Neuronal Signalling Studied with Light-Activated Ion

Channels to Target Interneurons, Entrain Hippocampal

Gamma Oscillations and Suppress Epileptiform Activity.

15th August 2013

Thesis submitted by

Laura Mantoan, MD MRCP

for the award of the degree

Doctor of Philosophy in Neuroscience

at the

Institute of Neurology, University College London.

# Declaration

I, Laura Mantoan, confirm that the work presented in this thesis is my own. Where information has been derived from other sources, I confirm that this has been indicated in the thesis.

# Abstract

The versatility and the electrophysiological characteristics of the light-sensitive ion-channels channelrhodopsin-2 (ChR2) and halorhodopsin (NpHR) make these optogenetic tools potent candidates in controlling neuronal firing in models of epilepsy and in providing insights into the physiology and pathology of neuronal network organization and synchronization. The experiments described in this thesis were designed to determine if the ChR2/NpHR system allows specific targeting and manipulation of interneuron activity in cortex and hippocampus, if it allows modulation of gamma oscillations in the hippocampal CA3 area, and if it constitutes a reliable toolbox enabling systematic analysis of epileptic neural circuits and a novel anti-epileptic treatment strategy that relies on optical activation of neurons to interrupt seizures. After successful generation of lentiviral constructs containing opsin genes driven by the interneuron-specific promoters glutamic acid decarboxylase (GAD) 67 and cholecystokinin (CCK) and the production of high-titre lentivirus, it was possible to demonstrate that both microbial opsins are expressed in neuronal cultures and rat motor cortex and hippocampus. Expression of the constructs, however, was not specific for interneurons and expression levels were low compared to the same opsins driven by the calcium calmodulin-binding kinase 2a (Camk2a) promoter: either fluorescence was only visible after immunofluorescent labelling or optical control of neural activity was not achievable despite visible fluorescence. In a separate set of experiments, stimulation of Camk2a–ChR2 with ramps of blue light induced oscillations in hippocampal area CA3. Oscillations entrained to modulated ramps over a wide range of frequencies with a frequency-dependent phase relationship. Finally, optical stimulation of halorhodopsin successfully reduced high frequency epileptic EEG activity in a tetanus toxin rat model of focal epilepsy. These results demonstrate that targeting opsins to interneurons with the GAD67 and CCK-promoters is not specific, that the CA3 network has properties that allow it

to entrain and synchronize to input from the dentate gyrus, which may help explain how coherence between these two anatomically coupled networks arises, and finally, that optical inhibition of HF discharges with NpHR targeted to pyramidal neurons represents an exciting new tool to be pursued in models of epilepsy both to dissect epileptic networks and for the development of other optogenetic neuromodulation therapies.

# Contents

# List of Tables

# List of Figures

# Acknowledgments

I would like to express my deep gratitude to Prof. Dimitri Kullmann, my principal supervisor, for his enthusiastic support, his invaluable and tireless review of my research project, for his guidance and teaching, scientifically and professionally, over the past five years.

I would like to extend this gratitude to Prof. Mary Collins and Dr. Stephanie Schorge, my secondary supervisors, for their incredible generosity, their invaluable advice and discussions on lentiviral physiology and molecular biology, the review of my thesis and for allowing me to become members of their team.

I would also like to extend my thanks to Prof. Matthew Walker, for allowing me to attend his clinics and see fascinating cases, for his immense support with clinical projects and for all he has taught me about sleep and epilepsy.

My thanks and gratitude also go to Dr. Douglas Macdonald, Dr. Rob Wykes, Dr. David Escors, Dr. Frederick Arce, Dr. Thomas Akam, Dr. Emily Ferenczi and Dr. Francesca Cacucci for sharing their knowledge, experience and experiments with me, and for their friendship.

I would like to thank Prof. John Parnavelas, Dr. Francesca Chiara, Dr. Anna Cariboni, Dr. William Andrews and Dr. Arianna Zito for teaching me how to perform immunohistochemical experiments, for sharing their laboratory, their materials and protocols. I would also like to thank Prof. Steve Davies, for allowing me to use his freezing vibratome equipment.

My thanks also extend to Dr. Karl Deisseroth and his team, for his generosity in sharing viral constructs, protocols and knowledge, for his invaluable course and for supporting our publication.

I wish to thank all the postdocs, staff, students and colleagues in the lab, at the Institute of Neurology, at the National Hospital of Neurology and

# Presentations

- Invited Lecture for the Epilepsy Specialist Interest Group at the Joint Meeting of the American and British Neurological Associations and Poster Presentation: "Optogenetic Treatment for Focal Epilepsy", Boston, USA, 8th October 2012.

- Poster Presentation: "Optogenetic Inhibition of Epileptic Activity", UCL Neuroscience Symposium 2012. London, June 2012.

- Platform Presentation and Prize for Best Platform Presentation: "Optogenetic Suppression of High Frequency EEG Activity in a Model of Focal Epilepsy" at the International League Against Epilepsy, UK Chapter Meeting. London, 27th April 2012.

- Poster Presentation: "Optogenetic Suppression of High Frequency EEG Activity in a Model of Focal Epilepsy"at Society for Neuroscience meeting. Washington, USA, 15th November 2011.

- Poster Presentation: "Optogenetic Inhibition of Epileptic Activity", International Epilepsy Congress. Rome, Italy, 29th August 2011.

- Poster Presentation: "Optogenetic Inhibition of Epileptic Activity", World Congress of Neuroscience, International Brain Organization. Florence, Italy, 15th July 2011.

- Poster Presentation: "Optogenetic Inhibition of Epileptic Activity", UCL Neuroscience Symposium 2011. London, July 2011.

- Poster presentation at the 3rd London-Innsbruck Colloquium on Acute Seizures and Status Epilepticus. Oxford, UK, 7-9 April 2011.

- Presentation at the Short Course in Optogenetics, Optogenetic Innovation Lab, Stanford University. Stanford, USA, 31st March 2011.

- Poster Presentation: "Optogenetic Inhibition of Epileptic Activity", Queen Square Symposium 2011, Institute of Neurology, UCL. London, February 2011.

- Lab Seminar, Experimental Epilepsy Group, Institute of Neurology, UCL. London, 18th November 2010.

- Invited Talk on"Neuronal Signalling Studied with Light Activated Ion Channels", Mike Haeusser Lab, UCL. London, 25th May 2010.

- Poster Presentation and 2nd Poster Prize: "Neuronal Signalling Studied with Light Activated Ion Channels", UCL Neuroscience Symposium 2010, London, March 2010.

- Poster Presentation: "Neuronal Signalling Studied with Light-Activated Ion Channels" at the Queen Square Symposium 2009, Institute of Neurology, UCL. London, February 2010.

- Presentation: "Microelectrode Amplifiers" at the lab retreat of the Department of Experimental Epilepsy. Axamer Lizum, Austria, March 2010.

- MPhil/PhD Upgrade Presentation, Department of Clinical and Experimental Epilepsy, Institute of Neurology, UCL. London, 21st January 2010.

- MSc Lecture: "The Biophysics of the Action Potential", MSc Neuroscience programme, Institute of Neurology, UCL. London, November 2009, 2010, 2011.

- Lectures: "The Examination of the Cranial Nerves" and "Movement Disorders", 4th Year Medical Students, Faculty of Medicine, UCL. London, Academic Years 2010 and 2011.

- Presentation and Critique of the Grant Proposal "Optogenetic Manipulation of Interneuron Development and Function" at the lab retreat of the Department of Experimental Epilepsy. Wales, 31st May 2009

- Poster Presentation: "Neuronal Signalling Studied with Light-Activated Ion Channels" at the Queen Square Symposium 2009, Institute of Neurology, UCL. London, 20th March 2009.

- Journal Club: Berndt A, Yizhar O, Gunaydin LA, Hegemann P, Deisseroth K. Bi-stable neural state switches. *Nat Neurosci.* 2008. Synapse Journal Club, Institute of Neurology, UCL. London, 10th March 2009.

## Publications

- Mantoan L, Eriksson SH, Nisbet AP, Walker MC. Adult-onset Non-REM Parasomnia with Hypnopompic Hallucinatory Pain: a Case Report. *Sleep*. Accepted for publication Sep 2012.

- Wykes RC*, Heeroma JH*, Mantoan L*, Zheng K, Macdonald DC, Deisseroth K, Hashemi KS, Walker MC, Schorge S, Kullmann DM. Optogenetic and Potassium Channel Gene Therapy in a Rodent Model of Focal Neocortical Epilepsy. * these authors contributed equally. *Sci Transl Med*, **4**(161):161ra152, (2012).

- Akam T, Oren I, Mantoan L, Ferenczi E, Kullmann DM. Oscillatory dynamics in the hippocampus support dentate gyrus–CA3 coupling. *Nat Neurosci*, **15**(5):763-8, (2012).

- Mantoan L, Amin Y, Kullmann D, Walker M. Status Epilepticus in the Intensive Care Unit: Frequency, Management and Impact on Outcome. *Epilepsia*, **52**:76-76, (2011).

- Mantoan L, Kullmann DM. Evaluating first seizures in adults in primary care. *Practitioner*, **255**(1743):25-8, (2011).

- Mantoan L, Wykes R, Schorge S, Walker MC, Kullmann DM. Optogenetic Inhibition of Epileptic Activity. *Epilepsia,* **52**:42-42, (2011).

- Mantoan L, Walker M. Treatment Options in Juvenile Myoclonic Epilepsy. *Curr Treat Options Neurol,* **13**(4):355-70, (2011).

- Kovac S, Miserocchi A, Scott C, Allen P, Mantoan L, Smith S, Walker M, Mc Evoy A, Scherg M, Hoechstetter K, Diehl B. Scalp EEG Source Analysis in Extratemporal Lobe Seizures: Comparison with Intracranial Findings. *Epilepsia,* **51**:24-24, (2010).

# Chapter 1

# Introduction

Opsins are a family of photosensory receptors found in all animal kingdoms, where they subserve a wide diversity of functions: from phototaxis in algae to eyesight in vertebrates (Briggs and Spudich, 2005). "Optogenetics" is a novel technology that combines optics and genetics by optical control of opsins targeted to living cell membranes. This fascinating technique has revolutionized neuroscience in recent years, allowing specific control of neuronal function with a spatiotemporal resolution and genetic specificity that are far greater than those achieved with electrophysiology (Davidson and Breakefield, 2003). Expression of these microbial light-sensitive proteins has been used to study specific classes of neurons *in vitro* (Boyden et al., 2005; Zhang et al., 2007b) and in intact brain tissue *in vivo*, in vertebrate (Aravanis et al., 2007; Diester et al., 2011) and invertebrate models (Hwang et al., 2007). More recent applications have focused on opsins as potential therapeutic tools (Tonnesen et al., 2009; Busskamp et al., 2010).

Building upon these recent technological advances, the aims of my work were threefold: Firstly, to target light-sensitive ion-channels to interneurons by lentiviral delivery. Secondly, to study the mechanisms of gamma oscillation synchronization and coherence in the hippocampus. Thirdly, to use optogenetic tools to investigate epileptic networks and suppress seizures.

Targeting the two major opsins channelrhodopsin-2 (ChR2) and halorhodopsin (NpHR) to interneurons to manipulate interneuron populations as a whole or as individual subclasses is desirable, as this would open up the possibility to study the individual functions of interneuron classes, understand how interneurons shape principal cell activity and neuronal oscillations, and define their role in epileptic networks. Viral delivery of opsins offers the unique advantage of targeted, cell subtype-specific and long-term expression. Two interneuron-specific promoters, glutamic acid decarboxylase (GAD) 67 and cholecystokinin (CCK), have successfully been used for virally-mediated delivery of transgenes (Chhatwal et al., 2007; Teschemacher et al., 2005; Jasnow et al., 2009), but the targeted expression of light-sensitive ion-channels to interneurons as a whole, or specifically CCK-positive interneurons, had not been attempted previously.

In collaboration with Thomas Akam, we set out to investigate whether ChR2 could be used to study synchronization mechanisms between local networks in the hippocampal area cornu ammonis 3 (CA3). Local network oscillations are known to be involved in input selection, consolidation of synaptic modifications and linking of distant cell populations, to mention just a few functions (Buzsáki and Draguhn, 2004). It is also known that network oscillations can become linked between regions and that synchronization is altered or disrupted in certain disease forms such as autism (Dinstein et al., 2011) and schizophrenia (Dinstein et al., 2011). How synchronization is accomplished, however, is unclear. We used optogenetic tools to control of a subset of neurons and bias their oscillations to defined frequencies. At the same time, oscillation entrainment and the interaction with other intrinsic oscillating networks was recorded by monitoring population activity with electrophysiological methods.

My final aim was to investigate whether optogenetic tools would allow modulation of epileptic activity. To date there is only one report on the therapeutic potential of light-activated inhibition in an *in vitro* model of

epileptiform activity (Tonnesen et al., 2009), and only one very recent comparable study *in vivo*, where thalamic stimulation was found to abolish stroke-induced seizures (Paz et al., 2012). An optimal therapeutic strategy would be minimally invasive, targeted to the epileptogenic zone, and would only suppress neuronal activity when needed. The versatility and the electrophysiological characteristics of ChR2 and NpHR make optogenetic tools potent candidates to control neuronal firing in models of epilepsy and to provide insights into the pathophysiology of epileptic network organization and synchronization.

The following sections will provide a review of the published literature and provide background information to the subsequent results chapters.

## 1.1 Opsins

Photosensory receptors deliver to organisms the information carried by light by absorbing single photons (Hecht et al., 1942; Van der Velden, 1946) and transducing these quanta of electromagnetic energy into a chemical form recognizable by cellular biochemical pathways. Many of these receptors, like our own visual pigments, are proteins that combine with the vitamin-A derived chromophore retinal (or retinaldehyde). This family of proteins are also termed retinylidene proteins or opsins [1]. They are the molecular basis for a variety of light-sensing systems from phototaxis in flagellates to eyesight in animals.

### 1.1.1 General Structure

Opsins are 25 - 50 kD membrane-bound proteins with a seven-transmembrane $\alpha$-helical structure (Fig. 1.1) (Briggs and Spudich, 2005). They reversibly and covalently bind retinal in Schiff base [2] linkage, by condensation of the aldehyde group of retinal to the positively charged amino group of a lysine residue in the

---

[1] Rhodopsin refers to the entire molecule comprising the opsin protein and the cofactor retinal.
[2] Compounds having the structure RN=CR2 bearing a hydrocarbyl group on the nitrogen atom R2C=NR′ (R′ ≠ H) (McNaught and Wilkinson, 1997 (online version 2012)).

seventh transmembrane alpha helix. Because this linkage is a protonated Schiff base, the result is a buried positive charge in the protein, and light-induced transfer of this proton within the binding pocket is important to function of rhodopsins.

Retinal acts as a chromophore: it is the part of the opsin molecule that photoisomerizes and causes a conformational change when absorbing light of a certain wavelength. This conformational change activates downstream G-protein signalling cascades or ion-transport mechanisms.

### 1.1.2 Classification

Primary sequence alignments divide opsins into two distinct phylogenetic classes, type 1 or microbial, and type 2, found in visual pigments and in pineal and hypothalamic receptor proteins of higher vertebrates. The two types of opsins differ in physical size and in the position of the 7th transmembrane helix in the membrane (Palczewski et al., 2000). Type 2 rhodopsins, such as visual pigments, exhibit a different domain organization from type 1 opsins: Whereas microbial rhodopsins have minimal interhelical loops, half of human retinal rhodopsin is buried in the membrane of rod cells, with the other half in hydrophilic loops protruding into the aqueous medium from both membrane surfaces. This different domain organization reflects how visual pigments transduce information from photons into biochemical signalling molecules: the intracytoplasmic loops enable type 2 opsins to bind heterotrimeric G proteins, receptor kinases, and other signalling proteins (Khorana, 1993; Sakmar, 1998). The microbial rhodopsins, on the other hand, function largely within the membrane to pump ions or to function as light-activated ion channels (Spudich, 1998). The isomeric configuration and ring/chain conformation of the retinal and the photoisomerization step also differ between the two opsin classes (Fig. 1.2): Rhodopsins found in prokaryotes and algae commonly contain an all-*trans* retinal isomer in the planar 6-*s-trans* conformation at the ground state that
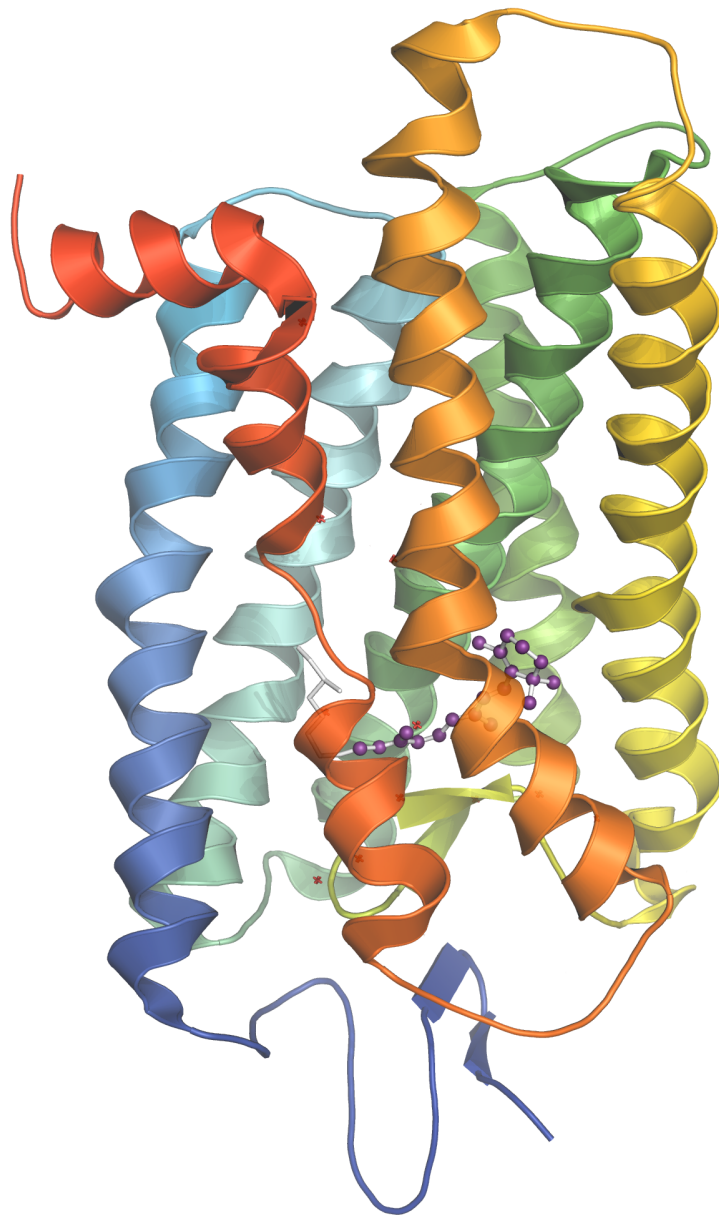
Figure 1.1: **Crystal structure of bovine rhodopsin in three dimensions**: Helices 1-6 are coloured in blue to orange, Helix 7 in red, retinal in purple. Reconstructed on PyMOL (Schrödinger, LLC, 2010) from PDB ID: 1GZM (Li et al., 2004) on www.pdb.org (Berman et al., 2000)).

Figure removed due to copyright restrictions.

Figure 1.2: **Retinal conformation and isomerization steps in opsins type 1 and 2.** The atomic structure of retinal in type 1 microbial opsins (left) in the all-*trans* (top) and 13-*cis* state (bottom) after absorption of photons. The conformation of visual pigment-like type 2 opsin retinal (right) in the 11-*cis* (top) state, which isomerizes to the all-*trans* state (bottom) after absorption of light (from (Spudich et al., 2000)).

isomerizes to 13-*cis* upon light activation, whilst type 2 opsins bind an 11-*cis* isomer of retinal in 6-*s-cis* conformation in the dark, which undergoes photoisomerization to an all-*trans* retinal when activated by a photon. Finally, despite having similar molecular structure and sharing functional features, direct sequence comparison revealed no evident homology between the two opsin groups, suggesting that the fundamental mechanism for detecting light using an "opsin-like" protein was exploited twice independently during the course of evolution (Fernald, 2006).

### 1.1.3   Microbial Opsins (Type 1)

The visual pigment rhodopsin was originally extracted from bovine retina using bile salts in 1878 (Kuehne, 1878). Half a century later, G. Wald provided evidence that visual pigment is composed of a protein conjugated with an unidentified retinoid (Wald, 1935) and went on to characterize the primary physiological and chemical visual processes in the eye[3]. He had also suggested that there may be a retinal protein mediating phototaxis in such motile unicellular organisms as the alga *Chlamydomonas*. In the following 30 years, research on microbial rhodopsins focused on four proteins found in the membrane of the halophilic archaeon *Halobacterium salinarum* and the only microbial retinylidene proteins known prior to 1999*:* the light driven ion pumps bacteriorhodopsin (BR) (Oesterhelt and Stoeckenius, 1973) and halorhodopsin (HR) (Matsuno-Yagi and Mukohata, 1977; Schobert and Lanyi, 1982), and the phototaxis receptors sensory rhodopsin I and II (SRI and SRII) (Bogomolni and

---

[3]For which he was eventually awarded the Nobel Prize in Physiology or Medicine in 1967.

24

Spudich, 1982; Takahashi et al., 1985). From 1999 onwards, genome sequencing of cultivated microorganisms has revealed the previously unknown presence of homologs of photosensory microbial rhodopsin in the other two domains of life: Bacteria (Beja et al., 2001; Jung et al., 2003) and Eukarya (Bieszke et al., 1999; Sineshchekov et al., 2002). Since then, a remarkable 782 different partial sequences homologous to type 1 rhodopsins was found by whole genome "shotgun sequencing" of microbial populations collected *en masse* from sea water samples in the world's oceans (Beja et al., 2001; de la Torre et al., 2003; Man et al., 2003; Man-Aharonovich et al., 2004; Sabehi et al., 2003; Venter et al., 2004). Rhodopsin genes have been identified in microorganisms that inhabit the most diverse environments from salt flats, soil, fresh water, surface and deep sea water, to glacial sea habitats and human and plant tissues as fungal pathogens (Briggs and Spudich, 2005). Studies of the microbial rhodopsins have made them some of the best understood membrane proteins in terms of structure and function at the atomic level. Atomic resolution structures, which exist for fewer than 60 membrane proteins, have been obtained from electron and X-ray crystallography from BR[4] (Grigorieff et al., 1996; Pebay-Peyroula et al., 1997; Essen et al., 1998; Luecke et al., 1999), HR (Kolbe et al., 2000), SRII (Luecke et al., 2001) and, most recently, from Channelrhodopsin-2 (Müller et al., 2011) and a chimera from Channelrhodopsin-1 and -2 from *Chlamydomonas reinhardtii* (Kato et al., 2012)*.* These proteins share a nearly identical positioning of the seven transmembrane helices and 80% identity in the 22 residues forming the retinal binding pocket. Finding type 1 rhodopsin homologs is based on identifying these conserved protein residues in other organisms.

The remainder of this section will explore the archaeal rhodopsins, including halorhodopsin, and the rhodopsins found in green flagellate algae, including channelrhodopsin.

---

[4]Including a 1.55Å structure reported for BR, in which bound water molecules are visible (Luecke et al., 1999).

Figure 1.3: (Spudich et al., 2000)) .

### 1.1.3.1  Archaeal Rhodopsins

Sixteen variants of BR, HR, SRI and SRII have been documented in related
halophilic archaea such as *Natronomonas pharaonis*.

As briefly alluded to in the previous section, the functions and photocycles of
the four archaeal rhodopsins have been well characterized and I would like to
sketch the major determinants of their activation process in more detail:

A photon of visible light absorbed by BR provides sufficient energy for the
structural transformation from quiescence into a signalling protein (Hecht et al.,
1942; Van der Velden, 1946), a process described as photoisomerization: Within
femtoseconds, photon absorption causes rapid rearrangement of electrons in
the molecule, which results in *trans* → *cis* isomerization at the C13 = C14 double
bond , causing transformation of all-*trans* to 13-*cis* retinal. Photoisomerization
of retinal initiates a sequence of photochemical events producing a series of
structural alterations in the opsin protein. The absorption spectrum of the
molecule is sensitive to conformational changes throughout the protein, and
therefore the sequentially different states of the opsin can be detected as so
called photointermediates with different absorption spectra. In the dark, the
unphotolyzed states of the pigments exhibit absorption maxima in the visible
range (BR 568 nm, HR 578 nm, SR I 587 nm, and SR II 487 nm), whilst the
absorption maxima of the photointermediates are shifted to either the red or
blue. To complete the cycle, the retinal needs to re-isomerize to all-*trans*: in
microbial rhodopsins the photointermediates spontaneously (i.e. by thermal
processes in the dark) return to the unphotolyzed state, completing a
photochemical reaction cycle (photocycle) (Spudich et al., 2000). Additionally, a
photochemical intermediate of the HR cycle can be photochemically
reconverted to the ground state by blue light, a two-photon reaction which is
also known for the M intermediate of bacteriorhodopsin (Hegemann et al.,

1985). As a general rule, more than 10-fold faster photocycling rates distinguish the archaeal transport (photocycles typically are < 30 ms) from the sensory pigments (photocycles typically are > 300 ms) (Spudich et al., 2000).

Functionally, archaeal rhodopsins have either transport or sensory functions. BR and HR are light-driven ion pumps for protons and chloride, respectively. BR and HR hyperpolarize the membrane by proton ejection or electrogenic chloride uptake thereby creating a negative inside/positive outside membrane potential and an inwardly directed electrical gradient for net proton uptake. This is especially important in alkaline conditions for pH homeostasis. BR also converts light to a proton gradient which in turn is used by a second membrane protein, ATP synthase to generate chemical energy in the form of ATP and to drive substrate active transport and other energy-requiring processes. SRI and SRII are receptors controlling the cell's phototactic responses to changes in light intensity and colour. In Archea, for example, they control the cell's swimming behaviour (Briggs and Spudich, 2005). If progenitors of these opsins existed before the divergence of archaea, eubacteria and eukaryotes in early evolution, then light-driven ion transport as a means of obtaining cellular energy may have preceded the development of photosynthesis and may represent one of the earliest means by which organisms used solar radiation as an energy source (Briggs and Spudich, 2005).

### 1.1.3.2   Rhodopsins in Green Flagellate Algae

The rhodopsins found in the green flagellate algae *Chlamydomonas reinhardtii* (Nagel et al., 2002, 2003; Sineshchekov et al., 2002), and *Volvox carteri* (Zhang et al., 2008) are important mediators of light control of phototaxis and the photophobic response. The photoreceptor currents mediating phototactic orientation are confined to the pigmented eyespot region, a single, asymmetrically placed photoreceptor apparatus. The presence of rhodopsin receptors in green flagellate algae was initially suggested based on their action

spectra for phototaxis (the rate of phototaxis plotted against light wavelength) (Foster and Smyth, 1980) and then confirmed by the results of retinal reconstitution studies in "blind" Chlamydomonas mutants (Lawson et al., 1991; Foster et al., 1984; Hegemann et al., 1991; Takahashi et al., 1991; Zacks et al., 1993; Sineshchekov et al., 1994). The receptor proteins themselves were not identified until the search of Chlamydomonas complementary deoxyribonucleic acid (cDNA) database revealed the presence of two sequences homologous to archaeal opsins. The two opsin proteins were reported independently by several research groups and named Chlamydomonas sensory rhodopsin A and B (CSRA and CSRB (Sineshchekov et al., 2002)), channelopsin 1 and 2 (Chop-1 and 2 (Nagel et al., 2002, 2003)) and Archaeal type Chlamydomonas opsin 1 and 2 (Acop-1 and Acop-2 (Suzuki et al., 2003)). In this thesis we will use channelrhodopsin-1 (ChR1) and channelrhodopsin-2 for the retinal-bound proteins and Chop-1 and 2 for their apoprotein or "opsin" forms without retinal. The N-terminal domains (7-TM domain) of the encoded opsin apoproteins form seven membrane-spanning helices and, in Xenopus oocytes, the light-dependent currents and current-voltage relationships were shown to be the same in full-length and 7-TM domains of ChR1 and 2, demonstrating that the extensive C-terminal domain is not involved in the photocurrents measured (Nagel et al., 2002, 2003). Under physiological conditions photoreceptor currents are carried mainly by $Ca^{2+}$, but $Sr^{2+}$, $Ba^{2+}$ and $Mg^{2+}$ are also conducted albeit less efficiently (Holland et al., 1996). When the eyespot region is exposed to low pH a second ($H^+$-mediated) photoreceptor current component appears (Ehlenbeck et al., 2002). Expression of Chop-1, or of only the hydrophobic core, in Xenopus laevis oocytes in the presence of all-*trans* retinal produced a light-gated current that showed characteristics of a channel selectively permeable for protons, suggesting that ChR1 is the photoreceptor system that mediates the $H^+$-mediated photoreceptor current (Nagel et al., 2002). ChR2 was subsequently shown to be a directly light-switched cation-selective ion channel (Nagel et al., 2003). This channel opens rapidly (<

$$C \longrightarrow C^* \longrightarrow O \longrightarrow D \longrightarrow C$$

10 - 400 ms     60 ms - 2 s

0.2 ms
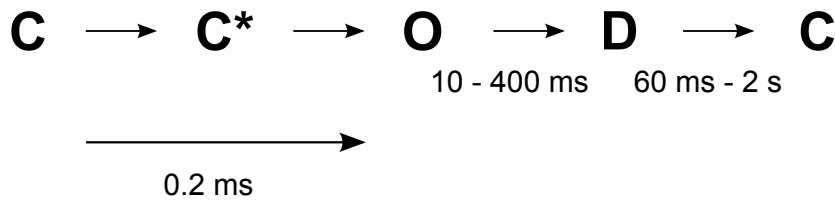
Figure 1.4: **ChR2 photocycle.** Schematic exemplifying time constants for ChR2 photoreactions modelled from electrophysiological data available (Müller et al., 2011; Kato et al., 2012).

200 µs) after absorption of a photon to generate permeability for monovalent and divalent cations. It desensitizes in continuous light to a smaller steady-state conductance. Recovery from desensitization is accelerated by extracellular $H^+$ and negative membrane potential, whereas closing of the ChR2 ion channel is decelerated by intracellular $H^+$. ChR2 is expressed in *Chlamydomonas* under low-light conditions, suggesting involvement in photoreception in dark-adapted cells (Nagel et al., 2003). The action spectra of the observed photocurrents in *Chlamydomonas* cells correlated with those measured for ChR1 and 2 (Sineshchekov et al., 2002) and showed that ChR2 absorption is blue-shifted (maximum at ~460 nm) as compared with ChR1 (maximum at ~500 nm). The ChR2 photocycle is only hypothetical due to only few crystallographic data available (Müller et al., 2011; Kato et al., 2012), but could be modelled from electrophysiological data as follows (Fig. 1.4) : (within 1 ns) photon absorption leads to an excited state of ChR2 (C*). In slower dark reactions this is followed by an open state (O), a closed, desensitized state (D), and a closed ground state (C). From experimental data, a 1 ms time period leads from a closed ground state (C) to the open state (C → C* → O). Closing to the desensitized state (D) occurs within 10–400 ms, depending on intracellular pH. As opening (C → C* → O) is so fast, the four-state transitions model (C → C* → O → D → C) is further reduced to a three-state transitions model (C → O → D → C). Time constants are 0.2 ms for light-activated opening (C → O), 20 ms for closing (O → D) and 2 s for recovery from desensitization (D→ C). When using these time constants, then the model predicts a much smaller stationary

light-activated current than experimentally observed. This may indicate that two photons are absorbed during the photocycle (in analogy with the two-photon cycles of other rhodopsins (Hegemann et al., 1985)), with an effective light-activated $D \rightarrow C$ transition time constant of 60 ms (Nagel et al., 2003). Expression of ChR2 in oocytes or mammalian cells was shown to be a powerful tool to increase cytoplasmic $Ca^{2+}$ concentration or to depolarize the cell membrane, simply by illumination (Nagel et al., 2003).

### 1.1.4 Opsin Expression in Neurons: Replacing the Electrode with Light?

Since Galvani first reported a method for the direct stimulation of nerves over 200 years ago (Galvani, 1791), the basic approach based on the use of metal electrodes has changed surprisingly little. Electrical stimulation involves the use of metal or electrolyte-filled glass pipette electrodes to trigger action potentials in individual neurons or groups of neurons. This technique suffers from three key limitations: it lacks specificity , as current can spread from the electrode beyond the tissue in physical contact with it, inhibiting neurons is difficult, and it is invasive (Scanziani and Häusser, 2009). Optical probes are promising tools that obviate the need of physical contact with the tissue studied(Scanziani and Häusser, 2009). Miesenboeck's team at Yale first developed optical techniques ranging from caged compounds, phototransduction components of *Drosophila* expressed in neurons (Zemelman et al., 2002) and combinations of heterologous expression of ligand-gated channels and injected photolabile caged compounds in fruit flies (Lima and Miesenböck, 2005). Since 2005, substantial progress was made by the groups of Deisseroth at Stanford University[5] and Nagel at the Max Planck Institute for Biophysics (Boyden et al., 2005): They developed opsins with the necessary temporal resolution to probe neurons at the resolution of single spikes. These tools were developed in a remarkable series of experiments over only a couple

---

[5]www.stanford.edu/group/dlab/optogenetics/

of years and subsequently further developed at both institutions (Kleinlogel et al., 2011; Yizhar et al., 2011a) and by Boyden's team at the Massachusetts Institute of Technology (MIT) (Chow et al., 2010). Table 1.1 and 1.2 summarizes the main spectral and kinetic characteristics of opsins available to date.

ChR2 was chosen to attempt genetically targeted photostimulation with fine temporal resolution due to the efficacy and speed of its natural light-transduction mechanisms. Knowing that the long C-terminus of ChR2 was not involved in the generation of photocurrents, lentiviruses were engineered containing a ChR2, whose C-terminus was fused with a yellow fluorescent protein (YFP) gene. These viruses successfully targeted ChR2 to mammalian neurons. Expression of ChR2 was shown to be was stable over weeks and safe, as it did not alter the electrical properties or survival of neurons (Boyden et al., 2005). Furthermore, ChR2 could drive neuronal depolarization without necessitating addition of external cofactors, as the retinal present in the mammalian brain was shown to be sufficient to constitute a functional rhodopsin (Boyden et al., 2005; Ishizuka et al., 2006; Li et al., 2005). Illumination with blue light induced rapid (opening rate of ~1.21 ms at 19.8 mW/mm$^2$ light intensity (Lin, 2011)), large amplitude (496±336 pA (mean±s.d.) at peak (Boyden et al., 2005)) depolarizing currents, which rapidly recovered (closing rate of 13.5 ms at 19.8 mW/mm$^2$ light intensity (Lin, 2011)). Pulsed optical activation of ChR2 was also able to elicit precise, repeatable spike trains in a single neuron, and to drive sustained naturalistic trains of spikes in a physiologically-relevant spike range (5–30 Hz). Finally, ChR2 was shown to drive subthreshold depolarizations and to control excitatory and inhibitory synaptic transmission (Boyden et al., 2005).

Soon, a complementary high-speed hyperpolarizing Cl$^-$-pump was found by screening halorhodopsins from two strains of archaea, *Halobacterium salinarum (*HsHR) and *Natronomonas pharaonis* (NpHR) (Zhang et al., 2007b). Illumination of HsHR- or NpHR-expressing *Xenopus* oocytes led to rapid outward currents

Table 1.1: **Optogenetic tools available to date - excitatory and bistable opsins.** Adapted from (Yizhar et al., 2011a). *Decay Kinetics are temperature dependent. The given values were measured at room temperature, except for ChRGR that was measured at 34°C. An ~50 % decrease in $\tau_{off}$ is expected at 37 °C (Yizhar et al., 2011a).

| Opsin | Peak Activation $\lambda$ [nm] | Off Kinetics $\tau$ [ms] | Reference |
|---|---|---|---|
| **Excitatory Opsins (Cation Channels)** | | | |
| ChR2 | 470 | ~10 | (Boyden et al., 2005; Nagel et al., 2003) |
| ChR2(H134R) | 470 | 18 | (Nagel et al., 2005; Gradinaru et al., 2007) |
| ChR2(T159C) | 470 | 26 | (Berndt et al., 2011) |
| ChR2(L132C) | 470 | 16 | (Kleinlogel et al., 2011) |
| ChETA: ChR2(E123A) | 470 | 4 | (Gunaydin et al., 2010; Berndt et al., 2011) |
| ChETAs: ChR2(E123T) | 490 | 4 | (Gunaydin et al., 2010; Berndt et al., 2011) |
| ChETA: ChR2(E123T/T159C) | — | 8 | (Gunaydin et al., 2010; Berndt et al., 2011) |
| ChIEF | 450 | ~10 | (Lin et al., 2009) |
| ChRGR | 505 | 4–5* | (Wang et al., 2009; Wen et al., 2010) |
| VChR1 | 545 | 133 | (Zhang et al., 2008) |
| C1V1 | 540 | 156 | (Yizhar et al., 2011b) |
| C1V1 ChETA(E162T) | 530 | 58 | (Yizhar et al., 2011b) |
| C1V1 ChETA(E122T/E162T) | 535 | 34 | (Yizhar et al., 2011b) |
| **Bistable Opsins** | | | |
| ChR2-step function opsins | 470–590 | 2 s - 29 min | (Berndt et al., 2009; Bamann et al., 2010; Yizhar et al., 2011b) |
| VChR1- SFOs | 560–390 | 32 s - 5 min | |

Table 1.2: **Optogenetic tools available to date - inhibitory opsins and biochemical modulators.** Adapted from (Yizhar et al., 2011a). *Decay Kinetics are temperature dependent. The given values were measured at room temperature. An ~50 % decrease in $\tau_{off}$ is expected at 37 °C (Yizhar et al., 2011a).

| Opsin | Peak Activation $\lambda$ [nm] | Off Kinetics $\tau$ [ms] | Reference |
|---|---|---|---|
| **Inhibitory Opsins** | | | |
| eNpHR3.0 (Chloride Pump) | 590 | 4.2 | (Gradinaru et al., 2010) |
| Arch/ArchT (Proton Pump) | 566 | 9 | (Chow et al., 2010) |
| eBR (Proton Pump) | 540 | 19 | (Gradinaru et al., 2010) |
| Mac | 565 | | (Chow et al., 2010) |
| **Biochemical Modulators** | | | |
| *increased G-protein signalling :* | | | |
| opto-β2AR | 500 | 0.5 s | (Airan et al., 2009) |
| opto-α1AR | 500 | 3 s | (Airan et al., 2009) |
| Rh-CT (5-HT1A) | 485 | 3 s | (Oh et al., 2010) |
| *increased cAMP :* | | | |
| bPAC | 453 | 12 s | (Stierl et al., 2011) |
| BlaC | 465 | 16 s | (Ryu et al., 2010) |

with excitation maxima near 580 nm, which, importantly, is red-shifted from the known ChR2 maximum of 470 nm. This spectral separation indicated that ChR2 and a halorhodopsin could be activated independently or in synchrony to effect bidirectional optical modulation of membrane potential. $Cl^-$ currents were reliable for both halorhodopsins across all physiological voltage regimes. On the basis of NpHR's higher extracellular $Cl^-$ affinity and stability, it was selected for experiments in neurons. Expression of NpHR-EYFP was successful in hippocampal neurons using lentiviruses carrying the ubiquitous elongation factor 1 a (EF1a) promoter[6] and expression was maintained for weeks after transduction. In voltage-clamp experiments, illumination of NpHR-EYFP cells with yellow light from a 300 W Xenon lamp induced outward currents with a peak of 43.86±25.9 pA with rise and decay time constants of $t_{on}$=6.1±2.1 ms and $t_{off}$=6.9±2.2 ms, respectively (no light intensity given in published literature) (Zhang et al., 2007b). NpHR-mediated hyperpolarization was also able to abolish evoked firing over a wide range of time-scales (up to 8 min) and with single spike precision in current-clamped neurons illuminated with light of 21 mW/mm$^2$ intensity. Furthermore, co-expression of NpHR and ChR2 in cultured neurons confirmed that ChR2 and NpHR can be combined to achieve bidirectional, independently addressable modulation of membrane potential in the same neuron (Zhang et al., 2007b). Both NpHR and ChR2 were also functionally expressed in the mammalian brain *in vivo* where they were shown to operate at high speed without necessitating cofactor addition (Zhang et al., 2007b; Li et al., 2005; Ishizuka et al., 2006).

### 1.1.4.1   Channelrhodopsin and its Variants

Despite the advantages of ChR2, its limitations became quickly apparent: the single channel conductance of ChR2 is small, requiring either strong expression or high levels of illumination to the tissue to effectively depolarize neurons. Prolonged or high frequency light stimulation desensitizes 80% of the channels,

---

[6]LV-EF1a-NpHR–enhanced yellow fluorescent protein [EYFP]

implying that five times more ChR2 needs to be expressed to achieve equivalent depolarization of the neuron as when ChR2 is not desensitized. ChR2 expression can also cause the accumulation of intracytoplasmic aggregates and cell toxicity. These shortcomings were tackled by developing better viruses and mutant ChR2 variants (Lin, 2011; Mattis et al., 2012) as shown in table 1.1. The first approach at developing improved ChR2 versions consisted in substituting amino acids involved in the channel kinetics, its spectral or membrane trafficking properties. The following channelrhodopsins (ChRs) were developed by this technique (mutation in brackets): ChR2(H134R) with large photocurrents but slower channel kinetics (Nagel et al., 2005), ChETA(E123T) with fast channel kinetics but small current amplitudes advantageous for reducing the depolarization block caused by overexpression of ChR2 (Gunaydin et al., 2010), a ChR2 including both mutations (H134R)+(E123T) with accelerated kinetics, and large photocurrents (Gunaydin et al., 2010), ChR2-step function (C128T) with long-lived open channel states but slow kinetics (Berndt et al., 2009)[7], and CatChR, a $Ca^{2+}$ translocating ChR2, which is fast and 70-fold more light sensitive than wildtype ChR2 but has not been tested *in vivo* or slices. The T159C mutation (ChRTC) generates large photocurrents at low light intensities and can be used with weaker promoters and long experiments. ChR ET/TC (E123T/T159C) has accelerated and voltage-independent kinetics and is good for high frequency activation, has no plateau depolarization and $Na^+$ channel inactivation, with its optimal wavelength slightly red shifted to 505 nm (Berndt et al., 2011). In addition to selectively mutagenizing ChR2, chimerae of ChR1 and 2 were made to exploit the faster kinetics and smaller desensitization properties of ChR1: a chimera of ChR1 and 2 called ChIEF has the best photocurrent responses when stimulated continuously or with high frequency pulses of light due to its high steady state and peak photocurrent. It requires

---

[7]Originally developed as a bistable switch driven by different colours of light (blue and yellow), but it was eventually shown that the channel was not suitable for long stimulation paradigms, as ChR did not desensitize well in darkness and was therefore not "bistable" (Schoenenberger et al., 2009).

desensitization with pulses of 570 nm light, as it does not recover in the dark (Lin et al., 2009). Finally, the green-light driven chimera ChRGR has fast kinetics with minimal desensitization (Wen et al., 2010). As a third approach to enrich the optogenetic toolbox, new excitatory opsins were sought: a cation conducting channelrhodopsin (VChR1) was found in *Volvox carteri*. It can drive spiking at 589 nm, with its excitation maximum red-shifted by 70 nm compared with ChR2 species (Zhang et al., 2008). VChR1 was recently improved to C1V1, a far-red shifted version of ChR2, which is compatible with Fura-2 and GCaMP $Ca^{2+}$ imaging techniques (Yizhar et al., 2011b). If C1V1 was used with the blue-shifted ChR2, it would allow combined stimulation of different neuronal subpopulations with light of different wavelengths. Finally, by mutating a cysteine residue, ChR2 variants with very long deactivation constants (up to 30 min) have been engineered (Berndt et al., 2009; Bamann et al., 2010; Yizhar et al., 2011b). The long lasting photocurrent can still be interrupted by deactivating the opsin with flashes of green/yellow light (560-590 nm (Berndt et al., 2009)). Since these opsins have bistable behaviour, allowing step-like control of the membrane potential, they have been termed step-function opsins (SFO).

In parallel to the excitatory channels, so-called "optoXRs" were developed: a chimeric opsin–G protein coupled receptor protein (GPCR) was engineered by replacing the intracellular loops of bovine rhodopsin (physiologically coupled with $G_t$–protein) with those of two specific adrenergic receptors ($G_q$–coupled human α1-adrenergic receptor and $G_s$–coupled hamster β2-adrenergic receptor). These optoXRs were shown to allow optical control of GPCR signalling cascades by activation with 500 nm light (Airan et al., 2009). They are responsive to timed light pulses, can be targeted to specific cell-types, and are functional within mammals *in vivo* (Airan et al., 2009).

### 1.1.4.2 The Problem of a Good Inhibitor

Experimenters soon found that NpHR had shortcomings: it activates slowly and generates small photocurrents. In addition, with high expression levels of NpHR, intracellular accumulations of NpHR-EYFP started to become apparent. They were mainly localized to the endoplasmatic reticulum (ER). To improve trafficking of NpHR to the cell membrane, a number of different peptides modulating membrane trafficking were screened and a combination of two motifs was identified that markedly promoted membrane localization and ER export: an N-terminal signal peptide and a C-terminal ER export sequence. The modified 'enhanced' NpHR (eNpHR2.0 or simply NpHR2.0) displayed high-level expression in mammalian neurons, increased peak photocurrent in the absence of aggregations or toxicity, and optical inhibition was observed, not only *in vitro*, but also *in vivo* (Gradinaru et al., 2008). Later, a membrane trafficking signal from an inward rectifier potassium channel (Kir2.1) was added to the NpHR sequence, generating NpHR3.0, with even better photoactivation and kinetic properties and a spectrum of activation shifted up to 680 nm(Gradinaru et al., 2010). A second group developed archaerhodopsin-3 (Arch) and an opsin from the fungus *Leptosphaeria maculans* (Mac), two proton-pumps activated by yellow and blue light, respectively (Chow et al., 2010). Arch expresses *in vivo* and silences currents of up to 900 pA, it spontaneously recovers and has no inactivated state. If used together, Arch and Mac could potentially allow "multicolour silencing", in the same way as the ChR2 variants allow "multicolour activation" of neurons. A comparison of kinetics of the three major inhibitors is given in Table 1.3 .

### 1.1.4.3 Applied Optogenetics

Expression of microbial light-sensitive proteins has been used to interrogate specific classes of neural cells, from cultured neurons to intact brain tissue *in vivo*. Targeting specific neuronal subpopulations will be discussed in a

Table 1.3: **Kinetics of the optogenetic inhibitors.** Details available of NpHR2.0, NpHR3.0 and Arch spectral and kinetic characteristics compared with those of ChR2. Values are expressed as mean±s.d. except for Arch (mean±standard error). No kinetic data were found on Mac (Boyden et al., 2005; Zhang et al., 2007b; Chow et al., 2010; Gradinaru et al., 2010).

| | ChR2 | NpHR2.0 | NpHR3.0 | eBR | Arch |
|---|---|---|---|---|---|
| **Recovery time [s]** | 5.1 ± 1.4 | — | — | — | — |
| **Current rise time [ms]** | 6.1 ± 2.1 | — | — | — | 8.8 ± 1.8 |
| **Voltage rise time [ms]** | 8.0 ± 1.9 | 35.6 ± 15.1 | — | — | — |
| **Current decay time [ms]** | — | 6.9 ± 2.2 | — | — | 19.3 ± 2.9 |
| **Voltage decay time [ms]** | — | 40.5 ± 25.3 | — | — | — |
| **Peak current [pA]** | 496 ± 336 | 43.8 ± 25.9 | — | — | 863 ± 6.2 |
| **Steady state current [pA]** | 193 ± 177 | 214.1 ± 24.7 | 747.2 ± 93.9 | 46.4 ± 7.2 | — |
| **Max. hyper-polarization [mV]** | — | 57.2 ± 6.8 | 101 ± 24.7 | 10.8 ± 1.0 | 76.2 ± 10.1 |
| **Shortest light time published [ms]** | 15 | 50 | 5 | 1000 | 15 |

subsequent chapter, but, briefly, can be achieved using cell-type specific promoters in viral vectors and in transgenic animals (Cardin et al., 2009) or cre-lox systems, or by employing both. To allow optical stimulation *in vivo*, an integrated fiberoptic and optogenetic technology was developed. The interface employed an implanted fiber guide to target the brain region of interest (Zhang et al., 2010). The fiber guide was used for two purposes: to deliver the engineered viruses that render specific neuronal types optically sensitive through ChR2 expression, and to direct the illumination beam of an optical fiber coupled with a laser to the ChR2 positive neurons. This interface was then superseded by direct implantation of a custom-made fiberoptic cannula into an area of viral injection or in transgenic mice expressing ChR2 and NpHR2.0 under the neuron specific Thymocyte differentiation antigen 1 (Thy1) - promoter (Wang et al., 2007; Arenkiel et al., 2007; Zhao et al., 2008). The interface has been implemented in rat, mouse and monkey models, and was used to target specific neuronal cell types without evidence of a functional immune response *in vivo* (Aravanis et al., 2007; Han et al., 2009a; Cardin et al., 2010; Diester et al., 2011). Following these advances, there has been an explosion in scientific output using optogenetic techniques. Among the notable results obtained with this technology are these findings: Using lentiviral targeting of ChR2 to hypocretin neurons in the lateral hypothalamus, electrical activity arising from hypocretin neurons was sufficient to drive awakening from sleep states (Adamantidis et al., 2007). Opsins were used to to elucidate the link between the firing of locus coeruleus neurons and arousal (Carter et al., 2010), between astrocyte activity and breathing patterns (Gourine et al., 2010), and to dissect the amygdala circuitry (Stuber et al., 2011; Tye et al., 2011). Optical microstimulation of ChR2 was used to drive perceptual decisions and learning behaviour in the barrel cortex of mice (Huber et al., 2008), to manipulate neural synchrony without perturbation of other parameters such as spiking rate (Han et al., 2009b; Han and Boyden, 2007) and to induce gamma oscillations (Cardin et al., 2009; Adesnik and Scanziani, 2010; Carlén et al., 2011). More recent

applications have focused on opsins as potential therapeutic tools: Optical microstimulation of ChR2 was used to rescue inner retinal neurons and restore visual function in a mouse model of retinal degeneration (Bi et al., 2006; Lagali et al., 2008), whilst halorhodopsin was able to reactivate human photoreceptors in retinitis pigmentosa (Busskamp et al., 2010) and to control epileptiform activity in organotypic hippocampal slice cultures (Tonnesen et al., 2009). Optical stimulation of the direct-pathway circuitry in the basal ganglia rescued the motor deficits in a mouse model of Parkinson's disease (Kravitz et al., 2010), whilst stimulation of the medial prefrontal cortex had an antidepressant effect in mice (Covington et al., 2010). More recently, further development of viral vectors and opsins has made it possible to selectively stimulate projection tracts rather than only somata (Tye et al., 2011), and to achieve pathway-specific targeting of specific subpopulations of neurons (Gradinaru et al., 2010).

## 1.2   Viral Vectors

Transfer of foreign genes into terminally differentiated cells such as neurons is desirable for experimental and therapeutic purposes and can be accomplished with nonviral or viral methods. Nonviral methods comprise the use of transfection reagents or of physical means such as ballistic, ultrasound, or electroporation-based DNA injection. Transfection relies on the principle that chemicals such as calcium phosphate, diethylaminoethyl-dextran (DEAE-Dextran) (Pagano and Vaheri, 1965) and cationic liposomes coat or neutralize the DNA's negative charge, thereby enabling it to cross the plasma membrane via endocytosis or phagocytosis.

Calcium-phosphate precipitation is an inexpensive technique developed in the 1970s, which has changed little over time and is based on the principle that when calcium phosphate is added to a DNA suspension in controlled conditions (pH and temperature), it precipitates (Graham and van der Eb, 1973). These precipitates are added to a cell culture, where the DNA/calcium

complexes are thought to be taken up by endocytosis. A major drawback of the technique is a low transfection efficiency in most culture systems including neurons (Dudek and Bertram, 2010) and the fact that little or no expression is observed *in vivo*. A further potential problem is that it loads neurons with $Ca^{2+}$, which may be toxic.

Cationic liposomes are vesicles composed of positively charged synthetic lipids[8] in bilayer formation (Felgner et al., 1987). The lipid-DNA complexes (lipoplexes) are stable and the positive charge of the complex interacts with the net negative charge of plasma membranes leading to internalization. The advantage of their low immunogenicity is counterbalanced by low transfection rates and cytotoxicity, thereby limiting their application. The cytotoxicity of lipoplexes manifests as cell shrinking, vacuolization of the cytoplasm and cell death via apoptosis, and is related to the lipid-DNA molar charge ratio and the dose administered. Since transfection efficiency also depends on the charge ratio (as well as the lipid composition and the vesicle size), in practice this means that cationic liposomes can only be used in limited quantities to avoid cytotoxicity, which results in low transfection efficiencies (Kongkaneramit et al., 2008; Masotti et al., 2009). In neurons some success can be achieved with commercially available cationic liposome formulations such as Lipofectamine[TM] (Invitrogen) (Dalby et al., 2004) and Fugene[TM] (Roche) (Wiesenhofer and Humpel, 2000).

Physical methods of gene transfer include electroporation and biolistic particle delivery (e.g. gene gun) methods (Gamper and Shapiro, 2006). Electroporation is based on the principle that an electric pulse applied to a cell perturbs the plasma membrane forming pores, that facilitate entry of DNA into the cytoplasm (Shigekawa and Dower, 1988). It can be used to transfect neurons by single cell electroporation via a patch pipette (Haas et al., 2001) or to transfect periventricular neurons by in utero electroporation (Tabata and Nakajima,

---

[8]1,2-di-O-octadecenyl-3-trimethylammonium propane, DOTMA

2001). Biolistic delivery consists in propelling complementary deoxyribonucleic acid (cDNA) coated gold particles at the nucleus of the cells of interest and can be used in cultured neurons (Gamper and Shapiro, 2006) and brain slices (Lo, 2001). Whilst the nonviral methods of gene transfer described above can be employed in many experimental paradigms, there are significant drawbacks: transfection is not specific for neurons and targets only a small volume of cells, and for therapeutic purposes, the techniques are not applicable to the central nervous system. These limitations can be overcome with neurotropic viral vectors, which have effectively evolved to target specific subpopulations of human cells, lead to long-term expression of viral genes and evade the attack of the immune system. Viral gene transfer into the nervous system has been successful *in vitro* and *in vivo* using vectors derived from simple retroviruses (such as Moloney murine leukaemia virus (MoMLV) (Mohajeri et al., 1999)) or from complex retroviruses (such as lentivirus (LV) (Bloemer et al., 1997)), from adenoviral vectors (such as adenovirus (Thomas et al., 2000) and adeno-associated virus (AAV) (Bartlett et al., 1998)), from herpes-simplex virus (HSV) (Wilson et al., 1999), Sindbis virus (Ehrengruber et al., 1999; D'Apuzzo et al., 2001), and from Semliki virus (Ehrengruber et al., 1999). The following section will describe the use of lentivirus and adeno-associated virus for viral gene delivery to the nervous system.

### 1.2.1   Lentiviruses

Lentiviral vectors were created to harness the powerful capacity of the human immunodeficiency virus (HIV) to infect post-mitotic cells and stably insert a stretch of genetic material into the cell genome. Lentiviruses are enveloped viruses belonging to the *Lentiviridae* subfamily of the *Retroviridae* family. They are the aetiologic agents for acquired immunodeficiency syndromes for a broad range of animal species including humans, primates, cats, horses, sheep and goats. The name lentiviruses (from the latin *lenti* = slow) originated from the prolonged incubation period needed for the infecting virus to induce the

disease. The first lentiviral gene transfer vector derived from HIV was described in 1996 (Naldini et al., 1996) as a promising tool for gene therapy. With time and design modification, this vector would also become an important laboratory tool: the ability to infect post-mitotic cells and a resistance to epigenetic silencing once integrated into the host genome, permitted the transduction of terminally differentiated cells such as neurons, achieving widespread and long-term gene expression in the brain (Bloemer et al., 1997). Further advances in lentiviral design have recently yielded non-integrating lentiviruses (Philippe et al., 2006; Apolonia et al., 2007), whose nucleic acids do not integrate into the host genome because either the integrase gene or the viral long-terminal repeats (LTRs) are mutant, thus avoiding the risk of mutagenesis and oncogenesis.

### 1.2.1.1 Structure and Viral Genome Organization

A complete lentiviral particle, or virion, consists of a lipid bilayer envelope derived from the host cell membrane and carrying glycoproteins coded for by the viral and host genomes, a protective protein core called nucleocapsid (comprising the viral protein p24) containing reverse transcriptase and a rod-shaped nucleoid made up of two copies of positive (i.e. coding) single-stranded RNA molecules. The whole virion is spherical and measures 80–100 nm in diameter.

The viral cDNA integrated into the host genome is called provirus and its length averages 9–10 kilobases (Federico, 2003). The genetic structure of a prototypic lentivirus is detailed in Fig.1.5. Both ends of the lentiviral proviruses are constituted by homologous regions of approximately 600–900 nucleotides, which are called long-terminal repeats (LTR). They are required for viral integration, replication and expression. LTRs can be divided in three functionally distinct regions: U3, R and U5. The U3 region contains sequences that interact with cellular factors during viral transcription, as well as elements with modulatory-, enhancing- and basal-promoting activity. The R region
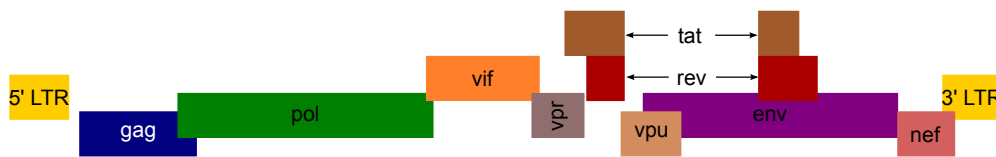
Figure 1.5: **Structure and genome of HIV-1** (redrawn from (Federico, 2003)). Genes and function of the expressed protein: *gag*: Gag polyprotein, physical infrastructure, *pol*: viral enzymes, viral replication machinery, *env*: viral glycoprotein gp120 and gp4, *tat, rev*: regulatory proteins Tat and Rev, *nef*: negative factor, promotes viral release and infectivity, *vif*: blocks a cellular inhibitor of viral replication, *vpr*: participates in migration of the pre-integration complex to the nucleus, arrests cells in G2, *vpu*: facilitates viral release, LTR (long-terminal repeats). Genes drawn at different levels when overlapping to facilitate view.

includes the transcription initiation site [9] and sequences that form stable loops in the growing RNA molecules. These RNA loops bind Tat (transactivator of transcription), a 15-kDa viral protein, whose effect results in a dramatic increase in the rate of viral genome transcription (Federico, 2003). The lentiviral genome codes for three structural proteins (Gag, Pol, Env) and contains open reading frames for regulatory genes necessary for the viral replication and transduction. It is the presence of these regulatory genes that differentiates lentiviruses from other retroviruses.

*gag* codes for the Gag polyprotein, which provides the physical infrastructure of the virus and is processed to matrix protein (p17); capsid protein (p24); spacer peptide 1 (p1); nucleocapsid protein (p7); spacer peptide 2 (p2) and p6 (Freed, 1998). *pol* provides the viral replication machinery and codes for the viral enzymes reverse transcriptase (synthesis of viral cDNA from genomic RNA), integrase (integration of viral cDNA into host genome), and HIV protease (cleavage of Gag-Pol precursor proteins) (Li et al., 1997). *env* codes for a precursor of the viral surface glycoprotein gp120 and the transmembrane glycoprotein gp41, which are critically involved in the cell receptor recognition and the fusion of viral to cell membranes (Wyatt and Sodroski, 1998). Of the regulatory proteins, Tat dramatically increases levels of viral transcription at the

---

[9]It is interesting to note, that as the first nucleotide of the R region corresponds to the transcription initiation site, the structure of the proviral cDNA does not fully overlap with that of the genomic RNA. The genomic RNA has in fact the structure R-U5-genes-U3-R (Federico, 2003).

level of the elongation of viral transcripts by binding to cellular factors and to a tat-activation region on the growing viral RNA. Rev (regulator of virion) is a 21-kDa protein involved in the export of viral RNA containing a rev-responsive element from the nucleus to the cytoplasm in the presence of Rev, unspliced RNA for the synthesis of the viral structural proteins Gag-Pol and single-spliced RNAs for the expression of env and some regulatory genes are effectively transported into the cytoplasm. In the absence of *rev*, viral transcripts are multispliced so that only the smaller RNAs for regulatory proteins can leave the nucleus and be translated (Federico, 2003; Purcell and Martin, 1993).

### 1.2.1.2 The Life Cycle of a Lentivirus

Lentiviruses attach target cells by the interaction of their envelope glycoproteins with cell surface receptors. Through pH-independent fusion of the viral envelope with the cell membrane, the nucleocapsid is released into the cell cytoplasm, where the capsid disassembles and reverse transcriptase transcribes genomic viral RNA into double-stranded DNA. Notably, both LTRs in the proviral DNA originate from the 3' LTR present on the genomic RNA. The most important feature distinguishing lentiviruses from other retroviruses is their ability to enter the nucleus independently of cell duplication, and hence independently of the nuclear membrane disassembling. Inside the nucleus, the provirus arranges in a circular form and is integrated into the host genome by viral integrase. Recent studies show that lentiviral cDNA insertion does not occur at random, as previously thought, but that lentiviruses integrate preferentially into transcriptionally active sites (Mitchell et al., 2004). The expression of viral proteins is tightly regulated and begins with the synthesis of small regulatory proteins, including Rev, which is then followed by nuclear export of unspliced and single spliced RNA into the cytoplasm, where the synthesis of viral proteins is accomplished. The later steps in the viral life cycle are common among all retroviruses and comprise the assembly of a mature viral particle containing two identical copies of full-length viral RNA (Federico,

2003).

### 1.2.1.3 Recombinant Lentiviruses

Recombinant lentiviral particles carry a highly deleted viral genome, to avoid the generation of replication-competent lentiviruses. For biosafety reasons, the genes encoding the structural proteins Gag/Pol and Rev, the envelope protein and the gene of interest have been separated onto three different plasmids (four in third generation lentiviral packaging plasmids): a transfer vector deprived of all regulatory elements and carrying the sequences to be engineered as well as the sequences for replication, packaging and expression; a packaging plasmid expressing *gag/pol* and *rev* (supplied on a separate plasmid in 4th generation lentiviruses) and a vector encoding *env*, which is often derived from a heterologous virus (a process known as pseudotyping). The most frequently used *env* is derived from the vesicular stomatitis virus (VSV) due to the high stability and broad tropism of its G protein (VSVg). VSVg enables viral entry through interaction with a ubiquitous host cell receptor (Escors and Breckpot, 2010), although a wide range of viral envelope proteins have been used to achieve cell type specificity in the brain (Bouard et al., 2009; Escors and Breckpot, 2010). Pseudotyping with VSVg leads to preferential neuronal gene delivery, although injection into white matter will transduce cells of all major macroglial types (Rahim et al., 2009). Of note, the packaging and envelope plasmids do not carry the encapsidation signal sequence and therefore lentiviral particles incorporate only the RNA from the transfer vector (Federico, 2003). Lentiviruses are usually produced in a producer cell line (e.g. human embryonic kidney cells - HEK 293 or 293FT) by co-expressing the transfer vector, the packaging plasmid and the envelope plasmid. Lentiviruses have a capacity to carry transgenes of approximately 8 kb (compare with: adeno-associated virus: 4.5 kb, adenovirus: 20 kb and HSV amplicon: up to 150 kb) and induce no immune response when injected into the brain parenchyma. Their transgene expression can persist for prolonged periods, providing

efficient and long-term gene delivery (Davidson and Breakefield, 2003).

### 1.2.1.4 Safety Issues

The most frequently used lentiviral vectors are derived from HIV-1, a highly pathogenic human virus. The main biosafety concerns regarding lentiviral vector use are (a) the possibility of generation of replication-competent viruses, (b) promoter activity of the 3' LTR, which could theoretically switch on the transcription of downstream genes leading to dysregulation and oncogenesis (Federico, 2003), and (c) insertional mutagenesis. The generation of replication-competent viruses can be minimized by improved design of the packaging system, trying to avoid regions of homology with the vector system to avoid recombinations and by ensuring that only the transfer vector is incorporated into mature viral particles. Fortunately, human endogenous retroviruses, which make up 1% of the human genome and can act as recombination partners with viral sequences, are mainly derived from onco- and spumaretroviridae. Homologous sequences of lentiviruses have not yet been found in mammalian genomes (Trono, 2002). To avoid any undesired gene dysregulation by the viral promoter in the 3' LTR, lentivirus vectors of the most recent generation, also called self-inactivating vectors (SIN), have a chimeric LTR, where the HIV promoter was replaced with transcriptional control elements from heterologous viral (e.g. cytomegalovirus, CMV) or cellular promoters (Zufferey et al., 1998; Federico, 2003). Lentiviral integration carries the intrinsic risk of disrupting and thereby possibly activating or inactivating host genes. The possibility of insertional oncogenesis is presently hotly debated and whilst there is evidence that non-Hodgkin lymphomas in late stage AIDS patients can be caused by an activation of cellular oncogenes (Shiramizu et al., 1994), there are no other reports about insertional activation of oncogenes by HIV (Trono, 2002). This might be due to the fact that HIV-infected cells tend to die quickly thereby preventing tumour development. However, lentiviral vectors for gene therapy would not kill their target cells, in addition, microglial

cells proliferate and the central nervous system (CNS) also contains a limited source of neural stem cells. Hence, insertional mutagenesis remains a real possibility and should be considered when developing clinical grade lentiviruses.

## 1.2.2 Adeno-Associated Virus (AAV)

As one of the smallest viruses, AAVs were discovered 1965 as contaminants of Adenovirus (Ad) cultures. Because AAV needs a helper virus for replication (which does not need to be an adenovirus), it is called a defective virus. Despite 80% of humans being seropositive for AAV serotype 2, no human disease is known to be attributable to it (Gonçalves, 2005). AAV consists of a capsid and a stretch of linear single-stranded DNA (plus or minus stranded genomes are packaged with equal efficiency) terminating in inverted terminal repeats (ITRs). ITRs are multipalindromic sequences folded up in a hairpin structure and contain the origin of replication. No polymerase is encoded by the viral genes, and the virus relies on cellular polymerases. The AAV genes are *rep* (coding for non structural proteins) and *cap* (structural proteins): Rep proteins have overlapping functions, whilst the *cap* gene encodes 3 different virion proteins (VP1, 2 and 3) that make up the capsid with icosahedral symmetry. The molar ratio between VP1, VP2 and VP3 in AAV particles is 1:1:10. The capsid is assembled in the nucleoplasm and has pores through which the de novo synthesized single-stranded DNA reaches the inside of an empty particle. AAVs use heparan sulphate proteoglycans as receptors for attachment and integrin receptors for internalization. As these proteins are ubiquitous, this explains the broad tropism of the virus for human and non-human cells. AAV5 additionally also uses the platelet-derived growth factor receptor and N-linked sialic acids. Uptake of the virus is via receptor-mediated endocytosis and the virion escapes from endosomes via a low pH dependent process. Each endosome contains one virion only. How the virion then enters the host cell nucleus is unclear. Whether the viral capsid enters the cell nucleus intact or modified depends on the

48

presence or absence of a helper virus (Gonçalves, 2005).

### 1.2.2.1 The Life Cycle of an AAV

Once AAV is inside the nucleus, it can follow one of two routes: If a cell latently infected with AAV is infected with a helper virus, the AAV genome is excised, and the DNA replicated and packaged into virions, which are then released by cell lysis (lytic route). If no helper virus has co-infected the cell, then AAV genes are auto repressed, and AAV DNA is integrated into the region called AAVS1 on the long arm of the human chromosome 19 (19q13.3-qter) and the lysogenic route is taken (Kotin et al., 1991). This targeted site-specific integration of the AAV provirus is a unique phenomenon among all eukaryotic viruses, and it allows the provirus DNA to be passed on through cell division (Gonçalves, 2005). The ITR, a Rep-binding element harbouring sequence and either one of the two largest Rep proteins are necessary for DNA integration. If a helper virus, such as Ad or HSV, has infected the cell, the lytic route is followed. This rescue programme is also activated if the cell is subject to metabolic inhibitors and DNA damaging agents e.g. UV (Yalkinoglu et al., 1988), and if no helper virus and no genotoxic agents are present (but the process is less efficient). Recombinant AAVs (rAAVs) are based on the fact that the ITRs are separate from virally encoding genes and that ITRs contain all cis-acting sequences necessary for genome replication, viral integration and packaging. It is therefore possible to follow a "gutless" approach by analogy to retroviruses by removing all virus encoding sequences and providing them in *trans* (Gonçalves, 2005). Viral production is based on AAV serotype 2 (AAV2) as the "prototype" and consists in transfection of virus-producing cell lines with rAAV DNA containing ITRs and a gene of interest, together with a *rep* and *cap* plasmid. Originally, wild-type Ad was used as helper virus, but it was later discovered that co-transfection of certain Ad RNAs is sufficient (the scale of vector production remains limited by the problem of co-transfection). Purification of the virus is possible via chromatography. The tropism of AAV depends on the

receptor content of the host cell, but low transduction rates can also result from problems with virion trafficking or single to double strand DNA conversion. AAV tropism can be broadened by rationally adding specific ligands to the capsid or by using capsid genes of other AAVs with different tropism, e.g. using *rep* of AAV2 and *cap* of a different AAV (Gonçalves, 2005). This approach solves the problems presented by neutralizing antibodies to capsid components in seropositive individuals or in patients in need of vector re-administration. It is important to remember that recombinant AAVs (rAAVs) are devoid of viral genes; this has two important implications: 1) The absence of Rep proteins prevents DNA integration at the AAVS1 locus. 2) As no viral genes are present, single-to double strand conversion and integration of the viral DNA depend on state of the cell and its physiological activities. Single to double strand form conversion of DNA is a prerequisite of gene expression and can be accomplished either by host cell polymerases or by passive annealing of plus and minus strands. Integration of rAAV is a passive process that depends on naturally occurring chromosomal breaks and host-cell enzymes. Therefore, rAAVs do not generate chromosomal breaks, nor do they have viral promoters active on host cell genes; this makes them less oncogenic than lentiviruses. However, it is still possible that rAAV sequences could cause a change in cell genes, since they are preferentially inserted in transcriptionally active sites. The main limitations of AAVs include the generation of neutralizing antibodies to viral proteins and the small packaging capacity of 4.5 kb. The latter can be overcome by a variety of techniques: through intermolecular recombination of rAAVs whose ITRs had been spliced out (the efficiency of this strategy is lower than with just one vector) or by hybrid technologies, for example including long double-stranded rAAV genomes in capsids of larger viruses e.g. Ad, HSV, baculovirus. Finally, rAAVs have the advantage that, rather than just adding genes, rAAVs can also be used to disrupt or correct mutant genes by homologous recombination; as an example AAVs were (successfully) used to disrupt mutant collagen genes in mesenchymal stem cells of individuals with

osteogenesis imperfecta (Chamberlain et al., 2004).

### 1.2.2.2 Safety Issues

One of the great advantages of AAV vectors is that the risks of insertional mutagenesis are minimal for the reasons described above. However, several risks remain to be addressed for adeno-viral approaches: Overexpression of the transgene may cause cell toxicity and implies that we will need to develop molecular switches or use inducible promoter systems. Transgene expression can occur in non-target tissue, although at least vertical AAV transfer has so far been ruled out in animal models (Favaro et al., 2009). Horizontal virus shedding in body fluids can occur for AAVs in the first 10 days after vector administration but disappears thereafter (Manno et al., 2006). The main concern surrounding the use of AAV in humans is its immunotoxicity, as T cells against capsid antigens and neutralizing antibodies have been documented in clinical trials (Mingozzi and High, 2011).

### 1.2.3 Targeting Viral Delivery

For many applications, it is mandatory to target the delivery of a transgene to a specific subset of cells. This can be achieved at the level of vector entry into the cell (transductional targeting), or at the level of transgene expression (transcriptional targeting). Transductional targeting is achieved by using envelope glycoproteins of different types of neurotropic viruses such as Rabies-, Mokola-, Ross-River-, HSV- and VSVg-viruses (Kang et al., 2002; Mazarakis et al., 2001; Watson et al., 2002). The most commonly used surface glycoprotein for targeting lentiviruses is the G-Protein derived from the *Rhabdovirus* Vesicular Stomatitis Virus (VSVg), as it is highly stable and confers broad tropism by binding to a cell surface lipid (Burns et al., 1993; Schlegel et al., 1983). Neuronal tropism of lentiviral vectors is mainly due to the VSVg envelope (de Almeida et al., 2001). Redirecting transgene transcription for targeted expression is a relatively easier task but it has been challenging to

control the level and specificity of lentivirus expression. Frequently used promoters for this task are strong promoters of viral, cellular or hybrid origin, including the cytomegalovirus (CMV) promoter and the CMV enhancer sequence (Klein et al., 2006, 2002). Even strong promoters, however, may be inactivated by methylation over time. In contrast, lack of expression does not necessarily mean the neuron is uninfected, as the expression levels might simply be below detection threshold (Davidson and Breakefield, 2003; Federico, 2003). Physiological long-term transcription in the nervous system can be achieved by using strong neuronal promoters including synapsin-1 (Glover et al., 2002), elongation factor 1a (EF-1a) (Zhang et al., 2007b), calcium calmodulin-binding kinase 2a (Camk2a) (Aravanis et al., 2007) specific for excitatory neurons, neuron-specific enolase (Klein et al., 1998), prepro-hypocretin (Hcrt) specific for hypocretin neurons (Adamantidis et al., 2007), glial fibrillary acidic protein (GFAP) specific for astrocytes (Gourine et al., 2010), tyrosine hydroxylase for targeting catecholaminergic neurons (Min et al., 1994) and neurofilament (Zhang et al., 2000), or by adding enhancing cassettes or intronic sequences to the transgene of interest (Benzekhroufa et al., 2009; Davidson and Breakefield, 2003).

The cell specificity and different transduction efficiencies of rAAVs depend on serotype: rAAV2 has broad tropism as its receptor is a common molecule, a complex of 3 components including heparan sulphate proteoglycans, integrin and the fibroblast growth factor receptor (Flotte and Berns, 2005). AAV5 is known to achieve more widespread expression, whilst AAV6 and 8 can achieve "body-wide" transduction efficiencies in striated muscle or hepatocytes (Gonçalves, 2005). AAV9 is a promising serotype as it can be administered systemically (Moscioni et al., 2006) and is known to cross the blood - brain barrier (Foust et al., 2009; Duque et al., 2009; Fu et al., 2011).

### 1.2.4 Viral Vectors for Gene Delivery to the Nervous System

Therapeutic gene delivery to the nervous system poses several challenges because the brain is relatively inaccessible, protected by the blood-brain barrier and made up of post-mitotic non-dividing cells. In addition, neurological disease often affects large areas, if not the entire nervous system, implicating a large volume and a large number of cells to be targeted for therapeutic purposes. Viral vectors can solve some of these problems, because of their ability to transduce terminally differentiated cells and (for AAV9) to penetrate the blood-brain barrier. Strategies to achieve targeted viral expression include stereotactic injections into specific brain regions, muscle injections of viruses capable of retrograde transport and the use of viruses that can be transported trans-synaptically. More global spread of the virus can be achieved with multiple injections, and intraventricular and intravascular injections (Flotte and Berns, 2005).

Lentiviruses can transduce neurons at high efficiency, leading to long-term transgene expression, making them suitable vectors for experiments targeting genes to neurons, which have proven notoriously resistant to means of non-viral transduction. The host immune response to lentiviruses is minimal, due to the lack of sequences coding for viral proteins. Therefore readministration of the lentiviral vector is possible (Trono, 2002). In addition, their cloning capacity of 8 - 9 kb accomodates relatively large transgenes and, depending on the pseudotyped envelope, their tropism in the brain is very broad (Davidson and Breakefield, 2003; Federico, 2003). To date, lentiviruses have been successfully and stably expressed in the nervous systems of several different animal species including mice, rats, guinea pigs and non-human primates *in vivo* and *in vitro* (Naldini et al., 1996; Trono, 2002). Among goals of such work are: to mimic disease, to explore basic neurophysiological mechanisms, and to test therapeutic targets. The use of lentiviruses ranges from the expression of normal and mutant proteins to the delivery of antisense or

Table 1.4: **Summary of characteristics of viral vectors used to target the nervous system** (adapted from (Davidson and Breakefield, 2003)). Infectious units/ml (IU/ml) is the number (unit) of viral particles available to transduce target cells in 1 ml of suspension.

| Vector | Size [nm] | Titres [IU/mL] | Transgene Capacity [kb] |
|---|---|---|---|
| **Lentivirus** | 100 | $10^6 - 10^{10}$ | $8 - 10$ |
| *Advantages* | modest packaging capacity, no immune response, long term expression | | |
| *Problems* | integration into host genome, short distance transport | | |
| **Adenovirus** | $80 - 120$ | $10^{10} - 10^{12}$ | 20 |
| *Advantages* | retrograde transport, long term expression, transgene capacity. | | |
| *Problems* | adjuvant properties, immune response (capsid!), also transduces microglia, and ependymal cells. | | |
| **AAV** | $20 - 30$ | $10^9 - 10^{13}$ | 4.5 |
| *Advantages* | Non-toxic, neurons preferentially. | | |
| *Problems* | can integrate into genome, does not transduce neurons equally well, transgenes small. | | |
| **HSV** | $120 - 300$ | $10^{11}$ | 30 - 50 |
| *Advantages* | large transgenes, antero- and retrograde, episomal state, minimal toxicity. | | |
| *Problems* | Low-level expression of viral genes, not only neurotropic. | | |

small inhibitory RNA to suppress target protein expression (Davidson and Breakefield, 2003). Major obstacles to lentiviral use include poor transduction efficiency, and only transient and low transgene expression. Inducible systems such as tetracycline-regulated promoters can be used to switch transgene expression on and off at will, but in the off state there may still be low levels of transgene expression, making these approaches "leaky".

As mentioned in the previous section, other vector types, including adeno-associated viruses, retroviruses, adenoviruses and HSV, can be used to target genes to the nervous system. Their strengths and drawbacks are

summarized in Table 1.4. Adeno-associated viruses were the first viral vectors to be used in clinical trials for CNS disorders due to their neuronal tropism, stable transgene expression in quiescent cells, low toxicity and poor rate of integration in the host genome. The lack of pathogenicity in humans from the wild-type virus further distinguishes them from lentivirus and adenovirus (Towne et al., 2010). One of the biggest challenges facing AAV gene delivery is the host immune response. The host defense mechanism at the adaptive level is made up of cell-mediated and humoral immunity. The cell-mediated response functions at the cellular level, eliminating the transduced cells using cytotoxic T cells, whereas the humoural response produces neutralizing antibodies against capsid antigens, preventing the readministration of vector. Most clinical data relates to rAAV serotype 2, although other serotypes are starting to emerge due to their better distribution and higher number of transduced neurons (five-to eightfold in rAAV 1 and 5 compared to serotype 2). AAV serotypes 2 and 5 transduce mostly neuronal cell types, whilst serotype 4 transduces mostly ependymal cells (Flotte and Berns, 2005). Wide spread of virus also means that one injection may be sufficient for therapeutic purposes. If the gene is overexpressed this can lead to toxicity. So far transcriptional regulation of rAAV has not been convincingly demonstrated, nor have there been clinical trials involving regulated transgene expression. In addition to the low background expression present in most gene regulation systems (Haberman and McCown, 2002), the main problem of regulation systems for AAVs is that their sequences are long and that rAAVs have a finite packaging capacity. Splitting the regulating transgenes into 2 vectors, is possible but may affect the viral terminal repeats, which could in turn affect internal promoter function (Haberman and McCown, 2002). These problems need to be addressed before rAAVs can be used for therapeutic purposes.

In summary, to date, most strategies to cure human disease using viral vectors have concentrated on lentiviruses and AAVs, lentiviruses being mainly used for

ex-vivo transduction of haematopoietic and stem cells and AAVs for *in vivo* approaches. The major safety issue with LVs is represented by insertional mutagenesis, whilst the host immune response is the main hurdle for AAV approaches.

### 1.2.5 Clinical Trials of Gene Delivery to the Human Central Nervous System

Only a small number of clinical trials using viral vectors in humans have been done, and with little success[10] (Mingozzi and High, 2011). Targeting the central nervous system as a whole remains a challenge and is currently under investigation only in animal models. Some success of focal viral delivery has been documented in patients with Parkinson's disease (PD) (Palfi, 2010): "ProSavin", a lentivirus delivering three genes involved in dopamine synthesis, was injected into the striatum of PD patients. However numbers were very small (9 patients, only 6 months duration of the study, progress self-reported by 2–3 patients only). An improved version (Stewart et al., 2011) of the lentivirus is currently part of a dose-finding Phase II study in humans.

AAVs have been used to administer neurotrophic factors (Marks et al., 2008, 2010; Mandel, 2010) and enzymes responsible for metabolism of neurotransmitters (Christine et al., 2009; Eberling et al., 2008; Kaplitt et al., 2007; LeWitt et al., 2011). A safety study and a phase I trial were performed for the intraparenchymal administration of AAV2 encoding aspartoacylase cDNA to the brain of patients affected by Canavan's disease (Janson et al., 2002; McPhee et al., 2006; Leone et al., 2012), a severe and fatal neurodegenerative disease. A decrease in the metabolite *N*-acetyl-aspartate in the brain, an improvement in seizure frequency and stabilization of overall clinical status have recently been reported (Leone et al., 2012). Some improvement was detected in children with Batten's disease (caused by a mutation in ceroid lipofuscinosis, neuronal 2 gene

---

[10]http://www.wiley.com/legacy/wileychi/genmed/clinical/ maintains a list of ongoing clinical trials using AAVs or LVs.

(CLN2), which normally codes for a lysosomal protein. If mutated it causes toxic accumulation of metabolites in lysosomes and cell death.) injected with AAV (containing CLN2 cDNA) through six burr holes and two injections per hole (Worgall et al., 2008) (these results formed the basis of a Phase I/II trial). One child developed severe seizures 14 days after intracortical injections, which resulted in death. Challenges for successful gene delivery to the brain include the need to achieve whole brain transduction, to treat before severe neuronal loss ensues, as well as the difficulty in determining clinical endpoints for diseases where the patient population is small and there are often no biomarkers of disease.

In all viral vector approaches, extensive work still needs to be done to assess the biosafety of viral vectors including insertional mutagenesis and oncogenesis, seroconversion, biodistribution, germline transmission, recombination with endogenous viral sequences and the production of large scale clinical grade viral batches of high yields and better purity.

## 1.3   Interneurons

In the central nervous system (CNS), interneurons are neurons whose axons and dendrites lie within the same brain area as their soma (Freund and Kali, 2008). In contrast, pyramidal neurons can have long axons projecting to brain regions distant from their soma or the contralateral hemisphere. Interneurons have traditionally been classified into two main groups: spiny and aspiny (or sparsely spiny) non-pyramidal cells (Jones and Peters, 1984; DeFelipe et al., 2013). Aspiny inhibitory non-pyramidal cells comprise the majority of CNS interneurons, are found in all cortical layers and release γ-aminobutyric acid (GABA) or glycine (in the spinal cord) as predominant neurotransmitter (Freund and Kali, 2008; DeFelipe et al., 2013). In contrast, spiny non-pyramidal neurons are found in middle cortical layers and are glutamatergic (Feldmeyer et al., 1999). In the cortex, hippocampus and basal ganglia, GABAergic

interneurons also contain neuropeptides such as cholecystokinin (CCK), parvalbumin (PV), somatostatin (SOM), vasoactive intestinal polypeptide (VIP), and neuropeptide Y (NPY) among many others, which they may release under certain conditions. Several recent attempts have been made to classify GABAergic interneurons: they have excluded spiny non-pyramidal cells and focused on aspiny GABAergic interneurons as major component of cortical circuits Ascoli et al. 2008; DeFelipe et al. 2013. I will follow this approach and hereforth discuss only GABAergic interneurons.

Interneurons have a predominantly inhibitory action on their post-synaptic target, since GABA mediates hyperpolarization of the membrane by opening chloride (via the $GABA_A$-receptor) or potassium channels (via the G-protein coupled $GABA_B$-receptor). However, GABA is also known to mediate post-synaptic depolarization through action on $GABA_A$-receptors of immature neurons (Ben-Ari et al., 1989) and by perisomatic inhibition of mature pyramidal cells in both the hippocampus (Sauer et al., 2012) and neocortex (Gulledge and Stuart, 2003; Szabadics et al., 2006). Interneurons synapse onto local neurons and provide two fundamental types of inhibition: Feed-forward, if the input to the interneuron comes from a population/cell different to the one it inhibits, and feed-back, if the interneuron receives input from the same local cell it synapses on (Freund and Kali, 2008). The major function of interneurons is to regulate the gain of pyramidal cell input, control activity levels of local cell assemblies, coordinate and synchronize them (Freund and Kali, 2008). As mentioned above, interneurons are a heterogenous group of neurons that differ on the basis of their morphological, electrophysiological and molecular criteria. This diversity can be used to classify interneurons into distinct groups (Somogyi and Klausberger, 2005; Ascoli et al., 2008; Freund and Kali, 2008; DeFelipe et al., 2013).

## 1.3.1 Diversity and Classification of Interneurons

The classification of neurons is still a hotly debated area and multiple attempts have been made at obtaining reliable, objective, reproducible criteria for classifying interneurons and a standardized terminology (Ascoli et al., 2008; DeFelipe et al., 2013). Most recently, software tools analysing databases of neuronal features have been developed and implemented for an automated classification of interneurons (Druckmann et al., 2012; DeFelipe et al., 2013). The major anatomical, molecular and electrophysiological classification criteria for interneurons can be summarized as follows:

### 1.3.1.1 Anatomical/Morphological

Aside from the anatomy of their soma and dendrites, interneurons can be subdivided according to their target specificity: innervating pyramidal cells, other interneurons or non-neural structures (e.g. blood vessels). Further, interneurons targeting pyramidal cells can be subdivided according to target location into axo-axonal or chandelier cells (target: axon initial segment), basket cells (target: perisomatic region), and interneurons targeting pyramidal cell dendrites. According to their axonal orientation relative to their layer of origin, basket cells can be classified as interneurons with tangential, radial, mixed or undetermined axons. Interneurons targeting dendrites can be distinguished according to which dendritic compartment they target (the shaft or the spines) and then further according to their axonal morphology. Shaft-targeting interneurons comprise willow and Martinotti cells. Spine targeting interneurons include horse-tail and neurogliaform cells (Ascoli et al., 2008).

### 1.3.1.2 Molecular

The Petilla classification (Ascoli et al., 2008) subdivides interneurons into five main groups, according to the expression of different neuropeptides: parvalbumin (including chandelier and basket cells), somatostatin (including

Martinotti cells), and cells expressing cholecystokinin, those expressing vasoactive intestinal polypeptide and those expressing neuropeptide Y. The five subtypes can be further characterized by their expression of other molecular markers such as transcription factors, synthesizing enzymes, connexins, voltage-gated ion-channels etc. The different types of voltage-gated ion-channels expressed on the interneuronal membrane endow the cell with different spiking properties and threshold responses to the frequency of stimulation, and contribute to the differential involvement of distinct interneuron subclasses in network oscillations of specific frequencies. As an example, PV-positive basket cells express $K^+$ channels of the Kv3 family, which contribute to the "fast-spiking" behaviour of this cell type, which among other characteristics supports the hypothesis of their crucial involvement in generating gamma oscillations (Freund and Kali, 2008; Buzsáki and Wang, 2012a).

CCK-positive and PV-positive basket cells will be discussed in further detail in the sections on CCK and neuronal oscillations, respectively.

### 1.3.1.3 Electrophysiological

Six main types of interneurons can be defined by physiological criteria (Ascoli et al., 2008; DeFelipe et al., 2013): Fast-spiking (non-adaptive spiking at steady state, short spikes, large afterhyperpolarizations), non-adaptive non-fast-spiking cells (no increase in inter-spike interval at steady state), adapting neurons (increase in inter-spike interval at steady state), accelerating neurons (decrease in inter-spike interval at steady state) and irregular spiking neurons (irregular inter-spike interval at steady state). Each neuron type contains further subclasses.

### 1.3.1.4 Functional

Interneurons can be functionally grouped according to the target they innervate and according to their firing patterns relative to different network oscillations

(Somogyi and Klausberger, 2005; Freund and Kali, 2008).

Since the dendrites are the site of major glutamatergic input and long- and short-term plastic changes, interneurons innervating the dendritic compartment modulate the efficacy and plasticity of the input to the pyramidal cell (Freund and Kali, 2008). Conversely, the soma is the site of summation of all post-synaptic conductances. Therefore, interneurons synapsing onto the soma or axon initial segment are ideally located to modulate pyramidal cell output. Furthermore, interneurons have been found to be involved in neurovascular coupling and to differentially modulate vascular tone, depending on their molecular profile: interneurons expressing VIP or nitric oxide synthase inducing vasodilatation in slices, whilst NPY and SOM expressing interneurons modulated vasoconstriction (Cauli et al., 2004; Kocharyan et al., 2008).

In addition to this target-related functional grouping, *in vivo* recordings in different hippocampal subfields have shown that anatomically/molecularly distinct classes of interneurons have similar firing patterns during a given brain state (such as different phases of sleep or behaviours) characterized by a specific network oscillation (Somogyi and Klausberger, 2005). As an example, during theta oscillations recorded extracellularly in the pyramidal cell layer, axo-axonic cells have the highest probability of firing during the peak of theta. Conversely, perisomatic basket cell are more likely to fire during the descending phase of theta. Other characteristic firing pattern have been established for distinct interneuron classes relative to gamma oscillations and sharp-wave ripples. These results imply that anatomically and molecularly defined classes of interneurons have also functionally similar roles (Somogyi and Klausberger, 2005; Freund and Kali, 2008).

### 1.3.2   The Interneuron Promoters GAD67 and CCK

A promoter consists of DNA elements flanking the transcription initiation site of a gene, which are involved in recruiting the transcription machinery (made up of transcription factors and RNA polymerase II) for the successful

transcription of a protein-coding gene. Promoter sequences also contain regulatory sites (enhancers, silencers, insulators) to which transcription factors bind (Smale and Kadonaga, 2003). These regulatory sites are scattered over hundreds of basepairs in mammalian genomes and it is the complex organisation of regulatory DNA that allows the detailed control of gene expression (Levine and Tjian, 2003). The process of designing tissue-specific promoters is made difficult by the fact that it is not possible to determine promoter enhancing and silencing sequences *a priori* and that even the 5′ untranslated region (5′ UTR) of a given gene might have unexpected effects on gene expression (Chhatwal et al., 2007). The screening of putative promoter sequences has traditionally been accomplished by two methods: expression of promoter-reporter cassettes *in vitro*, knowing that selectivity *in vitro* might equate to selectivity *in vivo*, or expression of constructs in transgenic animals or by lentiviral delivery *in vivo* (Chhatwal et al., 2007). Two cell-type specific promoters have been identified: the promoter regulating the transcription of glutamic-acid decarboxylase (GAD, EC 4.1.1.15), and of cholecystokinin. Glutamic acid decarboxylase catalyzes the rate limiting step in the synthesis of γ-aminobutyric acid (GABA): it decarboxylates L-glutamate to form GABA (Erlander and Tobin, 1991). GABA is the principal inhibitory neurotransmitter in the central nervous system of vertebrates and is released by 20-30% of CNS neurons (Szabó et al., 1996). Since its discovery in 1951, two GAD isoforms have been characterized as products of two different genes: they differ in molecular weight (GAD67, 67 kDa and GAD65, 65 kDa) and share a nearly identical distribution in the brain but differ in their subcellular localizations and their affinity for the co-factor pyridoxal phosphate (Erlander et al., 1991). The gene coding for GAD67 is mapped to chromosome 2 in mice and man (Brilliant et al., 1990). In mice, it spans more than 70 kb with at least 20 kb of 5′ regulatory sequences (Szabó et al., 1996). At the start of neuronal differentiation during development, GAD67 mRNA is detectable as early as embryonal day 10.5 (E10.5) in mice (the equivalent of E11.5 in rats), whilst the GAD67 protein
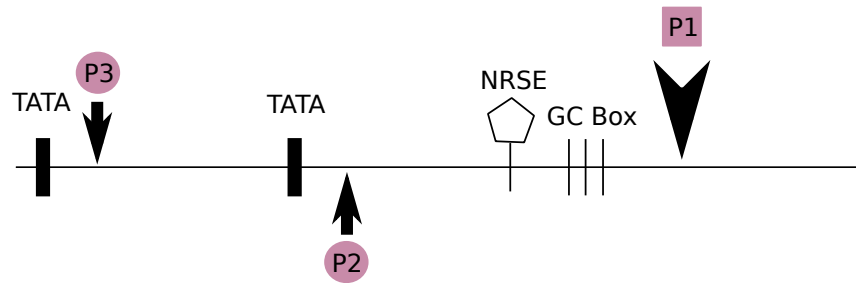
Figure 1.6: **Structure of the 5' flanking region of the murine GAD67 gene.** The arrows mark the transcripional start sites under control from the proximal house-keeping promoter (P1) and two more distal promoters (P2 and P3). P1 is made up of several GC boxes, P2 and 3 are made up of TATA boxes. NRSE, Neuron-restrictive silencer element. Redrawn from (Katarova et al., 1998).

becomes detectable one day later. In addition to the adult type mRNA, two 2 kb alternatively spliced mRNAs are detectable: they code for a 25 kDa leader peptide and a 44 kDa truncated form of the enzyme, which may play a role in the development of inhibitory synapses (Szabó et al., 1994). The promoter region P1 comprises the main group of transcription inititation sites at the 5' end of the GAD gene (Fig. 1.6), has binding sites for putative transcription factors and shares features of promoters of constitutively expressed housekeeping genes (Szabó et al., 1996). In addition to the main promoter, two further transcription initiation sites (P2 and P3) have been identified 130 and 295 bp upstream of P1. These promoters have characteristics of tissue-specific promoters, such as TATA and CAAT-like boxes. The 1.3 kb of the 5'-upstream sequences also contain neuronal-specific regulatory and silencing elements, as well as the putative binding sites for several transcription factors such as AP2, Hox, E-box, egr-1 and NF-$\varkappa$B (Szabó et al., 1996). GAD67 expression in transgenic mice carrying 5'-upstream regulatory elements of the GAD67 gene and lacZ as a reporter, was shown to be crucially dependent on the increasing length of the GAD67 5'-upstream region included in the construct. The proximal promoter P1 was not sufficient to confer orthodox expression patterns, indicating that P1 is negatively regulated. Only by including the region-specific enhancers between 1.3 and 9 kb upstream of the first exon, was a nearly fully

correct expression pattern achieved (Katarova et al., 1998). Various segments of the GAD67 regulatory sequences have since been used successfully to drive transgene expression in interneurons. Examples include gene gun delivery to organotypic cortical slice cultures (Jin et al., 2001) and adenoviral delivery to slice cultures of the brainstem (Teschemacher et al., 2005).

Cholecystokinin (CCK) was originally discovered as a hormone of the digestive tract and represents one of the most abundant neuropeptides in the brain, where it is mainly present in the form of an octapeptide (Fink et al., 1998). A 3 kb promoter including the 5' UTR region of the CCK gene has recently been described and is capable of selectively targeting CCK-positive cells in the hippocampus (Chhatwal et al., 2007) and the basolateral amygdala (Jasnow et al., 2009). Whilst CCKmRNA is also present in neocortical pyramidal neurons, the actual CCK protein is mainly expressed in GABAergic interneurons (Lee and Soltesz, 2011). In the hippocampus, CCK is expressed at high levels, CCK-positive interneurons are found in all layers and subfields, and they represent approximately 10% of the hippocampal population of interneurons. Of particular importance, CCK is expressed in one of two subpopulations of hippocampal basket cells (the other one expressing parvalbumin and discussed below). CCK-positive basket cells are thought to provide the fine-tuning of pyramidal cell input, due to their slow membrane time constants and the modulatory input they receive from subcortical structures (Glickfeld and Scanziani, 2006; Scanziani and Häusser, 2009). Additionally, CCK is able to excite PV-positive basket cells and to depress GABA release from CCK[+]-interneurons via indirect action on axonal cannabinoid-type 1 (CB1) receptors (cannabinoids are released by pyramidal cells innervated, in turn, by CCK[+]-interneurons) (Miller et al., 1997; Katona et al., 1999; Karson et al., 2008; Lee and Soltesz, 2011). CCK[+]-interneurons have therefore been compared to molecular switches, gating different sources of perisomatic inhibition. CCK has also been found in another two populations of

interneurons of the hippocampus: Schaffer-collateral associated cells (targeting the apical dendrites of CA1 pyramidal cells) and perforant path-associated cells (targeting the apical tuft of pyramidal cells). These CCK$^+$-interneurons were found to fire at specific frequencies and phases of ripple and theta oscillations, suggesting that whilst PV$^+$-interneurons may synchronize pyramidal cells during oscillations, CCK$^+$-interneurons may be involved in differentiating groups of pyramidal cells forming assemblies (Klausberger et al., 2005). Finally, CCK has also been found to facilitate glutamate from most excitatory hippocampal pathways (Deng et al., 2010; Lee and Soltesz, 2011). These results indicate that despite its high expression levels throughout the nervous system, CCK exerts selective actions on different neuronal subpopulations, and it is therefore not surprising that CCK has been found to modulate mood and behaviour in health and disease states. CCK has been linked with anxiety states through its actions in the basolateral amygdala (Jasnow et al., 2009), and sleep states through activation of hypothalamic orexin neurons and modulation of thalamic rhythms (Cox et al., 1997; Tsujino et al., 2005). Both CCK and endocannabinoid systems have been linked to the regulation of satiety, nociception, , as well as interacting with dopaminergic, serotonergic and opioid systems (Fink et al., 1998; Noble and Roques, 2006; Lee and Soltesz, 2011). In schizophrenia, whole brain CCK levels were found to be low in post-mortem brains (Kerwin et al., 1992), whilst CCK receptor polymorphisms were demonstrated in schizophrenia and panic attack disorder (Kennedy et al., 1999; Sanjuan et al., 2004). Finally, CCK$^+$-interneurons were reduced in the hippocampus of kindled animals (Sayin et al., 2003) and CB1-receptors were upregulated in developmental seizure models, whilst blocking CB-1 receptors reduced hyperexcitability (Chen et al., 2003, 2007).

### 1.3.3 Choice of Interneuron Promoters

As briefly discussed in the introductory section, my original aim was to target opsins to interneurons by viral delivery. This approach would offer the

possibility to target opsins to interneurons in non-transgenic animals and, potentially, in humans. Ideally, ChR2 targeted to interneurons could then have been used to drive oscillations and to potentially inhibit epileptiform activity in behaving animals by activating interneurons. The choice of interneuron-specific promoters for the viral approach is limited by the fact that only the GAD67 and CCK promoters had been cloned and shown to be specific for interneurons or subpopulations thereof (Chhatwal et al., 2007; Jasnow et al., 2009; Katarova et al., 1998; Jin et al., 2001; Teschemacher et al., 2005). Additionally, the promoter had to be small enough to be cloned into a lentiviral vector (i.e. under 10 kb in size). Despite the biological limitations, had the GAD67 and CCK promoters been specific, they would have helped clarify the role of interneurons as a whole and of CCK[+]-interneurons in particular in the generation and entrainment of hippocampal gamma oscillations. As CCK[+]-interneurons have been shown to be reduced in kindling models of epilepsy, the contribution of cortical CCK[+]-interneurons could have been studied in the tetanus toxin model of epilepsy used in my experiments. Further molecular characterization of tissue-specific promoters or transcription factors may allow a better target in future studies. For the study of hippocampal gamma oscillations (further discussed below), an ideal approach would have targeted the opsin-containing virus to PV-basket cells. A possible alternative solution would consist of crossing a PV-Cre with a floxed-ChR2 transgenic mouse line, resulting in ChR2 expressing PV-basket cells. This approach has been used successfully in previous studies (Cardin et al., 2010; Carlén et al., 2011) and could be complemented by using red-shifted opsins targeted to principal cells using a Camk2a or EF1a promoter to drive principal cells and PV cells independently. Further alternative approaches would be to express opsins in SOM-Cre, GAD67-Cre dependent mice by injecting AAV or LV carrying floxed ChR2 or NpHR, to study the contribution of these neurons to gamma oscillations.

## 1.4    Neuronal Oscillations and Synchronization

### 1.4.1    Brief Overview

An oscillation is the periodic variation of a physical measure above and below a central value. It is characterized by three variables: frequency, amplitude and phase. Neuronal oscillations are rhythmic voltage fluctuations in time that arise at the level of the individual neuron and at the level of a neuronal population, in which case the term "neuronal oscillation" describes the collective behaviour of ensembles of neurons. Individual neurons display rhythmic changes in their post-synaptic potentials and subthreshold membrane depolarizations that can oscillate at given frequencies (Hutcheon and Yarom, 2000; Llinás, 1988). Although synaptic transmembrane currents are the majour source of the local field potential (LFP, i.e the electric potential measured by an extracellularly placed electrode), $Na^+$ and $Ca^{2+}$ spikes, ion fluxes through ligand and voltage-gated ion-channels and membrane voltage oscillations significantly contribute to shaping the LFP (Buzsáki et al., 2012). Conversely, the same oscillation measured on the LFP may be generated by different cellular mechanisms. Whilst the extracellular signal gives us information about the behaviour of a population of neurons, when we record a macroscopic oscillation on LFP, we can not infer any underlying microscopic mechanism (the 'inverse problem') (Buzsáki et al., 2012). The intrinsic property to generate rhythmic changes of the membrane potential depends on the expression and the function of voltage-gated ion channels and is described by differential equations in the Hodgkin-Huxley model (Hodgkin and Huxley, 1952, 1990). In addition, neurons are interconnected with each other, creating a local network in which neurons can synchronize and oscillate. The oscillation frequency of a network depends on the size of the network (i.e. the number of neurons involved) and the speed of neuronal signalling (limited by axon conductance and synaptic delays) (Buzsáki and Draguhn, 2004). Most connections among neurons are local, with few long range connections, a network design similar to

"small-world" networks (Watts and Strogatz, 1998). Therefore, the oscillation frequency of a network is mainly correlated with its size: small local networks of neurons are recruited in high frequency oscillations, large networks in slow frequency oscillations (Buzsáki et al., 2004). Oscillation frequencies in mammals span four orders of magnitude (0.5 - 200 Hz) and are preserved throughout evolution (Buzsáki and Draguhn, 2004). Table 1.5 gives a brief overview of the oscillation nomenclature (excluding sleep and pathological rhythms). Mammalian brains however, differ in size across species, bringing up the intriguing question of how to synchronize neurons in big brains. At the local level, higher mammals have inhibitory interneuron networks (Buzsáki et al., 2004) and electrical coupling by gap junctions (Gouwens et al., 2010). In addition there are a limited number of long range connections: they reduce synaptic path lengths between distant networks. The advantages of this architectural design are that bigger brains can maintain the same functions and synchronize distant regions using oscillators, which require less energy than wiring (Buzsáki and Draguhn, 2004).

The function of oscillations is thought to depend on the underlying neuronal substrate in which they arise. However, there are several main functions of oscillations that can be generalized at the level of the neuronal network. Briefly, they are: input selection (i.e. an oscillating network is less responsive to an external input e.g thalamocortical sleep spindles during sleep (Riedner et al., 2011), or to a sensory input that is not timed correctly (Hutcheon and Yarom, 2000)), linking of distant cell populations oscillating at similar frequency (for subsequent concerted activation of downstream pathways) (Buzsáki and Draguhn, 2004), consolidation of synaptic modification by replay during slow-wave sleep (Buzsáki, 1998) and representation of information by phase (i.e. action potential spike precession in relation to the phase of the hippocampal theta oscillation for representation of spatial short-term memory (O'Keefe and Recce, 1993)).

Table 1.5: **Neuronal Oscillation Nomenclature** (adapted from (Steriade, 2005; Uhlhaas et al., 2008)).

| Name | Frequency [Hz] | Cell Assemblies Involved | Putative Function |
|---|---|---|---|
| **Delta** | $1-4$ | thalamocortical and corticothalamic neurons | physiologically found in deep sleep |
| **Theta** | $4-8$ | septohippocampal cholinergic system (clock), dentate granule cells and CA1 pyramids | Spatial navigation, working memory, cognitive control, sensory gating, synaptic plasticity, top-down control, long-range synchronization |
| **Alpha** | $8-12$ | largely unknown, likely generated within the cortex itself, surface-parallel intracortical connections are important for spread | Inhibition, attention, consciousness, top-down control, long-range synchronization |
| **Beta** | $12-30$ | cells from some thalamocortical nuclei (e.g. centrolateral (CL) intralaminar thalamic nucleus), cortex and amygdala | Sensory gating, attention, perception, motor control, long-range synchronization |
| **Gamma** | $30 - 200$ | hippocampus (pyramidal cells synchronized by fast-spiking $PV^+$ interneurons) | Attention, perception, motor control, memory, consciousness, synaptic plasticity |

Correlation of local network oscillations between regions can be described in relation to amplitude, frequency or phase. "Synchronization" in animal experiments refers to correlation between spikes in two regions or between spikes and local field potentials (LFPs) (Tiesinga et al., 2008; Fell and Axmacher, 2011). The latter is also termed spike-field coherence. Furthermore, studies have analyzed the phase correlation between LFPs in different regions. How synchronization is accomplished, however, is poorly understood but is important: frequency-specific networks emerge during perceptual tasks and the degree of frequency synchronization correlates with task performance in humans (Hipp et al., 2011). Phase synchronization underlies long-term and working memory (Fell and Axmacher, 2011), and synchronization is thought to be disrupted between hemispheres of autistic children (Dinstein et al., 2011) and in schizophrenia (Uhlhaas and Singer, 2010).

### 1.4.2   An Introduction to Gamma Oscillations

Neuronal oscillations in the gamma range (35-45 Hz) were first described by Jasper and Andrews in 1938, who probably recognized that they had different behavioural correlates than slower EEG rhythms (Jasper and Andrews, 1938; Buzsáki and Wang, 2012a,b). The term was rediscovered and became popular in the 1980ies and was officially reintroduced by Freeman, who used it to describe the oscillation band between 30-90 Hz. Eventually, the nomenclature of brain rhythms should be based on the underlying physiological mechanism, but since our knowledge is incomplete, the names of brain rhythms respect historical traditions. The nomenclature of rhythms above 90 Hz is discussed in the epilepsy chapters. Gamma rhythms have been described in animals *in vivo* since the very early days of neurophysiology (Adrian, 1942; Eckhorn et al., 1988; Gray and Singer, 1989) and revolutionized the field of neuronal oscillations when found *in vitro* (Fisahn et al., 1998). Coherent, sensory stimulus-induced gamma oscillations were first described in the olfactory system of the hedgehog (Adrian, 1942), and subsequently in other mammalian sensory systems,

including the visual cortex of cats (Eckhorn et al., 1988; Gray and Singer, 1989). The notion that brain areas could be synchronized with millisecond-scale precision more than just a cortical column apart, and without oscillation of the tissue in between, led not only to the idea that synchronized oscillations could "bind" different areas of cortex responding to the same stimulus, but also to the fascinating hypothesis that such synchrony could be associated with perception (Roelfsema et al., 1994; Fries et al., 1997) and perhaps awareness (Traub and Whittington, 2010). Gamma oscillations are not specific to visual cortex, and have been found to be induced by sensory stimuli in somatosensory (Buhl et al., 1998), auditory (Palva et al., 2002) and olfactory cortex (Neville and Haberly, 2003), as well as during slow-wave sleep. Gamma oscillations have also been found in entorhinal cortex (Chrobak and Buzsáki, 1998), amygdala (Halgren et al., 1977), hippocampus (Buzsáki et al., 1983; Whittington et al., 1995), striatum (Berke et al., 2004) and thalamus (Pinault and Deschênes, 1992). Although gamma oscillations *in vivo* have been found in mammals (Fries et al., 1997; Buhl et al., 1998; Fisahn et al., 1998) and other species (Ramcharitar et al., 2006), sensory-induced oscillations are not universally encoded in the gamma range[11]. It has been postulated that mammals may use frequencies in the gamma range to encode sensory-induced oscillations, as the period of a gamma oscillation may interface with time constants of processes involved in synaptic plasticity, such as the calcium concentration changes within dendrites (Traub and Whittington, 2010). The first persistent gamma oscillations to be found *in vitro* in brain slices were obtained by adding carbachol, a cholinergic agonist, to the bathing solution, and by a careful slicing technique aimed at preserving the inhibitory circuitry (Fisahn et al., 1998). These findings were revolutionary because *in vitro* gamma oscillations subsequently enabled researchers to study the physiopharmacology of gamma oscillations *in vitro*. It also became apparent that gamma oscillations required fast inhibitory cell firing and $GABA_A$-receptor

---

[11]Beta frequencies have been reported in the turtle visual system (Prechtl, 1994) and insect olfactory system (Laurent et al., 1996).

mediated inhibition. On the basis of current data from experiments and computational modelling, two models have been proposed to explain the emergence of gamma oscillations:

In the I-I model (or interneuron network gamma (ING) model (Whittington et al., 2000)), a subset of interneurons (I) are mutually connected. Gamma oscillations arise when interneurons start discharging synchronously and generate inhibitory postsynaptic potentials (IPSPs) in the downstream interneurons, which will only start firing again when the hyperpolarization mediated through GABA$_A$ receptors has decayed (Wang and Rinzel, 1992; Whittington et al., 1995; Wang and Buzsáki, 1996). Pyramidal neurons in this network are synchronized by inhibitory input. The frequency of the gamma oscillation in this model is determined by the IPSPs kinetics and the net-excitation of the interneuron assembly (Wang and Buzsáki, 1996; Buzsáki and Wang, 2012a).

In the E-I model (or pyramidal-interneuron network gamma (PING) model (Whittington et al., 2000)), excitatory and inhibitory neurons are reciprocally connected. A synchronous excitatory volley from the excitatory (E) neurons activates interneurons (I), which in turn generate a synchronous inhibitory volley. Once the E neurons recover from inhibition they can generate the next synchronous excitatory volley. This was the earliest model for oscillations (Wilson and Cowan, 1972), and has since been refined by many investigators. Long-distance coupling of oscillations is poorly understood, but one recent hypothesis is that the axons of principal cells may be coupled via gap-junctions (Traub and Whittington, 2010). Although this is a minority view, I find the model compelling and would like to briefly outline here how it explains the generation of gamma oscillations (Traub and Whittington, 2010): Pyramidal cells axons can generate spontaneous action potentials, which initiates a wave of activity (termed very fast oscillations (VFO), ~250 Hz) transmitted to other

network axons through gap junctions [12]. The wave of activity leads to near-synchronous phasic depolarization of fast-spiking interneurons, which in turn generate IPSPs in pyramidal cell somas. This produces hyperpolarization and reduced action potential propagation along pyramidal cell axons, thereby reducing the VFO. Once the IPSPs fade, the process is repeated, giving rise to the next gamma period. The frequency of the gamma oscillation in this model depends on the axon conduction and the synaptic delays between excitatory and inhibitory reciprocal synapses. An alternative view on mechanisms to temporally coordinate distant oscillators includes interleaving assemblies (Vicente et al., 2008) and long-range interneurons (Buzsáki and Draguhn, 2004) with thicker axons and large diameter myelin sheaths, allowing for rapid signal propagation. Both models were developed to explain gamma oscillations in the cortex. In the cornu ammonis 1 (CA1) area of the hippocampus, a hybrid network made up of both I-I and E-I networks has been suggested, as interneurons display both phase advance (as postulated in the I-I model, where interneurons synchronize pyramidal cells) or delay (as in the E-I model, where the interneuron "inherits" the spike from an excitatory neuron (Buzsáki and Wang, 2012a)) relative to the spikes of pyramidal cells (Bragin et al., 1995; Brunel and Wang, 2003; Mizuseki et al., 2011; Belluscio et al., 2012). Other mechanisms may be responsible for gamma oscillations in other brain areas (Buzsáki and Wang, 2012a). In addition to our basic understanding of the mechanisms underlying gamma oscillations, it is known that the coherence of gamma oscillations across regions varies depending on sleep/wake states (Bragin et al., 1995; Montgomery et al., 2008) and task demands (Montgomery and Buzsáki, 2007). Different gamma synchronization patterns are thought to be important for information flow through the hippocampus (Salinas and Sejnowski, 2001; Akam and Kullmann, 2010), but the factors that govern gamma oscillation coherence across brain regions is poorly understood.

---

[12]Interestingly, both *in vitro* and *in vivo* experiments in Connexin-36 (a neuronal gap-junction protein) knock-out mice have demonstrated that hippocampal gamma oscillations are selectively impaired (Hormuzdi et al., 2001; Buhl et al., 2003).

### 1.4.3 Interneurons and Gamma Oscillations

Several lines of evidence support the involvement of fast-spiking PV-positive interneurons in gamma oscillations: In behaving rats, trains of spikes at gamma frequency recorded from fast-spiking interneurons (putative and histologically verified PV-basket cells) are correlated with the LFP theta oscillation (Buzsáki et al., 1983). Further, post-synaptic potentials recorded *in vitro* in pyramidal cells during carbachol-induced gamma oscillations are phase locked to the LFP gamma rhythm. These postsynaptic potentials reverse their polarity at the equilibrium potential for chloride, indicating that they are mediated by $GABA_A$-receptors. In addition, the maximum discharge from basket cells precedes the depolarisation of pyramidal cells recorded in slices during carbachol-induced gamma oscillations, as suggested in E-I models (Buzsáki and Wang, 2012a). These findings suggest that extracellularly recorded gamma oscillations represent pyramidal cells' IPSPs driven by fast-spiking PV-interneurons (Buzsáki et al., 1983; Bragin et al., 1995; Hasenstaub et al., 2005; Freund and Katona, 2007; Hájos and Paulsen, 2009). As mentioned above, the molecular and neurophysiological characteristics of PV-positive basket cells further support their role in the induction of gamma oscillations: They include their low spike threshold, their fast-spiking properties and narrow spikes conveyed by the expression of KV3.1/3.2 channels and their resonance at gamma frequency (Buzsáki et al., 1983; Gulyás et al., 1993; Lien and Jonas, 2003; Pike et al., 2000; Cardin et al., 2009). Other subclasses of interneurons are more likely to contribute to slower rhythms (Martinotti cells e.g. have resonance at theta) and to establish cross-frequency coupling between gamma and theta (Buzsáki and Wang, 2012a).

### 1.4.4 Neuronal Oscillations and Optogenetic Tools

Optogenetic tools offer the unique possibility to drive a subset of neurons at different frequencies, without perturbing others, and to measure the effect on

the local field potential or on single unit recordings. Most importantly they allow to experimental testing of the function of neuronal ensembles and to establish cause and effect of oscillations when they are optically activated (Tiesinga and Sejnowski, 2009). Optogenetic tools were first used to selectively drive fast spiking parvalbumin-positive interneurons at a range of frequencies (8-200Hz), which resulted in selective amplification of gamma oscillations in barrel cortex of mice (Cardin et al., 2009). Subsequently, opsins were used to show that *N*-Methyl-*D*-aspartate (NMDA) receptors in parvalbumin-positive interneurons play a critical role in the induction and maintenance of gamma oscillations in sensory cortex (Carlén et al., 2011), whilst another group studied how the horizontal projections of pyramidal cells in layer 2/3 of the cortex modulate cortical activity by exciting ChR2 and eliciting gamma oscillations in pyramidal cells with ramps of blue light (Adesnik and Scanziani, 2010). Our study describes the first use of optogenetic techniques to study gamma oscillations in the hippocampus.

## 1.5   The Neurobiology of Focal Neocortical Epilepsy

### 1.5.1   Terminology

"Epilepsy" is not a single disease but comprises a variety of disease forms with different aetiologies and clinical manifestations (Panayiotopoulos, 2005). In addition, the definitions of "epilepsy" and "seizures" are still debated and not uniformly accepted by specialists in the field (Panayiotopoulos, 2005). The classification of epileptic seizures and syndromes is updated at regular intervals by the Commission on Classification and Terminology of the International League against Epilepsy (ILAE), to ensure that the classification of this disease matches our advances in knowledge based on new research findings in molecular biology, genomic technologies and imaging (Berg et al., 2010). It is therefore important to define the terminology (Table 1.6) that will be used here and to delineate the subtype of "epilepsy" that will be discussed in the

Table 1.6: **The terminology of epilepsy**

**Epilepsy:** the liability to recurrent clinically manifested seizures of any type (Panayiotopoulos, 2005).

**Epileptic seizure**: a clinical manifestation presumed to result from an abnormal and excessive discharge of a set of neurons in the brain. The clinical manifestation consists of a sudden and transitory abnormal phenomena which may include alterations of consciousness, motor, sensory, autonomic, or psychic events perceived by the patient or an observer (Commission-ILAE, 1993).

**Pharmacoresistant seizures**: Seizures that fail to respond to two or more first-line drugs alone or in combination.

**Focal seizures**: Seizures that originate primarily within networks limited to one cerebral hemisphere. For each seizure type there is one consistent onset zone. The network underlying the ictal onset zone may be localized or more widely distributed within one hemisphere. Focal seizures can propagate to involve cortical areas different from the onset zone and to the contralateral hemisphere (Berg et al., 2010).

**Generalized seizures**: originate within, and rapidly engage, bilaterally distributed networks. The networks include cortical and subcortical structures and seizures may be asymmetric (Berg et al., 2010).

**Ictal epileptiform patterns** (Chartrian et al., 1974): sharp wAves, spikes, spike-wave complexes and polyspike-wave complexes

**Spike**: a transient lasting between 20-75 ms that is clearly distinguishable from the baseline (Chartrian et al., 1974; White et al., 2010).

**Sharp wave**: a transient lasting between 75-200 ms that is clearly distinguishable from the baseline(Chartrian et al., 1974).

**Spike-wave complexes**: a spike followed by a slow wave (4-7Hz)

**Polyspike-wave complexes**: 2 or more spikes followed by 1 or more slow wAves

Table 1.7: **Forms of neocortical epilepsy with genetic causes** (Panayiotopoulos, 2005; Crompton et al., 2010; Meisler et al., 2010; Bellini et al., 2011)

**Benign familial neonatal seizures** (mutations in KCNQ2, also known as Kv7.2, and KCNQ3, also known as Kv7.3).

**Benign familial infantile seizures** (linked to chromosomes 2, 19 and the PRRT2 gene on chromosome 16)

**Benign familial neonatal–infantile seizures** (missense mutations in SCN2A gene)

**Autosomal dominant nocturnal frontal lobe epilepsy** (mutations in the CHRNA2, CHRNA4, and CHRNB2 genes)

**Familial temporal lobe epilepsy**:

- **Mesial familial temporal lobe epilepsy** (gene unknown)

- **Lateral familial temporal lobe epilepsy** (LGI-1 gene mutations in chromosome 10q)

**Familial focal epilepsy with variable foci** (linkage with chromosome 2q and 22q but gene not cloned yet)

following paragraphs.

## 1.5.2   Epidemiology - the Burden of the Disease

Epilepsy is one of the commonest neurological disorders and a major public health concern, affecting approximately 50 million people worldwide (Radhakrishnan, 2009) and 450,000 people in the UK. 60-70% of epilepsies may involve focal seizures, half of which arise from the temporal lobes (Panayiotopoulos, 2005). According to the revised ILAE terminology for the classification of epilepsy and seizures (Berg et al., 2010), epilepsies can be classified according to their aetiology as genetic, metabolic/structural and of unknown cause.

Genetic forms of epilepsy manifesting with focal seizures include the familial (autosomal dominant) electroclinical syndromes detailed in Table 1.7. Some of them are monogenic forms of epilepsy now belonging to a group of disorders

termed channelopathies, due to mutations in susceptibility genes coding for ion-channel subunits.

Structural and metabolic causes of focal seizures include malformations of cortical development, tumors, infections, inflammation, stroke, peri-natal insults, trauma and other injuries. The exact incidence and prevalence of these aetiologies is unknown and is different in westernized and developing countries, with infections (cysticercosis and tuberculosis) being the most common cause in the developing world (Panayiotopoulos, 2005). The old ILAE classification of epilepsies further distinguished between focal seizures arising from limbic structures (mesial temporal lobe epilepsies and others defined by location and aetiology), versus the neocortex (frontal, parietal, occipital and lateral temporal neocortical seizures) (Engel and ILAE, 2001).

The following chapters will concentrate on the focal epilepsies arising from frontal neocortical networks in humans and the tetanus toxin (TT) rodent model of this disease (Nilsen et al., 2005).

### 1.5.3 Clinical and Electrophysiological Features of Focal Seizures Arising from the Frontal Neocortex

Based on cytoarchitectural and functional studies, the frontal neocortex can be subdivided into primary motor cortex, premotor cortex and prefrontal cortex, and seizures may originate from anywhere within it. Frontal lobe seizures present diagnostic challenges both clinically and electrographically: they are characterized by rapid spread to other areas and by a varied semiology and electroencephalographic (EEG) features due to varied patterns of spread (Panayiotopoulos, 2005), which are, in turn, facilitated by the manifold connections of the frontal lobe with other brain regions.

Clinically, frontal lobe seizures are generally short and can occur without warning and with little post-ictal confusion. They frequently occur out of sleep, and can cluster in 5-6 seizures per night. The ictal manifestiations range from

tonic and clonic motor manifestations with preserved consciousness (the typical Jacksonian motor seizure), to ictal posturing of the limbs (ipsi-, contra or bilateral) preceded by a somatosensory aura of numbness or tingling when arising from more anterior areas such as the supplementary motor area (SMA), to complex stereotyped behaviour (often referred to as "hypermotor") in seizures arising from the frontopolar, opercular-insular, anterior cingulate and orbitofrontal regions. The rapid spread of the seizures between the hemispheres can cause sudden hyper- or hypotonia manifesting as drop attacks with risk of serious injury (Sisodiya and Manford, 2009). Autosomal dominant nocturnal frontal lobe epilepsy is a familial form of frontal lobe epilepsy with Mendelian inheritance, stereotyped nocturnal seizures and association with mutations in the beta-2 or alpha-4 subunit of nicotinic receptors.

Electroencephalographic recordings often fail to help in the diagnosis of frontal lobe seizures for the following reasons: 1) The considerable size of the frontal lobes, which makes it difficult to detect discharges in the deep or distant cortical structures by scalp recordings, 2) The fact that frontal lobe seizures have motor manifestations, implying that the EEG recording is obscured by motor activity during the seizure, 3) The fact that EEG recording is inherently inaccurate, as even depth EEG electrodes detect discharges only near the electrode and intracranial grids sample only superficial signals.

Imaging can aid diagnosis but the detection rate of abnormalities is lower than for temporal lobe epilepsies, with computed tomography (CT) identifying 20% of lesions with localizing value, magnetic resonance imaging (MRI) identifying a further 30-40% and positron emission tomography often detecting non-specific changes (Kellinghaus and Lüders, 2004; Sisodiya and Manford, 2009).

Despite these shortcomings, the increased use of intracranial recordings (which, unlike the surface EEG, do not suffer from the low-pass filtering effect of the skull and scalp) and of hardware capable of higher sampling rates (>1000 Hz)

(Jacobs et al., 2009a) has recently led to identification of ictal EEG activity in the frequency range between 80 and 200 Hz. These brief synchronous neuronal discharges have been called epileptic high frequency oscillations (HFO) or "ripples" and are implicated in ictogenesis (Bragin et al., 2000; Engel et al., 2009). Clinically, HFOs have been detected at the seizure onset zone of patients with neocortical epilepsy undergoing pre-surgical evaluation and several reports have shown that they can be detected at the onset of a neocortical seizure and inter-ictally (Traub et al., 2001; Worrell et al., 2004). They can occur independently from interictal spikes and have a better localizing value than spikes. Surgical resection of the tissue, wherein HFOs have been recorded, leads to a favourable outcome (Jacobs et al., 2008; Modur et al., 2011). The clinical usefulness of HFOs has yet to be established, but they are being investigated as a clinical tool to precisely define and limit the seizure onset zone both in neocortical and temporal lobe epilepsy.

Frontal lobe seizures must be differentiated from parasomnias (sleep disorders characterized by motor activity and stereotyped or complex behaviour during sleep). Behaviour in parasomnias is usually less stereotyped, more complex and does not usually cluster more than once or twice per night. A polysomnogram with video-EEG often aids in differentiating these disorders from seizures. A further differential diagnosis is non-epileptic attacks, which involve complex behaviour with retained awareness combined with a normal scalp EEG. Attacks arising from sleep, of short duration and of stereotyped nature should raise suspicions of an ictal phenomenon.

### 1.5.4   Mechanisms of Focal Epileptogenesis and Modelling Focal Epilepsy

Broadly speaking there are genetic and acquired forms of epilepsy (implying that they develop and occur after an insult to the brain). The pathophysiological processes underlying both forms of epilepsy can be investigated by studying

Table 1.8: **Animal models of chronic focal epilepsy**

| Local Application of | Effect |
| --- | --- |
| Acetylcholine | Acute seizures during local infusion, but no spontaneous ones (Ludvig et al., 2006; Baptiste et al., 2010) |
| Tetrodotoxin | Elvax polymer containing tetrodotoxin sheets did not produce spontaneous epileptiform events in rats (Graber and Prince, 1999) |
| Cobalt | Focal seizures, but run down after a few days or weeks (cobalt wire (Chang et al., 2004)). |
| Iron | Gives rise to a chronic epileptic focus in albino rats and cats but with iron salt deposition and activation of macrophages and glial proliferation (Willmore et al., 1978). |
| Penicillins | Selectively block GABA receptors and generate acute focal seizures within several minutes but do not develop into chronic epilepsy (Silfverhuth et al., 2011). |
| **Injection of** | **Effect** |
| Alumina gel | Used as a non-human primate model of complex partial seizures but not used in rodents (Ribak et al., 1998). |
| Tetanus Toxin | Neocortex or hippocampus as a model of chronic focal epilepsy (Carrea and Lanari, 1962; Mellanby and Thompson, 1977; Mellanby et al., 1977). |

human tissue from post-mortem brains or surgical resections, or by replicating the electrographic features of seizures in cell culture systems or brain slices. Although useful for answering a set of questions, these experimental setups do not allow one to observe the behavioural phenomena and comorbidities associated with seizures and epilepsy. Certainly it is possible to study epilepsy and epileptogenesis in the human patient, but these studies focus on imaging and electrographic approaches and cannot investigate these processes at the molecular and cellular level. An alternative approach to better understand epilepsy in a living organism consists of trying to reproduce the human pathology in animal models (Table 1.8). Animal models, too, have their limitations, which need to be acknowledged. If used in a responsible way, however, they provide important tools not only to understand epilepsy but also

to develop and test new drugs and diagnostic tools.

How can animal models be used? After several decades of research, it has become apparent that many cellular and molecular alterations can lead to seizures and that multifactorial processes act at multiple levels - from genes to networks (Dudek et al., 2001). Consequently, each model of focal epileptogenesis may answer only part of the scientific puzzle. Table 1.8 summarizes animal models available today to study chronic focal epilepsy in adults.

### 1.5.4.1   The Tetanus Toxin Model of Neocortical Epilepsy

The effects of intracerebral tetanus toxin (TT) and its antitoxin were described by Roux and Borrell in 1898 (Roux and Borrell, 1898). They had pioneered a short-lived intracerebral antitetanus injection technique for the treatment of tetanus. Short-lived because after four years the treatment was shown to be inferior to the subcutaneous or parenteral route of injection of the antitoxin (Wilson, 1997). The first use of tetanus toxin to generate seizures was described by Carrea and Lanari (Carrea and Lanari, 1962) in dogs in an attempt to establish a model of chronic focal epilepsy based on the hypothesis that tetanus toxin selectively blocked inhibitory synapses . The equivalent rodent model was introduced by Mellanby and colleagues (Mellanby et al., 1977) and has since been used in rat hippocampus and cortex (Nilsen et al., 2005) to generate spontaneous recurrent focal seizures with very little morphological damage.

The model mimics temporal lobe or limbic complex partial seizures if the toxin is injected into the hippocampus. If TT is injected into the neocortex the model mimics focal neocortical epilepsy with or without secondary generalization and epilepsia partialis continua. Epilepsia partialis continua is defined as 'spontaneous regular or irregular clonic muscle twitching of cerebral cortical origin, sometimes aggravated by action or sensory stimuli, confined to one part of the body, and continuing for a period of hours, days or weeks' (Obeso et al.,

1985).

The experimental procedures will be described in detail in the methods section but, briefly, consist in a stereotaxtic injection of 4–50 ng TT into the hippocampus or neocortex of adult rats (injection of TT is also possible in the neonatal hippocampus). The toxin is very labile and can lose toxicity if it binds to surfaces and if agitated too vigorously. The use of an inert protein, such as bovine serum albumin (BSA) can prevent the loss of toxicity (Pitkaenen et al., 2006). The dose of the TT is critical in the neocortical model, as too low a dose produces no seizures at all, whilst too high a dose causes severe convulsions and death.

Seizures develop from day 3–8 in the adult hippocampal model, and from day 3–14 in the neocortical model, depending on the dose. In the hippocampal model seizures can occur up to 30 times a day at their peak, but they rarely last longer than 2 minutes. They are characterized by behavioural arrest, clonic movements and secondary generalization with the EEG showing bursts of 2–3 Hz activity in the hippocampus, increasing to synchronized 20 Hz before slowing down again and ending at 2–5 Hz (Finnerty and Jefferys, 2002). In the neocortical model seizure manifestations comprise behavioural arrest and focal twitching, which can be subtle. They are associated with bursts of fast activity (>20 Hz) (Nilsen et al., 2005). Spontaneous seizures remit spontaneously at 6–8 weeks in the adult hippocampal model, but all animals have impaired memory and learning (Mellanby et al., 1999). In the neocortical model seizures can persist for many months (Nilsen et al., 2005).

**Mechanism of Action of Tetanus Toxin**    Tetanospasmin (referred to as "tetanus toxin") is one of the two exotoxins[13] produced by the gram-positive bacillus *Clostridium tetani* and is one of the most potent toxins known to man[14]. Tetanospasmin is a zinc-metalloproteinase synthesized as a single 150 kDa

---

[13]The second exotoxin is tetanolysin, which subserves a hitherto unknown function.
[14]with an estimated lethal dose of 2.5 ng per kg in humans

progenitor toxin, which is then cleaved by a protease into the active toxin composed of a 50 kDa light chain and a 100 kDa heavy chain by a protease (Pellizzari et al., 1999). Both fragments remain connected by a disulfide bridge, which is required for the neurotoxicity of the protein (Schiavo et al., 1990). Clostridia present in the soil can contaminate wounds, where they secrete the tetanospasmin. The TT diffuses in body fluids to presynaptic cholinergic or sympathetic peripheral axon terminals, where it binds to glycoproteins and glycolipids with high affinity and specificity (Schiavo et al., 1991; Pellizzari et al., 1999). These binding sites are implicated in the peripheral neuron-specific binding of the TT (Schiavo et al., 1991). The precise mechanism by which TT reaches the CNS is unknown but the following description summarizes the fascinating steps, which are thought to take place (Pellizzari et al., 1999): TT is first internalized into the peripheral neuron via an endocytic vesicle and is transported retrogradely along the axon into the central nervous system. On reaching the distal dendrites, the toxin is released into the synaptic cleft. TT then binds to the presynaptic membrane of an inhibitory interneuron by a different receptor to the one that mediated its uptake into the peripheral nerve. Uptake into the central neuron is again via an endocytic vesicle. An acidic pH is required to mediate the translocation of the toxin from the vesicle to the cytoplasm, where it can exert its proteolytic activity. The acidic pH is thought to expose hydrophobic residues of the proteins, which are eventually capable of tunnelling the toxin into the cytosol, either via a pore or via vesicle lysis. Once TT has reached the cell cytosol, the light chain cleAves synaptobrevin at a single site (Schiavo et al., 1992) [15]. Synaptobrevin is one of the proteins making up the SNARE (Soluble NSF Attachment Protein Receptor proteins) tetrahelix - a protein complex involved in vesicular release of neurotransmitters - and its cleavage prevents the release of inhibitory GABA and glycine, thereby causing

---

[15]Strikingly, botulinum toxin serotype B cleAves synaptobrevin at the exactly same site, suggesting that the different clinical symptoms derive from the different sites of intoxication (from a different ability to undergo retrograde transport: botulinum toxin cleAves synaptobrevin at the neuromuscular junction but tetanus toxin is transported transsynaptically into inhibitory terminals), rather than from a different molecular mechanism of the two toxins (Pellizzari et al., 1999)

paroxysmal increases in motoneuron activity, manifesting as intense muscle spasms accompanied by autonomic instability, which can eventually prove fatal. The clinical symptoms of tetanus intoxication would suggest a role of TT in blocking inhibitory neurotransmission at the level of the spinal cord. However, there is no conclusive data demonstrating that the toxin is selective for interneurons. On the contrary, *in vitro* and *in vivo* data have shown that TT has a differential effect on inhibitory and excitatory synapses which are time and dose-dependent: After a latent period, TT effects become apparent in spinal cord neuronal cultures as bursts of activity called paroxysmal depolarizing events (PDEs) that are due to the following mechanisms: evoked glycine release[16] and the frequency of inhibitory postsynaptic potentials (IPSPs) are blocked more rapidly and at lower TT concentrations, whereas inhibition of evoked glutamate release and excitatory postsynaptic potentials is achieved later and at higher toxin doses (Bergey et al., 1983; Williamson et al., 1992). After several hours of toxin exposure there is total loss of synaptic activity (Bergey et al., 1987). Therefore the apparent selectivity of TT for interneurons may be due to the following two reasons: peripheral infections with TT result in very small concentrations of the toxin (picomolar (Pellizzari et al., 1999)) at the synaptic cleft, thereby affecting preferentially the more sensitive interneurons at lower concentrations as detailed above. In addition there may be a morphological reason behind a preferred disinhibition of central pathways: interneurons synapse at the soma and proximal dendrites of spinal motor neurons, whilst excitatory inputs are located at the distal dendrites. Therefore, when arriving at the peripheral cell soma, the toxin may affect proximal synapses earlier in its retrograde travel (Bergey et al., 1987). Both mechanisms in combination can explain an early central disinhibition as a net clinical effect.

What then isthe action of tetanus toxin in generating seizures when injected into the cortex and hippocampus? In both models measurement of radiolabelled

---

[16]TT inhibits the $Ca^{2+}$-dependent but not spontaneous release of neurotransmitters (Williamson et al., 1992).

GABA reveals decreased GABA release and IPSPs in the early stages post-injection (37 hours) (Empson et al., 1993; Empson and Jefferys, 1993), whilst no difference in $Ca^{2+}$-dependent GABA release was detected at four weeks (Empson et al., 1993). Inhibitory responses, however, remain depressed (Vreugdenhil et al., 2002). It is conceivable that an initial short term inhibition of GABA release causes hyperexcitability leading to epileptogenesis. This would require changes in transcription or down-stream events leading to altered channel expression. TT is cleared from the central nervous system within 45 days, as supported by experiments measuring elimination of radio-labelled TT from the brain (Mellanby, 1989), and by experiments measuring cleaved vesicle-associated membrane protein/synaptobrevin as a function of the proteolytic activity of TT (Mainardi et al., 2012). Despite rapid clearance, TT leAves long-lasting changes in local connectivity in a cortex rendered epileptic. In support of this hypothesis, alterations of the intrinsic excitability of layer 5 pyramidal neurons were shown in the cortex of TT injected rats (Wykes et al., 2012) up to 20 days post-injection. At the cellular level, minimal cell loss was reported in the low-dose hippocampal and cortical models (Louis et al., 1990; Benke and Swann, 2004), whilst subcellular molecular and genetic changes have not been described in detail. One report describes increased expression of GAD67 and NMDA receptor subunits (Liang and Jones, 1997).

Limitations of the model comprise the need for surgical equipment and stereotaxic injection into the brain, as well as the variability of the toxin batches, whose potency can vary considerably, depending on the mode of production and the subsequent handling and storage of the toxin (Schiavo personal communication).

### 1.5.5 Therapeutic Challenges

Treatment of focal neocortical seizures is usually with lamotrigine or carbamazepine monotherapy (Marson et al., 2007), or a combination of two

drugs upon failure of two first line antiepileptic drugs (AED). Patients who have failed to respond to adequate doses of two first-line drugs have a less than 20 % chance of achieving seizure freedom with the addition of a new AED (Schiller and Najjar, 2008). Pharmacoresistance is especially common in focal neocortical epilepsy with up to 49 % of patients being reported as having drug-resistant seizures (Sillanpää, 1993; Beleza and Pinho, 2011): patients continue to have seizures as well as suffering the side effects of medication, the risk of injury and death and only a small minority are candidates for surgery. Focal extratemporal epilepsy is particularly problematic, as neocortical seizure foci are not always amenable to surgery because they are difficult to localize despite modern imaging tools (positron emission tomography, 3-Tesla magnetic resonance imaging, surface rendering and diffusion weighted imaging), the function of the underlying cortex is difficult to determine and map out, making it difficult to predict post-surgical deficits, and because the seizure foci are sometimes localized in eloquent cortical areas and therefore not amenable to surgical resection at all (Rothman, 2009). This explains why only 10-20 % of patients in surgical series suffer from frontal lobe epilepsy. Epilepsy surgery options include lesionectomy, frontal lobe resection or corpus callosotomy (the transection of the corpus callosum to slow seizure spread to the contralateral hemisphere or secondary generalization), which is a palliative procedure sometimes performed in devastating drop attacks. Overall, surgery has limited success with only 20-40 % of patients achieving seizure freedom (compared to a success rate of 70 % in temporal lobe epilepsy). Alternatives are limited and involve implantation of a titanium encased vagal nerve stimulator (VNS) with two stimulating electrodes tunnelled subcutaneously and then wrapped around the vagus nerve fibres. Vagal nerve stimulation can be used as adjunct treatment of partial seizures but its mechanism of action remains speculative, with modulation of ictal events and activation of the noradrenergic, the reticular activating, the limbic and autonomic systems as putative modes of action (George and Aston-Jones, 2010).

### 1.5.5.1 New Therapeutic Approaches for Focal Epilepsy

The main therapeutic goal in any form of epilepsy is freedom of seizures with a well tolerated treatment. In women of childbearing age this includes freedom from potential teratogenic effects of the drugs or treatment on the developing foetus. But curing epilepsy also includes preventing the development of seizures in subjects at risk, as well as striving to find a more specific way of targeting medical and surgical treatments to maximize benefits and avoid side effects (Jacobs et al., 2009b). This is why new therapeutic approaches are needed. The efforts made to develop new treatment strategies in humans have been aimed at suppressing neuronal excitability in two ways:

1. Using non-specific physical methods such as therapeutic cooling, magnetic devices and deep brain stimulation (DBS), and repetitive transcranial magnetic stimulation (rTMS) (Löscher et al., 2009; Rothman, 2009; George and Aston-Jones, 2010)

2. Specific targeting of treatment by viral delivery of genes involved in neurotransmission. The following paragraph will outline the most recent approaches tested in humans.

**Physical Methods**

**Deep Brain Stimulation**　The idea to stimulate the nervous system with electricity to influence it therapeutically is surprisingly old, with the first documented use in the year 46AD, when the electric shocks of the torpedo ray were described to treat headaches and peripheral pain (Alotaibi et al., 2011). But it was not until 1954 that the first therapeutic use of deep brain stimulation was demonstrated clinically, in a woman with Parkinson's Disease (Pool, 1954). The therapeutic effects of brain stimulation on seizures were demonstrated a year later in a cat model of seizures (Cooke and Snider, 1955). Whilst the initial interest of deep brain stimulation (DBS) in epilepsy was diverted to stimulation

of the cerebellum due to its main inhibitory GABA-ergic output through Purkinje cells (Cooke and Snider, 1955), the regions of the brain that are currently being evaluated in clinical trials include the subthalamic nucleus, the thalamus (anterior and centromedian nuclei), the caudate nucleus, the amygdalohippocampal complex, locus coeruleus, mammillary body and the mammillothalamic tract (reviewed in (Alotaibi et al., 2011; Kahane and Depaulis, 2010)). Overall, electrical stimulation to suppress seizures can be directed at the epileptic focus itself (as in amygdalohippocampal, cortical or lesional stimulation), or, more commonly, at structures thought to influence epileptic activity remotely, as is the case in stimulation of the subthalamic nucleus, the thalamus (anterior and centromedian nuclei), the caudate nucleus and the so called "overdrive method" of stimulation, where white matter structures connected to the epileptic focus are stimulated. Whilst these techniques receive no feed-back of the stimulation effect from the stimulus-delivering electrode, a new method called responsive neurostimulation comprises a closed-loop feed-back system and the stimulus itself is triggered by EEG events (ictal or pre-ictal) that are analyzed using software algorithms and differ from patient to patient (Alotaibi et al., 2011). Responsive neurostimulation relies on the development of precise seizure detection algorithms and stimulation parameters (Kahane and Depaulis, 2010), but it may eventually prove to be more physiological than chronic stimulation of the brain.

**Magnetic Devices**   Repetitive transcranial magnetic stimulation (rTMS) is based on the principle that a strong magnetic field generates a current in superficial neurons perpendicular to the coil. Low frequency stimulation (<1 Hz) seems to decrease cortical activity, whilst high frequency stimulation increases it (Pascual-Leone et al., 1999). Of all nervous system stimulation techniques, it is the least invasive. Reports of rTMS in refractory partial epilepsy, however, are conflicting with some authors reporting a significant

decrease in seizure frequency (Fregni et al., 2006; Sun et al., 2011), whilst a double-blinded placebo controlled trial found no difference against placebo (Cantello et al., 2007).

**Therapeutic Cooling**   Low temperatures have a number of beneficial effects on limiting injury to the nervous system: they suppress metabolic activity, decrease tissue adenosine triphosphate and oxygen consumption, and reduce glutamate release, mitochondrial dysfunction and calcium overload. In addition, the blood-brain barrier becomes less permeable, thereby limiting oedema, and inflammation is mitigated (Polderman, 2008). There are a number of reports documenting the therapeutic effect of external therapeutic hypothermia in cases of status epilepticus (Cereda et al., 2009; Corry et al., 2008; Elting et al., 2010). The degree of hypothermia used is usually between 30–35 °C and the most common side effects include vein thrombosis, pulmonary embolism, cardiac arrhythmias and infections. Shivering has to be controlled with neuromuscular blockade. Focal cooling of the brain parenchyma with cold saline has been reported to stop seizures (Karkar et al., 2002), and has the additional advantage of fewer systemic side effects. The final goal would is the development of an implantable thermoelectric device built into a closed loop system and capable of cooling a defined area of the brain when seizure activity is detected. A simple thermoelectric device has been shown to be successful in terminating seizures in a rat model, without causing neuronal damage (Rothman, 2009). Despite the enthusiasm generated by a number of case reports, no randomized trials have been conducted to assess the benefits of therapeutic hypothermia on epileptic patients, and until more evidence becomes available, mild hypothermia should be reserved to the most refractory cases of status epilepticus only.

**Gene Therapy**   Gene therapy approaches are problematic: Embryonic stem cells raise a variety of ethical issues, xenografts have tolerance problems and the first xenograft of GABA cells failed to survive (Riban et al., 2009).

Gene therapy approaches using viral vectors have not been attempted in human patients with epilepsy. Different viral vectors, however, have been tested in rodent epilepsy models. We have recently been able to demonstrate that lentiviral gene therapy for epilepsy was successful in the TT model of focal epilepsy: We showed that lentiviral overexpression of the potassium channel Kv1.1 not only prevented epileptogenesis when the virus was co-injected with TT, but also that epileptogenesis was prevented when the lentivirus was administered into an established epileptic focus (Wykes et al., 2012).

AAVs have been the most commonly used viruses in epilepsy models so far: they have been used to suppress gene expression of excitatory neurotransmitters or to overexpress genes involved in neuronal inhibition. In the kainic acid rat model of epilepsy, AAVs expressing neuropeptide Y (NPY) delivered to the piriform cortex alone or in combination with the NPY receptor Y2, were able to suppress seizures (Foti et al., 2007; Richichi et al., 2004; Woldbye et al., 2010; Noe et al., 2010; McCown, 2009), whilst delivery of galanin, a neuroactive peptide, through constitutive expression from AAV, attenuated seizure sensitivity and reduced hilar cell death (Haberman et al., 2003; Lin et al., 2003). Adenosine kinase downregulation via AAV serotype 8 antisense DNA was recently shown to suppress seizures (Theofilas et al., 2011). Herpes-based vectors were used to overexpress the neurotrophic factors fibroblast growth factor-2 (FGF-2) and brain-derived neurotrophic factor (BDNF) in a pilocarpine model of temporal lobe epilepsy: this resulted in increased neurogenesis and reduced inflammation (reduced astrocytosis, microcytosis and interleukin-beta production) and behaviourally in reduced seizure frequency and severity (Paradiso et al., 2009; Bovolenta et al., 2010). How the pathogenic epileptic milieu influences the transduction efficacy and viral tropism for neurons is currently the subject of investigations (Weinberg et al., 2011).

# Chapter 2

# Research Questions

The experiments proposed here were designed to determine:

1. if an interneuron promoter-driven ChR2/NpHR system allows specific targeting and manipulation of interneuron activity in cortex and hippocampus,

2. if opsins allow modulation of gamma oscillations in the hippocampal CA3 area,

3. if opsins constitute a reliable toolbox enabling systematic analysis of epileptic neural circuits and

4. whether NpHR could be used as a novel anti-epileptic treatment strategy that relies on optical inhibition of neurons to interrupt seizures.

# Chapter 3

# Materials and Methods

## 3.1 Plasmid Design and Construction

Lentiviral plasmids used to target excitatory neurons contained NpHR2.0–EYFP (enhanced yellow fluorescent protein, EYFP) and ChR2-mCherry under the excitatory neuron specific promoter Camk2a (gift of K.Deisseroth, Stanford University (Aravanis et al., 2007), see Appendix Fig.A.1 for a list of original plasmids used for cloning). They were used as backbones to generate the constructs carrying the GAD67 (gift of S. Kasparov (Teschemacher et al., 2005)) and CCK promoters (gift of K. Ressler (Chhatwal et al., 2007)). The vectors contain the HIV-1 central polypurine tract (cPPT) (Zennou et al., 2001) and the Woodchuck Hepatitis Virus Post-transcriptional Regulatory Element (WPRE) (Brun et al., 2003) to improve transduction efficiency. To construct the vectors pLenti-CCK-NpHR–EYFP and pLenti-CCK-ChR2-mCherry, I inserted an *Xba*I site into pLenti-CCKpro-GFP (green fluorescent protein, GFP) by mutagenizing it with the following primers: forward 5'-acaaaaacaaattacaaaaattcaaaattttatctagatttcccagggaagatgaagaa-3' and reverse 5'-ttcttcatcttccctgggaaatctagataaaattttgaatttttgtaatttgttttttgt-3'. The ~3 kb CCK promoter sequence was subsequently removed (*Xba*I/*Bam*HI fragment) and ligated into pLenti-Camk2a-NpHR2.0–EYFP and pLenti-Camk2a-ChR2-mCherry cut with the restriction enzymes *Xba*I/*Bam*HI. I

generated a further construct to capitalize from the combined use of
pAAV-double floxed-hChR2(H134R)-mCherry-WPRE-pA (gift of K.Deisseroth,
Stanford University) and the CCK-driven Cre-recombinase in the lentiviral
vector pCCKp-cre-IRES-DsRED (gift of K. Ressler (Chhatwal et al., 2007)): I
cloned the inverse double-floxed sequence (*Bam*HI/*Eco*RI fragment) into
pLenti-Camk2a-NpHR2.0–EYFP and pLenti-Camk2a-ChR2-mCherry after
removing channel and fluorophore by digestion with *Bam*HI and *Eco*RI. I
amplified plasmids using conventional kits (Quiagen) and confirmed all
sequences by restriction enzyme digesting and sequencing. GAD67 subcloning
was outsourced to Entechelon GmBH, Regensburg, Germany. The adenoviral
vector (AVV) shuttle carrying 3.7 kb of GAD67 promoter sequences was
mutagenized and a *Pac*I site inserted 5'-upstream of the *Pml*I site. The Camk2a
promoter was subsequently removed from pLenti-Camk2a-NpHR2.0–EYFP
and pLenti-Camk2a-ChR2-mCherry via restriction digest with *Pac*I/*Pml*I and
the GAD67 promoter cloned in (see Appendix Fig.A.2 for cloned constructs).

## 3.2   Lentiviral Production and Titration

I generated VSVg pseudotyped Lentiviruses according to local protocols
(provided by Collins, Towers and Escors) in Prof. Mary Collin's laboratory
(Division of Infection and Immunity, UCL): 293FT cells (Invitrogen) were
seeded 24 hours prior to transfection and should have reached 90% confluence
the following day. Cells were co-transfected with the transfer vector, p8.91
(*gag/pol* expressor) and pMD.G (VSVg expressor) in Fugene 6 (Roche),
Optimem and sterile Tris-Ethylenediaminetetraacetic acid buffer (both
Invitrogen), pH 8. Approximately 24, 48 and 72 hours after transfection,
lentivirus-containing supernatant was harvested and the HEK cell medium was
replaced with fresh complete medium (Dulbecco's Modified Eagle Medium
(DMEM) containing 10% Fetal Bovine Serum and 1% Penicillin/Streptomycin).
The supernatant was pooled and stored at 4 °C, then filtered through a 0.45 µm

filter (Fisher Scientific) into polyallomer ultracentrifuge tubes and a 20% 1x Hanks' balanced salt solution (HBSS) with a sucrose cushion added at the bottom of the tubes to remove cell debris. Six centrifuge tubes were spun at 20,000 rpm for 2 hours at 4 °C in a swing-out rotor ultracentrifuge (Beckman Coulter). After centrifugation, the supernatant was carefully decanted, the tubes filled with 300 µl 1x HBSS and left to rest for one hour on ice. The virus was then re-suspended, aliquoted and stored long term at -80 °C. I determined the concentrated viral titer by quantitative polymerase chain reaction (PCR) to be between $10^8$ and $10^9$ infectious units (IU)/ml.

## 3.3   Primary Neuronal Cell Cultures

I used a modified version of the protocol presented by Deitch and Fischer (Deitch and Fischer, 1999) on tissue from neonatal (postnatal day 0, p0) Sprague-Dawley rats or knock-in mice expressing GFP in GABAergic neurons (GAD67-GFP mice) (Tamamaki et al., 2003): Cortex and hippocampi were dissected in ice-cold balanced salt solution (BSS) containing 10 x Hanks' balanced salt solution and 10 mM HEPES, pH 7.3. Meninges were removed to minimize contamination with fibroblasts and the collected tissue treated with 2.5% trypsin for 15 minutes at 37 °C. After removing the trypsin, hippocampi were washed with BSS and triturated with a fire-polished Pasteur pipette. Cell density and the fraction of viable cells were identified with trypan-blue. Cells were plated in neuronal medium (Neurobasal Medium containing GlutaMAX-I and B27 serum-free supplement, Invitrogen) containing 10% fetal calf serum (FCS) on Poly-D-Lysine(PDL)/Laminin coated coverslips (prewashed overnight in $HNO_3$ and sterilized with dry heat 230 °C for 2 h). Plating density was 100,000 neurons per well in 24-well plates. I replaced half the culture volume with serum-free neuronal medium, changed it twice a week and added cytosine arabinoside (1-β-D-arabinofuranosylcytosine) on day 3 to a final concentration of 1 µM to curb glial proliferation. Neuronal cultures from the ganglionic

eminence (embryonal day 14) were made by W. Andrews and A. Zito in Prof. John Parnavelas' lab (Department of Cell and Developmental Biology, UCL). Although neuronal medium contains B27 and hence retinyl acetate, the neurophysiological experiments were conducted in solutions devoid of retinal.

## 3.4   Viral Transduction *In Vitro*

Day 7 hippocampal cultures were transduced with fourfold serial dilutions of the lentivirus ($\sim 1 \times 10^5 – 1 \times 10^7$ IU/ml). pLenti-Camk2a-NpHR2.0–EYFP was applied to wild-type neuronal cultures, whilst pLenti-Camk2a-ChR2-mCherry was transduced in GAD67-GFP expressing cultures, to confirm that lentiviruses targeted only excitatory neurons. Images were taken using a Nikon Fluorescence microscope. Cultures were incubated at 37 °C for 7–11 days before electrophysiological experiments or fixed in 4 % paraformaldehyde (PFA) for 10 minutes and then stained for immunofluorescence.

## 3.5   Electrophysiology and Imaging in Cultures

These experiments were performed with Volynski and Ermolyuk (Department of Clinical and Experimental Epilepsy, UCL): We acquired live confocal images on a Zeiss LSM 510 confocal microscope using EYFP and mCherry filter settings on day *in vitro* 14–18 (DIV). Neurons were patched in whole-cell mode with borosilicate glass micropipettes (Warner, pipette resistance $\sim 4$ M$\Omega$). The intracellular solution contained (in mM) KGluconate (97), KCl (38), EGTA (0.35), HEPES (20), Mg ATP (4), Na GTP (0.35), NaCl (6), Phosphocreatine (7) (equilibrated to pH 7.28 with KOH) (Boyden et al., 2005). Experiments were performed at room temperature (22–24 °C) as in (Boyden et al., 2005) and recordings were obtained with an Axon Instruments Multiclamp 700B Amplifier. Brief pulses of light were delivered using a 473 nm laser for activation of ChR2 and an XCite exacte mercury burner and a standard

bandpass excitation 530–560 nm filter for activation of NpHR. Spiking behaviour was measured during flashes, while holding patched neurons at -70 mV in current clamp and delivering brief depolarizing steps (~200 pA) to induce firing. LabView (National Instruments) software was used to record all data.

## 3.6    Acute Hippocampal Slicing and Neurophysiology

Acute hippocampal slices of 250 μm thickness were cut on a Leica VT1200 vibratome in ice-cold cutting solution containing (in mM): NaCl (64), $NaHCO_3$ (25), Glucose (10), Sucrose (120), KCl (2.5), $NaH_2PO_4$ (1.25), $CaCl_2$ (0.5), $MgCl_2$ hexahydrate (7). Slices were then allowed to rest for 45 min in carbonated artificial cerebrospinal fluid containing (in mM): NaCl (124), KCl (3), $NaHCO_3$ (26), $NaH_2PO_4$ (1.25), $CaCl_2$ (2.4), $MgCl_2$ hexahydrate (1.3), Glucose (10), equilibrated with 95% $O_2$ and 5% $CO_2$. Neurons were patched in whole-cell mode with borosilicate glass pipettes (Resistance 3–7 MΩ, Warner) and intra- and extracellular solutions as published in (Aravanis et al., 2007). Neurophysiological experiments were performed on an Olympus BX50WI microscope at room temperature. Fluorescent neurons were visualized with an HBO 100 Olympus Mercury Burner and filter sets for EYFP (Exciter HQ500/20x, Dichroic Q515LP, Emitter HQ535/30m, Chroma) and HcRed (Exciter HQ575/50x, Dichroic Q610LP, Emitter HQ640/50m, Chroma). Optical stimulation was performed with fibre-coupled lasers with TTL and/or analogue modulation: a blue 473 nm laser (LD pumped all-solid state, CNI), a green 461 nm laser (diode pumped, Crystalaser) and a yellow 593 nm laser (LD pumped all-solid state, Laser 2000) through an Olympus 60x water immersion objective (LUMPLFL 60x W/IR/0.90, Olympus). Recordings were performed with an Axopatch 1D Amplifier and visualized and recorded in LabView software. Membrane currents were low-pass filtered at 2 kHz, digitized at 10 kHz, with current command routines written in Labview.

Electrophysiological data were analyzed offline in Octave (an OS Matlab$^{TM}$ clone) and QtiPlot open source software.

For the oscillation experiments in slices (Akam et al., 2012) we used animals injected with AAV5-Camk2a-ChR2(H134R)-mCherry into CA3. Slice thickness was 400 μm to preserve the circuitry involved in gamma oscillations. Optical stimulation was performed with a blue 470 nm light emitting diode (LED) (OptoLED, Cairn) coupled to the epifluorescence illuminator tube of a Zeiss Axioskop FS microscope and the slices visualized with an amber LED and an LED filter set for red fluorescence (Exciter 572 nm/Dichroic 660 nm/Emitter HQ640/50m) under a 60x water immersion objective. For the sinusoidal stimulus experiments, the ramp current was multiplied by 0.25 and an offset of 1 to give a sinusoid whose amplitude was 25% of the stimulus amplitude at any given time during the ramp. Light intensity and local field potential (LFP) during a 'ramp-kick' experiment consisted of a 5 ms boost of light intensity by 20–40% (of the immediately preceding ramp value) at 500 or 750 ms into the ramp stimulus. Traces of 500 ms duration (centered around stimulus) were low-pass filtered with a 6$^{th}$ order Butterworth filter (cut-off frequency 4 times the estimated oscillation frequency). Since filtering causes changes in oscillation shape and phase, we calculated cycle averaged local field potentials (LFPs) by resampling all pre-stimulus cycles to a length of 200 samples. Wavelet transform graphs were created in Matlab (Mathworks) by using the continuous wavelet function (cwt), once the traces had been down sampled to 1 kHz. The relationship between averaged LFP and modulation phase was computed as in (Akam et al., 2012), after eliminating the first 200 ms of stimulation.

## 3.7 *In Vivo* Experiments

### 3.7.1 Animals

Male postnatal day 20 (p20) Sprague-Dawley rats were used for *in vivo* viral injections. Postnatal day 20 was the youngest age allowed for injections at our institution, since the injected rat had to be quarantined for 24 hours post-injection before being allowed back to its dam and p20 is the usual weaning age for rats. Young rats were desirable, as juvenile tissue survives longer and is healthier in patch clamp experiments, which were usually performed at least 14 days after lentivirus injection (and up to 4 weeks for AAVs) to ensure viral expression was present. As there is no brain atlas for the juvenile rat, the correct coordinates for the hippocampal injection site had to be identified by injection of Trypan Blue. Rats were terminally anaesthetized with isoflurane and 1–1.5 µl (cortex and hippocampus, respectively) Trypan Blue injected into the putative target area. Brains were sliced acutely, the site of injection measured and the coordinates adjusted. For the TT model, 5–10 week old male Sprague-Dawley rats were used. All animals were housed on a 12-hour light/dark cycle in a temperature- and humidity-controlled environment with free access to food and water. All efforts were made to minimize animal suffering and to reduce the number of animals used. Animal experiments were conducted in accordance with the Animals (Scientific Procedures) Act 1986 and local ethical review.

### 3.7.2 Stereotaxic Surgery and Viral Transduction *In Vivo* for Targeting Opsins to Interneurons

For the stereotaxic operation each rat was anaesthetized with isoflurane (Forane; Abbot). The animals were placed in a stereotaxic frame (Kopf instruments). Surgery was performed under a Leica S6E microscope. In the first set of experiments, a permanent guide cannula (Plastics One, Seven Oaks, Kent, UK) was implanted and secured with screws and dental cement. For the NpHR

group the implantation was targeted to the right motor cortex at the following stereotaxic coordinates, measured in millimetres from bregma in the anterior-posterior (AP) and lateral (L) planes and ventral from dura in the vertical (V) plane: AP +1, L +2.5, V -1.5. To target the cornu ammonis 3 (CA3) area of the hippocampus in juvenile rats, the guide cannula was implanted at AP -3.5, L +4, V -2.6. Five days after stereotaxic surgery, animals were lightly sedated with isoflurane, and lentivirus (lentiviral titres ~$10^8$ IU/ml) injected with a microinjector unit (UMP3-1, World Precision Instruments) via an internal cannula at a rate of 0.1 µl/min. Later, permission was granted to inject lentivirus directly with a Hamilton syringe (5 µl Hamilton Syringe, 900 Series, liquid tight with reinforced plunger; 33 G blunt needle; injection rate 200 nl/min with a microinjector unit) without the implantation of a guide cannula. Injection volume was of 1 µl to cortex at the following stereotaxic coordinates AP -1.5 , L -1.5, V -1.45, and 1.5 µl to dorsal CA1/3 at AP -2.8 , L +3.6, V -2.9 and ventral CA3: AP -4.1, L +4.45, V +5.35. Before lightening anaesthesia, rats were injected with 0.05 mg/kg subcutaneous (s.c.) buprenorphine analgesia and 1–2 ml s.c. 0.9% saline and the animal allowed to recover.

### 3.7.3 Modelling Focal Epilepsy

Five to ten-week old male Sprague-Dawley rats were stereotaxically injected into the right motor cortex (between the forelimb and hind limb cortical representations) with 12.5 - 17.5 ng tetanus toxin (gift of G. Schiavo). The toxin suspension was diluted in an isoosmotic solution containing 150 mM NaCl, NaOH HEPES 10 mM and 0.1% bovine serum albumin (BSA, pH 7.0–7.2) in 0.5–1.25 µl high-titre virus. Injection coordinates in mm from bregma for antero-posterior (AP) and lateral (L) and from pia for depth (V) were as follows: AP +1, L +2.4, and V -1. Depending on experimental protocols, the viral vectors used included: 1) lentivirus carrying NpHR tagged with EYFP under the Camk2a promoter (viral titre $10^8$–$10^9$ IU/ml, made by myself as detailed above), 2) lentivirus carrying GFP under the EF1a promoter as control

(pCDH-CMV-MCS-EF1a-copGFP, SBI systems), 3) AAV serotype 5, carrying an eNpHR3.0-2A-ChR2 construct (abbreviated as eNPAC (Gradinaru et al., 2010)) under the Synapsin (hSyn) promoter (gift of K. Deisseroth and produced by UNC vector core, titre $10^{12}$). Control animals were injected with fluorescent beads (Invitrogen, F8834) in Dulbecco's Phosphate-Buffered Saline (D-PBS) or control virus as in 2). An optic fibre (core diameter 200 µm, numerical aperture 0.22, cannula length 1.5–1.8 mm, Doric Lenses, Canada) and an EEG electrode were subsequently implanted above the injection site. A reference electrode soldered to a screw was fixed to the skull anterior to bregma on the left side. Both electrodes (stainless steel coiled wire with silicone insulation) had been tunnelled subcutaneously from a wireless transmitter (A3019D, Open Source Instruments Inc.) for continuous EEG recording (sampling frequency 512 Hz, bandwidth 0.7–160 Hz) (Chang et al., 2011) implanted in the left dorsal region in a subcutaneous pouch. After recovery rats were housed singly in cages placed inside a large Faraday enclosure for continuous EEG telemetry from the first post-operative day.

### 3.7.4   Optogenetic Stimulation *In Vivo*

Optogenetic studies were performed on day 7–10 post-surgery. For optogenetic studies, the implanted optic cannula was connected to a 561 nm laser (Crystalaser) via fiberoptic patch cord (NA 0.22, Doric Lenses) and a rotary commutator (Doric Lenses), and stimulated on and off in 20 second intervals for sessions of 1000 second duration. The laser output was calibrated with a digital optical power meter (PM100D, ThorLabs), aiming for an intensity of 25 mW at the implantable fibre tip, corresponding to an irradiance of approximately 22 mW/mm$^2$ at a distance of 0.5–1 mm, previously reported to be sufficient to inhibit 98% of spikes in brain slice experiments (Zhang et al., 2007b).

### 3.7.5 EEG Acquisition and Analysis

The implanted wireless transmitter (A3019D, Open Source Instruments Inc) has two analogue input filters: a 0.7 Hz high-pass filter and a three-pole low-pass anti-aliasing filter (cut off frequency 160 Hz) with a sharp roll-off. Following analogue to digital conversion, the EEG signal is visualized and analyzed with software scripts within the the Neuroarchiver software environment (Open Source Instruments Inc.): signal peaks greater than 5 x RMS were removed and power bands were computed for 2 s EEG epochs. The EEG data were also analyzed by measuring the coastline (sum of the absolute difference in voltage between consecutive sample points (Korn et al., 1992)) for successive 2 s segments. We complemented this with an automated event classifier that detected all episodes of duration 250–1000 ms that exceeded 5 times baseline power, and grouped them according to key features such as periodicity, amplitude and asymmetry into 4 groups: "short high frequency bursts" (<250 ms), "long high frequency bursts" (>250 ms, event power >6 x baseline), "long high frequency bursts of low amplitude" (>250 ms, event power 5–6 x baseline), and "high frequency spikes", referencing them back to a library of events that had previously been validated by a blinded operator on a large group of animals as being linked to seizures, artefacts or being normal[1]. Data were analyzed offline in QtiPlot open source software.

### 3.7.6 Tissue Processing

For electrophysiological recordings, animals were sacrificed up to 6–8 weeks following viral injection, by an overdose of pentobarbitone and perfused transcardially with ice-cold sucrose-based solution (Aravanis et al., 2007) for 2 min. For immunohistochemistry, rats were perfused transcardially with ice-cold artificial cerebrospinal fluid, decapitated and the brains removed and post-fixed for 24 h in 4 % paraformaldehyde (adjusted to pH 7.4 with 1 M HCl)

---

[1]At http://www.opensourceinstruments.com/Electronics/A3018/Seizure_Detection.html

at 4°C. They were then transferred to a solution containing 30 % sucrose in 1x phosphate buffered saline (PBS) and left at 4°C until they had sunk. Using a Leica freezing vibratome (laboratory of Prof. Steve Davies, UCL), 30 μm coronal sections were cut through the targeted brain regions. For immunohistochemistry, sections were stored in 24-well plates in 250 μl volume. Every section from each series was taken and stained for either GAD67, CCK and GFP, GFAP or activated Caspase-3 as a marker of apoptosis, and 4',6-diamidino-2-phenylindole (DAPI) to visualize cell nuclei.

## 3.8 Immunohistochemistry

Immunohistochemical staining was conducted on free floating sections. Sections were washed in PBS and permeabilized in PBS, 0.2% Triton X-100 for 10 minutes and then blocked with DAKO-blocking medium (Dako) for 1 hour on a shaker. Series of sections were incubated for 2 days in the primary antibodies against γ-amino butyric acid (GABA, 1:100-1:200, Thermo Scientific, PA1-18027), cholecystokinin-8 (CCK-8, 1:100-1:200, Thermo Scientific, PA1-18016), CaMKIIα (1:100-1:200, Thermo Scientific, #MA1-048), green-fluorescent protein (GFP, 1:3000, Abcam, ab13970 or Aves 1:800), dsRed and mCherry (1:200, Living Colors® DsRed or mCherry Monoclonal Antibody, catalogue no. 632392 and 632543), activated Caspase-3 (1:200, kindly gifted by A. Cariboni and J.Parnavelas) or glial fibrillary acidic protein 46 (GFAP, 1:200, Millipore clone GA5, #MAB3402). Following washing in PBS (3 x 15 min), the sections were incubated in secondary antibodies (1:1000, all Abcam and labelled with Alexa Fluor (AF) 488, AF 568 or Tetramethylrhodamine, all gift of A. Cariboni and J. Parnavelas) overnight at 4°C. After further washing in PBS, sections were incubated in DAPI for 5 minutes. The free floating sections were mounted onto microscope slides and allowed to dry. They were subsequently coverslipped using Mowiol Mounting Medium (gift of A. Cariboni and J. Parnavelas). A similar protocol was developed to stain cultured neurons. As fixation with 4%

PFA greatly reduces the fluorescent signal, constructs carrying NpHR-EYFP were always stained with primary antibodies against EYFP and secondaries labelled with AF 488 to detect expression of the virus, whilst constructs carrying ChR2-mCherry were always counterstained with primary antibodies against dsRed or mCherry and secondary antibodies labelled with AF 561 or Tetramethylrhodamine. For colocalization studies, primary antibodies against GABA, CCK, GFAP and CaMKIIα were labelled with secondary antibodies carrying a red fluorophore (for the NpHR-EYFP expressing slices) or a green fluorophore (for the ChR2-mCherry expressing slices). Slices from adult male GAD67-GFP mice expressing GFP in interneurons were used as positive controls for anti-GAD67, anti-CCK and anti-CaMKIIα antibodies. As there is no GAD67-, CCK- or CaMKIIa knockout line available to me, a true negative control experiment was not possible. The anti-GFP antibody could have been tested on the GAD67-GFP mice using a red fluorochrome-labelled secondary antibody to detect co-localization with GFP cells. However, as fixation in 4% PFA destroys at least part of the GFP signal, this experiment was not considered suitable as a positive control. Instead, control stains without primary, without secondary and without any antibody were run alongside the main experiments. All immunohistochemical experiments were performed in the laboratory of Prof. John Parnavelas , UCL, with help from F. Chiara and A. Cariboni.

## 3.9  Morphological Analysis

The evaluation and acquisition of morphological data was performed on a Leica DM2500 Upright confocal microscope (Rockefeller Biomedical Research Unit, UCL) with a 40x oil immersion objective and the following excitation laser lines: 488 nm, 532 nm, 405 nm (see Appendix Table A.1). Slices were first analyzed by fluorescence illumination for expression of the fluorochrome in the targeted area. Image acquisition was performed with Leica LAS AF software. The colocalization of opsin-expressing cells and neuronal or glial cell markers

(GABA, CCK, CaMKIIα) was analyzed in the cortex and hippocampus. To compare the extent of viral expression volumes of different constructs, the size of the area exhibiting EYFP fluorescence was measured at 5–10-fold magnification in the cortex and hippocampus. Volumetric analysis was performed using Octave open source analysis software. Immunostained sections were digitized by means of a high-resolution video camera. All stained sections were evaluated. Image analysis and cell counting was performed using GIMP (GNU Image Manipulation Program) and Image J open source software[2].

## 3.10   Statistical Analysis

Data were analyzed with paired or unpaired non-parametric tests and paired and unpaired *t-tests*, implemented in R open source software[3] and InStat V3 software (Graphpad, LaJolla, CA). Statistical analysis will be discussed as part of each result chapter.

---

[2]http://www.gimp.org/ and http://rsbweb.nih.gov/ij/
[3]http://www.R-project.org

# Chapter 4

# Targeting Opsins to Interneurons

The experiments I will discuss in this chapter were aimed at exploring whether it was possible to generate lentiviral constructs containing opsin genes driven by the interneuron-specific promoters glutamic acid decarboxylase 67 (GAD67) and cholecystokinin (CCK). Further experiments were aimed at demonstrating whether expression of these constructs *in vitro* and *in vivo* was possible and if expression was restricted to interneurons. Finally, I will discuss the construction of an optogenetic setup and the experiments aimed at photoactivating opsins expressed under the Camk2a, GAD67 and CCK promoter *in vitro*.

## 4.1    Plasmid Construction and Assessment of Promoter Activity *In Vitro*

After generating five lentiviral constructs as outlined in the methods section (Appendix Fig. A.2), and before producing active lentiviruses, I transfected the viral constructs carrying the GAD67 and the CCK promoters into 293FT HEK cells (Fig. 4.1) to assess if both promoters were able to drive transgene expression and to compare their level of expression with a control virus (carrying a CMV promoter driving GFP expression) and with the original constructs (LV-CCKpro-GFP, pLenti-Camk2a-NpHR2.0–EYFP and pLenti-Camk2a-ChR2-mCherry). Transgene expression was defined by
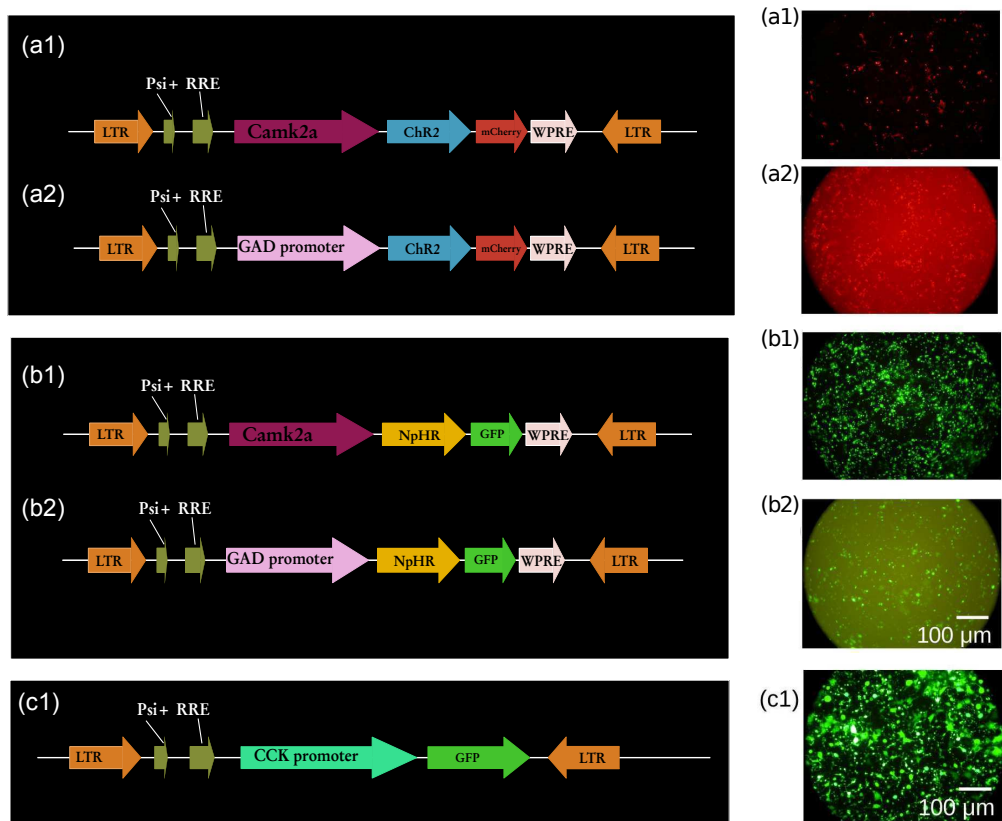
Figure 4.1: **Cloned lentiviral constructs and assessment of promoter activity *in vitro*. (a-c)** Left panels: schematic of the viral vector; right panels: fluorescence micrographs of transfected HEK cells. Micrograph a2 and b2 were taken with a different filter setting.

visualization of the fluorophore in all cases, as in all ChR2/NpHR containing vectors, the fluorophore is fused in-frame to the N-terminus of the opsin gene. HEK cells expressed visible fluorescence with all plasmids, although fluorescence levels were lower (in terms of brightness and numbers of fluorescing cells on visual inspection) in the GAD67/CCK constructs. No inference on GAD67/CCK promoter strength can be drawn, however, as the lentiviral plasmid still contains the 5′ LTR and its promoter, which may be interfering with the internal GAD67/CCK promoter[1].

## 4.2   Lentiviral Generation

### 4.2.1   Lentiviral Production and Titration

The successful production of lentiviral particles is a process fraught with variables that have to be controlled to be able to get high enough titres to ensure expression in neurons. After testing a number of various methods (Lipofectamine protocol by G. Towers, one or more rounds of centrifugations, different resuspension media, different types of HEK cells), I found that there was a highly significant difference in viral titres (Fig. 4.2, $p < 0.01$, two-tailed, unpaired *t-test*) when the viral suspension was centrifuged once only versus when I used two rounds of centrifugation. Two rounds of centrifugation are used when a cleaner viral preparation is necessary, such as in vaccination or *in vivo* experiments, where cell debris could otherwise trigger unwanted immune reactions. The protocol described in the methods section and provided by D. Escors (Prof. Collins' lab), yielded the best results with consistent titres as high as $10^8$–$10^9$ IU/ml. Titration experiments also needed optimization: Fluorescent-activated cell sorting (FACS) analysis is advantageous in that it

---

[1]As discussed in the introductory section both LTRs in the proviral DNA originate from the 3′ LTR present on the genomic RNA. To avoid any undesired gene dysregulation by the viral promoter in the 3′ LTR, lentivirus vectors of the last generation, also called self-inactivating vectors (SIN), have a chimeric LTR, where the HIV promoter was replaced with transcriptional control elements from heterologous viral (e.g. CMV) or cellular promoters (Federico, 2003): when DNA provirus integrates into the host cell genome, expression will only depend on the internal promoter.
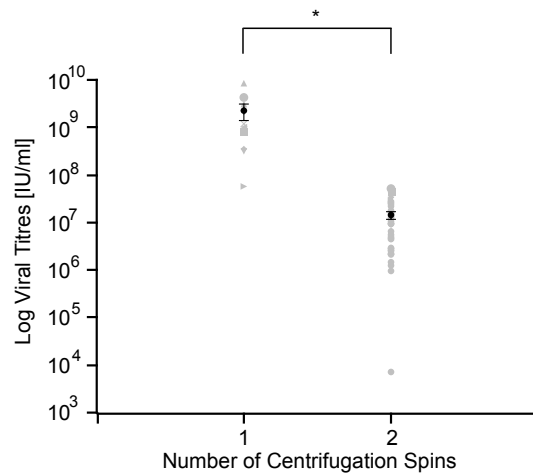
Figure 4.2: **Viral titres depending on number of centrifugation steps.** Viral titres of pLenti-Camk2a-NpHR2.0–EYFP batches concentrated with two rounds of ultracentrifugation (n = 36) had significantly reduced titres (p < 0.01, two-tailed, unpaired *t-test*), compared to viral batches centrifuged only once (n = 10). In black mean values and SEM.

gives a direct readout of the expression of the gene of interest, providing there is

a reporter fluorophore. In the constructs I used, the opsin gene is fused to the

fluorophore gene, therefore fluorescence would have indicated expression of

the opsin, too. FACS, however, cannot distinguish the total amount of lentiviral

DNA in a fluorescent cell and is thought to underestimate real titres (Sastry

et al., 2002). Also, FACS analysis depends on the available laser wavelengths

used to excite the fluorophores. Unfortunately, the FACS analyzers available

did not have a laser line for the excitation of mCherry. Therefore, I found that

the best method of titration for both mCherry and EYFP constructs was

quantitative PCR (qPCR)[2].

---

[2]qPCR enables one to determine the total amount of lentiviral DNA in a sample relative to total cellular DNA. It hence allows calculation of the infectious units per unit volume if the amount of virus and the number of cells transduced are known
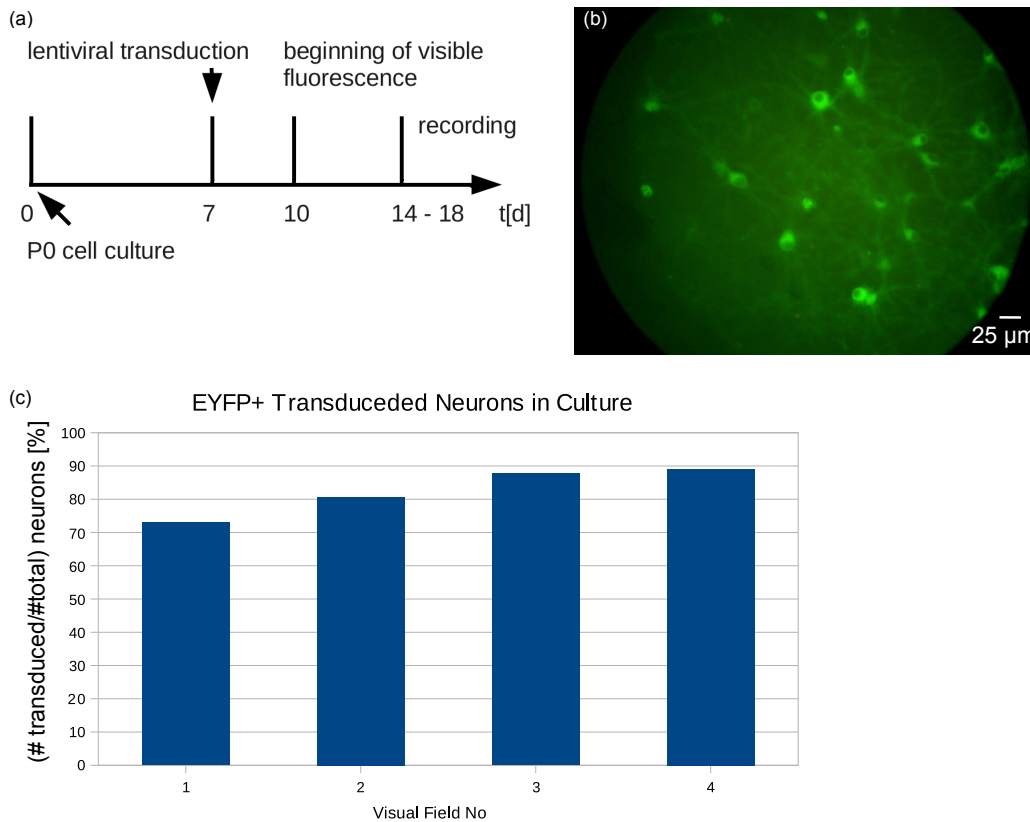
Figure 4.3: **Expression of Camk2a driven ChR2 and NpHR in neuronal cultures. (a)** Timeline of experiments. **(b)** Fluorescent images of neurons expressing pLenti-Camk2a-NpHR-EYFP in culture at 20x magnification. **(c)** Evaluation of expression levels by counting fluorescent EYFP-positive neurons in 4 visual fields (n=1) of transduced cultures revealed high expression levels (73–89% of total neurons).

## 4.3 Study of Camk2a-driven ChR2 and NpHR in Neuronal Cultures

### 4.3.1 Viral Transduction in Primary Neuronal Cell Cultures

Lentiviruses expressing ChR2 or NpHR under the Camk2a promoter were initially tested in primary neuronal cultures . Both opsins were successfully expressed in postnatal hippocampal cultures of rat or mouse, with fluorescence visible as early as day 4 post-transduction in NpHR and day 5 post-transduction in ChR2-expressing neurons (Fig. 4.3a, b). Expression persisted in healthy looking neurons without signs of cytotoxicity as long as
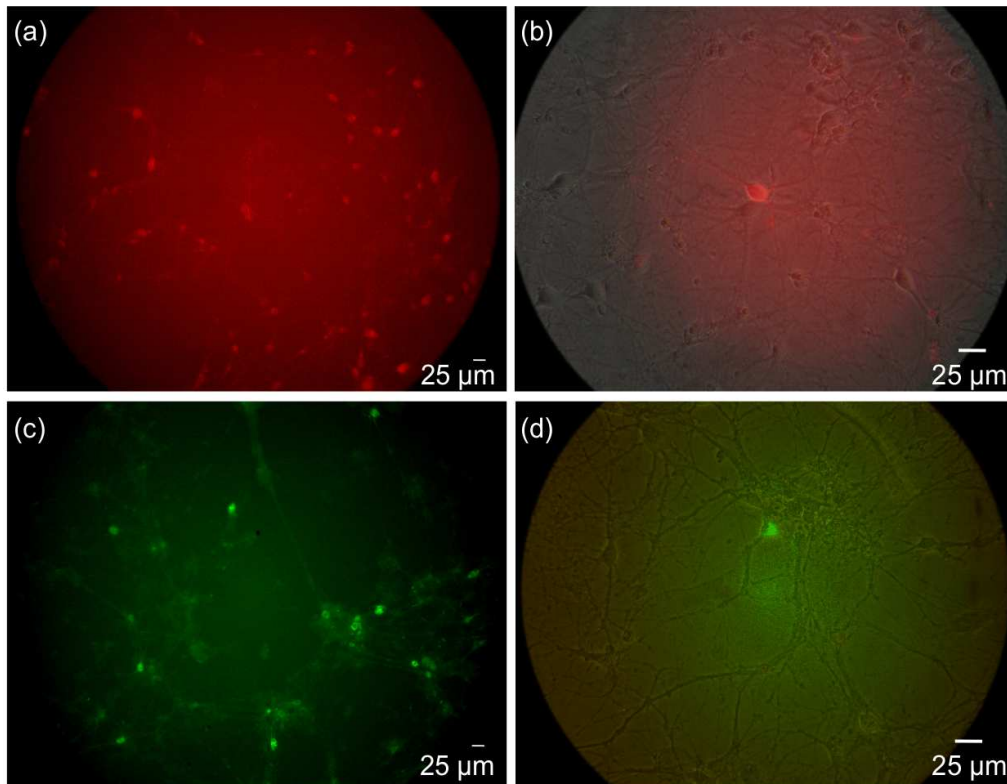
Figure 4.4: **GAD67- and CCK-driven opsins in hippocampal neuronal cultures. (a)** LV-CCK-ChR2-mCherry, **(b)** LV-GAD67-ChR2-mCherry, **(c)** LV-CCK-NpHR2.0-EYFP, and **(d)** LV-GAD67-NpHR2.0-EYFP expressed at low levels in wild-type neuronal cultures.

cultures survived. Evaluation of expression levels by counting fluorescent EYFP-positive neurons in 4 visual fields of transduced cultures revealed high expression levels (73–89 % of total neurons, Fig. 4.3b, c). When I tested the GAD67/CCK-driven opsin vectors in wildtype p0 rat hippocampal or cortical cultures, the results reflected the low levels of endogenous expression, with very little or no expression visible at all when transduced with different concentrations of lentivirus, ranging from $10^5$–$10^7$ IU/ml (Fig. 4.4 and Fig. 4.54.6). It has been known for a long time that both neuronal activity and growth factors such as brain-derived neurotrophic factor (BDNF) regulate soma size, levels of GABA and dendrite morphology in inhibitory interneurons in culture (Marty et al., 1997). Also, co-culturing neurons with astrocytes, rather than on Poly-D-Lysine (PDL) alone, accelerates the appearance of GABA- and
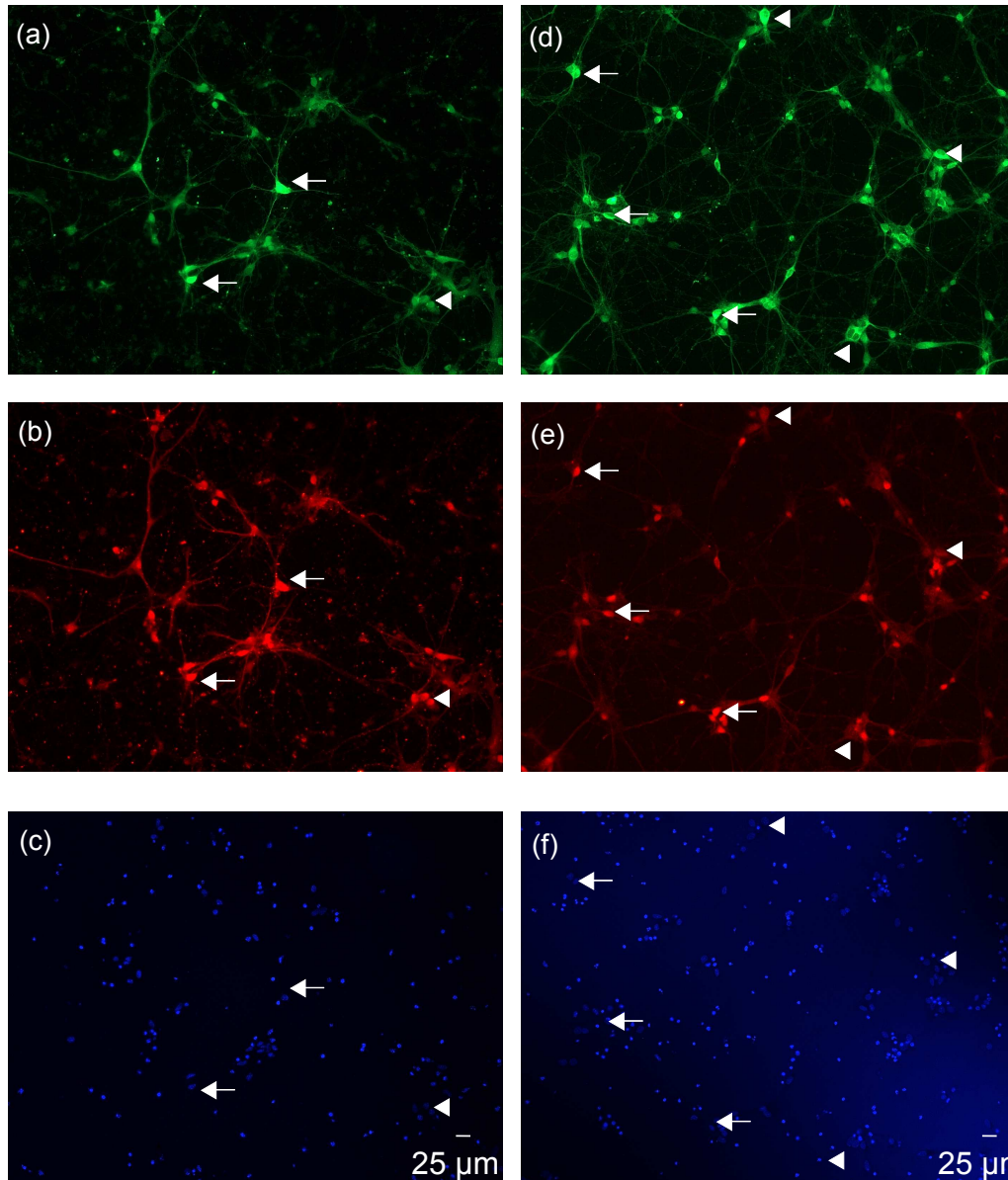
Figure 4.5: **CCK- and GAD67-driven opsins in ganglionic eminence neuronal cultures.LV-CCK-NpHR2.0-EYFP: (a)** LV-CCK-NpHR2.0-EYFP expresses in GE neuronal cultures (in green). Approximately 90% of LV-CCK-NpHR2.0-EYFP expressing neurons (in green) also stain for anti-CCK antibody (**b**, in red). Arrows depict examples of colocalizing neurons, arrowheads non-colocalizing neurons. **(c, f)** DAPI stain was used to aid cell counting (n=1). **LV-GAD67-NpHR2.0-EYFP: (d)** LV-GAD67-NpHR2.0-EYFP expresses in GE neuronal cultures (in green) and co-localizes with GABA-antibody (**e**, in red): 40% of LV-GAD67-NpHR2.0-EYFP expressing neurons (in green) also stain for GABA-antibody (in red). Arrows and arrowheads used as above (n=1).
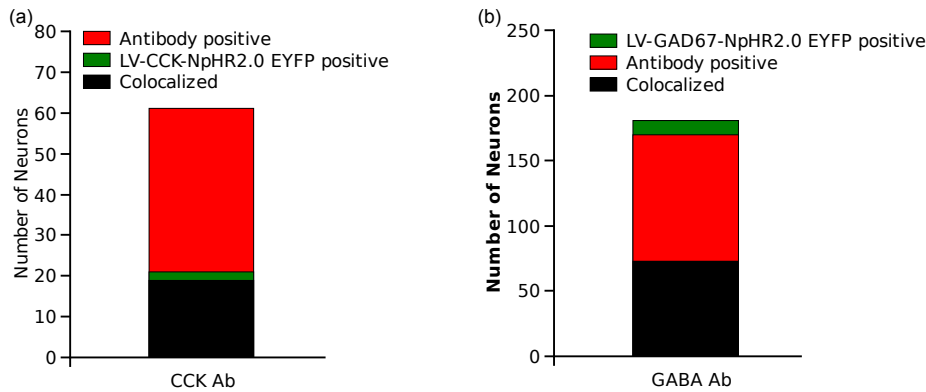
Figure 4.6: **Cell counts of CCK- and GAD67-driven opsins in ganglionic eminence neuronal cultures.** Bar plot **(a)** shows that 19/21 LV-CCK-NpHR2.0-EYFP expressing neurons are also CCK-antibody positive (n=1). Bar plot **(b)** shows 73/181 LV-GAD67-NpHR2.0-EYFP neurons also stain for GABA antibodies (n=1).

glutamatergic transients (present at 24 hours in cultures in the former, versus at 4 days in the latter case) (Li et al., 1999). In view of the remote possibility that transducing hippocampal neurons cultured on PDL-coated coverslips failed because there was too small a percentage of inhibitory neurons on day 7 *in vitro*, I decided to increase the number of inhibitory cells in the culture by using neuronal cultures from the ganglionic eminence (GE), the birthplace of interneurons. Embryonal day 14 (E14) GE neuronal cultures were provided by A. Zito and W. Andrews (Prof. Parnavelas' lab). GAD67 is already expressed at E14 and the cultures were transduced at days 5-7 *in vitro* with $10^6$ IU/ml per well. Fluorescence was visible for LV-GAD67-NpHR2.0 EYFP and LV-CCK-NpHR2.0-EYFP but not for the ChR2-mCherry constructs: ~90 % of cells expressing LV-CCK-NpHR2.0-EYFP also stained for anti-CCK antibody (19/21 cells, 4 visual fields (VFs)). 40% of LV-GAD67-NpHR2.0-EYFP expressing neurons were also anti-GABA antibody positive (73/181 cells, 4 VFs). Caveats remain due to the small numbers in the experiments.

### 4.3.2 ChR2 Mediates Neuronal Depolarization *In Vitro*

We were able to demonstrate in pilot experiments that our lentiviral particles carrying LV-Camk2a-ChR2-mCherry successfully transduced hippocampal neurons of GAD67-GFP expressing mice (Fig. 4.7). The red fluorescence of mCherry was exclusively detected in neurons not expressing GFP, indicating that targeted expression to principal cells had been successful. Neurons expressing mCherry were patch-clamped in whole cell mode as described above (with help from Y. Ermolyuk and K. Volynski) and the cell flashed with blue light. Brief flashes of blue light of 200 ms elicited reliable depolarization and spiking of current-clamped neurons (Fig. 4.7c).

### 4.3.3 NpHR Inhibits Neuronal Firing *In Vitro*

In a pilot experiment, consistent with previous data (Zhang et al., 2007b), we were able to show not only that the NpHR is stably expressed in cultured neurons without disrupting cellular morphology, but also that the Cl$^-$-pump was functional (data not shown). Green fluorescing cultured hippocampal neurons expressing LV-Camk2a-NpHR2.0 EYFP were patched in whole cell mode and their membrane potential measured. We first verified that the neuron was capable of firing action potentials by current injection. Then neurons were flashed with yellow light at random intervals during firing. Increasing intensities of light led to inhibition of spiking evoked by current injection. However, flashing patch-clamped LV-GAD67-NpHR2.0-EYFP and LV-CCK-NpHR2.0-EYFP expressing neurons in a GE neuronal culture with yellow light from an amber or white LED (irradiance values between 1.15 and 8.55 mW/mm$^2$ at the 40x objective) was not sufficient to inhibit neuronal firing.

In summary, in the first experimental period, I generated new lentiviral constructs carrying ChR2 and NpHR2.0, each driven by the interneuron-specific promoters GAD67 and CCK. I generated high-titre lentivirus of the Camk2a, GAD67 and CCK driven constructs and tested them *in vitro* on neuronal
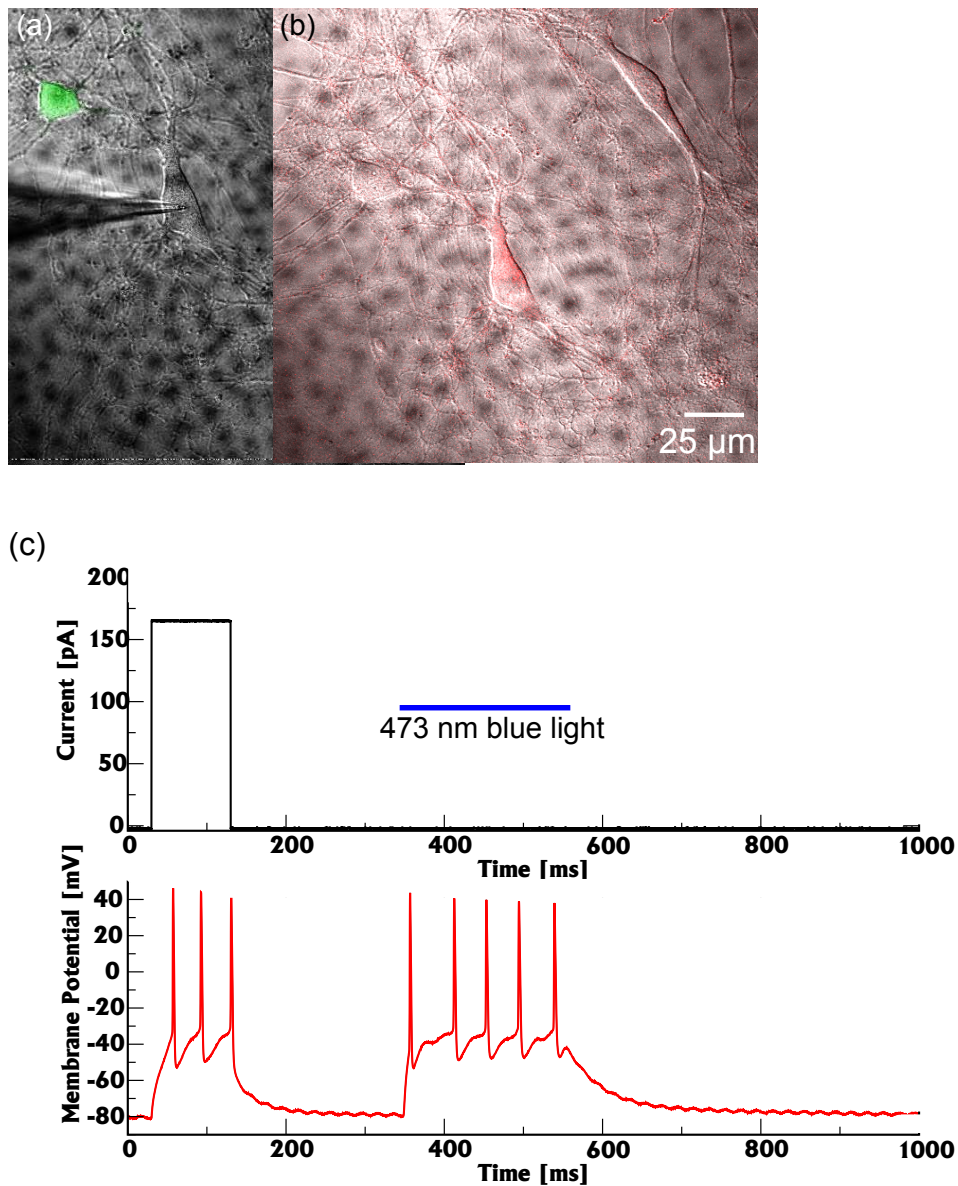
Figure 4.7: **Neurophysiology of Camk2a driven ChR2 in neuronal cultures. (a, b)** Transduction of neuronal cultures from GAD67-GFP mice with LV-Camk2a-ChR2-mCherry, showing green fluorescence in interneurons **(a)**, whilst the virally transduced neurons are principal cells **(b)**. **(c)** Neurons expressing mCherry were recorded in whole-cell patch-clamp mode as described above and the cell flashed with blue light if healthy. Brief flashes of 473 nm blue laser light elicited reliable depolarization and spiking of current clamped neurons (n=1).

cultures. All constructs expressed, but at low levels for the GAD67 and CCK driven constructs. CCK was specific for CCK neurons in GE neuronal cultures (but numbers are small), whilst GAD67 was not specific. Patch-clamp experiments with optogenetic excitation or inhibition of neurons succeeded in the Camk2a driven constructs only.

## 4.4   Opsin Expression *In Vivo*

We went on to explore if we could achieve reliable expression of the lentiviral vectors carrying NpHR and ChR2 *in vivo*. NpHR was of particular interest as a promising candidate for inhibition of neuronal spiking in focal and *in vitro* epilepsy models.

### 4.4.1   Morphological Characterization of Opsin Expression Levels in Rat Cortex and Hippocampus

All rats injected with 500–1250 nl of lentivirus carrying NpHR2.0-EYFP under the Camk2a, GAD67 and CCK promoters (titre $3 \times 10^8$ or $5 \times 10^8$ IU/ml) exhibited strong fluorescence in both cortex and hippocampus in stained sections, which was also clearly visible in acutely sliced sections. Conversely, lentivirus vectors expressing ChR2-mCherry under the Camk2a, GAD67 and CCK promoters were only visible on stained sections. To compare expression levels between LVs and AAVs, a group of animals (n=1 for each virus) were injected with either AAV5-eNpHR3.0-2A-ChR2-EYFP (eNPAC) (UNC vector core, titres $10^{12}$ IU/ml), or to evaluate and compare opsin expression between promoters and between LVs and AAVs, sliced and fixed sections were stained with an anti-GFP, anti-dsRed or an anti-mCherry primary antibody[3] (Living Colors®). The antibody signal was amplified by using a secondary antibody labelled itself with GFP or a red fluorophore (Tetramethylrhodamine or Alexa

---

[3]As EYFP is a derivative of GFP and mCherry one of dsRed, they have sequence homologies (Shaner et al., 2004) and can therefore be detected by anti-GFP and anti-dsRed antibodies, respectively.
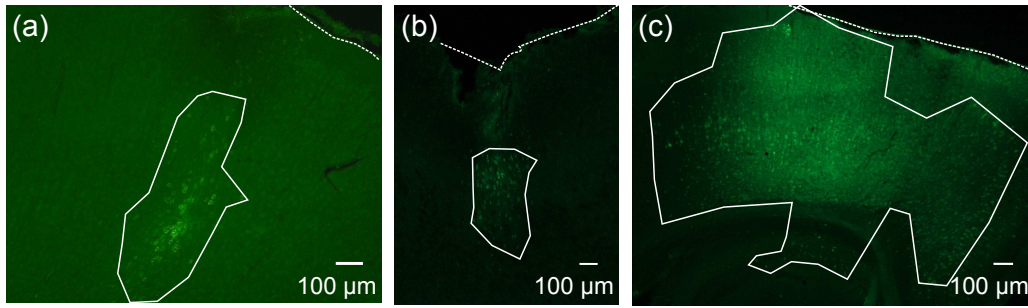
Figure 4.8: **Comparison of expression levels in cortex.** Fluorescence Micrographs at 10x magnification obtained from cortex of animals injected with **(a)** LV-CCK-NpHR2.0-EYFP, **(b)** LV-Camk2a-NpHR2.0-EYFP and at **(c)** 5x magnification showing expression of AAV-eNPAC. Continuous line denotes the area of fluorescence, dashed line the pial surface. Slices were counterstained with anti-GFP antibodies and AF 488 secondaries to amplify the GFP signal; n=1; injection volume 1–1.25 µl.

| Cortex | LV-Camk2a-NpHR2.0-EYFP | AAV5-eNpHR3.0-2A-ChR2-EYFP (eNPAC) |
|---|---|---|
| Viral Titre | $10^8$ IU/ml | $2 \times 10^{12}$ IU/ml |
| Injection Volume | 1.25 µl | 1 µl |
| Expression Volume | 0.04 mm$^3$ | 0.09 mm$^3$ |

Table 4.1: **Comparison of expression in cortical slices injected with LV vs. AAV (n=1).**

Fluor 589). Only the areas of direct injection were studied: Calculation of

volume of expression was performed by measuring the area exhibiting strongly

fluorescent neurons under 5x or 10x magnification in all slices available for one

animal and computing the volume by multiplying the areas with the thickness

of the slice. Since all slices showing fluorescence were examined, the result

should therefore represent the entire volume of viral expression (Fig. 4.8 and

Table 4.1 for results in cortex, Fig. 4.9 and Table 4.2 for results in hippocampus).

Expression volumes were greatest in AAV injected animals, approximately

five-fold of the values obtained in areas injected with Camk2a lentivirus.

However, 1 in 3 animals injected with AAVs showed diffuse axonal staining
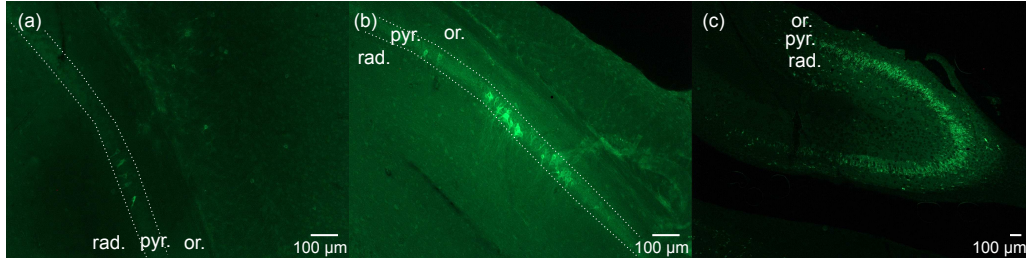
Figure 4.9: **Comparison of expression levels in hippocampus.** Fluorescence micrographs showing extent of expression in hippocampus (n=1) injected with 1.5 µl of either **(a)** LV-CCK-NpHR2.0-EYFP, **(b)** LV-GAD67-NpHR2.0-EYFP (both 10x magnification), or **(c)** 1 µl AAV-eNPAC (5x magnification). Slices were counterstained with anti-GFP antibodies and AF 488 secondary antibodies to amplify the GFP signal. Stratum radiatum (rad.), pyramidale (pyr.; dotted lines) and oriens (or).

| Hippocampus | LV-CCK-NpHR2.0-EYFP | LV-GAD67-NpHR2.0 EYFP | AAV5-eNpHR3.0-2A-ChR2-EYFP (eNPAC) |
|---|---|---|---|
| **Viral Titre** | $10^8$ IU/ml | $10^8$ IU/ml | $2 \times 10^{12}$ IU/ml |
| **Injection Volume** | 1.5 µl | 1.5 µl | 1 µl |
| **Expression Volume** | $0.009\,\mathrm{mm}^3$ | $0.013\,\mathrm{mm}^3$ | $0.08\,\mathrm{mm}^3$ |

Table 4.2: **Comparison of expression in hippocampal slices injected with LVs carrying different promoters and LV vs. AAV (n=1).**

rather than expression of virus in cell somata. The interneuron-promoter driven opsins had the lowest levels of expression.

### 4.4.2 Evaluation of Promoter Specificity

The quantitative data described here are based on observations of fluorophore labelling in confocal or fluorescent micrographs: To count and score cells, the fluorophores were sequentially visualized, then their images merged in RGB space. Slices from adult male GAD67-GFP mice expressing GFP in interneurons were used as positive controls (Fig. 4.10) . I found LV-Camk2a-NpHR2.0-EYFP to be specific for pyramidal cells (Aravanis et al., 2007), with ~74 % of LV-Camk2a-NpHR2.0-EYFP-expressing cells staining for CaMKIIα-antibody (38/51 cells). The GAD67- and CCK-driven constructs were counted in the hippocampus, because of the better penetration of the anti-GAD67 antibody into hippocampal slices compared with cortex[4]. LV-GAD67-ChR2-mCherry was found not to be selective for interneurons in CA1 and CA3 with only 2.6% of GABA-antibody stained cells also expressing LV-GAD67-ChR2-mCherry (Fig. 4.11a, Fig. 4.12a-cdelete: 4.11a). Conversely, 3% of pyramidal cells stained with anti-CaMKIIα also expressed LV-GAD67-ChR2-mCherry (Fig. 4.11a,4.12 d-edelete:4.11a).

Strong dendritic expression and spread to dentate gyrus (DG) was noted, although the latter was most likely due to virus spread rather than retrograde transport into mossy fibres, as there is no evidence so far that VSVg pseudotyped lentiviruses are transported in a retrograde fashion (Mazarakis et al., 2001; Wong et al., 2004). LV-GAD67-NpHR2.0-EYFP was found to be expressed in only ~15% of hippocampal GABA positive interneurons, but also in ~10% of CaMKIIα positive neurons (Fig. 4.11b, Fig. 4.13 delete:4.11b) . LV-CCK-ChR2-mCherry was found to stain only very few neurons in the hippocampal pyramidal layer, and was difficult to find on microscopy. Only 4

---

[4]Some antibodies had a low penetration into the myelinated cortex compared with the hippocampus, which did not improve despite varying the concentration of the permeabilizing agent.
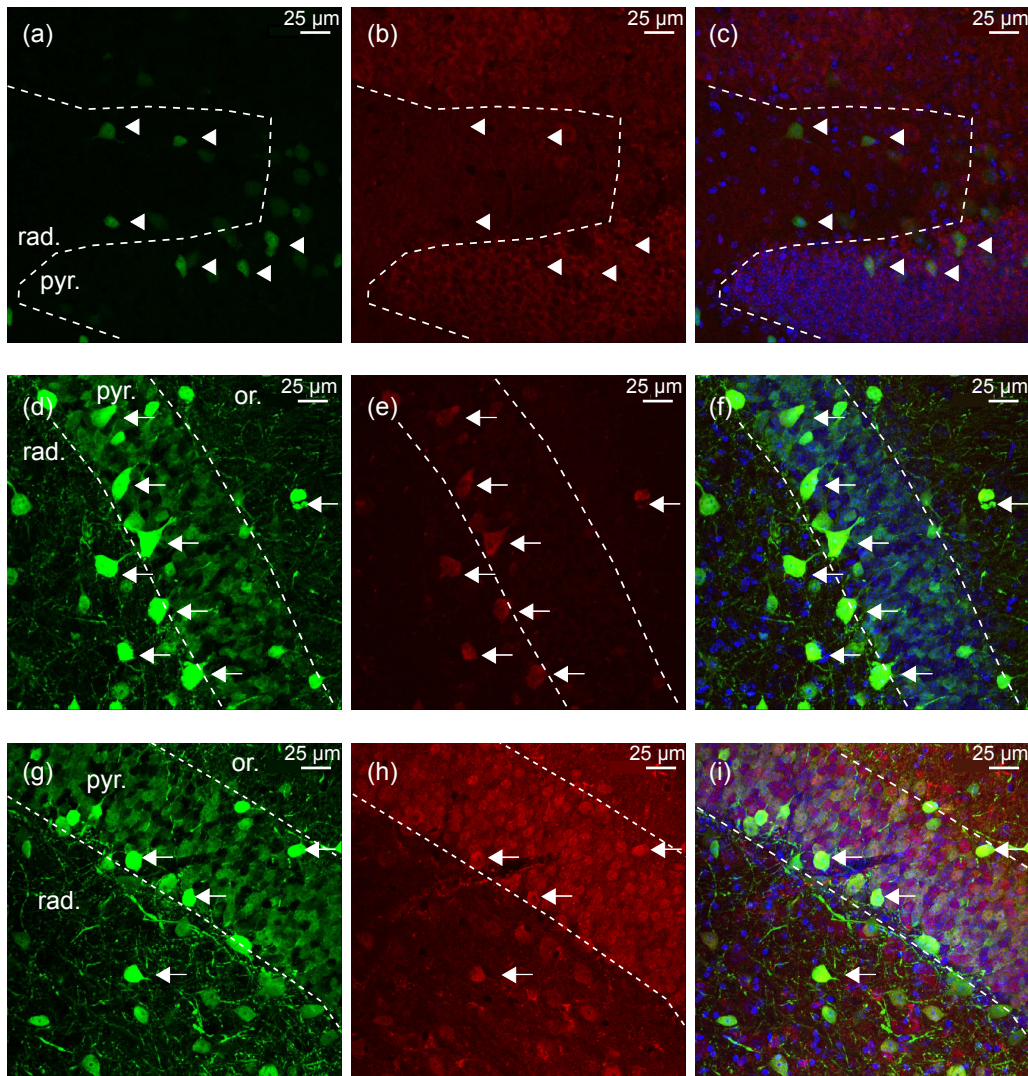
Figure 4.10: **Immunohistochemistry on control sections.** Fluorescent micrographs from GAD67-GFP mice used as positive controls for anti-GAD67, anti-CCK and anti-CaMKIIα antibodies (n=1 animal). **(a), (d), (g)** Interneurons expressing GFP under the GAD67 promoter. **(b)** Anti-CaMKIIα stains neurons in the pyramidal layer of the hippocampus (n = 97) and none of the neurons expressing GFP (n = 23; arrowheads). **(c)** shows overlay images of the green (a), red (b) and blue (DAPI) channels. **(e)** All GABA-antibody stained neurons (n = 14) expressed green fluorescence (arrows). **(f)** showing overlay images of (d), (e) and the blue (DAPI) channel. **(h)** CCK-antibody stained neurons **(i)** overlay image: 80% (7/9) of CCK-antibody stained neurons (red) expressed GFP (green) . One third of GFP expressing interneurons (green) also stained for CCK-antibody (9/27; arrows). Stratum radiatum (rad.), pyramidale (pyr.; dotted lines) and oriens (or).
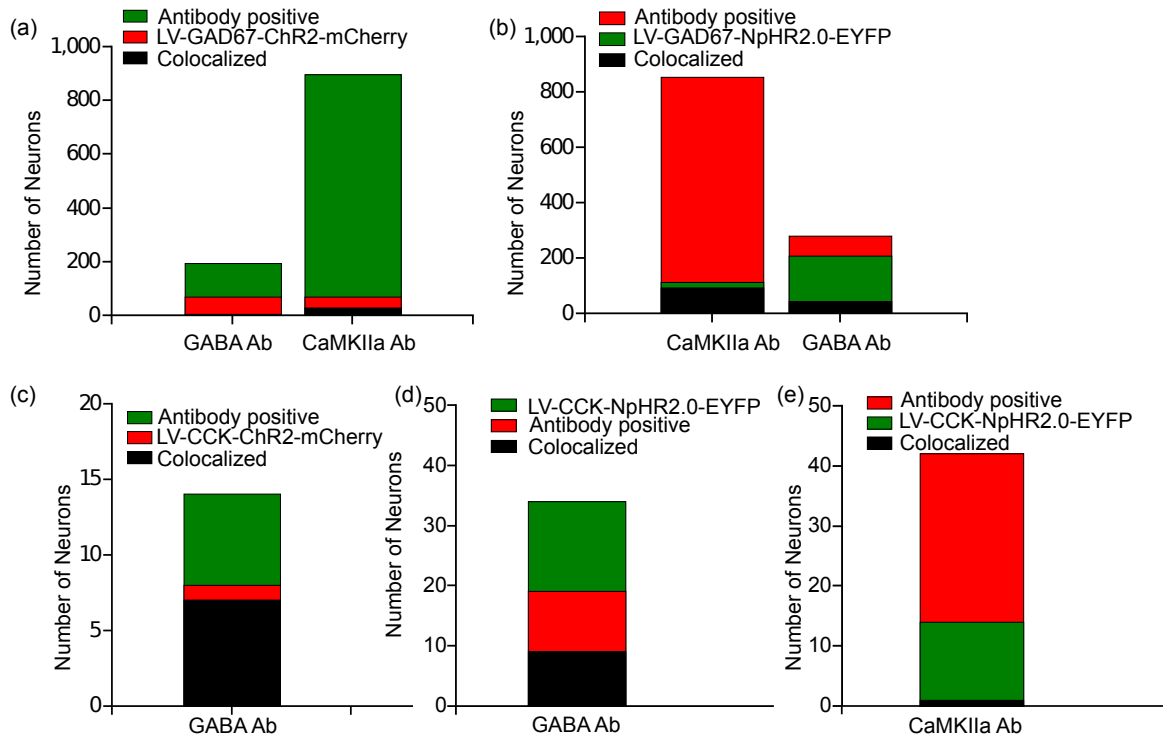
Figure 4.11: **Colocalization data. (a) LV-GAD67-ChR2-mCherry:** Only 5/193 (20 visual fields (VFs), 3 slices, 1 animal) anti-GABA antibody stained neurons also expressed LV-GAD67-ChR2-mCherry. 27/895 anti-CaMKIIα antibody stained neurons also expressed LV-GAD67-ChR2-mCherry (15 VFs, 2 slices, 1 animal). **(b) LV-GAD67-NpHR2.0-EYFP:** 91/852 anti-CaMKIIα antibody stained neurons also expressed LV-GAD67-NpHR2.0-EYFP (12 VFs, 2 animals). 43/279 anti-GABA antibody stained neurons also expressed LV-GAD67-NpHR2.0-EYFP (23 VFs, 3 animals). **(c) LV-CCK-ChR2-mCherry:** 7/14 anti-GABA antibody stained neurons also expressed LV-CCK-ChR2-mCherry (4 VFs, 1 animal). 7/8 LV-CCK-ChR2-mCherry positive cells stained for anti-GABA antibody. **(d) LV-CCK-NpHR2.0-EYFP:** 9/19 anti-GABA antibody stained neurons also expressed LV-CCK-NpHR2.0-EYFP (1 VF cortex and 2 VFs hippocampus, 3 animals). **(e) LV-CCK-NpHR2.0-EYFP:** 1/42 anti-CaMKIIα antibody stained neurons also expressed LV-CCK-NpHR2.0-EYFP (4 VFs, 1 animal).
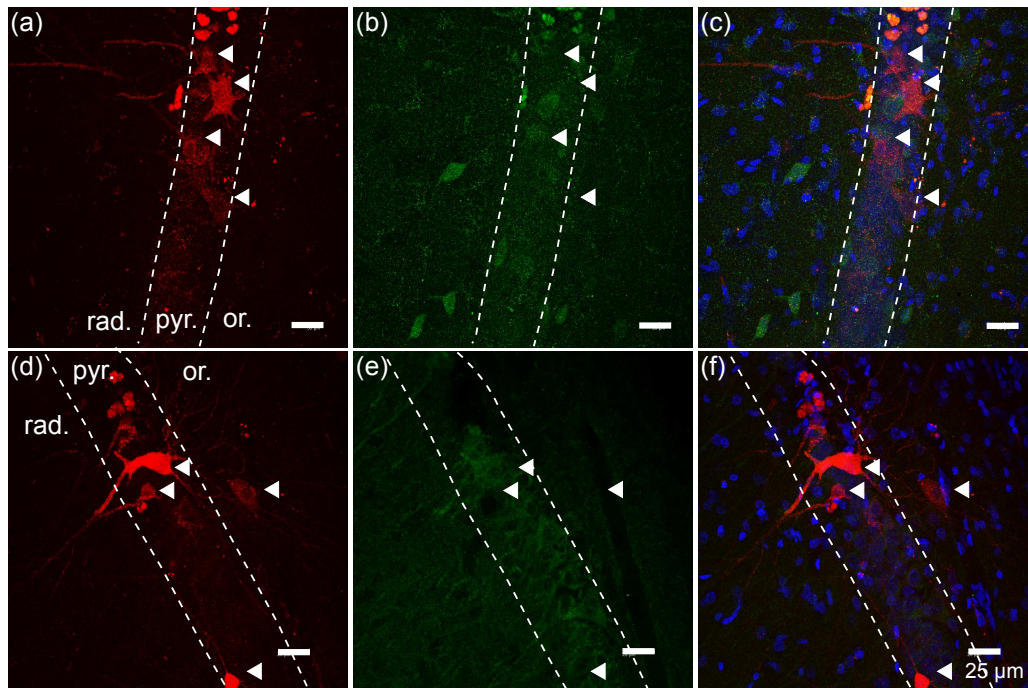
Figure 4.12: **Immunofluorescence study of LV-GAD67-ChR2-mCherry in hippocampus.** **(a)** LV-GAD67-ChR2-mCherry-expressing neurons in red (arrowheads), **(b)** anti-GABA positive interneurons in green and **(c)** overlay (with DAPI) show that LV-GAD67-ChR2-mCherry is not specific for GABAergic interneurons. **(d)** LV-GAD67-ChR2-mCherry-expressing neurons in red (arrowheads) are not stained with **(e)** anti-CaMKIIα antibody. **(e)** Anti-CaMKIIα antibody positive pyramidal cells in green and **(f)** overlay with DAPI to visualize cell nuclei. The scale bar is 25 μm for all images. Stratum radiatum (rad.), pyramidale (pyr.; dotted lines) and oriens (or).

Figure 4.13: **Immunofluorescence of colocalization of LV-GAD67-NpHR2.0-EYFP in hippocampus.** **(a)** LV-GAD67-NpHR2.0-EYFP-expressing neurons in green (arrowheads), **(b)** anti-CaMKIIα positive pyramidal cells in red and **(c)** overlay with DAPI to visualize cell nuclei. Approximately 10% of anti-CaMKIIα stained neurons also express LV-GAD67-NpHR2.0-EYFP. **(d)** LV-GAD67-NpHR2.0-EYFP-expressing neurons in green (arrowheads), **(e)** anti-GABA positive interneurons in red and **(f)** overlay (with DAPI) show that LV-GAD67-NpHR2.0-EYFP is not specific for GABAergic interneurons. The scale bar is 25 μm for all images. Stratum radiatum (rad.), pyramidale (pyr.; dotted lines) and oriens (or).
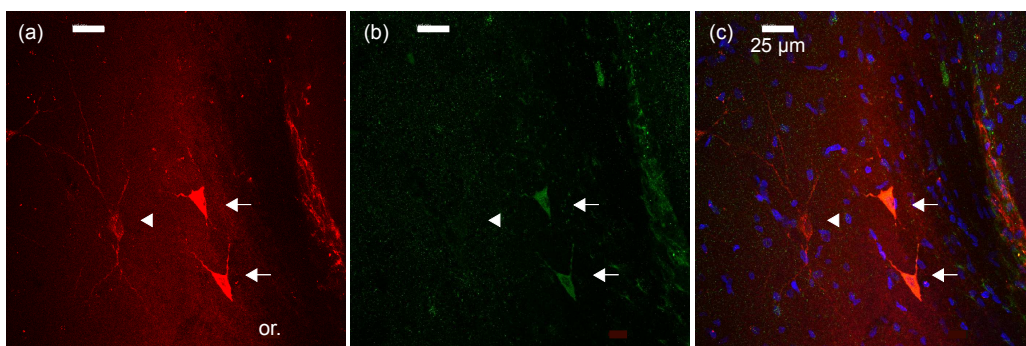


Figure 4.14: **Immunofluorescence and colocalization of LV-CCK-ChR2-mCherry in stratum oriens (or). (a)** LV-CCK-ChR2-mCherry-expressing neurons in red (arrows), **(b)** anti-GABA positive cells in green and **(c)** overlay with DAPI to visualize cell nuclei. Arrowhead points to LV-CCK-ChR2-mCherry positive neuron, which does not co-localize with GABA antibody stained cells. The scale bar is 25 μm for all images.
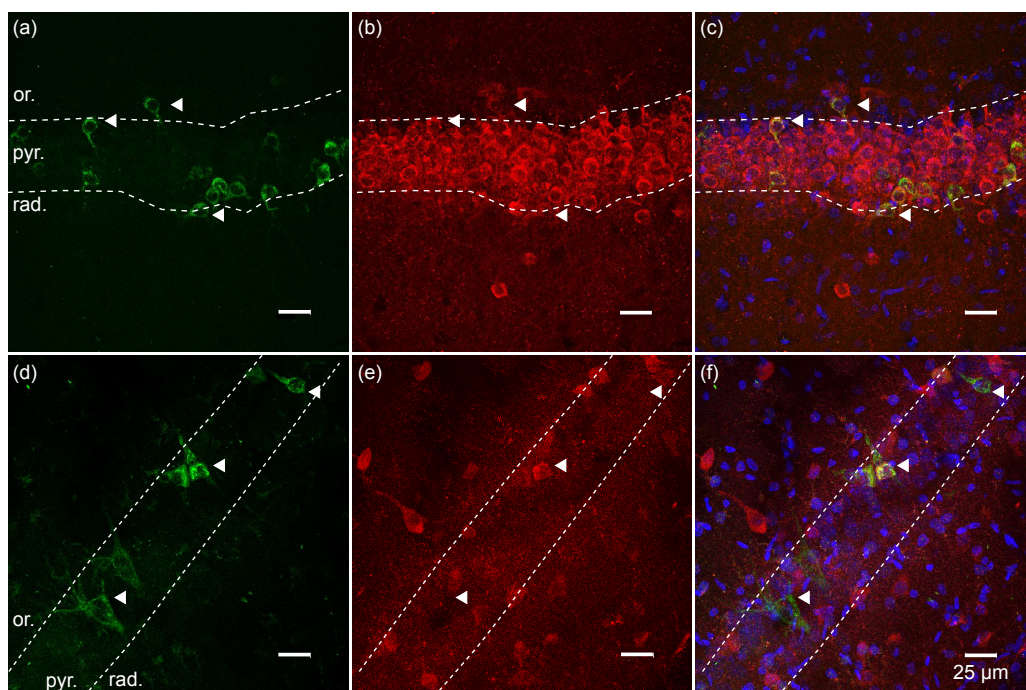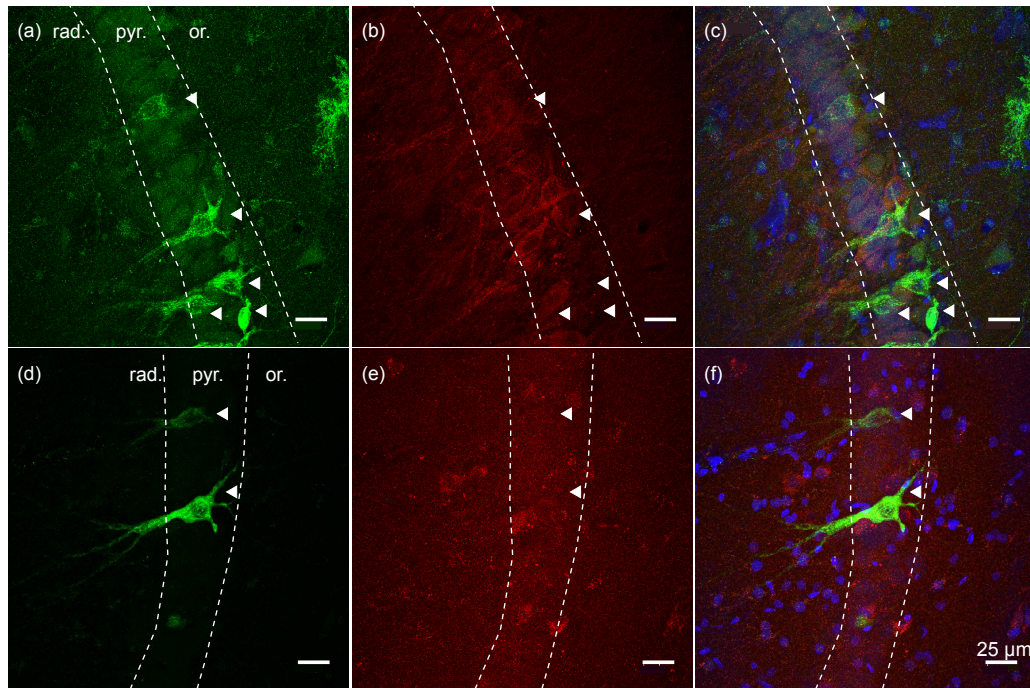
Figure 4.15: **Immunofluorescence of colocalization of LV-CCK-NpHR2.0-EYFP in hippocampus. (a)** LV-CCK-NpHR2.0-EYFP-expressing neurons in green, **(b)** anti-CaMKIIα positive pyramidal cells in red and **(c)** overlay with DAPI to visualize cell nuclei. Arrowheads points to LV-CCK-NpHR2.0-EYFP-expressing neurons, which do not colocalize with anti-CaMKIIα antibody stained cells. **(d)** LV-CCK-NpHR2.0-EYFP-expressing neurons in green, **(e)** anti-GABA positive interneurons in red and **(f)** overlay (with DAPI). Arrowheads points to LV-CCK-NpHR2.0-EYFP-expressing neurons, which do not colocalize with anti-GABA antibody stained cells. Stratum radiatum (rad.), pyramidale (pyr.; dotted lines) and oriens (or).

VFs were evaluated in hippocampus, with 7/8 LV-CCK-ChR2-mCherry positive cells (in red) also stained with anti-GABA (Fig. 4.11c, Fig. 4.14 delete: 4.11c).

LV-CCK-NpHR2.0-EYFP appeared to be slightly more specific for interneurons but the numbers of transduced cells was small. 47% of anti-GABA antibody-stained cells also expressed LV-CCK-NpHR2.0-EYFP (Fig. 4.11d and Fig. 4.15 delete: 4.11d). 2.4% of anti-CaMKIIα antibody stained neurons also expressed LV-CCK-NpHR2.0-EYFP in hippocampus (Fig. 4.11e and 4.15 delete: 4.11e). The CCK antibody failed to stain neurons in these sections and could not be evaluated.

Finally, AAV5-eNpHR3.0-2A-ChR2-EYFP (eNPAC) was evaluated:

approximately 30% of all AAV-eNPAC-expressing cells stained for anti-GABA antibody (34/112 cells, 2 VFs). 70% of all AAV-eNPAC expressing cells stained for anti-CaMKIIα antibody (108/154 cells). Evaluated separately, 67.5% of all anti-CaMKIIα stained cells also expressed AAV-eNPAC (108/160 cells). Approximately 83% of all anti-GABA stained cells also expressed AAV-eNPAC (34/41 cells, 2 VFs).

In conclusion, *in vivo* the GAD67 and CCK promoter-driven constructs expressed at lower levels than the Camk2a-driven opsins and were not specific for interneurons. AAV-eNPAC expressed in larger volumes than LV in cortex and hippocampus, and stained both interneurons and pyramidal cells.

## 4.5   Optical Requirements and Development of a Laser Setup

Immunohistochemistry directed against mCherry confirmed that all ChR2-mCherry constructs were detectable. Why the NpHR 2.0-EYFP and ChR2-mCherry lentiviral constructs in acute slices had different expression levels presented a puzzle, as all viruses had been made in the same batch and had similar viral titres. Different batches were tested and different volumes of injection (up to 2 μl in the hippocampus). In addition, using a Cre recombinase/floxed opsin approach by co-injection of a LV-CCK-Cre recombinase and a double floxed ChR2-mCherry lentivirus under a strong promoter[5] gave the same results. I was using an LED system for combined fluorescence visualization/opsin excitation on the rig (OptoLED light source, Cairn Research) at this stage. Since I was also having difficulties in photoactivating the clearly visible NpHR2.0-EYFP constructs with an amber LED, it seemed plausible that both the light intensity for the mCherry excitation and for the NpHR2.0 photoactivation were too low at maximum LED current.

---

[5]This was done to test the hypothesis that expression of Cre recombinase, even if weak, would be sufficient to invert the floxed ChR2-mCherry sequence in the second lentivirus, thereby allowing expression of the construct under the strong promoter (see Appendix Fig. A.2).
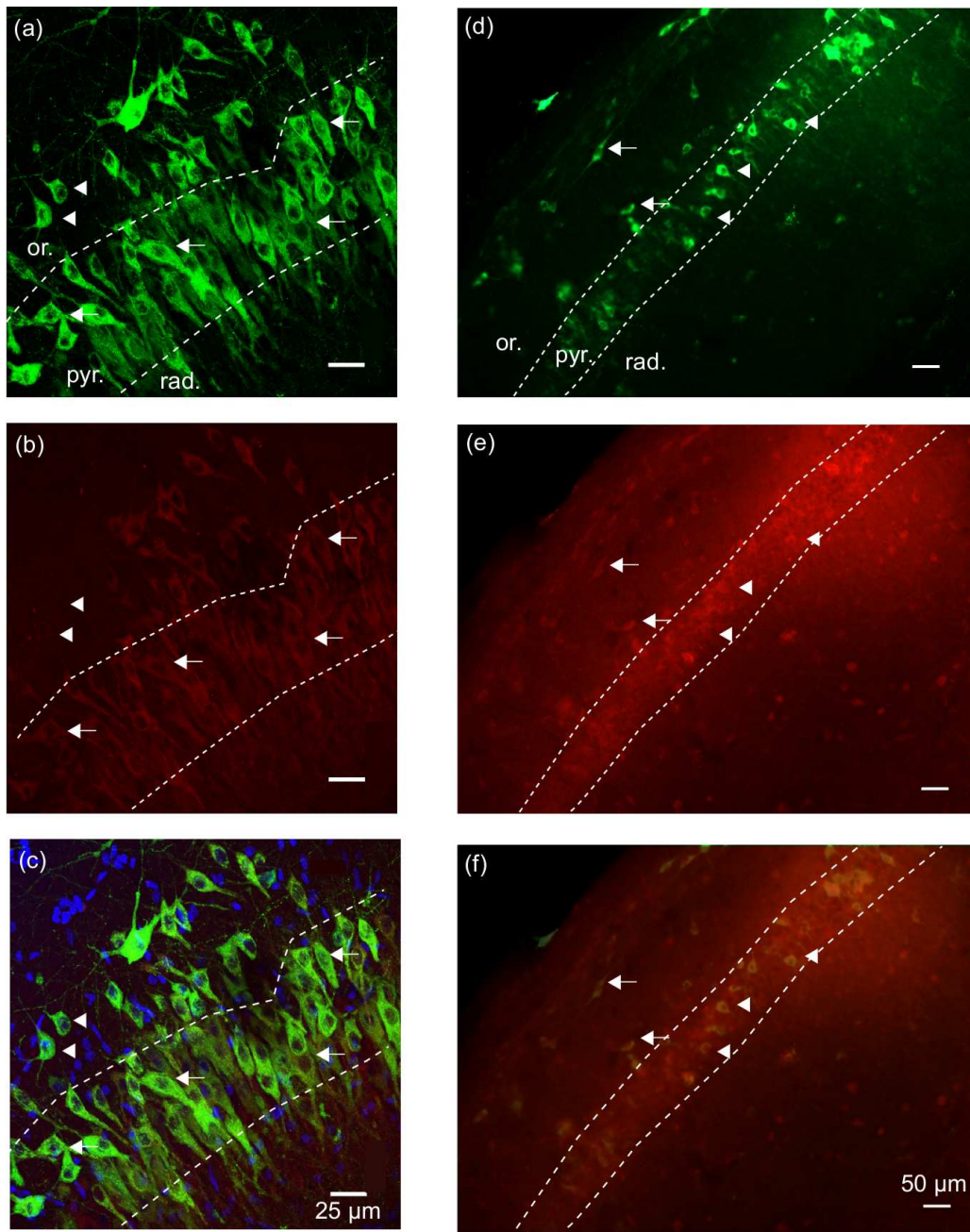
Figure 4.16: **Colocalization of AAV-eNPAC. (a)** Confocal fluorescence micrographs showing expression of AAV-eNPAC (in green) and **(b)** anti-CaMKIIα stained pyramidal cells in red. Arrows point to AAV-eNPAC expressing (green) neurons stained with anti-CaMKIIα antibody (red). Arrowheads point to AAV-eNPAC-expressing (green) neurons, which do not stain for anti-CaMKIIα antibody (red). **(c)** overlay (with DAPI to identify cell nuclei), scale bar 25 μm for a-c. **(d-f)** Fluorescence micrographs showing expression of **(d)** AAV-eNPAC (green) in neurons, which also stain for **(e)** GABA-antibody (in red; arrows). **(f)** overlay of (d) and (e). Arrowheads point to AAV-eNPAC-expressing (green) neurons not stained with anti-GABA antibody. The scale bar for (d) and (e) is 50 μm. Stratum radiatum (rad.), pyramidale (pyr.; dotted lines) and oriens (or).

Initially I tried to increase the light intensity measured with a power meter (Thorlabs) at the level of the microscope chamber by changing the excitation filters, to optimize light transmission, as well as trying a brighter amber LED that had just come out on the market (Jan-Feb 2011) and by trying various permutations of excitation filters/LEDs/dichroic mirrors (Table 4.3) . I then visualized slices from parvalbumin (PV)-TomatoRed transgenic mice and pipettes filled with AF 594 as a control for the visualization of red fluorescence, comparing them to the fluorescence intensity from a mercury burner on a colleagues' microscope and concluded that the mercury burner provided far higher intensities of light. In addition, I had used AAV5-eNPAC for patch-clamp experiments as a control and managed to excite ChR2 with the 473 nm blue LED, but not at the level of temporal precision and the degree of depolarization expected (Gradinaru et al., 2010), whilst I remained unable to optically activate NpHR3.0 in the same construct with LEDs. A period of intense exchange with other laboratories using opsins followed, including Marco Capogna's at Oxford (successfully using an LED system for activation of ChR2 of commercial AAV expressed in slices) and Karl Deisseroth's at Stanford (only using mercury burners or lasers on their set-ups). I concluded that I needed to increase the light intensity on the microscope set-up. To optimize the optical system with help from Georg Ritter, I reinstalled a mercury burner (BX-FLA, Olympus) on my microscope, achieving light intensities greater than with the LED by an order of magnitude (Table 4.4). An ideal set-up would have allowed me to visualize fluorescence with a mercury burner and flash the opsins with a mercury burner or a laser. However, a fast shutter was not available to generate light pulses with the mercury burner, and could not have been mounted because of space restrictions inside the Faraday cage. Flashing the opsins with a Cairn Xe-Flash system and a self-built optrode (optic fibre attached to patch pipette) was attempted, but was also unsuccessful because the power supply could not be triggered precisely and because the light intensity fluctuated excessively. The Xe-arc lamp also generated excessive electrical

| LED setup | Wave-length [nm] | Power‡ [mW] | Irradiance‡ [mW mm$^{-2}$] | Power‡ [mW] | Irradiance‡ [mW mm$^{-2}$] |
|---|---|---|---|---|---|
| **‡ at Objective** | | **40x** | | **10x** | |
| 572nm emitter / amber LED | 593 | 0.59 | 2.95 | 2.43 | 0.63 |
| 560 nm emitter / amber LED | 593 | 0.23 | 1.15 | 0.87 | 0.23 |
| 560 nm emitter / white LED | 593 | 1.71 | 8.55 | 6.8 | 1.77 |
| White LED and 660 dx | 593 | 1.2 | 6 | 10.58 | 2.75 |
| Amber LED and 660 dx | 593 | 0.33 | 1.65 | 7.4 | 1.92 |
| eEndow GFP filter and blue LED | 488 | 2.6 | 13 | 10.5 | 2.73 |

**Irradiance requirement (Irradiance [mW mm$^{-2}$] at 40x**

| | | |
|---|---|---|
| ChR2 | | 8–12 (Boyden et al., 2005) |
| NpHR2.0 | | 21.7 (Zhang et al., 2007b) |

Table 4.3: **Light requirements and LEDs.** Light requirements of opsins and fluorophores, and the intensities achieved with the LED system at the chamber, measured with a power meter (Thorlabs). LED light was used at maximal intensity and current (blue LED 1 A, white LED 0.96 A, amber LED 1.01 A). To get maximal light intensity for NpHR, a 560 and a 572 nm emitter mirror were tested with an amber or white LED, respectively; 660 dx = 660 nm dichroic mirror; compare with light intensities required by opsins (Aravanis et al., 2007; Berndt et al., 2009).

| Fluorescence filter | Wavelength [nm] | Power‡ [mW] | | Irradiance‡ [mW/mm² ] | |
|---|---|---|---|---|---|
| ‡at Objective | | 10x | 40x | 10x | 40x |
| endow GFP | 488 | 29.3 | 6 | 7.618 | 30 |
| EYFP | 514 | 11.8 | 2.5 | 3.068 | 12.5 |
| HcRed | 587 | 147 | 45.2 | 38.22 | 226 |
| HcRed | 593 | 139 | 29 | 36.14 | 145 |
| 660 Dichroic Mirror alone | 593 | — | 66 | — | — |

Table 4.4: **Mercury burner light intensity.** Light intensities achieved with the Olympus Mercury burner through the microscope objective.

noise, which made it difficult to record from cells. It became clear that it was necessary to develop a modular system that would allow laser light to be fed into the microscope, whilst maintaining the mercury burner for fluorescence visualization. The lasers were however kept separated from the setup, in order to use them for the *in vivo* part of the project. The following modular set-up was therefore designed and assembled with help from G. Ritter: a lens tube system consisting of a microscope port adapter, cage rods, a focussing lens, together with a fiber optic mating sleeve (all Thorlabs) were mounted onto the second camera port of an Olympus dual-port adapter above the fluorescence illuminator (Fig. 4.17). This allowed coupling of the optic fibres running from the laser head to the fiber optic mating sleeve at the top of the lens tube system, whilst keeping the lasers and optic fibres independent from the microscope set-up. The irradiance values obtained with laser stimulation under the 10x Objective were 0.3–9 mW for the 473 nm laser, 0.06–13.5 mW for the 561 nm laser and 0.76–13 mW for the 593 nm laser. Figure 4.18 shows the calibration line for the 561 nm laser. It is important to note that there is considerable power loss through coupling the light into optic fibres and the type of the optic fibre ending, core size, numeric aperture and coupling have to be chosen with care to minimize losses.
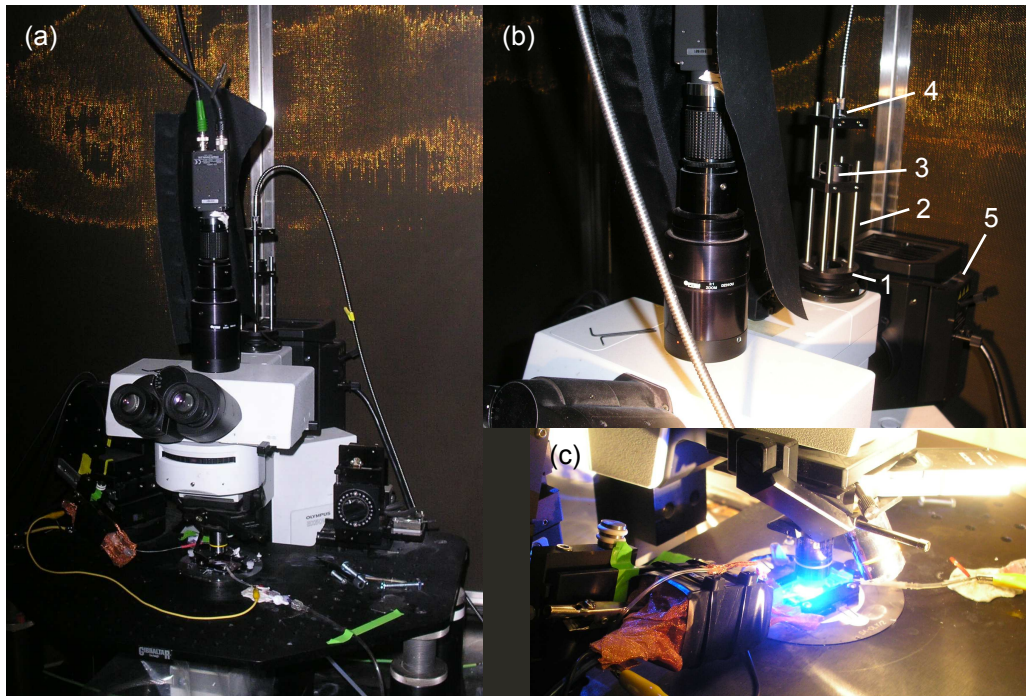
Figure 4.17: **Optogenetic microscope setup. (a)** Olympus BX50WI microscope setup, front view. **(b)** Detail of the lens tube system consisting of a microscope port adapter (1), cage rods (2), a focussing lens (3), together with a fiber optic mating sleeve (4) (all Thorlabs) mounted onto the second camera port of the Olympus dual-port adapter above the fluorescence illuminator (5). This allowed coupling of the optic fibres running from the laser head to the fiber optic mating sleeve at the top of the lens tube system, whilst keeping the lasers and optic fibres independent from the microscope set-up. The first port of the Olympus dual-port adapter is used for visualization with a CCD camera, whilst the fluorescence illuminator (Olympus BX-FLA) is attached to the rear port of the microscope. **(c)** 488 nm light delivered through the 60x water immersion objective (LUMPLFL 60x W/IR/0.90, Olympus) to the slice preparation.
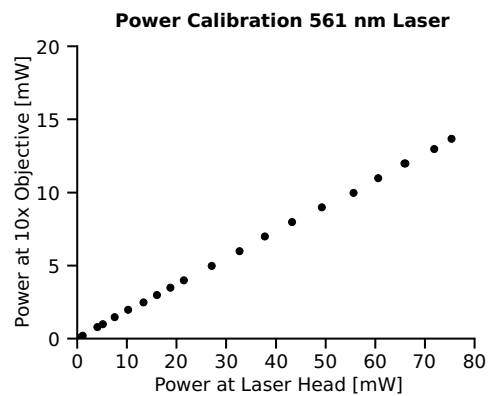


Figure 4.18: **Calibration of the 561 nm Laser.**

## 4.6 Neurophysiology and Optogenetic Activation in Slices

Successful optogenetic experiments were performed in acute slices strongly expressing AAV5-eNPAC (containing both ChR2 and NpHR3.0) in hippocampus. Using the Cairn LED system, it was possible to photoactivate ChR2 in AAV5-eNPAC-expressing cells with the blue 470 nm LED and an 470/40x excitation filter.

At the maximum LED current of 0.9 A, the irradiance[6] was of <10 mW/mm$^2$ under the 40x objective. Only at maximal LED current of 0.9 A was depolarization possible (Fig. 4.19a, b). A minimum LED light duration of 50 ms was required to drive APs; with trains of 10 ms pulses at 10 Hz there were many AP failures (Fig. 4.19 b). In contrast, previous reports have shown that ChR2(H134R) within the eNPAC construct is capable of driving firing at up to 20 Hz with 5 ms pulses (Gradinaru et al., 2010). Pulses lasting 1 ms elicited subthreshold depolarizations but could not generate trains of action potentials. Conversely, when flashed with a blue 473 nm laser (CNI Laser), short 1 ms laser pulses were able to drive reliable action potentials (Fig. 4.19 c, d, 4.20e; Irradiance calibrated prior to experiments to be 5 mW/mm$^2$). The 561 nm green laser (CrystaLaser), however, was unable to activate NpHR3.0 and did not inhibit firing but instead co-activated ChR2. This phenomenon can be explained by the overlap of the activation spectra of ChR2 and NpHR3.0 at 561 nm, resulting in photocurrents of cations and chloride in the same direction to

---

[6]Irradiance or power density is defined as the light intensity in mW per illuminated area of view in mm$^2$. The irradiance over the area of view of the objective, can be calculated as follows:
  field diameter = field number/magnification of objective
  The field number can be found on the eyepieces and for the BX 50 microscope is 22
  Calculation for a 40x objective:
  field diameter = 22/40
  field diameter = 0.55 (for 10x objective field diameter = 2.2)
  area of view with 40x objective:
  A=2$\pi$(0.55/2)$^2$
  A=0.23 mm$^2$ (for 10x obj A=3.8)
  meaning that if you get 1mW over the detector area, in theory you should get that 1mW over your area of view (Irradiance) =>
  Irradiance = 5mW/mm$^2$ (for 10x Obj Irradiance= 0.26mW/mm$^2$).
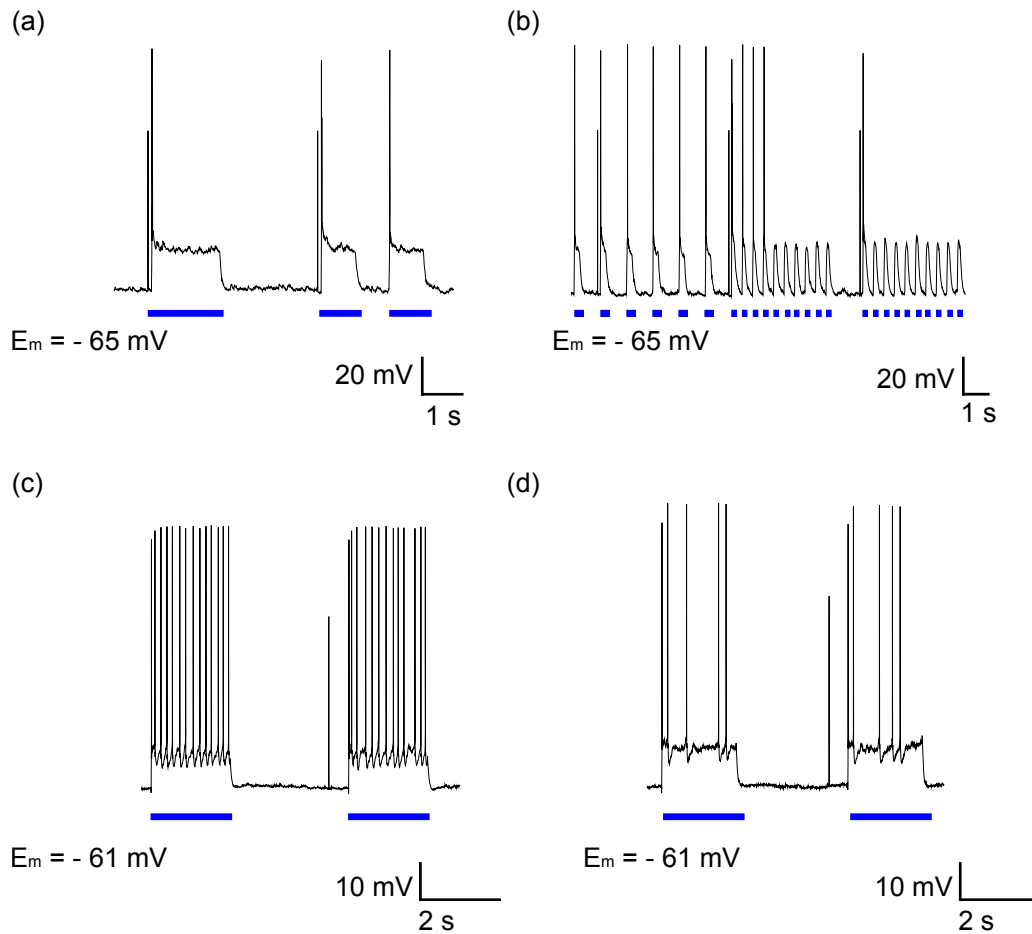
Figure 4.19: **Optogenetic experiments in slices -1. (a-b)** Current clamp traces of cortical neuron expressing AAV5-eNPAC 5 weeks post AAV injection illuminated with a blue LED. **(a)** A 2 s and two 1 s pulses of 473 nm LED light depolarize the neuron above threshold, but only 1 AP is triggered. **(b)** Six 50 ms pulses elicit reliable spiking, whilst 10 ms light pulses are unable to consistently drive action potentials. **(c-f)** Laser experiments **(c)** Sample trace of a CA3 pyramidal neuron expressing AAV5-eNPAC illuminated with 2 s pulses of 473 nm light (irradiance 5 mW/mm$^2$) at the beginning of a 13 min protocol (2 pulses, 1 Hz). **(d)** The last two traces at the end of the stimulation protocol show a reduction in the number of APs fired from a mean of 13.6 at t = 0, to a mean of 5 at t = 13 min. The decrease in the number of APs may be due to laser instability or opsin desensitization. Membrane potential ($E_m$).
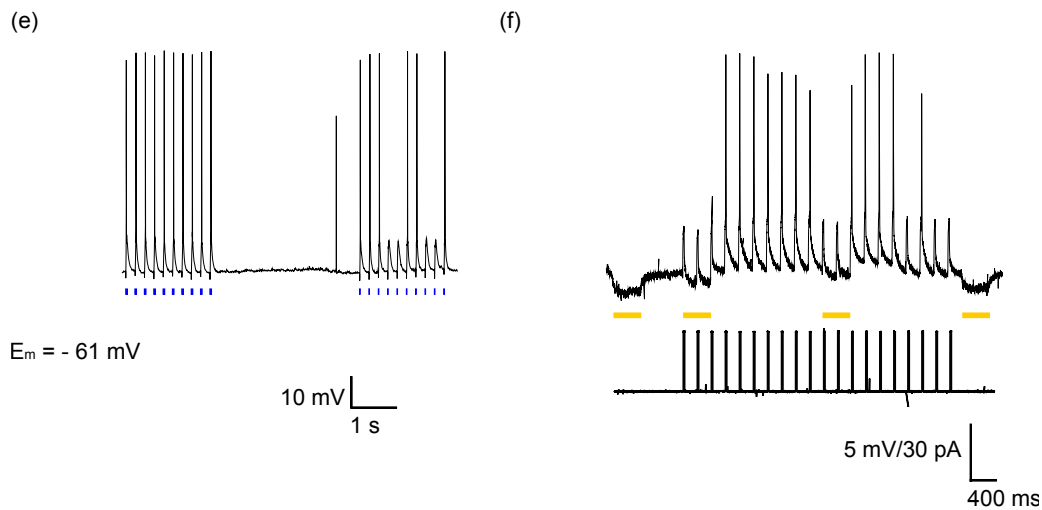
Figure 4.20: **Optogenetic experiments in slices -2.(e)** 5 ms blue laser pulses (left part of trace) reliably drive spike firing, and even 1 ms pulses (right part of trace) are able to elicit APs. **(f)** A CA1 neuron expressing AAV5-eNPAC is stimulated with a 593 nm laser (13 mW at 10x objective). Yellow light hyperpolarized the membrane (400 ms pulse duration), albeit by only by 2.5 mV, and inhibited action potential firing during current injection (30 pA, 20 ms pulses). Membrane potential ($E_m$).

cancel each other out (for the excitation of NpHR3.0 stimulation at the very end

of the spectrum was advised - personal communication, V. Gradinaru, Stanford)

(Gradinaru et al., 2010). After purchase of a longer wavelength 593 nm yellow

laser (Laser 2000), it was possible to successfully depolarize the resting

membrane potential and to independently activate NpHR and inhibit spike

firing elicited by current injection (Fig. 4.20delete: 4.19f)[7].

## 4.7 Discussion

In this final section of the chapter I will discuss the differences in

adeno-associated and lentiviral expression of opsins, the results of the

interneuron-targeted strategies and some of the reasons behind the difficulties

in visualizing and photoactivating opsin constructs.

My experiments have shown that constructs delivered with AAV serotype 5

were strongly expressed within the hippocampus and cortex and and over a

---

[7]The yellow laser had no analogue modulation input and had to be switched on and off manually.

wider spatial extent than when delivered with lentiviruses. AAV serotype 2 and 5 are known to transduce mostly neurons (Flotte and Berns, 2005) and diffuse spread of virus also has the advantage that a single injection would be sufficient for experimental or therapeutic purposes. On the down side, however, in our hands roughly 30% of animals injected with AAV only showed diffuse axonal staining but no somatic fluorescence. All animals had had the same type, volume and batch of virus injected on the same day of surgery and rats were of the same age and the same litter. The reasons for this difference are not clear, but it is known that since recombinant AAVs do not contain viral genes, the fate of viral DNA depends on the presence of host cell polymerases and therefore on the state of the cell. In addition, AAVs have a hitherto unexplained differential neuronal tropism, not only due to the specificity of the promoter, but also influenced by capsid proteins and other sequences[8]. Certainly, if the mechanisms of this tropism were known, they could be exploited to effectively target gene delivery. The reason to use lentiviral vectors in my project was the advantage of their large transgene capacity (8-10 kb in LVs vs 4.5 kb in AAVs), which would have allowed one to shuttle the relatively large GAD67 and CCK promoter sequences (3.5 and ~3 kb, respectively). As discussed in the introductory chapter, there are ways to split larger transgenes onto 2 complementary AAVs. However the techniques are complex, and the success rate in generating the constructs perhaps lower. Also, if considering viral vectors as therapeutic tools, LVs are relatively invisible to the immune system, as they do not carry or cause expression of viral proteins in transduced cells, whilst AAVs can cause generation of neutralizing antibodies. This really is the main obstacle to using AAVs for repeated therapeutic applications. However, AAVs have the powerful advantage of site-specific integration, which avoids the risks of insertional mutagenesis carried by LVs. Eventually, it will be

---

[8]Some authors have claimed a general bias of AAVs towards inhibitory neurons and of LVs towards excitatory neurons. However there is no conclusive evidence to prove this interesting thought: many other authors have used AAVs to target excitatory neurons and the bias of LVs towards interneurons has not been replicated in other studies (Nathanson et al., 2009).

important to continue working on both types of vectors, in order to make better tools but also better treatments: manipulating capsid proteins of AAVs may be a way to reduce the immune response and increase neuronal specificity, whilst among the lentiviral secrets to unravel are how, for example, the secondary intermediate RNA structure of the virus influences its packaging, what variables determine LV packaging efficiency and titres (Neve, 2011), and whether the LTRs could be modified in order to achieve site-specific integration to avoid disruption of genomic sequences. An alternative approach would be the use of non-integrating lentiviral vectors, which has proven successful in delivering transgenes to dendritic cells as a vaccine carrier in mice (Hu et al., 2009, 2010), or herpes simplex virus, which give reliable expression in neurons, can carry a large payload (up to 100 kb) and are capable of retrograde transport. But ultimately, before being able to use any viral vector for human use, we will need to achieve controllable regulation of expression and manage to produce clinical grade viruses on a large scale and at affordable prices.

On immunofluorescent and morphological criteria, expression of the GAD67-promoter driven constructs was not specific for interneurons in slices and cultures. The CCK-driven constructs may be slightly more specific for interneurons as a whole in slices and for CCK interneurons in ganglionic eminence (GE) neuronal cultures, but the numbers of neurons stained are too small to make inferences. In the hippocampus, GABA is specific for interneurons, making up 7–11% of all neurons (Freund and Buzsáki, 1996). In the adult central nervous system, GAD67 and GAD65 colocalize with GABA in most if not all GAD-positive cells, although GABA is also known to be expressed in non-neuronal cells (Katarova et al., 1998), more so in the periphery (Erdö and Wolff, 1990). GAD67 and GAD65 are expressed and colocalize with GABA as early as E10.5, showing that embryonic GABA is synthesized by the same enzyme isoforms present in the adult (Katarova et al., 2000). CCK is already expressed at prenatal day 14 (Giacobini and Wray, 2008), and persists

throughout postnatal migration (Morozov et al., 2006). Therefore, postnatal neuronal cultures should have been capable of expressing the GAD67/CCK-driven constructs. Expression of the constructs only succeeded in GE neuronal cultures. However, whilst using the same virus, this was not the case in postnatal hippocampal cultures (neither wildtype, nor in GAD67-GFP mice). Conversely, the Camk2a-driven constructs expressed in both GE and hippocampal cultures. Whilst there is evidence in the literature that some promoters may be correctly regulated in transgenic mice but not in cultures (Katarova et al., 1998), this clearly should have applied to both pre- and postnatal types of culture. Both types of culture were plated on PDL-coated coverslips (i.e. without astrocytic support) and transduced on day 7 *in vitro*, therefore neither type of culture could be considered as mature from a point of view of synaptic connections and GABA and glutamatergic synaptic events. Perhaps the only difference is that the number of interneurons is much higher in GE neuronal cultures; therefore the virus transduces fewer principal cells that will not be able to express the construct, thereby allowing visible expression of fluorescence in interneurons.

In the *in vivo* experiments, two problems need addressing: Firstly, why expression of the GAD67/CCK constructs was not specific for interneurons, and secondly, why the Camk2a-ChR2 constructs were not visible in acute slices. To answer the first question, I would first like to focus on the GAD67 promoter, described by Katarova et al. (Katarova et al., 1998) and made available to us by S. Kasparov, Bristol. The promoter used in my experiments contains 3.7 kb of 5′ upstream sequences of the GAD67 promoter, containing the first intron and part of the second exon, and has been used to target GABAergic nucleus of solitary tract interneurons in organotypic slice cultures (Teschemacher et al., 2005). However, as discussed previously, the original authors also showed that only by including longer 5′ upstream regulatory sequences, did GAD67 drive correct expression of reporter genes. Transgenic mouse lines containing 3 to 7 kb of 5′ upstream sequences of the GAD67 promoter (called short and intermediate

constructs) showed variable staining of hippocampal interneurons at best, as well as ectopic expression (in hippocampal pyramidal neurons e.g. that express low levels of GAD mRNA (Cao et al., 1996)), and even the longest construct showed patterns of mixed correct and ectopic expression both in the hippocampus and the cortex, whilst correctly labelling cerebellar Purkinje cells (Katarova et al., 1998). In an attempt to test whether my constructs would correctly express in Purkinje cells, I injected the rat cerebellar vermis but was unable to obtain any expression, in concordance with previous results on the "short construct" (Katarova et al., 1998). Also, evaluating expression at different time points did not alter the pattern of expression. I would therefore argue that the GAD67 promoter, in the form I used it, may contain all regulatory sequences for correct expression in brain regions of high GABA content, which develop early (Katarova et al., 1998) but not for specific targeting of interneurons in the hippocampus or cortex. The CCK promoter, on the other hand, has been used to label interneurons of the hippocampus and the basolateral amygdala (Chhatwal et al., 2007; Jasnow et al., 2009). On a closer look, however, previous authors convincingly show hippocampal staining of the interneuron-rich polymorphic layer of the dentate gyrus (whilst the excitatory granule cell layer is not stained), which co-localizes with CCK-mRNA in situ hybridization. However, CCK-mRNA in-situ hybridization shows strong staining throughout the pyramidal cell layer of CA1 and CA3, and the authors have not confirmed whether these neurons are indeed interneurons (Chhatwal et al., 2007; Jasnow et al., 2009). In this sense, having used the same CCK promoter (gift of K. Ressler), LV-CCK-NpHR2.0-EYFP shows the same good expression in the polymorphic layer of the dentate gyrus but in CA1 they only stain very few cells, which are undoubtedly pyramidal, both in their morphology and antibody staining pattern. In addition, the LV vector used is not a self-inactivating vector[9]; therefore even at the viral level, both promoters

[9]As discussed in footnote 1 at the beginning of this chapter, SIN have a chimeric LTR, where the HIV promoter was replaced with transcriptional control elements from heterologous viral (e.g.CMV) or cellular promoters (Federico, 2003): when DNA provirus integrates into the host

GAD67 and CCK may have been influenced by the 5' LTR promoter. Furthermore, CCK-mRNA is found in the somata of neurons in many brain regions, including CA3 pyramidal cells, albeit without expression of the octopeptide (Schiffmann and Vanderhaeghen, 1991), indicating that staining for the octopeptide, rather than using in situ hybridization, is more specific to detect expression of the actual neurotransmitter. Other authors have tried alternative promoters, e.g. using small promoters from *Takifugu rubripes* (fugu) to restrict expression specifically to interneurons, with the advantage that they could be used in AAV vectors because of their small size (Nathanson, 2009). However, interneurons were identified mainly morphologically and without quantitative data as to the percentage of interneurons stained by the fugu-AAV. More work is required to understand which and how regulatory elements determine promoter function. This will allow us to use promoters or their regulatory elements to target specific cell subtypes.

The last questions to address include 1) why it was not possible to visualize the ChR2-mCherry constructs or to photoactivate NpHR driven by GAD67/CCK, and 2) what really are the photoactivation requirements of opsins. My hypotheses for the difficulty in visualizing ChR2-mCherry is that expression levels were too low to become visible or that the protein was misfolded, since the antibodies targeted to mCherry revealed that the protein had been expressed. Protein misfolding could be explained by the fact that I used a ChR2 of an early generation, and that subsequent ChR2 versions have been improved. It is likely that NpHR could not be photoactivated with the LED system because of the higher light requirements and smaller photocurrents of NpHR2.0. NpHR2.0 has recently been superseded by NpHR3.0 . It might well be that with NpHR3.0 and other (better) opsin inhibitors on the market, light from an LED system will be sufficient to inhibit neuronal firing. This would greatly facilitate *in vivo* (and clinical) applications. Overall, (and in hindsight) it is important to test the adequacy of the flashing system as one of the key parameters when

cell genome, expression will only depend on the internal promoter.

using optogenetic tools. In later experiments in collaboration with F. Cacucci and T. Wills, UCL, we measured the 470 nm laser output by looking at the photodiode sensor/power meter output. We also fed the voltage from the power meter box directly into an oscilloscope. Both studies revealed a very noisy laser output trace, which could be explained by problems in the cavity geometry - a known problem in diode laser design (material temperature coefficients, long term distance stability, mechanical shocks, etc.) or crystal damage (personal communication). More worryingly, it became clear that the laser took 1–2 s to reach full power. It became also clear that when using short pulses of 5–10 ms, the light intensity achieved would have been a lot smaller than at steady state. This implies that some of the experiments might have failed due to lack of light to the preparation. Undoubtedly, many of these problems will be overcome with the development of better and more affordable light sources.

# Chapter 5

# Optogenetic Induction and Entrainment of CA3 Oscillating Networks

The experiments discussed in this chapter were aimed at understanding the dynamical properties of CA3 networks by answering the following questions:

1. Can gamma oscillations be induced in the hippocampus by optogenetic activation of excitatory neurons (by analogy with experiments in cortex (Adesnik and Scanziani, 2010))?

2. How do optogenetic induced gamma oscillations compare with carbachol-induced oscillations?

3. Are phase-response curves derived for optogenetic and electrical alveus/dentate gyrus stimulation consistent with results predicted by the Wilson-Cowan Model?

4. Can gamma oscillations entrain to periodic inputs?

This part of my PhD project was developed and executed in collaboration with T. Akam and E. Ferenczi, and the experiments described form an integral part of
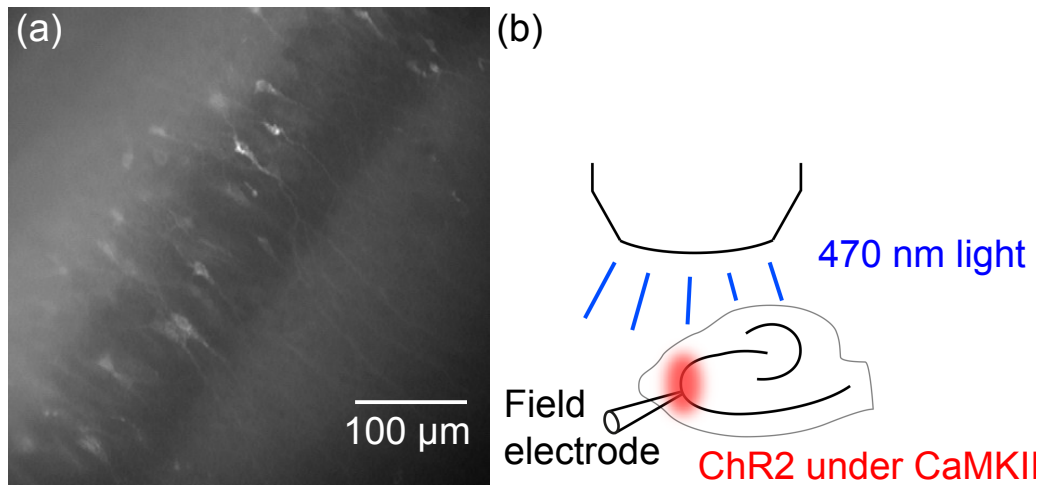
Figure 5.1: **Optogenetic induction of gamma oscillations.** (a) Fluorescent micrograph showing expression of AAV5-Camk2a-ChR2(H134R)-mCherry in the pyramidal layer of CA3. Typically, 4 - 5 sections of 400 µm thickness each would exhibit fluorescence. (b) Schematic of the experimental setup for excitation with 470 nm light from an LED coupled to the microscope **(Akam et al., 2012)**.

T. Akam's project aimed at testing the predictions of a computational model to confirm its accurate description of large scale coherence dynamics *in vivo* (Akam and Kullmann, 2010). E. Ferenczi performed the alveus stimulation experiments under supervision of T. Akam. Because this was a collaborative project to which my contribution was the development and application of optogenetic tools, I shall describe the results relatively briefly. They are published in (Akam and Kullmann, 2010). Experimental procedures are described in detail in the method section. Since a newer generation ChR2 had become available in AAV (ChR2(H134R) (Gradinaru et al., 2007)), we employed this novel vector in these experiments. Briefly, we injected postnatal day 20 (p20) male Sprague-Dawley rats with AAV5-Camk2a-ChR2(H134R)-mCherry into dorsal and ventral CA3, which resulted in widespread somatic red fluorescence in the pyramidal layer (Tye et al., 2011; Lee et al., 2010) of CA3 (Fig. 5.1). Some 30% of the animals, however, showed diffuse fluorescence throughout CA3 and no somatic staining. This may have been due to variability of the viral aliquot (titre, damage to the virus through handling) or uneven distribution of viral particles in the syringe, which was usually pre-filled to be used to inject 2 animals in the same session.
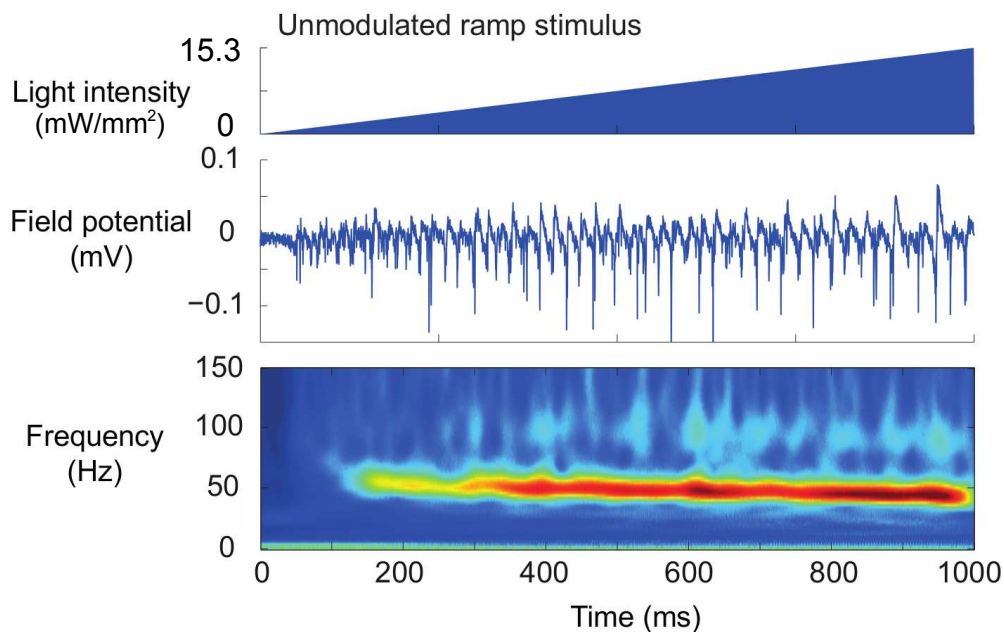
Figure 5.2: **Induction of gamma oscillations by ChR2 activation (Akam et al., 2012).** A 1 s ramp of blue light (top panel) elicits gamma oscillations of 52.6 ± 5.1 Hz (middle panel), n=7. The bottom panel shows the average wavelet transform amplitude (12 traces, 1 slice).

Stimulation of ChR2 was performed by delivering a 1 s ramp of blue light with a blue LED (Cairn Instruments) coupled through the epifluorescence illuminator of a Zeiss Axioscope microscope. To deliver the light ramp, the LED current was kept in the linear input-output range with the light intensity delivered to the slice ranging from 0 to $< 15.3 \, \text{mW}/\text{mm}^2$ irradiance. Ramps were delivered every 45 seconds. A ramp was delivered instead of a square pulse to avoid channel desensitization (Adesnik and Scanziani, 2010). The recording field electrode was placed adjacent to the pyramidal cell layer of CA3 where maximum fluorescence was visible.

## 5.1   Induction of Gamma Oscillations by Light

Stimulation of CA3 pyramidal cells with ramps (0–15.3 mW/mm$^2$ irradiance) of 470 nm blue light for 1000 ms induced self-organized oscillations in the gamma range (n=7, Fig. 5.2). The light stimulus imposed the start and end of the
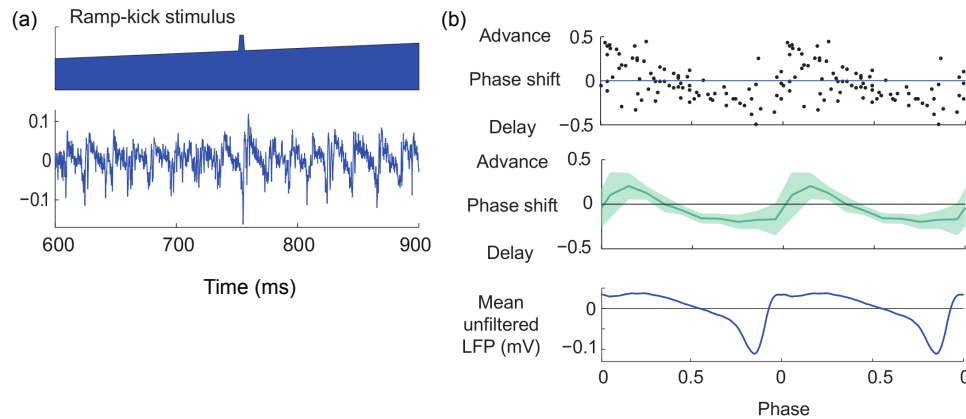
Figure 5.3: **Optogenetic rephasing of gamma oscillations (Akam et al., 2012).**
**(a)** Light intensity and local field potential (LFP) during a ramp-kick experiment,
consisting in a 5 ms boost of light intensity by 20–40% (of the immediately pre-
ceding ramp value) at 500 or 750 ms into the ramp stimulus. **(b)** The stimulus
induces a biphasic response curve as demonstrated in a single slice (top panel)
and a population (middle panel, n = 4, 95% confidence interval in shaded green)
aligned with the mean unfiltered LFP (bottom panel).

rhythmic activity, but not its frequency[1].

## 5.2    Rephasing of Gamma Oscillations by ChR2

To analyze the effect of the light stimulus on the CA3 gamma oscillation, we

evaluated the phase response curve (PRC). The phase of an oscillation is defined

as the time $\varphi$ elapsed relative to the origin of the oscillation. $\varphi$ is normalized by

the period $T$ of the oscillation, and is therefore given as a variable between 0

and 1 (Winfree, 1967). A PRC shows the alteration of the phase of an oscillation

due to a stimulus as a function of the oscillation phase. Delivering a light "kick"

stimulus to an oscillating slice elicited a biphasic phase response curve. This

implies that the ChR2-activated conductance advances or delays the phase of

the gamma oscillation depending on the timing of the perturbation (Fig. 5.3).

---

[1]Note that the frequency of the ChR2-induced gamma oscillations was higher than that in-
duced by carbachol (Akam et al., 2012) as in Appendix Fig. A.3, suggesting that, although both
light activation of ChR2 and carbachol activated pyramidal neurons, the network effect on oscil-
lation frequency was different, perhaps because different subsets of interneurons were activated
(Pálhalmi et al., 2004) or because carbachol depolarized interneurons directly (Pitler and Alger,
1992).

## 5.3 Comparison with Carbachol-induced Gamma Oscillations in CA3

We then asked, how optogenetically-induced gamma oscillations compare to carbachol-induced gamma oscillations and their PRCs. These experiments were performed by T. Akam and E. Ferenczi. In brief, gamma oscillations were induced in CA3 by perfusing slices with 20 μM carbachol. The LFP was recorded in CA3 and 60-100 stimuli delivered with bipolar electrodes in the alveus or dentate gyrus every 1.5–2 s (Fig. 5.4a). We found that carbachol-induced gamma oscillations also exhibit biphasic PRCs on weak alveus stimulation, but that the maximum phase advancement occurs later than in optogenetically-induced oscillations (Fig. 5.4b, c).

Strong alveus stimulation led to resetting of the oscillation, independent of stimulus phase (Fig. 5.4d). Stimulation of dentate gyrus led to the same rephasing behaviour with biphasic PRCs on weak stimulation and resetting of the oscillation with strong stimuli (Akam et al., 2012)[2].

## 5.4 Phase Response Curves are Consistent with Predictions from the Wilson-Cowan Model

We proceeded to test if our phase-response curves obtained through optogenetic and alveus/dentate gyrus stimulation were correctly predicted by the Wilson-Cowan Model[3] (Wilson and Cowan, 1972). This is a simple model of

---

[2]Akam and Ferenczi classified stimulation strength based on their effect on the oscillation rather than based on the parameters of the stimulation. One reason for this was that there was no ideal objective measure of stimulation strength: Measures based on the strength of electrical stimulation were problematic because the exact position of the stimulating electrode and how intact the fiber pathway was in the slice would both effect the amount of synaptic input recruited for a given stimulation intensity. Finally, for different strength stimuli in a single slice they observed a qualitative change in the shape of the PRC as the stimulation strength was increased. Therefore they used weak vs strong to describe stimuli that produced these different shape phase response curves. A quantitative measure of stimulation strength based on the effect on the oscillation was introduced at the end in order to combine data from different slices and is discussed in (Akam et al., 2012).

[3]Modelling was performed by T. Akam.
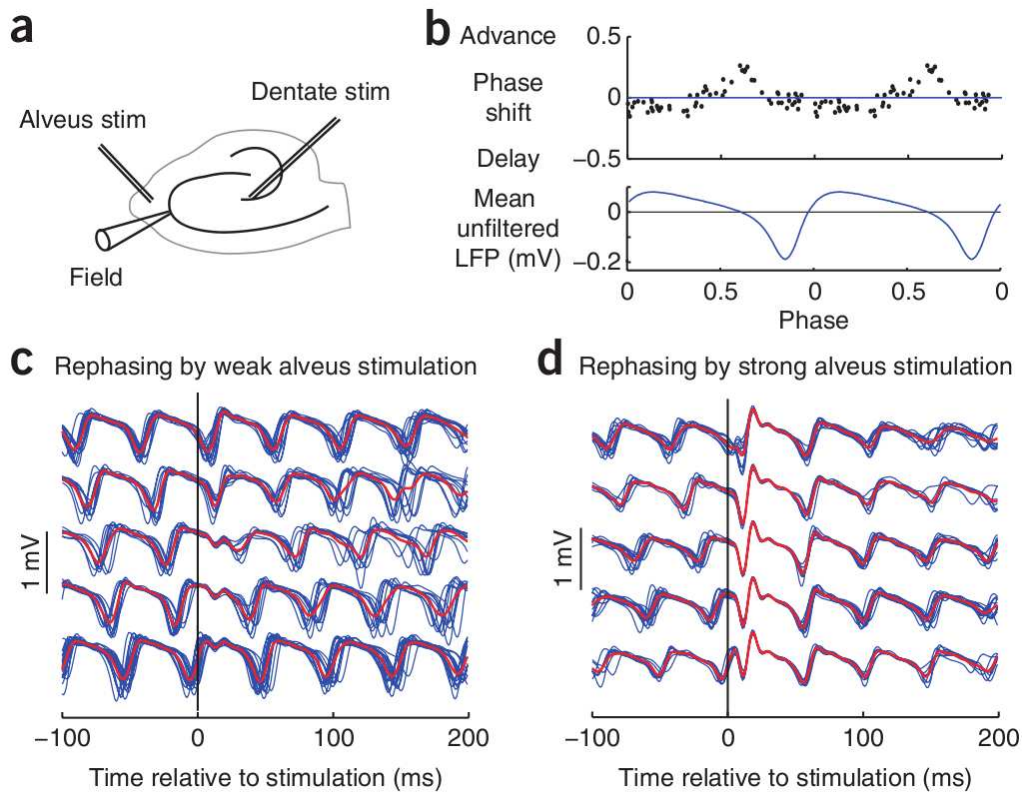
Figure 5.4: **Carbachol-induced gamma oscillations in CA3 (Akam et al., 2012).**
**(a)** Experimental setup for alveus and dentate gyrus stimulation. **(b)** CA3 gamma
oscillations have biphasic PRCs on weak alveus stimulation. The maximum
phase advance occurs later than with optogenetic rephasing. **(c)** Weak alveus
stimulation in one experiment. LFPs (in blue, with superimposed average in red)
grouped according to stimulation phase. **(d)** Strong alveus stimulation leads to
phase resetting (colour coded as in c).
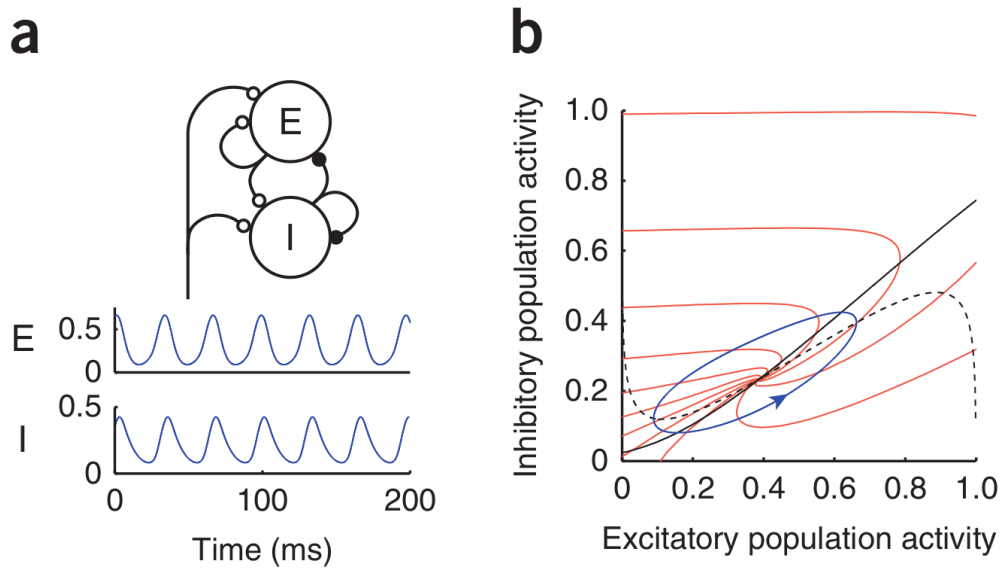
Figure 5.5: **Wilson-Cowan model** (Akam et al., 2012). **(a)** Schematic of the Wilson-Cowan Model depicting a network of excitatory and inhibitory populations of neurons. The bottom panel graphs depict E(t) (the proportion of excitatory cells firing per unit time at the time point t) and I(t) (the proportion of inhibitory cells firing per unit time at the time point t) over time when no noise perturbs the system. **(b)** Phase space diagram describing the state of (a) at any instant with the coordinates E(t) on the x-axis and I(t) on the y-axis. In blue the limit cycle. The limit cycle is a solution for dynamical systems, which repeats itself in time (a dynamical system is a mathematical model describing the evolution in time of a system). Depicted in red the isochrons (a set of parameters resulting in oscillations of the same phase). Nullclines (black: dashed, excitatory; solid, inhibitory; Nullclines are curves through points found solving a parent differential equation, for which the parent equation's slope will always be zero.

neural networks used in computational neuroscience. It is composed of recurrently and mutually connected excitatory and inhibitory populations of neurons (Fig. 5.5a), which are regarded as an oscillator and can be described by a differential equation.

Solutions to the system equations are found numerically. These are graphically depicted in phase plane plots (Fig. 5.5b). Both solutions and phase plane plots describe and predict dynamic interactions of the two populations of neurons. In the model, the two key variables are defined as follows (Wilson and Cowan, 1972): I(t) as the number of inhibitory cells firing per unit time at the time point t, E(t) as the number of excitatory cells firing per unit time at the time point t.
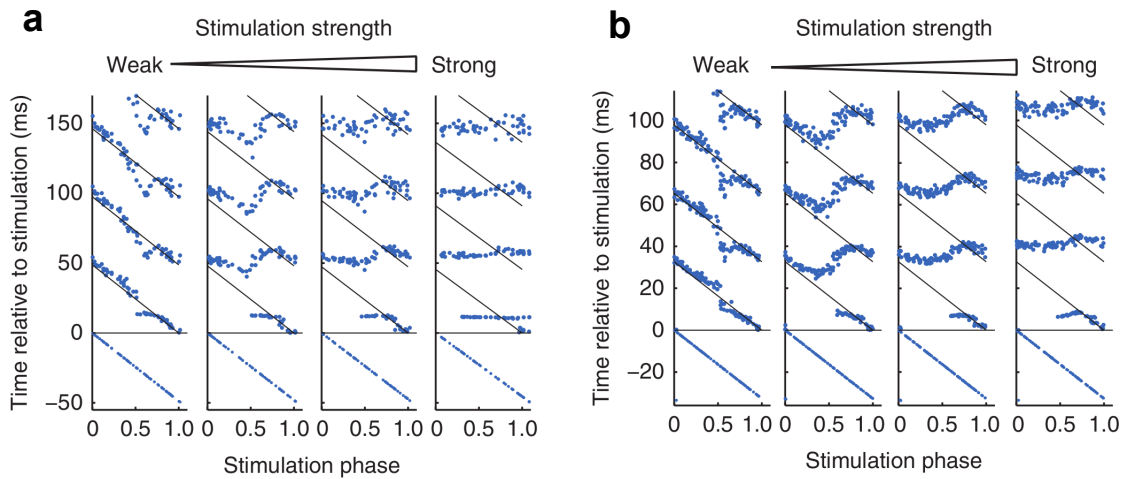
Figure 5.6: **Wilson-Cowan model and alveus stimulation rephasing** (Akam et al., 2012). **(a)** Experimental data on rephasing of gamma oscillation in a hippocampal slice with alveus stimulation of four different strengths. Blue dots represent the troughs of the oscillation and are represented along the x-axis according to the phase before the stimulus. Four troughs are shown for each oscillation after the stimulus (blue dots along a vertical line), with the diagonal grey lines depicting the expected position of the troughs had the stimulus been absent. As shown in Fig. 5.4 there is phase advancement of the oscillation on weak alveus stimulation and resetting of the oscillation to the same phase on strong stimulation. **(b)** Shows Wilson-Cowan model derived graphs for rephasing gamma oscillations on alveus stimulation, which are consistent with experimental data in (c).
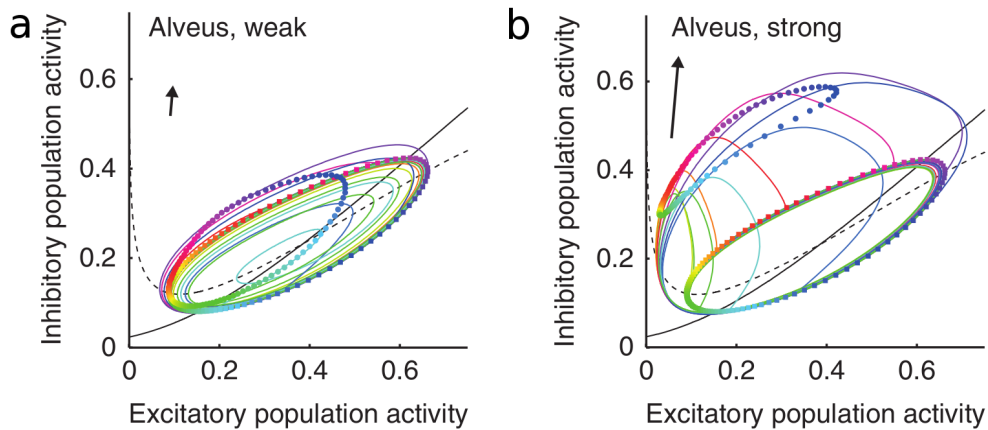


Figure 5.7: **Phase space diagrams for (a) weak and (b) strong alveus stimulation** (Akam et al., 2012). Coloured squares represent positions at the time of alveus stimulation for 100 simulations. Coloured circles represent positions 6 ms after the stimulus. Coloured lines show trajectories of 10 points from the time of stimulation until their return to the original limit cycle. The black vertical arrow describes the direction (ratio of inhibitory vs excitatory input) of the input stimulus.

I(t) and E(t) depend on the number of cells not refractory to stimulation and the amount of synaptic connectivity between the cells. The differential equation also contains variables for the strength of the connectivity between the cells, the amount of external input to excitatory neurons and a term for the stimulus decay. Unperturbed, the synaptic interactions between excitatory and inhibitory populations give rise to an oscillatory state resulting in an anti-clockwise oriented limit cycle in the model's phase space. Very simplistically, the model predicts that if this state is perturbed by a stimulus, this will push the oscillation away from the stable limit cycle.

To understand how the system behaves when perturbed, the concepts of latent phases and isochrons need to be introduced. The latent phase of a point x off the limit cycle is defined as the phase of a point y on the limit cycle, for which trajectories coming off point x and y will converge as t approaches infinity. Lines connecting points with the same latent phase are called isochrons. A stimulus that pushes the oscillation perpendicular to the vertical axis (representing I(t)) towards isochrons of increased latent phase will advance the phase of the oscillation, pushing the oscillation towards isochrons of decreased latent phase will delay the oscillation. If the oscillation is pushed parallel to the isochrons, the phase of the oscillation will not change.

The Wilson-Cowan model correctly predicted the rephasing behaviour for alveus/dentate gyrus and for optogenetic stimulation. The rephasing behaviour after weak alveus stimulation was reproduced in the model by an input that was biased towards the inhibitory population (corresponding to a nearly vertical input vector in the phase plane), thereby advancing the phase of the oscillation, as the limit cycle is pushed in the vertical direction and points on the limit cycle now cross isochrons with an advanced latent phase (Fig. 5.6 and 5.7a). The model also correctly described the resetting of the oscillation phase after strong alveus stimulation (Fig. 5.6 and 5.7b). At the end of the strong stimulus the points on the limit cycle reach new positions. These new positions
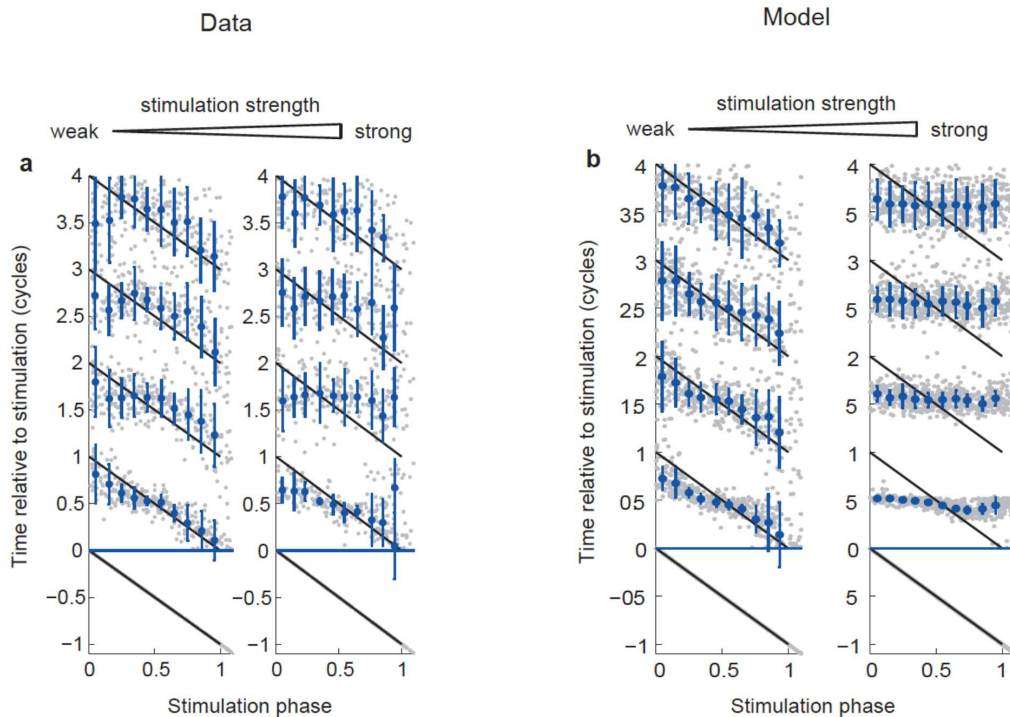
Figure 5.8: **Optogenetic rephasing in the Wilson-Cowan model (Akam et al., 2012). (a)** Experimental data on rephasing of gamma oscillation in hippocampal slices (n=4) with optogenetic stimulation of two different strengths (weak: LED current increment by 20-30%, strong: LED current increment by 40%). Data are represented as in Fig. 5.6c delete: 5.5. Phase advancement of the oscillation occurs earlier in the oscillation phase than on weak alveus stimulation. Strong light stimuli elicited discontinuous PRCs and reset the oscillation to the same phase as on strong alveus stimulation. **(b)** Shows Wilson-Cowan Model derived graphs for rephasing gamma oscillations by optogenetic stimulation, consistent with experimental data in (a).

define a loop that is so displaced compared to the original limit cycle, that only

a fraction of isochrons are crossed. This implies that independent of the phase

before stimulation, a strong stimulus will reset the oscillation to only a small

range of phases. The Wilson-Cowan model also corresponded with the

experimental optogenetic rephasing data as shown in Fig. 5.8 . In this case the

rephasing behaviour was reproduced in the model, if the input stimulus was

targeted more towards the excitatory population, resulting in a PRC with earlier

phase advance.
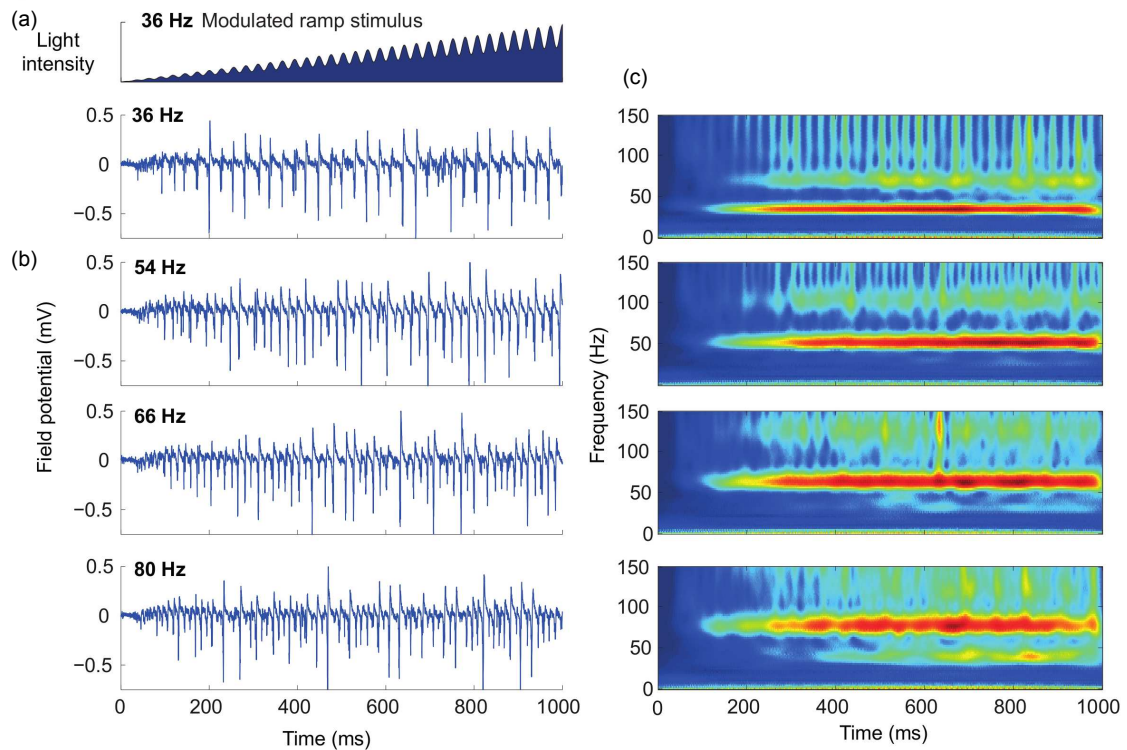
Figure 5.9: **Entrainment of oscillations by modulated ramps (Akam et al., 2012).** **(a)** Light intensity stimulus modulated by a 30 Hz sinusoid. **(b)** LFP entraining at stimulus frequencies between 30 and 80 Hz. **(c)** Averaged wavelet transforms for each frequency (n = 4 slices).

## 5.5 Entrainment of Oscillations by Modulated Light Ramps

Finally, we tested the hypothesis that the gamma oscillation frequency could be modulated or entrained by the frequency of an oscillatory stimulus. We delivered a light ramp with sinusoidal modulation (25% of the stimulus amplitude) at frequencies from 30–80 Hz, which entrained the oscillating local field potential (LFP), as shown in Fig. 5.9. With higher modulation frequencies there was a gradual advancement of the oscillation phase (Gutkin et al., 2005). Figure 5.10 shows that in our experiments, the phase of the LFP trough relative to the modulation cycle is advanced when the modulation frequency is greater than the unmodulated gamma frequency, and retarded when the modulation frequency is smaller than the unmodulated gamma frequency. When the

150
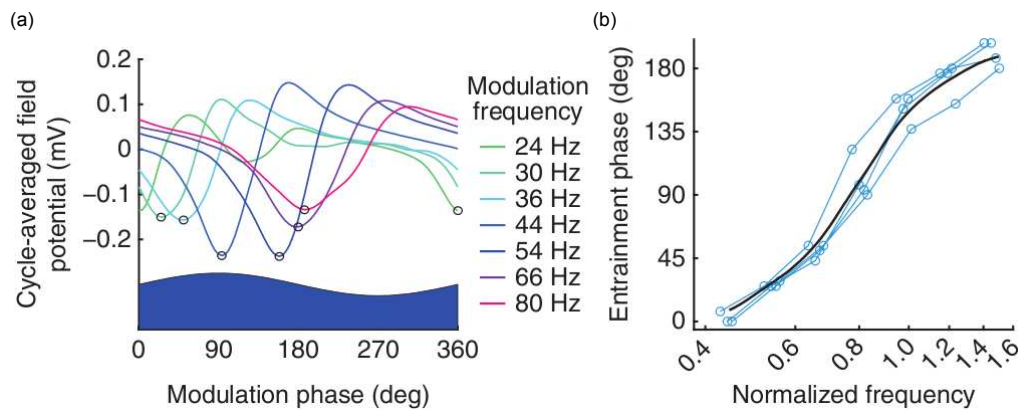
Figure 5.10: **Relationship between LFP phase and modulation frequency (Akam et al., 2012). (a)** The cycle averaged field potentials at each modulation frequency (shown in different colours for each frequency) as a function of the light stimulus modulation phase (bottom blue curve). The relationship between LFP phase and modulation frequency remains constant for each modulation frequency, but there is advancement of the LFP trough (black circles) with modulation frequencies higher than the unmodulated gamma frequency (n = 4 slices). The amplitude of the cycle averaged field potential is maximal at the resonant frequency of 52.6 ± 5.1 Hz. **(b)** Relationship between the entrainment phase and the normalized modulation frequency (Gaussian weighted moving average in black, individual slice data in blue).

modulation frequency approaches the unmodulated gamma frequency of 52.6 ±

5.1 Hz, the amplitude of the LFP is maximal denoting resonance. The

relationship between the trough phase of the LFP and the modulation

frequency is constant. We conclude, that the phase relationship of input

stimulation and output frequency is frequency dependent .

## 5.6 Discussion

In this final section I would like to discuss the answers to the four questions posed at the beginning of this chapter:

1. Can gamma oscillations be induced in the hippocampus by optogenetic activation of excitatory neurons (by analogy to experiments in cortex (Adesnik and Scanziani, 2010))?

2. How do optogenetic-induced gamma oscillations compare with carbachol-induced oscillations?

3. Are phase-response curves derived for optogenetic and electrical alveus/dentate gyrus stimulation consistent with results predicted by the Wilson-Cowan Model?

4. Can gamma oscillations entrain to periodic inputs?

We had set out to explore the characteristics of CA3 networks underlying gamma oscillations. Our original aim was to drive different subclasses of hippocampal neurons at various frequencies, to study how synchronization between local networks is accomplished and what variables influence inter-region coherence of oscillatory activity. We would have liked to drive interneurons and pyramidal cells separately with light of different wavelengths, to disentangle how the two populations interact to generate an oscillation. With the optogenetic techniques available, we were able to accomplish part of the project and studied the influence of excitatory input to hippocampal gamma oscillations. We were able to drive excitatory neurons with ChR2 and show that also in CA3 (Adesnik and Scanziani, 2010) it is possible to generate oscillations in the gamma range. We showed that the PRC of the optogenetically-induced oscillations is biphasic, which is also the case in PRCs obtained on alveus and dentate gyrus stimulation during carbachol-induced oscillations. These results suggest that it may be a general property of CA3 networks to advance or delay gamma oscillations depending on the timing of synaptic input.

We were also able to show how gamma oscillations respond to periodic inputs, a principle that may help explain how oscillation coherence may arise in various brain regions. When driving oscillations with a sinusoidally modulated ramp, the oscillation frequency entrained over a broad range of frequencies. The phase relationship of the LFP trough to the modulation stimulus was strongly frequency dependent. We suggested that modulating the intrinsic oscillation frequency may be a mechanism to modulate the phase relationship of coupled networks. The fact that the modulated ramp was so effective in entraining the oscillation deserves attention, as one may have expected ChR2 to desensitize to the modulated ramp stimulus. Evidently, there was enough ChR2 expressed, so that even if some of the channels inevitably desensitised (within 18 ms) (Lin, 2011), there were still enough in an open or activatable state to generate the LFP oscillation. Most importantly, however, these *in vitro* data reproduced the simulated data computed from a model based on the Wilson-Cowan equations with a transient input pulse developed by T. Akam, confirming that neuronal mass models in general can be used to study synchronization dynamics (Akam et al., 2012). Also in the field of neuronal oscillations, optogenetic and viral approaches will be instrumental in acquiring new answers in the future: they will allow manipulation of oscillatory activity in the live animal and behavioural studies. They will also allow, as in our case, to flexibly tune individual input and output variables in an oscillatory system and thereby field test computational models and theories, a fundamental part of our attempts at understanding network behaviour.

# Chapter 6

# Optogenetic Inhibition of Epileptiform Activity

Epilepsy affects over 50 million people worldwide, of whom only 60–70% are seizure free on medication (Duncan et al., 2006). Pharmacoresistance is common in focal neocortical epilepsy, and resective surgery is only appropriate when the epileptogenic zone does not involve eloquent cortex (Schuele and Lueders, 2008). Because seizures are intermittent, developing a method for rapid and reversible suppression of activity in a restricted area of neocortex would be an important advance. High-frequency oscillations build up prior to neocortical seizure onset, and occur preferentially in epileptogenic areas (Worrell et al., 2004; Bragin et al., 2010). Although automated detection of such electroencephalographic (EEG) correlates of incipient seizures has attracted attention, progress in local manipulation of brain excitability has been slower, and is mainly focused on electrical brain stimulation (Kahane and Depaulis, 2010), focal brain cooling (Rothman, 2009) or targeted drug delivery (Heiss et al., 2010). A potentially powerful alternative way to suppress seizure activity 'on demand' is to photo-activate prokaryotic light-sensitive ion channels and transporters expressed in neurons (Zhang et al., 2007a; Miesenböck, 2011). Photoactivation of the chloride pump halorhodopsin from *Natronomonas*

154

*pharaonis* (NpHR) has been shown to suppress burst firing in organotypic hippocampal cultures (Tonnesen et al., 2009), and most recently, NpHR activation in thalamus was used to attenuate post-stroke seizures in rodent sensory cortex (Paz et al., 2012). I asked if NpHR photoactivation can attenuate epileptic activity in an established neocortical seizure focus *in vivo* and if the halorhodopsin system constitutes a reliable toolbox to study epileptic networks in the tetanus toxin model of focal neocortical epilepsy. Our long-term aim was to suggest a new approach to treatment for human disease and provide the backbone for the development of other optogenetic neuromodulation therapies.

## 6.1   Modelling Focal Neocortical Epilepsy

The choice of the tetanus toxin (TT) model of focal neocortical epilepsy to study optogenetic inhibition of epileptic activity was motivated by the following reasons: The possibility of targeted NpHR-lentivirus delivery into an epileptic focus would allow treatment of focal epilepsy, whilst avoiding the shut down of the entire brain. The study would build on established work of our laboratory, which demonstrated that stereotaxic application of tetanus toxin to motor cortex of rodent brain, gives rise to drug-resistant spontaneous seizures, characterized by behavioural arrest and bilateral facial twitching, mimicking those of neocortical epilepsy (Nilsen et al., 2005).

Some initial difficulties were related to finding the best dose and supplier of TT, as doses equal to or below 12.5 ng, and TT from Quadratech UK Ltd. (Epsom, Surrey, UK), or Sigma failed to elicit seizures. The TT used in the experiments described was a gift of G. Schiavo, Cancer Research Institute London, UK. The experiments were performed in Prof. Kullmann's lab, in collaboration with Dr. Rob Wykes, Postdoctoral Fellow.

Experimental procedures are described in the Methods chapter. Briefly, TT (12.5–17.5 ng) was injected into the motor cortex of 5–10 week-old Sprague-Dawley rats together with 1.25 µl high-titer ($10^8$ infectious units/ml)

2nd generation lentivirus carrying NpHR2.0 tagged with enhanced yellow fluorescent protein (EYFP) under the Camk2a promoter (Zhang et al., 2007b). We used two sets of control animals: one group was injected with NpHR lentivirus alone, and the other with TT and a lentivirus expressing only green fluorescent protein (GFP) or fluorescent beads. Immediately after the injection a cannula was implanted at the same site with a 200 μm diameter optic fiber. A cortical EEG electrode was also implanted, and connected to a subcutaneous wireless transmitter for continuous EEG recording (bandwidth 1 – 160 Hz). Between day 3 and 7 following tetanus toxin application, we observed the development of spontaneous bursts of high-frequency EEG activity (HFA) > 70 Hz in the motor cortex, near the site of TT injection, lasting over 5 weeks (Fig. 6.1 and 6.2). A more extensive characterization of the model was carried out by R. Wykes and J. Heeroma. With high doses of TT these electrographic phenomena can be accompanied by contralateral limb tonic posturing and clonus, head jerks, weight loss and/or status epilepticus (Wykes et al., 2012). Epileptogenesis is also accompanied by persistent changes in the intrinsic excitability of layer 5 pyramidal neurons (Wykes et al., 2012). There were also electrographic seizures, interictal spikes and slow wAves (Wykes et al., 2012). Behavioural arrest and forelimb myoclonus were documented on video recordings (Wykes et al., 2012). To allow comparison of the differences in the EEG traces in control and experimental animals, the EEG power was computed from 50 minutes of continuous 2–4 second EEG epochs for each frequency band by Fast Fourier transformation. Whilst control animals have a relatively linear relationship between log power and log frequency, TT injected animals have a significant increase in the high frequency components of the EEG between 70–120 and above 120 Hz (Fig. 6.1a). These changes, once apparent, persisted for the entire duration of the experimental protocol (or at least 35 days in animals monitored for longer periods of time).
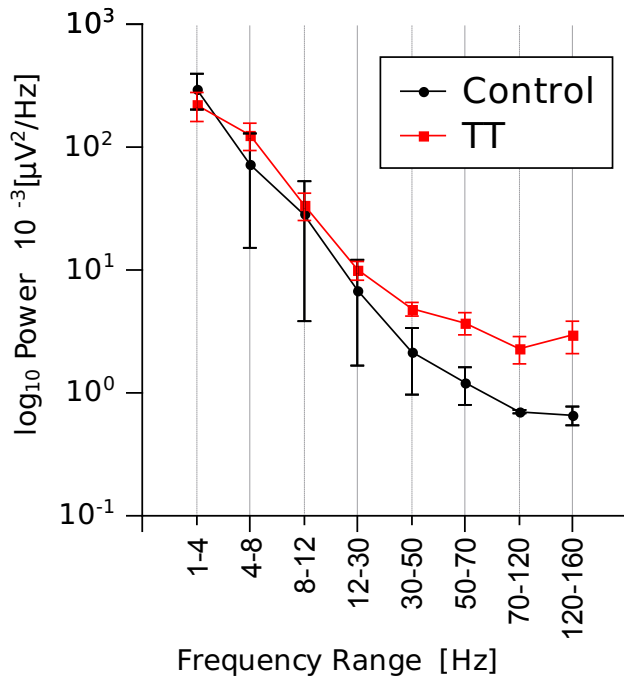
Figure 6.1: **The tetanus toxin model of focal epilepsy. (a)** Power values at different EEG frequency bands for control animals (n = 5) and TT injected animals (n = 6) recorded on day 7–10 post injection (displayed as mean ± standard error of mean (SEM)): delta (0–4 Hz), theta (4–8 Hz), alpha (8–12 Hz), beta (12–30 Hz), low gamma (30–50 Hz), high gamma (50–70 Hz), high frequency activity (HFA) > 70 Hz (displayed in two bands of HFA 70–120 Hz and HFA 120–170 Hz). The graph shows an increase in the HFA > 70 Hz in TT injected animals.
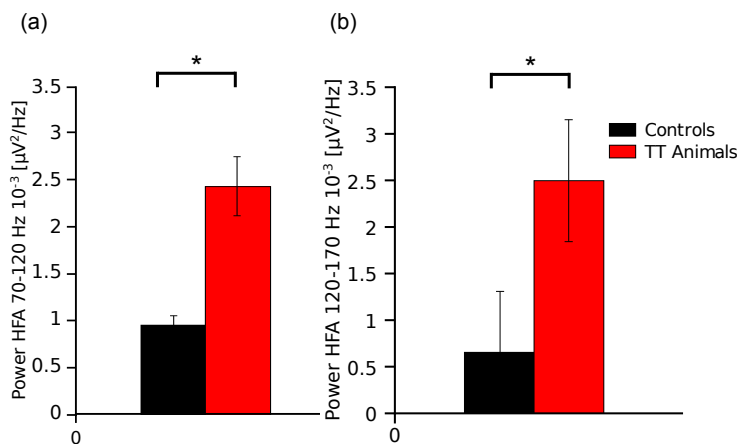


Figure 6.2: **High-frequency activity increase after TT injection. (a)** The HFA increase is significant in the 70–120 Hz band (p = 0.004, unpaired two-tailed $t$ test) and **(b)** 120–160 Hz band (p = 0.001, unpaired two-tailed $t$ test) of TT injected animals.
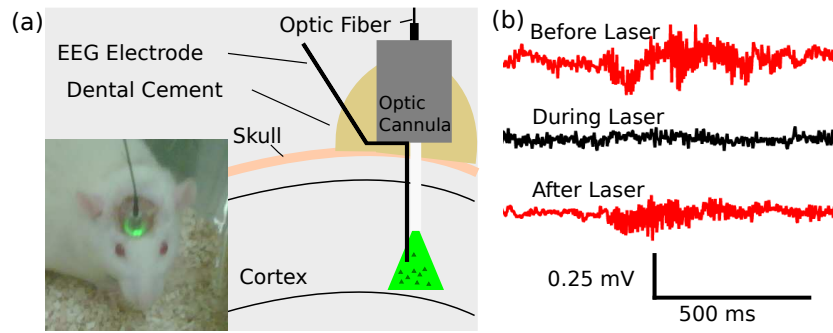
Figure 6.3: **The optogenetic setup. (a)** Schematic of the implanted headstage for simultaneous EEG recording and optical stimulation. **(b)** Representative EEG traces before, during and after 561 nm laser illumination, showing a decrease in HFA.

## 6.2 Optogenetic Setup

Optogenetic studies were performed on day 7–10 post-surgery, when both viral expression (on immunohistochemistry) and HFA bursts (on EEG) were present. An aim was to prevent animal suffering, as we had observed that a number of animals would be severely affected by the toxin and would go on to develop fixed limb posturing with constant HFA if kept alive for long periods of time. On the experimental day, the implanted optic cannula (Fig. 6.3a) was connected to a 561 nm laser (with analogue modulation, diode pumped, 75 mW nominal power, Crystalaser) via a fiberoptic patch cord (fibre core 200 µm, NA 0.22, Doric Lenses) and a rotary commutator (Doric Lenses) to prevent entanglement of the animal when connected to the fibre in the cage (Appendix Fig. A.4). Before *in vivo* experiments, the laser output was calibrated by setting up a test light path (laser → optic fibre → commutator → patch cord → implantable cannula) identical to the experimental setup to be used *in vivo*, and by measuring the light intensity at the tip of the test implantable cannula with a digital optical power meter (PM100D with Slim Photodiode Power Sensors S130C, ThorLabs). A stimulation intensity of 25 mW at the implantable fibre tip was chosen for the experiments, in light of the following considerations: 1) NpHR2.0 requires an irradiance value of 21.7 mW/mm$^2$ to inhibit 98% of spikes in slice experiments (Zhang et al., 2007b) and there is loss of light intensity through the tissue. 2)
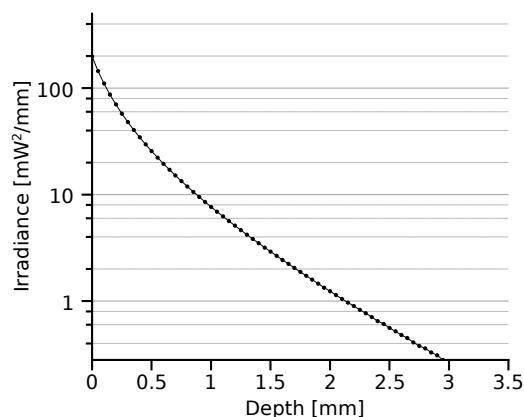
Figure 6.4: **Irradiance loss *in vivo*.** Irradiance values predicted at various tissue depths and computed by means of on line tissue calculator for laser wavelength 561 nm, NA 0.22, fiber core 0.2 mm, light intensity at fiber tip 25 mW. At 0.5 mm depth, the irradiance is ~22 mW.

Lentivirus expression volume is of approximately 0.04 mm$^3$. 3) To attain illumination with the required irradiance of 21.7 mW/mm$^2$ of most of the transduced volume, 25 mW were estimated to be adequate. Following my visit to Karl Deisseroth's lab, I was given a light transmission calculator for brain tissue (available on-line[1]), which allows one to compute the actual irradiance values (depending on the NA and the diameter of the fibre, the tissue and the wavelength used). Irradiance values at various distances from the fibre vary considerably (by more than one order of magnitude between 0 and 1 mm distance from the fibre tip), and even illumination of the transduced cortical volume is impossible (Fig. 6.4 ). I based the decision to continue using 25 mW at the fibre tip based on my immunohistochemical findings, which showed healthy neurons transduced at depths of more than 0.5 mm below the tip (Fig. 6.4). In view of the slow kinetics and high light intensity requirements of NpHR2.0 (Zhang et al., 2007b), we decided to deliver constant light pulses, but to avoid shifting the GABA reversal potential to depolarizing values by prolonged NpHR activation (Raimondo et al., 2012) and tissue damage through overheating, we limited pulse duration to 20 seconds. Laser stimulation was given on and off in 20 s intervals for sessions of 1000 s duration, preceded by a

---

[1]www.stanford.edu/group/dlab/cgi-bin/graph/chart.php
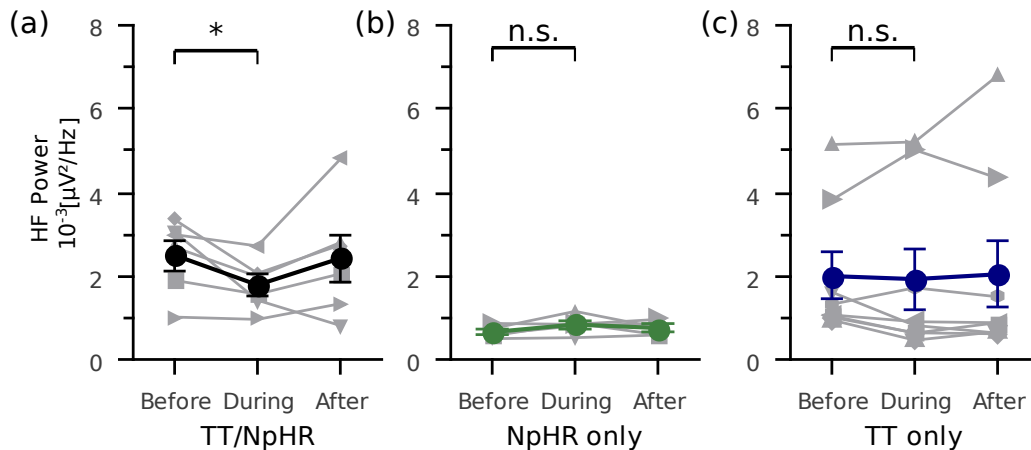
Figure 6.5: **Optogenetic suppression of neuronal excitability reduces high frequency activity in focal neocortical epilepsy. (a)** Mean EEG power in the 120–160 Hz band before, during and after laser stimulation in animals injected with TT and NpHR lentivirus (n = 6), showing a significant decrease (p < 0.05; grey: individual experiments; black: mean ± SEM). **(b)** Baseline HFA EEG power was lower in animals injected with NpHR lentivirus alone, and unaffected by laser illumination (n = 5; green: mean ± SEM). **(c)** Laser illumination had no effect on HFA EEG power in control animals injected with TT together with either GFP-expressing control virus or fluorescent beads (n = 8; individual experiments in grey, blue: mean ± SEM).

1000 s baseline and followed by a further period of 1000 s (Fig. 6.3b). The animals were observed for signs of discomfort or seizures throughout the stimulation paradigm but were never visibly adversely affected by the light, and displayed a variety of behaviours from grooming and exploration, to feeding, resting and falling asleep. Overt motor seizures occurred at too low a frequency to be expected during the 50 min duration of the experiment.

## 6.3 NpHR Reduces Epileptiform Activity *In Vivo*

We were able to demonstrate that suppressing network excitability by inhibiting a subset of neurons in the epileptic focus was sufficient to reduce epileptiform activity. To objectively quantify the differences in the EEG before, during and after laser experimentation (1000 s each), we employed three independent analysis methods. Firstly, we computed the mean power for 500 consecutive 2 s

EEG epochs in each frequency band: delta (1–4 Hz), theta (4–8 Hz), alpha (8–12 Hz), beta (12–30 Hz), low gamma (30–50 Hz), high gamma (50–70 Hz), high frequency activity (HFA) in the band 70–120 Hz and in the band 120–160 Hz. No assumption was made on the distribution of the data within the sets. The data before and during laser experiments were regarded as naturally linked as they were collected in the same animal. The Wilcoxon matched pairs signed-rank test was used to compare the means of the data before versus during experimentation and a probability value of 0.03 was regarded as significant. The unpaired two-tailed *t-test* was computed to compare mean power between the experimental animal groups. Illumination with 561 nm light in animals co-injected with TT and NpHR yielded a significant reduction in HF power in the 120–160 Hz band compared to the 1000 s baseline period (Fig. 6.5a, p = 0.03, Wilcoxon matched pairs signed-rank test). Lower EEG frequency bands (< 70 Hz) were not affected by the laser stimulation (Appendix Fig. A.5). Control animals injected with TT alone displayed a similar increase in the mean HFA (120-160 Hz) band of their EEG but HFA power was not significantly affected by laser stimulation with 561 nm light (Fig. 6.5b). In control animals injected with NpHR alone, HFA power in the 120–160 Hz band was significantly lower than in those with TT (p = 0.001, unpaired two-tailed *t-test*), and remained unaffected by laser activation (Fig. 6.5c).

The EEG data were also analyzed by measuring the coastline (sum of the absolute difference in voltage between consecutive sample points (Korn et al., 1987)) for successive 2 s segments and computed for 1000 seconds before the laser experiment, 1000 seconds during laser stimulation and the 1000 seconds period after the experiment. The EEG coastline length was significantly reduced from baseline in the TT/NpHR group during laser stimulation (Fig. 6.6a, p = 0.03, Wilcoxon matched pairs signed-rank test). The mean EEG coastline length was significantly shorter in the control group injected with NpHR alone (p = 0.001, unpaired two-tailed *t-test*) and again unaffected by laser illumination (Fig. 6.6b). In animals injected with TT and GFP virus (or beads), coastline was
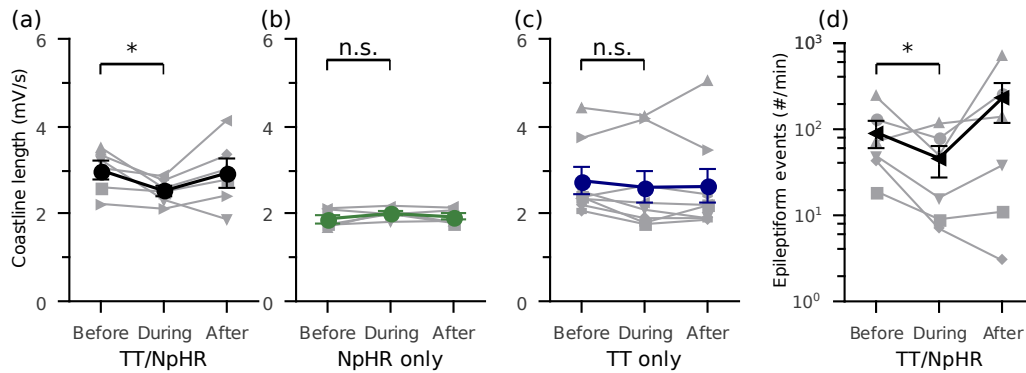
Figure 6.6: **Antiepileptic effect of NpHR assessed by coastline analysis and automated event detection. (a)** Mean EEG coastline length was significantly reduced by laser illumination in animals injected with TT/NpHR (symbols as in Fig. 6.5). **(b)** Baseline coastline was lower in animals injected with NpHR lentivirus alone, and unaffected by illumination. **(c)** EEG coastline length was unaffected by laser illumination in animals injected with TT together with GFP lentivirus or fluorescent beads. **(d)** Automated event classification used to detect bursts of high-frequency activity revealed a significant decrease upon laser illumination (n=8).

comparable to the baseline length in the TT/NpHR group, but was unaffected by laser illumination (Fig. 6.6c).

The analysis described above includes all the EEG throughout the 50–minute duration of the experiment. As neither the coastline length nor the HFA are specific for seizures, we complemented the analysis above with an automated event classifier as described in the Methods section, which allowed us to separate epileptiform activity from spontaneous behaviour artifacts such as from eating and grooming (Fig. 6.7 ). The number of events that fell into categories independently validated as characteristic of epileptic animals was counted prior to, during, and after intermittent illumination. The frequency of events was increased in the animals injected with TT/NpHR and was significantly reduced by illumination with 593 nm light, when analyzed with a paired *t-test* after logarithmic transformation (Fig. 6.6d, p = 0.048).
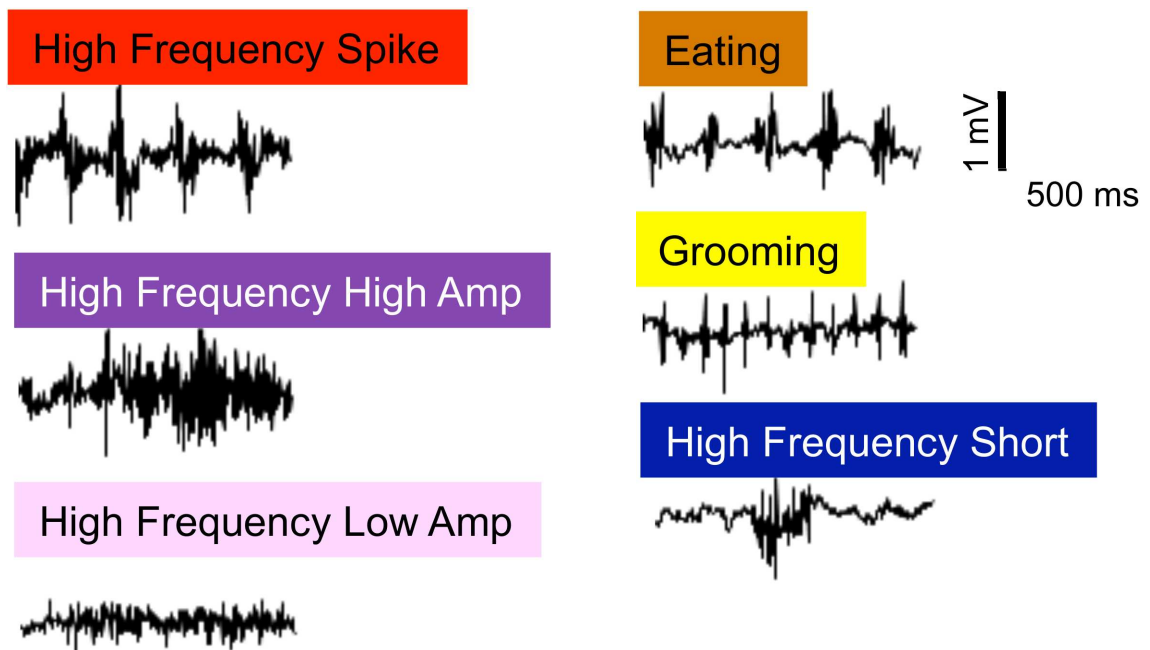
Figure 6.7: **Examples of EEG events detected by automated event classifier.** Sample traces of "short high frequency bursts" (<250 ms), "long high frequency bursts" (>250 ms, event power >6 x baseline), "long high frequency bursts of low amplitude" (>250 ms, event power 5–6 x baseline), and "high frequency spikes", and artefacts from eating and grooming (from (Wykes et al., 2012)).
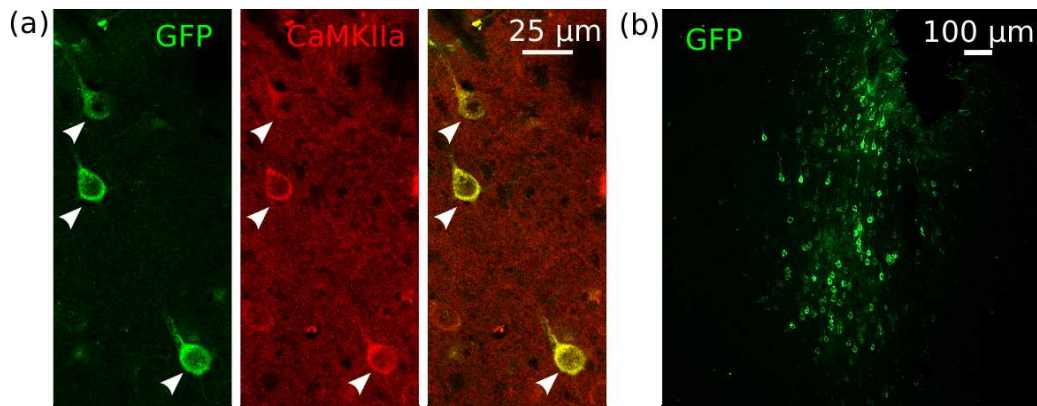
Figure 6.8: **Immunofluorescence for CaMKIIa in TT/NpHR injected animals.**
**(a)** Micrograph obtained from an animal sacrificed on day 6 after surgery, showing 38/51 EYFP positive cells (arrowheads) stained with Anti-GFP antibodies (left panel, green) also stained for CaMKIIα (central panel in red, and right panel showing overlay). **(b)** EYFP Immunofluorescence micrographs of 30 μm sections obtained one month after TT/LV–Camk2a–NpHR2.0-EYFP injection stained with Anti-GFP antibodies, confirming expression in layer 5 neurons.

## 6.4 NpHR targets CaMKIIα cells.

At the end of the experiments, the animals were terminally anaesthetized with isoflurane and a lethal dose of pentobarbitone, perfused with artificial cerebrospinal fluid (ACSF) and the brains fixed in 4% paraformaldehyde overnight. 30 μm sections were double labelled with an anti-CaMKIIα and an anti-GFP antibody to confirm expression of LV-Camk2a-NpHR2.0-EYFP in principal neurons as described in the Methods section. DAPI was used to stain nuclei and aid cell counting. Seventy-five percent of EYFP-expressing cells were found to be CaMKIIα positive (Fig. 6.8 a, 131 cells counted, 3 visual fields, 1 animal), when cerebral cortex was injected with 500 nl of LV. The volume of cortex containing all EYFP positive cells was estimated in an animal injected with 1.25 μl of LV at one month post injection as approximately 0.04 mm$^3$.

I wanted to address the question whether viral injection triggers a glial reaction. On day 4 post headstage implantation there were 39% more GFAP positive cells around the injection site than in a distant control area of cortex. There were also marked morphological differences with a larger soma and thicker processes of
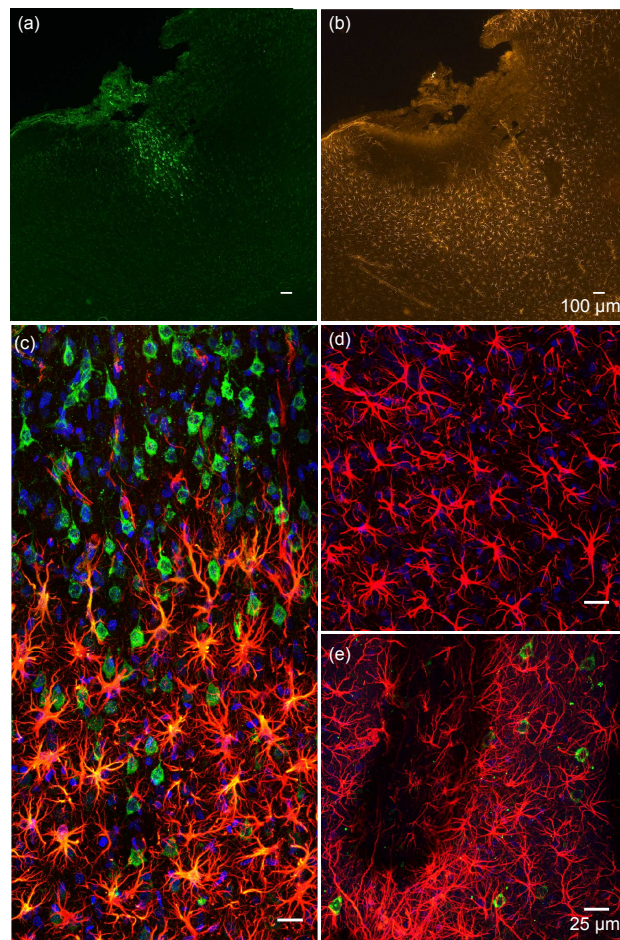
Figure 6.9: **Study of glial activation in virus-injected animals. (a)** Fluorescent micrograph (5x magnification) showing area of LV-Camk2a-NpHR2.0-EYFP/TT injection (day 4) and expression of GFP (counterstained with anti-GFP antibody). The cortical defect is due to the implantation of the optic cannula and recording electrode. Scale bar 100 µm. **(b)** Fluorescence micrograph (5x magnification) of the same section, shows increased numbers of GFAP positive cells (red). Scale bar 100 µm. **(c)** 40x magnified confocal fluorescence micrograph showing LV-Camk2a-NpHR2.0-EYFP/TT injected area and infiltration with bulky astrocytes. Day 4 post-injection; scale bar 25 µm. **(d)** Slender astrocyte morphology in control area of cortex. Day 4 post-injection; scale bar 25 µm. **(e)** LV-CCK-NpHR 2.0-EYFP injected animals (day 33 post injection) showing astrocytes clustering around injection site (confocal image, 40x magnification, anti-GFP and anti-GFAP stained). Scale bar 25 µm.

astrocytes at the injection site in the first days after injection (Fig. 6.9c and d). However, staining for GFAP revealed glial infiltration wherever screws (inserted for headstage stability) were accidentally touching or penetrating the cortical surface, and around the needle track in animals not implanted with a cannula (Fig. 6.9e). I concluded that infiltration by glial cells can be triggered just by mechanical trauma and is difficult to separate from glial infiltration due to viral injection only.

Further, I wanted to address whether LV injection initiates apoptotic cell death. I compared activated caspase-3 on day 6 versus at 1 month post injection. Caspases are cysteine-aspartic acid proteases, responsible for most proteolytic cleavages that lead to apoptosis. Caspase-3 is a key downstream effector caspase, whose activation has been shown to be a requirement for the execution of apoptotic cell death (Li and Yuan, 2008; Woo et al., 1998). There were more activated caspase-3 positive cells on day 6 (Fig. 6.10, 196 cells/mm$^3$, 1 animal) versus one month, where approximately half the amount of activated caspase-3 was counted (118 cells/mm$^3$, 1 animal (Fig. 6.10c, d). Only 5% of caspase positive cells at one month were fluorescent neurons. Since the animals were co-injected with TT, however, caspase activation might have been due to toxin effects on cells, the effects of increased excitation, HFA and seizures and generally due to the poorer health of the animals. Animals sacrificed at one month were usually less affected by the toxin and had fewer high HFA bursts, making it difficult to compare them with those sacrificed in the first week. Additionally, a positive control, where neurons were known to die by apoptosis, was not available, I therefore did not pursue this study further.

In summary, we confirmed that LV-Camk2a-NpHR2.0-EYFP was mainly expressed in principal cortical neurons and that expression was present in the first post-operative week and persisted for at least 4 months.
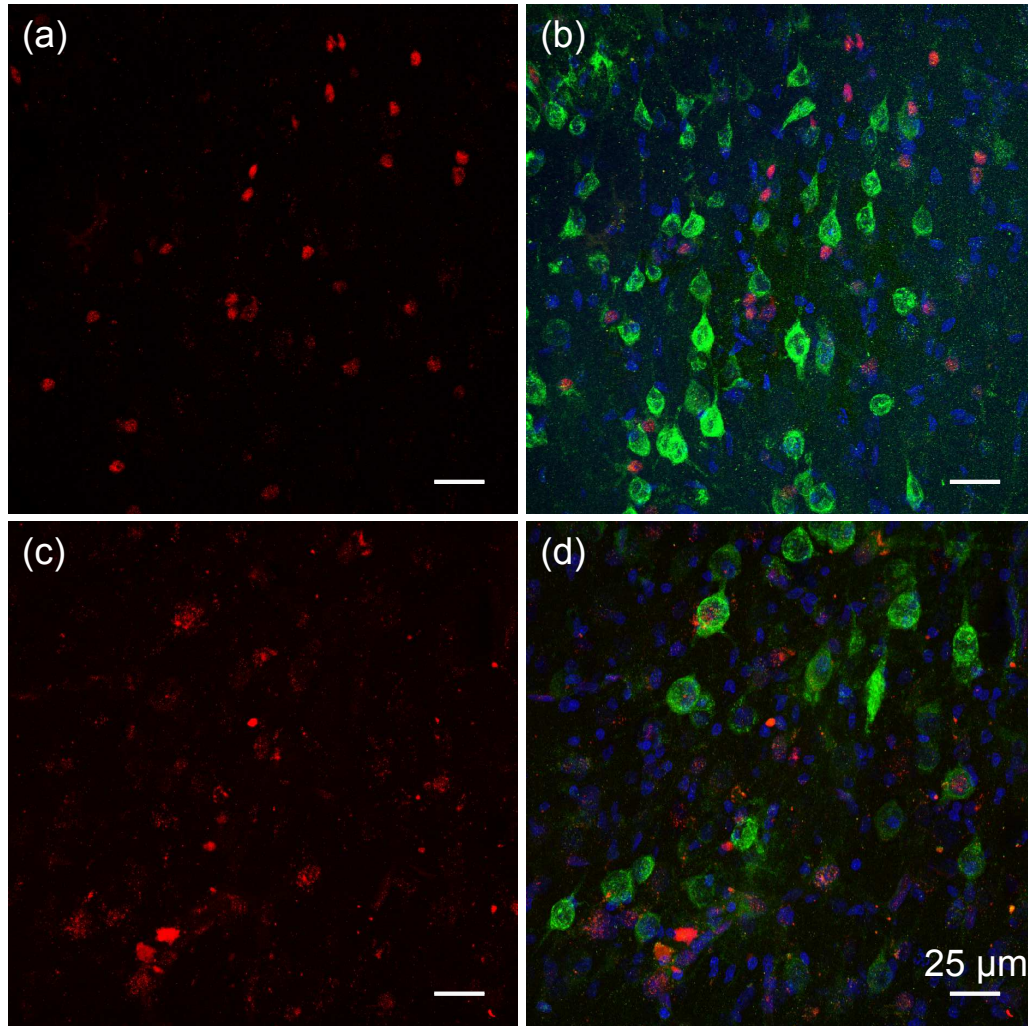
Figure 6.10: **Immunofluorescence for caspase-3 activation.** **(a)** Confocal micrograph showing only activated caspase-3 positive cells (in red) in the TT/LV–Camk2a–NpHR2.0-EYFP injected area on day 6 post injection. **(b)** Confocal micrograph showing the same area of cortex counterstained with anti-GFP (green) and anti-activated caspase-3 antibody (in red). **(c)** Confocal micrograph showing only activated casepase-3 positive cells (in red) in the TT/LV–Camk2a–NpHR2.0-EYFP injected area at 1 month post injection. Fewer nuclei are stained by the anti-caspase-3 antibody. **(d)** Confocal micrograph showing the same area of cortex counterstained with anti-GFP (green) and anti-activated caspase-3 antibody (in red). All images at 40x magnification; scale bar 25 μm in all images.

## 6.5 A Model to Dissect Epileptic Networks?

Despite the importance of HFA, it remains unclear how these oscillations are generated in the cortex. Since the thalamus is known to be able to generate rhythmic neuronal firing (Pedroarena and Llinás, 1997) in the cortex, such as during sleep (a simple schematic of thalamocortical connections to the primary motor cortex is sketched in Fig. 6.11a), one may tentatively hypothesize that HFA in primary motor cortex may involve thalamocortical connections. Optogenetic tools have already been used to discover pathway-specific feed-forward circuits between thalamus and cortex using LVs (Cruikshank et al., 2010). To investigate if thalamocortical networks play a role in generating HFA bursts in the TT model, in preliminary experiments I injected LV-Camk2a-NpHR2.0-EYFP into the venterolateral part of the anteroventral nucleus of the thalamus (AVVL), known to project to and excite the motor cortex (Zin-Ka-Ieu et al., 1998). Subsequently, I injected TT into primary motor cortex and implanted an optic cannula above the injection site (Fig. 6.11b). I hypothesized that if laser stimulation of primary motor cortex switches off HFA, this would suggest that CaMKIIα-expressing excitatory thalamocortical afferents are involved in the generation of HFA, either by driving the oscillation, or just by providing tonic excitation. LV was correctly expressed on day 8 post injection (Fig. 6.11c) although the fibres could not yet be tracked back to cortex (Fig. 6.11c top panel) and stimulation with light did not reduce HFA > 70 Hz (n = 2) 8 days after injection. Optogenetic experiments to be pursued in the future could address the timing of axonal expression of NpHR and whether NpHR expression in axons reaches the motor cortex. Further, experiments could test if NpHR inhibition of thalamocortical axons in primary motor cortex could be used to suppress glutamate release and HFA > 70 Hz.
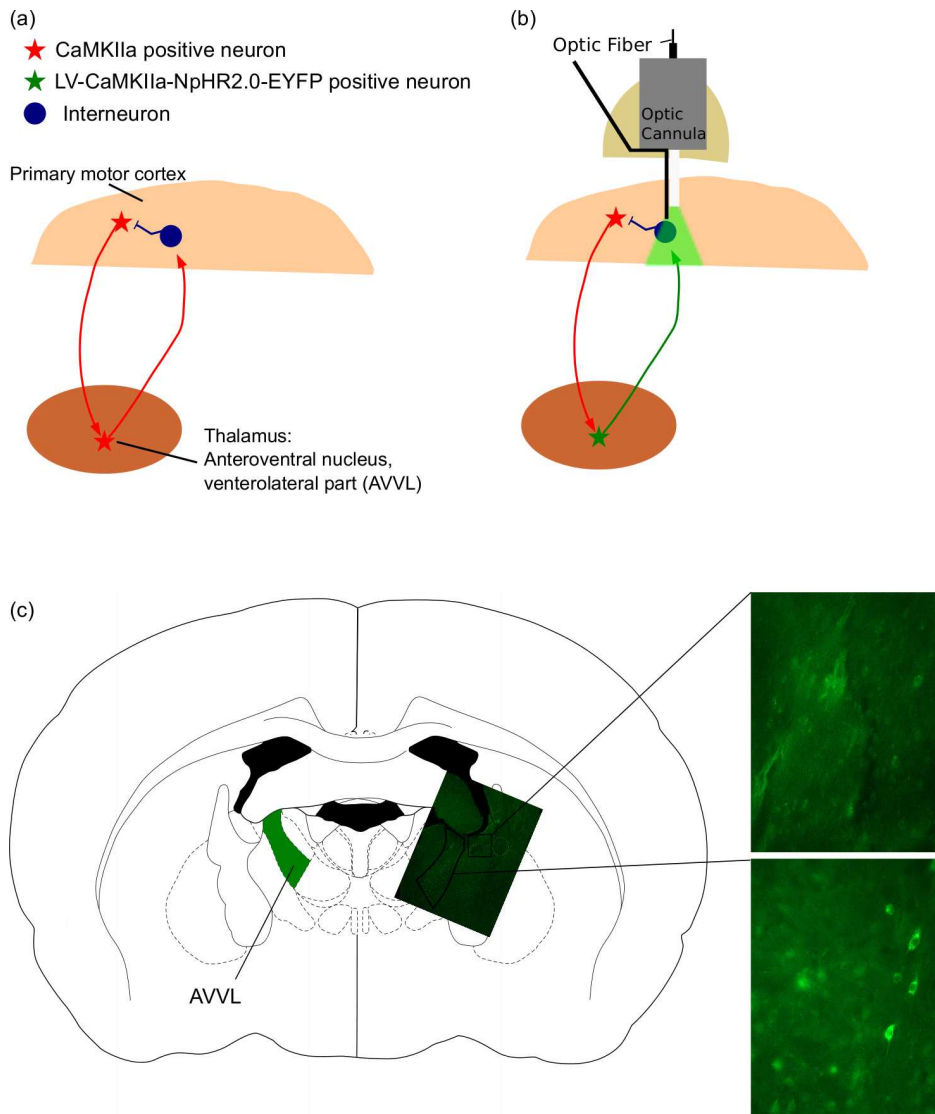
Figure 6.11: **Optogenetic inhibition of thalamocortical connections.** **(a)** Schematic of thalamocortical connections (Zin-Ka-Ieu et al., 1998). **(b)** LV-Camk2a-NpHR2.0-EYFP was injected into the venterolateral part of the anteroventral nucleus of the thalamus (AVVL) and an optic cannula with a recording electrode implanted in primary motor cortex, which was stimulated with 561 nm yellow light. **(c)** Schematic of coronal brain section at AV coordinates from bregma - 1.3 mm, showing the location of the AVVL and, on the right, a superimposed fluorescent micrograph (5x magnification) showing the correct expression of LV-Camk2a-NpHR2.0-EYFP (bottom micrograph, 40x magnification). On day 8 post injection, the fibre tracts were beginning to show fluorescence (top micrograph, 40x magnification) but did not yet reach the site of cannula implantation in primary motor cortex (AV +1 mm from bregma). Unsurprisingly, optical stimulation with 561 nm laser light did not reduce HFA in 2 experimental animals. Brain section redrawn from (Paxinos and Watson, 1986), plate 23.

## 6.6 Discussion

In this final section of the chapter, I would like to discuss my results in the context of the topic of high-frequency oscillations, how to modulate them and their relationship to epilepsy. I will then discuss further open questions suitable for optogenetic investigation in epilepsy models, and conclude by addressing the potential translation of optogenetic treatment approaches to human patients.

With the increased use of intracranial electrodes and the use of higher sampling frequencies for the evaluation of epilepsy surgery patients (Worrell et al., 2004, 2008), it has been possible to record EEG frequencies above the gamma range, which were undetectable by surface electrodes due to the low-pass filtering properties of the skull vault. As discussed in the introductory chapter, the oscillation frequency ranges above gamma have no strict definition or names. Many authors use the term "ripples" for frequencies between 80–200 Hz and "fast ripples" for frequencies above 200 Hz. The frequency range itself does not define whether an oscillation is physiological or pathological, and the two must be distinguished both in the hippocampus and in the cortex. In my work I have used the term high-frequency activity (HFA) to describe EEG frequencies above 70 Hz. I will use the term high frequency oscillations (HFOs) when this term has been used by authors in their published work. Physiological HFOs > 300 Hz can be readily observed in human somatosensory cortex during stimulation of peripheral nerves (Hashimoto, 2000; Hashimoto et al., 1999), as can HFOs > 200 Hz in rodent barrel cortex during stimulation of the thalamus or vibrissae (Jones et al., 2000) and ripples (80–200 Hz) in the neocortex of cats during vigilance or anaesthesia (Grenier et al., 2001). Fast ripple oscillations in the dentate gyrus (DG) were the first documented pathological HFOs (Bragin et al., 1999): they are not normally present in the DG and they are associated with interictal spikes and more generally only with tissue capable of epileptogenicity (Engel et al., 2009). This and the fact that they are detectable at the ictal onset,

supports the hypothesis that they must play a role in seizure generation (Bragin et al., 2005, 1999). "Epileptic" HFOs (60–100 Hz) have been documented in human neocortex on the electrocorticogram of focal epilepsy patients implanted with subdural electrodes both pre-ictally and during seizures (Worrell et al., 2004). HFO rates were significantly higher in the seizure onset zone (Jacobs et al., 2009b) (SOZ) and it has therefore been suggested that they be used as biomarkers for epilepsy by aiding the identification of the SOZ in presurgical patients. Additionally, two recent studies have reported a significantly better outcome in patients whose HFO-generating tissue was completely removed during epilepsy surgery (Akiyama et al., 2011; Jacobs et al., 2010). Some authors postulate that HFOs may represent localized activity of GABA-ergic interneurons (Hashimoto, 2000; Engel et al., 2009), whilst others favour a pyramidal cell network coupled by gap-junctions at the level of the axon, as the origin for very high frequency oscillations present in the epileptic human cortex (Roopun et al., 2010). It is not known whether interfering with the HFOs would improve seizure control in humans but recent studies have suggested that seizures may arise not from a discrete focus, as previously thought, but from concerted activity of epileptogenic networks. Therefore, modulating these networks with optogenetic tools or chemically (Etherington and Frenguelli, 2004; Hamil et al., 2012) may prove successful in preventing and treating ictal phenomena (Wilke et al., 2011).

The results of the experiments described above, may help answer a few of these open questions: we have shown that injection of TT into primary motor cortex models HFA bursts found in seizure onset zones of patients with focal epilepsy and have demonstrated rapid and reversible suppression of HFA upon photoactivation of NpHR. As to the networks generating the high-frequency oscillations, our findings would support the gap-junction hypothesis mentioned above, since halorhodopsin was targeted to excitatory neurons, and their inhibition with 561 nm light reduced the power of the HFA. Alternatively, two

other mechanisms could also explain our results: removal of tonic drive to interneurons (removal of metabotropic glutamate receptor activation (Whittington et al., 2000)) or attenuated inhibitory postsynaptic currents (iPSCs) in pyramidal cells due to intracellular accumulation of $Cl^-$ and a reduced GABA driving force.

Our data show that opsins are suitable tools to modulate and study epileptic networks with great precision and specificity. It was interesting to observe that in control animals, NpHR activation alone did not affect any of the EEG frequency bands. This finding was supported by the laser experiments performed in Karl Deisseroth's lab at the Short Course in Optogenetics (April 2011), where I implanted an optic cannula into the primary motor cortex of a transgenic Thy1-NpHR2.0 mouse and stimulated it with 593 nm yellow laser light, without detectable effect on the animal's behaviour or motor function. One may tentatively suggest that the modest chloride influx through NpHR 2.0 may only suffice to disrupt or modulate the effects of small pyramidal networks generating the HFOs. The smaller photocurrents generated by NpHR2.0 may also explain why chloride influx does not shift the chloride reversal potential and eventually cause $GABA_A$ receptor opening to lead to depolarization of the membrane potential (Tonnesen et al., 2009), whilst the contrary has been shown to be true when using NpHR3.0, which generates larger photocurrents and is more effective at silencing neurons (Raimondo et al., 2012).

Equally interesting was the observation that a previously healthy transgenic Thy1-ChR2 mouse developed a generalized tonic-clonic seizure when either the stimulation frequency or the 473 nm laser intensity were too high, indicating that the ictal activity did not remain localized to where photoactivation took place generating only a focal seizure (as perhaps would have been expected from focal stimulation of motor cortex) but that ictal activity rapidly spread and secondarily generalized in an otherwise normal brain (aside from surgical trauma from the implantation of the optic cannula). This observation supports

the idea that synchronization of small scale networks can recruit distant networks and quickly synchronize brain regions at considerable distance, again suggesting that epilepsy may arise from abnormal synchronization of local networks, which could therapeutically be perturbed without altering global brain function and behaviour.

Several unanswered questions about the nature of high-frequency oscillations and epilepsy can be addressed with optogenetic techniques: An intriguing one I started to address, was whether thalamocortical connections are involved in generating HFA in primary motor cortex. Instead of switching off principal cells in primary motor cortex to attenuate HFA in TT animals, I injected thalamic nuclei projecting to the primary motor areas with a Camk2a driven NpHR, and stimulated their afferents in the cortex with green light to study their effect on HFA, in analogy to previous work done on animal models of Parkinson's disease (Gradinaru et al., 2010). Further experiments are needed to understand whether thalamocortical connections play a role in the generation of cortical HFA. Optogenetic tools could further be used in epilepsy models to elucidate the precise mechanism of action of deep brain stimulation in different stimulation targets for different forms of focal and generalized epilepsy. Future studies will benefit from newer generation opsins and viruses, and should make use of an optogenetic proton-pump inhibitor to avoid influencing GABAergic synaptic transmission with newer generation NpHRs (Raimondo et al., 2012).

Finally, and most importantly, our results indicate that optical inhibition of neurons in the epileptogenic zone, combined with wireless telemetry and seizure detection algorithms, represents a promising new platform to dissect epileptic networks and to develop an automated device to stop seizures acutely, akin to an implantable defibrillator. Since HFA is linked to seizure foci and the removal of HFA containing cortex is linked with improved surgical outcome, it is conceivable that by manipulating excitation and reducing HFA, this may translate into reduced seizure activity. It will be important to test this

hypothesis and to continue to study epilepsy and epileptogenesis not only at the synaptic but at the network level, because "ultimately, curing epilepsy may require not only halting epileptogenic processes but returning synaptic networks to their pre-epileptic state or by creating a compensatory balance to suppress the excess excitability" (Jacobs et al., 2009b).

# Chapter 7

# General Discussion and Outlook

Several points have emerged from the experiments described in this thesis: In the chapter dedicated to targeting opsins to interneurons we have seen that the GAD67 and CCK promoters are not specific for interneurons or subsets of interneurons. I have shown that *in vivo*, AAVs are expressed over a larger volume than LVs, and I have discussed how to set up optogenetic experiments *in vitro* using adequate light sources. In the chapter discussing optogenetic induction and entrainment of CA3 oscillating networks I have shown that it is possible to elicit oscillations in the gamma range by stimulating CA3 principal cells with ChR2. I have also demonstrated how gamma oscillations respond to periodic inputs and described the relationship between oscillation phase and stimulus frequency. These results were adequately predicted by a model developed by T. Akam based on the Wilson-Cowan equations. In the final results chapter, I showed that injection of TT into primary motor cortex models HFA bursts found in seizure onset zones of patients with focal epilepsy. I then showed that halorhodopsin is reliably expressed and can be stimulated *in vivo* in rat motor cortex, without clinical signs of dysfunction in the live animal, nor histological features of cytotoxicity. Finally, I have demonstrated rapid and reversible suppression of epileptic EEG activity upon photoactivation of NpHR.

I would like to conclude by adding a few final remarks and ideas and an

outlook to the above mentioned main points:

Optogenetics has revolutionized neuroscience and provides the unique opportunity to selectively interrogate and manipulate ensembles of neurons. As better opsins are being developed, the technique will become more reliable and easier to implement but great care is necessary when setting up each component of the technique, from illumination to the choice of vector. The ability to study excitatory and inhibitory interneurons separately and how they interact is one of the main requirements of modern neuroscience. This can not be reliably achieved with the GAD67 and CCK promoter-driven opsins in their current form. If not by serendipity, it is unlikely we will achieve this goal if we do not fundamentally question what genetic and transcriptional factors determine the identity of an interneuron. Efforts to study this are already under way (Heinrich et al., 2010). Whilst optogenetics has given us the means to drive populations of neurons, it will be equally important to develop a 3-dimensional readout strategy, in order to acquire precise recordings of neural activity *in vivo*. So far, multielectrode arrays have had the disadvantage that they cause scarring and inflammation, but new materials and the advances in nanotechnology hold great promise for the future.

Viral vectors are important as study tools and for gene therapy of terminally differentiated cells, but also carry the risk of mutagenesis and immune system activation. Before viral gene therapy of the nervous system can be considered "safe" for human applications, several issues need addressing: First it is vital to establish the "gene dose" required and how to control it. The correct "dose" of the lentiviral vector "ProSavin" (Oxford Biomedica) is currently under investigation in a Phase II study in patients with Parkinson's disease. Further it is important, to achieve control over promoter activity and specificity to ensure that the therapeutic gene reaches the diseased cells. This could be achieved by inducible promoter systems. Finally, it is paramount to ensure no "spill-over" of virus occurs into germ cells. Overall I think the best option available to date

for human use would be a non-integrating lentivirus with an inducible promoter system.

In the second result chapter, I touched on some of the most fascinating questions in neuroscience: how brain activity is coordinated, information is processed and routed (which eventually translates into what we call cognition and behaviour). We demonstrated that the CA3 network has properties that allow it to entrain and synchronize to input from the dentate gyrus, which may help explain how coherence between these two anatomically coupled networks arises. Thoughts about function of the coherence between CA3 and dentate gyrus are only speculative, but we suggest it may help control information flow. Oscillations are perturbed in disorders such as schizophrenia, epilepsy and Parkinson's disease and it will be an important task to test if the cognitive and perceptual deficits associated with these disorders are due to the fact that networks cannot synchronize or that the disruption in oscillatory activity affects synaptic plasticity (Uhlhaas and Singer, 2010) in the hippocampus. To explore the interplay of neuronal subtypes in generating and synchronizing oscillations, a future strategy could exploit a far-red shifted ChR2 (Yizhar et al., 2011b) to drive principal cells under the Camk2a promoter and PV-Cre transgenic mice with a double-floxed stop blue-shifted ChR to drive fast-spiking interneurons. Most importantly, oscillatory activity in different subclasses of neurons could be perturbed or induced in the live animal to determine how this may impact on behaviour. The optogenetic tools that will continue to be developed will certainly help us find answers to these questions.

In the last result chapter, my experiments show that optogenetic treatment approaches for epilepsy are feasible and may in the future become viable for human patients. When considering opsins as future therapeutic tools, several challenges will need addressing: Firstly, optogenetic tools need to be optimized, with better and faster inhibitors generating large photocurrents and expressing long-term *in vivo*. Secondly, the random insertion of lentiviral vectors with their

inherent potential for mutagenesis, oncogenesis and the lack of control over transgene expression represents a significant risk to patients. As discussed in previous chapters, adeno-associated virus vectors with targeted insertions and a better understanding of inducible and cell-subtype specific promoters are required. Thirdly, caution must be taken in causing expression of potentially immunogenic proteins, although there is no evidence so far that long-term expression of opsins causes an immune response (Han et al., 2009a), possibly because neurons reside in immunologically privileged areas behind the blood-brain barrier. Further, the development of brighter and miniaturized LEDs with better light coupling into optic fibres will allow powering of the light source with a small battery and therefore development of implantable devices - some prototypes are already available for small animal work (e.g. Kendall Research Systems). Timing and duration of illumination will need to be optimized and reliable seizure detection algorithms developed and validated in human epilepsy. Eventually, this could lead to the development of implantable devices that will trigger the generation of a "defibrillator" light pulse once the electrical signature of a seizure onset is detected, yielding a radically new treatment alternative for human disease. In addition, in parallel with scientific tools, surgical techniques have advanced, too. Consequently, human brain tissue has become available for culturing (Gibbons and Dragunow, 2010) and for neurophysiological studies (Graebenitz et al., 2011; Roopun et al., 2010). It should now also be the study of epileptic human brain tissue that will take our knowledge of epilepsy a step further.

Finally, scientific collaboration across the fields of science will be crucial to generate new ideas, develop new techniques and interpret results. It is the prerequisite to advance our knowledge of the phenomena occurring in the brain in health and disease. And it is those scientific collaborators, supervisors, mentors, post-docs, friends and my husband I would like to thank for their inspiration and support. They have helped me find my way in science, greatly

advance my own understanding, and advance our shared knowledge a small

step forward.

# Bibliography

Adamantidis A.R., Zhang F., Aravanis A.M., Deisseroth K., and de Lecea L.
Neural substrates of awakening probed with optogenetic control of
hypocretin neurons. *Nature*, **450**(7168):420–424, (2007).

Adesnik H. and Scanziani M. Lateral competition for cortical space by
layer-specific horizontal circuits. *Nature*, **464**(7292):1155–1160, (2010).

Adrian E.D. Olfactory reactions in the brain of the hedgehog. *J Physiol*, **100**(4):
459–473, (1942).

Airan R.D., Thompson K.R., Fenno L.E., Bernstein H., and Deisseroth K.
Temporally precise in vivo control of intracellular signalling. *Nature*, **458**
(7241):1025–1029, (2009).

Akam T. and Kullmann D.M. Oscillations and filtering networks support
flexible routing of information. *Neuron*, **67**(2):308–320, (2010).

Akam T., Oren I., Mantoan L., Ferenczi E., and Kullmann D.M. Oscillatory
dynamics in the hippocampus support dentate gyrus-CA3 coupling. *Nat
Neurosci*, **5**:763-8, (2012).

Akiyama T., McCoy B., Go C.Y., Ochi A., Elliott I.M., Akiyama M., Donner E.J.,
Weiss S.K., Snead O.C., Rutka J.T., Drake J.M., and Otsubo H. Focal resection
of fast ripples on extraoperative intracranial EEG improves seizure outcome
in pediatric epilepsy. *Epilepsia*, , (2011).

Alotaibi F.A., Hamani C., and Lozano A.M. Neuromodulation in Epilepsy. *Neurosurgery*, , (2011).

Apolonia L., Waddington S.N., Fernandes C., Ward N.J., Bouma G., Blundell M.P., Thrasher A.J., Collins M.K., and Philpott N.J. Stable gene transfer to muscle using non-integrating lentiviral vectors. *Mol Ther*, **15**(11):1947–1954, (2007).

Aravanis A.M., Wang L.P., Zhang F., Meltzer L.A., Mogri M.Z., Schneider M.B., and Deisseroth K. An optical neural interface: in vivo control of rodent motor cortex with integrated fiberoptic and optogenetic technology. *J Neural Eng*, **4**(3):S143–S156, (2007).

Arenkiel B.R., Peca J., Davison I.G., Feliciano C., Deisseroth K., Augustine G.J., Ehlers M.D., and Feng G. In vivo light-induced activation of neural circuitry in transgenic mice expressing channelrhodopsin-2. *Neuron*, **54**(2):205–218, (2007).

Ascoli G.A., Alonso-Nanclares L., Anderson S.A., Barrionuevo G., Benavides-Piccione R., Burkhalter A., Buzsáki G., Cauli B., Defelipe J., Fairen A., Feldmeyer D., Fishell G., Fregnac Y., Freund T.F., Gardner D., Gardner E.P., Goldberg J.H., Helmstaedter M., Hestrin S., Karube F., Kisvárday Z.F., Lambolez B., Lewis D.A., Marin O., Markram H., Munoz A., Packer A., Petersen C.C.H., Rockland K.S., Rossier J., Rudy B., Somogyi P., Staiger J.F., Tamas G., Thomson A.M., Toledo-Rodriguez M., Wang Y., West D.C., and Yuste R. Petilla terminology: nomenclature of features of GABAergic interneurons of the cerebral cortex. *Nat Rev Neurosci*, **9**(7):557–568, (2008).

Bamann C., Gueta R., Kleinlogel S., Nagel G., and Bamberg E. Structural guidance of the photocycle of channelrhodopsin-2 by an interhelical hydrogen bond. *Biochemistry*, **49**(2):267–278, (2010).

Baptiste S.L., Tang H.M., Kuzniecky R.I., Devinsky O., French J.A., and Ludvig N. Comparison of the antiepileptic properties of transmeningeally delivered

muscimol, lidocaine, midazolam, pentobarbital and GABA, in rats. *Neurosci Lett*, **469**(3):421–424, (2010).

Bartlett J.S., Samulski R.J., and McCown T.J. Selective and rapid uptake of adeno-associated virus type 2 in brain. *Hum Gene Ther*, **9**(8):1181–1186, (1998).

Beja O., Spudich E.N., Spudich J.L., Leclerc M., and DeLong E.F. Proteorhodopsin phototrophy in the ocean. *Nature*, **411**(6839):786–789, (2001).

Beleza P. and Pinho J. Frontal lobe epilepsy. *J Clin Neurosci*, **18**(5):593–600, (2011).

Bellini G., Miceli F., Soldovieri M.V., del Giudice E.M., Pascotto A., and Taglialatela M. Benign Familial Neonatal Seizures. Gene Reviews NCBI, (2011).

Belluscio M.A., Mizuseki K., Schmidt R., Kempter R., and Buzsáki G. Cross-frequency phase-phase coupling between theta and gamma oscillations in the hippocampus. *J Neurosci*, **32**(2):423–435, (2012).

Ben-Ari Y., Cherubini E., Corradetti R., and Gaiarsa J.L. Giant synaptic potentials in immature rat CA3 hippocampal neurones. *J Physiol*, **416**:303–325, (1989).

Benke T.A. and Swann J. The tetanus toxin model of chronic epilepsy. *Adv Exp Med Biol*, **548**:226–238, (2004).

Benzekhroufa K., Liu B.H., Teschemacher A.G., and Kasparov S. Targeting central serotonergic neurons with lentiviral vectors based on a transcriptional amplification strategy. *Gene Ther*, **16**(5):681–688, (2009).

Berg A.T., Berkovic S.F., Brodie M.J., Buchhalter J., Cross J.H., van Emde Boas W., Engel J., French J., Glauser T.A., Mathern G.W., Moshé S.L., Nordli D., Plouin P., and Scheffer I.E. Revised terminology and concepts for organization of seizures and epilepsies: report of the ILAE Commission on Classification and Terminology, 2005-2009. *Epilepsia*, **51**(4):676–685, (2010).

Bergey G.K., MacDonald R.L., Habig W.H., Hardegree M.C., and Nelson P.G. Tetanus toxin: convulsant action on mouse spinal cord neurons in culture. *J Neurosci*, **3**(11):2310–2323, (1983).

Bergey G.K., Bigalke H., and Nelson P.G. Differential effects of tetanus toxin on inhibitory and excitatory synaptic transmission in mammalian spinal cord neurons in culture: a presynaptic locus of action for tetanus toxin. *J Neurophysiol*, **57**(1):121–131, (1987).

Berke J.D., Okatan M., Skurski J., and Eichenbaum H.B. Oscillatory entrainment of striatal neurons in freely moving rats. *Neuron*, **43**(6):883–896, (2004).

Berman H.M., Westbrook J., Feng Z., Gilliland G., Bhat T.N., Weissig H., Shindyalov I.N., and Bourne P.E. The Protein Data Bank. *Nucleic Acids Res*, **28**(1):235–242, (2000).

Berndt A., Yizhar O., Gunaydin L.A., Hegemann P., and Deisseroth K. Bi-stable neural state switches. *Nat Neurosci*, **12**(2):229–234, (2009).

Berndt A., Schoenenberger P., Mattis J., Tye K.M., Deisseroth K., Hegemann P., and Oertner T.G. High-efficiency channelrhodopsins for fast neuronal stimulation at low light levels. *Proc Natl Acad Sci U S A*, **108**(18):7595–7600, (2011).

Bi A., Cui J., Ma Y.P., Olshevskaya E., Pu M., Dizhoor A.M., and Pan Z.H. Ectopic expression of a microbial-type rhodopsin restores visual responses in mice with photoreceptor degeneration. *Neuron*, **50**(1):23–33, (2006).

Bieszke J.A., Braun E.L., Bean L.E., Kang S., Natvig D.O., and Borkovich K.A. The nop-1 gene of Neurospora crassa encodes a seven transmembrane helix retinal-binding protein homologous to archaeal rhodopsins. *Proc Natl Acad Sci U S A*, **96**(14):8034–8039, (1999).

Bloemer U., Naldini L., Kafri T., Trono D., Verma I.M., and Gage F.H. Highly

efficient and sustained gene transfer in adult neurons with a lentivirus vector. *J Virol*, **71**(9):6641–6649, (1997).

Bogomolni R.A. and Spudich J.L. Identification of a third rhodopsin-like pigment in phototactic Halobacterium halobium. *Proc Natl Acad Sci U S A*, **79** (20):6250–6254, (1982).

Bouard D., Alazard-Dany D., and Cosset F.L. Viral vectors: from virology to transgene expression. *Br J Pharmacol*, **157**(2):153–165, (2009).

Bovolenta R., Zucchini S., Paradiso B., Rodi D., Merigo F., Mora G.N., Osculati F., Berto E., Marconi P., Marzola A., Fabene P.F., and Simonato M. Hippocampal FGF-2 and BDNF overexpression attenuates epileptogenesis-associated neuroinflammation and reduces spontaneous recurrent seizures. *J Neuroinflammation*, **7**:81, (2010).

Boyden E.S., Zhang F., Bamberg E., Nagel G., and Deisseroth K. Millisecond-timescale, genetically targeted optical control of neural activity. *Nat Neurosci*, **8**(9):1263–1268, (2005).

Bragin A., Jandó G., Nádasdy Z., Hetke J., Wise K., and Buzsáki G. Gamma (40-100 Hz) oscillation in the hippocampus of the behaving rat. *J Neurosci*, **15** (1 Pt 1):47–60, (1995).

Bragin A., Engel J., Wilson C.L., Fried I., and Mathern G.W. Hippocampal and entorhinal cortex high-frequency oscillations (100–500 Hz) in human epileptic brain and in kainic acid–treated rats with chronic seizures. *Epilepsia*, **40**(2): 127–137, (1999).

Bragin A., Wilson C.L., and Engel J. Chronic epileptogenesis requires development of a network of pathologically interconnected neuron clusters: a hypothesis. *Epilepsia*, **41 Suppl 6**:S144–S152, (2000).

Bragin A., Azizyan A., Almajano J., Wilson C.L., and Engel J. Analysis of

chronic seizure onsets after intrahippocampal kainic acid injection in freely moving rats. *Epilepsia*, **46**(10):1592–1598, (2005).

Bragin A., Engel J., and Staba R.J. High-frequency oscillations in epileptic brain. *Curr Opin Neurol*, **23**(2):151–156, (2010).

Briggs W.R. and Spudich J.L. *Handbook of Photosensory Receptors*. Wiley–VCH, (2005). ISBN 3527310193.

Brilliant M.H., Szabó G., Katarova Z., Kozak C.A., Glaser T.M., Greenspan R.J., and Housman D.E. Sequences homologous to glutamic acid decarboxylase cDNA are present on mouse chromosomes 2 and 10. *Genomics*, **6**(1):115–122, (1990).

Brun S., Faucon-Biguet N., and Mallet J. Optimization of transgene expression at the posttranscriptional level in neural cells: implications for gene therapy. *Mol Ther*, **7**(6):782–789, (2003).

Brunel N. and Wang X.J. What determines the frequency of fast network oscillations with irregular neural discharges? I. Synaptic dynamics and excitation-inhibition balance. *J Neurophysiol*, **90**(1):415–430, (2003).

Buhl D.L., Harris K.D., Hormuzdi S.G., Monyer H., and Buzsáki G. Selective impairment of hippocampal gamma oscillations in connexin-36 knock-out mouse in vivo. *J Neurosci*, **23**(3):1013–1018, (2003).

Buhl E.H., Tamás G., and Fisahn A. Cholinergic activation and tonic excitation induce persistent gamma oscillations in mouse somatosensory cortex in vitro. *J Physiol*, **513 ( Pt 1)**:117–126, (1998).

Burns J.C., Friedmann T., Driever W., Burrascano M., and Yee J.K. Vesicular stomatitis virus G glycoprotein pseudotyped retroviral vectors: concentration to very high titer and efficient gene transfer into mammalian and nonmammalian cells. *Proc Natl Acad Sci U S A*, **90**(17):8033–8037, (1993).

Busskamp V., Duebel J., Balya D., Fradot M., Viney T.J., Siegert S., Groner A.C., Cabuy E., Forster V., Seeliger M., Biel M., Humphries P., Paques M., Mohand-Said S., Trono D., Deisseroth K., Sahel J.A., Picaud S., and Roska B. Genetic reactivation of cone photoreceptors restores visual responses in retinitis pigmentosa. *Science*, **329**(5990):413–417, (2010).

Buzsáki G. Memory consolidation during sleep: a neurophysiological perspective. *J Sleep Res*, **7 Suppl 1**:17–23, (1998).

Buzsáki G. and Wang X.J. Mechanisms of gamma oscillations. *Annu Rev Neurosci*, **35**:203–225, (2012).a.

Buzsáki G. and Wang X.J. What's in a name? A short history of gamma oscillations. *Annu Rev Neurosci*, **Supplemental Material: 35**:203–225, (2012).b.

Buzsáki G., Leung L.W., and Vanderwolf C.H. Cellular bases of hippocampal EEG in the behaving rat. *Brain Res*, **287**(2):139–171, (1983).

Buzsáki G. and Draguhn A. Neuronal oscillations in cortical networks. *Science*, **304**(5679):1926–1929, (2004).

Buzsáki G., Geisler C., Henze D.A., and Wang X.J. Interneuron Diversity series: Circuit complexity and axon wiring economy of cortical interneurons. *Trends Neurosci*, **27**(4):186–193, (2004).

Buzsáki G., Anastassiou C.A., and Koch C. The origin of extracellular fields and currents–EEG, ECoG, LFP and spikes. *Nat Rev Neurosci*, **13**(6):407–420, (2012).

Cantello R., Rossi S., Varrasi C., Ulivelli M., Civardi C., Bartalini S., Vatti G., Cincotta M., Borgheresi A., Zaccara G., Quartarone A., Crupi D., Laganà A., Inghilleri M., Giallonardo A.T., Berardelli A., Pacifici L., Ferreri F., Tombini M., Gilio F., Quarato P., Conte A., Manganotti P., Bongiovanni L.G., Monaco F., Ferrante D., and Rossini P.M. Slow repetitive TMS for drug-resistant epilepsy: clinical and EEG findings of a placebo-controlled trial. *Epilepsia*, **48**(2):366–374, (2007).

Cao Y., Wilcox K.S., Martin C.E., Rachinsky T.L., Eberwine J., and Dichter M.A. Presence of mRNA for glutamic acid decarboxylase in both excitatory and inhibitory neurons. *Proc Natl Acad Sci U S A*, **93**(18):9844–9849, (1996).

Cardin J.A., Carlén M., Meletis K., Knoblich U., Zhang F., Deisseroth K., Tsai L.H., and Moore C.I. Driving fast-spiking cells induces gamma rhythm and controls sensory responses. *Nature*, **459**(7247):663–667, (2009).

Cardin J.A., Carlén M., Meletis K., Knoblich U., Zhang F., Deisseroth K., Tsai L.H., and Moore C.I. Targeted optogenetic stimulation and recording of neurons in vivo using cell-type-specific expression of Channelrhodopsin-2. *Nat Protoc*, **5**(2):247–254, (2010).

Carlén M., Meletis K., Siegle J.H., Cardin J.A., Futai K., Vierling-Claassen D., Ruehlmann C., Jones S.R., Deisseroth K., Sheng M., Moore C.I., and Tsai L.H. A critical role for NMDA receptors in parvalbumin interneurons for gamma rhythm induction and behavior. *Mol Psychiatry*, , (2011).

Carrea R. and Lanari A. Chronic effect of tetanus toxin applied locally to the cerebral cortex of the dog. *Science*, **137**:342–343, (1962).

Carter M.E., Yizhar O., Chikahisa S., Nguyen H., Adamantidis A., Nishino S., Deisseroth K., and de Lecea L. Tuning arousal with optogenetic modulation of locus coeruleus neurons. *Nat Neurosci*, **13**(12):1526–1533, (2010).

Cauli B., Tong X.K., Rancillac A., Serluca N., Lambolez B., Rossier J., and Hamel E. Cortical GABA interneurons in neurovascular coupling: relays for subcortical vasoactive pathways. *J Neurosci*, **24**(41):8940–8949, (2004).

Cereda C., Berger M.M., and Rossetti A.O. Bowel ischemia: a rare complication of thiopental treatment for status epilepticus. *Neurocrit Care*, **10**(3):355–358, (2009).

Chamberlain J.R., Schwarze U., Wang P.R., Hirata R.K., Hankenson K.D., Pace J.M., Underwood R.A., Song K.M., Sussman M., Byers P.H., and Russell D.W.

Gene targeting in stem cells from individuals with osteogenesis imperfecta. *Science*, **303**(5661):1198–1201, (2004).

Chang J.H., Yang X.F., Zempel J.M., and Rothman S.M. The unilateral cobalt wire model of neocortical epilepsy: a method of producing subacute focal seizures in rodents. *Epilepsy Res*, **61**(1-3):153–160, (2004).

Chang P., Hashemi K.S., and Walker M.C. A novel telemetry system for recording EEG in small animals. *J Neurosci Methods*, **201**(1):106–115, (2011).

Chartrian G., Bergamini L., Dondey M., Klass E., Lennox-Buchtal M., and Petersén I. A glossary of terms most commonly used by clinical electroencephalographers. *Electroencephalogr Clin Neurophysiol*, **37**(5):538–548, (1974).

Chen K., Ratzliff A., Hilgenberg L., Gulyás A., Freund T.F., Smith M., Dinh T.P., Piomelli D., Mackie K., and Soltesz I. Long-term plasticity of endocannabinoid signaling induced by developmental febrile seizures. *Neuron*, **39**(4):599–611, (2003).

Chen K., Neu A., Howard A.L., Földy C., Echegoyen J., Hilgenberg L., Smith M., Mackie K., and Soltesz I. Prevention of plasticity of endocannabinoid signaling inhibits persistent limbic hyperexcitability caused by developmental seizures. *J Neurosci*, **27**(1):46–58, (2007).

Chhatwal J.P., Hammack S.E., Jasnow A.M., Rainnie D.G., and Ressler K.J. Identification of cell-type-specific promoters within the brain using lentiviral vectors. *Gene Ther*, **14**(7):575–583, (2007).

Chow B.Y., Han X., Dobry A.S., Qian X., Chuong A.S., Li M., Henninger M.A., Belfort G.M., Lin Y., Monahan P.E., and Boyden E.S. High-performance genetically targetable optical neural silencing by light-driven proton pumps. *Nature*, **463**(7277):98–102, (2010).

Christine C.W., Starr P.A., Larson P.S., Eberling J.L., Jagust W.J., Hawkins R.A., VanBrocklin H.F., Wright J.F., Bankiewicz K.S., and Aminoff M.J. Safety and tolerability of putaminal AADC gene therapy for Parkinson disease. *Neurology*, **73**(20):1662–1669, (2009).

Chrobak J.J. and Buzsáki G. Gamma oscillations in the entorhinal cortex of the freely behaving rat. *J Neurosci*, **18**(1):388–398, (1998).

Commission-ILAE Guidelines for epidemiologic studies on epilepsy. Commission on Epidemiology and Prognosis, International League Against Epilepsy. *Epilepsia*, **34**(4):592–596, (1993).

Cooke P.M. and Snider R.S. Some cerebellar influences on electrically-induced cerebral seizures. *Epilepsia*, **4**:19–28, (1955).

Corry J.J., Dhar R., Murphy T., and Diringer M.N. Hypothermia for refractory status epilepticus. *Neurocrit Care*, **9**(2):189–197, (2008).

Covington H.E., Lobo M.K., Maze I., Vialou V., Hyman J.M., Zaman S., LaPlant Q., Mouzon E., Ghose S., Tamminga C.A., Neve R.L., Deisseroth K., and Nestler E.J. Antidepressant effect of optogenetic stimulation of the medial prefrontal cortex. *J Neurosci*, **30**(48):16082–16090, (2010).

Cox C.L., Huguenard J.R., and Prince D.A. Peptidergic modulation of intrathalamic circuit activity in vitro: actions of cholecystokinin. *J Neurosci*, **17**(1):70–82, (1997).

Crompton D.E., Scheffer I.E., Taylor I., Cook M.J., McKelvie P.A., Vears D.F., Lawrence K.M., McMahon J.M., Grinton B.E., McIntosh A.M., and Berkovic S.F. Familial mesial temporal lobe epilepsy: a benign epilepsy syndrome showing complex inheritance. *Brain*, **133**(11):3221–3231, (2010).

Cruikshank S.J., Urabe H., Nurmikko A.V., and Connors B.W. Pathway-specific feedforward circuits between thalamus and neocortex revealed by selective optical stimulation of axons. *Neuron*, **65**(2):230–245, (2010).

Dalby B., Cates S., Harris A., Ohki E.C., Tilkins M.L., Price P.J., and Ciccarone V.C. Advanced transfection with Lipofectamine 2000 reagent: primary neurons, siRNA, and high-throughput applications. *Methods*, **33**(2):95–103, (2004).

D'Apuzzo M., Mandolesi G., Reis G., and Schuman E.M. Abundant GFP expression and LTP in hippocampal acute slices by in vivo injection of sindbis virus. *J Neurophysiol*, **86**(2):1037–1042, (2001).

Davidson B.L. and Breakefield X.O. Viral vectors for gene delivery to the nervous system. *Nat Rev Neurosci*, **4**(5):353–364, (2003).

de Almeida L.P., Zala D., Aebischer P., and Déglon N. Neuroprotective effect of a CNTF-expressing lentiviral vector in the quinolinic acid rat model of Huntington's disease. *Neurobiol Dis*, **8**(3):433–446, (2001).

de la Torre J.R., Christianson L.M., Béjà O., Suzuki M.T., Karl D.M., Heidelberg J., and DeLong E.F. Proteorhodopsin genes are distributed among divergent marine bacterial taxa. *Proc Natl Acad Sci U S A*, **100**(22):12830–12835, (2003).

DeFelipe J., López-Cruz P.L., Benavides-Piccione R., Bielza C., naga P.L., Anderson S., Burkhalter A., Cauli B., Fairén A., Feldmeyer D., Fishell G., Fitzpatrick D., Freund T.F., González-Burgos G., Hestrin S., Hill S., Hof P.R., Huang J., Jones E.G., Kawaguchi Y., Kisvárday Z., Kubota Y., Lewis D.A., Marín O., Markram H., McBain C.J., Meyer H.S., Monyer H., Nelson S.B., Rockland K., Rossier J., Rubenstein J.L.R., Rudy B., Scanziani M., Shepherd G.M., Sherwood C.C., Staiger J.F., Tamás G., Thomson A., Wang Y., Yuste R., and Ascoli G.A. New insights into the classification and nomenclature of cortical GABAergic interneurons. *Nat Rev Neurosci*, **14**(3):202–216, (2013).

Deitch J.S. and Fischer I. *The Neuron in Tissue Culture*. Wiley, (1999).

Deng P.Y., Xiao Z., Jha A., Ramonet D., Matsui T., Leitges M., Shin H.S., Porter J.E., Geiger J.D., and Lei S. Cholecystokinin facilitates glutamate release by

increasing the number of readily releasable vesicles and releasing probability. *J Neurosci*, **30**(15):5136–5148, (2010).

Diester I., Kaufman M.T., Mogri M., Pashaie R., Goo W., Yizhar O., Ramakrishnan C., Deisseroth K., and Shenoy K.V. An optogenetic toolbox designed for primates. *Nat Neurosci*, **14**(3):387–397, (2011).

Dinstein I., Pierce K., Eyler L., Solso S., Malach R., Behrmann M., and Courchesne E. Disrupted neural synchronization in toddlers with autism. *Neuron*, **70**(6):1218–1225, (2011).

Druckmann S., Hill S., Schürmann F., Markram H., and Segev I. A Hierarchical Structure of Cortical Interneuron Electrical Diversity Revealed by Automated Statistical Analysis. *Cereb Cortex*, , (2012).

Dudek F.E. and Bertram E.H. Counterpoint to "what is an epileptic seizure?" by d'ambrosio and miller. *Epilepsy Curr*, **10**(4):91–94, (2010).

Dudek H., Ghosh A., and Greenberg M.E. Calcium phosphate transfection of DNA into neurons in primary culture. *Curr Protoc Neurosci*, **Chapter 3**:Unit 3.11, (2001).

Duncan J.S., Sander J.W., Sisodiya S.M., and Walker M.C. Adult epilepsy. *Lancet*, **367**(9516):1087–1100, (2006).

Duque S., Joussemet B., Riviere C., Marais T., Dubreil L., Douar A.M., Fyfe J., Moullier P., Colle M.A., and Barkats M. Intravenous administration of self-complementary AAV9 enables transgene delivery to adult motor neurons. *Mol Ther*, **17**(7):1187–1196, (2009).

Eberling J.L., Jagust W.J., Christine C.W., Starr P., Larson P., Bankiewicz K.S., and Aminoff M.J. Results from a phase I safety trial of hAADC gene therapy for Parkinson disease. *Neurology*, **70**(21):1980–1983, (2008).

Eckhorn R., Bauer R., Jordan W., Brosch M., Kruse W., Munk M., and Reitboeck H.J. Coherent oscillations: a mechanism of feature linking in the visual

cortex? Multiple electrode and correlation analyses in the cat. *Biol Cybern*, **60** (2):121–130, (1988).

Ehlenbeck S., Gradmann D., Braun F.J., and Hegemann P. Evidence for a light-induced H(+) conductance in the eye of the green alga Chlamydomonas reinhardtii. *Biophys J*, **82**(2):740–751, (2002).

Ehrengruber M.U., Lundstrom K., Schweitzer C., Heuss C., Schlesinger S., and Gähwiler B.H. Recombinant Semliki Forest virus and Sindbis virus efficiently infect neurons in hippocampal slice cultures. *Proc Natl Acad Sci U S A*, **96**(12): 7041–7046, (1999).

Elting J.W., van der Naalt J., and Fock J.M. Mild hypothermia for refractory focal status epilepticus in an infant with hemimegalencephaly. *Eur J Paediatr Neurol*, **14**(5):452–455, (2010).

Empson R.M. and Jefferys J.G. Synaptic inhibition in primary and secondary chronic epileptic foci induced by intrahippocampal tetanus toxin in the rat. *J Physiol*, **465**:595–614, (1993).

Empson R.M., Amitai Y., Jefferys J.G., and Gutnick M.J. Injection of tetanus toxin into the neocortex elicits persistent epileptiform activity but only transient impairment of GABA release. *Neuroscience*, **57**(2):235–239, (1993).

Engel J. and ILAE A proposed diagnostic scheme for people with epileptic seizures and with epilepsy: report of the ILAE Task Force on Classification and Terminology. *Epilepsia*, **42**(6):796–803, (2001).

Engel J., Bragin A., Staba R., and Mody I. High-frequency oscillations: what is normal and what is not? *Epilepsia*, **50**(4):598–604, (2009).

Erdö S.L. and Wolff J.R. gamma-Aminobutyric acid outside the mammalian brain. *J Neurochem*, **54**(2):363–372, (1990).

Erlander M.G. and Tobin A.J. The structural and functional heterogeneity of glutamic acid decarboxylase: a review. *Neurochem Res*, **16**(3):215–226, (1991).

Erlander M.G., Tillakaratne N.J., Feldblum S., Patel N., and Tobin A.J. Two genes encode distinct glutamate decarboxylases. *Neuron*, **7**(1):91–100, (1991).

Escors D. and Breckpot K. Lentiviral vectors in gene therapy: their current status and future potential. *Arch Immunol Ther Exp (Warsz)*, **58**(2):107–119, (2010).

Essen L., Siegert R., Lehmann W.D., and Oesterhelt D. Lipid patches in membrane protein oligomers: crystal structure of the bacteriorhodopsin-lipid complex. *Proc Natl Acad Sci U S A*, **95**(20):11673–11678, (1998).

Etherington L.A.V. and Frenguelli B.G. Endogenous adenosine modulates epileptiform activity in rat hippocampus in a receptor subtype-dependent manner. *Eur J Neurosci*, **19**(9):2539–2550, (2004).

Favaro P., Downey H.D., Zhou J.S., Wright J.F., Hauck B., Mingozzi F., High K.A., and Arruda V.R. Host and vector-dependent effects on the risk of germline transmission of AAV vectors. *Mol Ther*, **17**(6):1022–1030, (2009).

Federico M. *Lentivirus gene engineering protocols*. Humana Press, (2003).

Feldmeyer D., Egger V., Lubke J., and Sakmann B. Reliable synaptic connections between pairs of excitatory layer 4 neurones within a single 'barrel' of developing rat somatosensory cortex. *J Physiol*, **521 Pt 1**:169–190, (1999).

Felgner P.L., Gadek T.R., Holm M., Roman R., Chan H.W., Wenz M., Northrop J.P., Ringold G.M., and Danielsen M. Lipofection: a highly efficient, lipid-mediated DNA-transfection procedure. *Proc Natl Acad Sci U S A*, **84**(21): 7413–7417, (1987).

Fell J. and Axmacher N. The role of phase synchronization in memory processes. *Nat Rev Neurosci*, **12**(2):105–118, (2011).

Fernald R.D. Casting a genetic light on the evolution of eyes. *Science*, **313**(5795): 1914–1918, (2006).

Fink H., Rex A., Voits M., and Voigt J.P. Major biological actions of CCK–a critical evaluation of research findings. *Exp Brain Res*, **123**(1-2):77–83, (1998).

Finnerty G.T. and Jefferys J.G.R. Investigation of the neuronal aggregate generating seizures in the rat tetanus toxin model of epilepsy. *J Neurophysiol*, **88**(6):2919–2927, (2002).

Fisahn A., Pike F.G., Buhl E.H., and Paulsen O. Cholinergic induction of network oscillations at 40 Hz in the hippocampus in vitro. *Nature*, **394**(6689): 186–189, (1998).

Flotte T. and Berns K. *Adeno-associated viral vectors for gene therapy*. Elsevier, (2005).

Foster K.W. and Smyth R.D. Light Antennas in phototactic algae. *Microbiol Rev*, **44(4)**:572-630, (1980).

Foster K.W., Saranak J., Patel N., Zarilli G., Okabe M., Kline T., and Nakanishi K. A rhodopsin is the functional photoreceptor for phototaxis in the unicellular eukaryote Chlamydomonas. *Nature*, **311**(5988):756–759, (1984).

Foti S., Haberman R.P., Samulski R.J., and McCown T.J. Adeno-associated virus-mediated expression and constitutive secretion of NPY or NPY13-36 suppresses seizure activity in vivo. *Gene Ther*, **14**(21):1534–1536, (2007).

Foust K.D., Nurre E., Montgomery C.L., Hernandez A., Chan C.M., and Kaspar B.K. Intravascular AAV9 preferentially targets neonatal neurons and adult astrocytes. *Nat Biotechnol*, **27**(1):59–65, (2009).

Freed E.O. HIV-1 gag proteins: diverse functions in the virus life cycle. *Virology*, **251**(1):1–15, (1998).

Fregni F., Otachi P.T.M., Valle A.D., Boggio P.S., Thut G., Rigonatti S.P., Pascual-Leone A., and Valente K.D. A randomized clinical trial of repetitive transcranial magnetic stimulation in patients with refractory epilepsy. *Ann Neurol*, **60**(4):447–455, (2006).

Freund T. and Kali S. Interneurons. **3**(9):4720, (2008).

Freund T.F. and Buzsáki G. Interneurons of the hippocampus. *Hippocampus*, **6**(4):347–470, (1996).

Freund T.F. and Katona I. Perisomatic inhibition. *Neuron*, **56**(1):33–42, (2007).

Fries P., Roelfsema P.R., Engel A.K., König P., and Singer W. Synchronization of oscillatory responses in visual cortex correlates with perception in interocular rivalry. *Proc Natl Acad Sci U S A*, **94**(23):12699–12704, (1997).

Fu H., Dirosario J., Killedar S., Zaraspe K., and McCarty D.M. Correction of neurological disease of mucopolysaccharidosis IIIB in adult mice by rAAV9 trans-blood-brain barrier gene delivery. *Mol Ther*, **19**(6):1025–1033, (2011).

Galvani L. De viribus electricitatis in motu musculari, commentarius. *Bonon. Sci. Art. Inst. Acad.*, **7**:364-415, (1791).

Gamper N. and Shapiro M.S. Exogenous expression of proteins in neurons using the biolistic particle delivery system. *Methods Mol Biol*, **337**:27–38, (2006).

George M.S. and Aston-Jones G. Noninvasive techniques for probing neurocircuitry and treating illness: vagus nerve stimulation (VNS), transcranial magnetic stimulation (TMS) and transcranial direct current stimulation (tDCS). *Neuropsychopharmacology*, **35**(1):301–316, (2010).

Giacobini P. and Wray S. Prenatal expression of cholecystokinin (CCK) in the central nervous system (CNS) of mouse. *Neurosci Lett*, **438**(1):96–101, (2008).

Gibbons H.M. and Dragunow M. Adult human brain cell culture for neuroscience research. *Int J Biochem Cell Biol*, **42**(6):844–856, (2010).

Glickfeld L.L. and Scanziani M. Distinct timing in the activity of cannabinoid-sensitive and cannabinoid-insensitive basket cells. *Nat Neurosci*, **9**(6):807–815, (2006).

Glover C.P.J., Bienemann A.S., Heywood D.J., Cosgrave A.S., and Uney J.B. Adenoviral-mediated, high-level, cell-specific transgene expression: a SYN1-WPRE cassette mediates increased transgene expression with no loss of neuron specificity. *Mol Ther*, **5**(5 Pt 1):509–516, (2002).

Gonçalves M.A.F.V. Adeno-associated virus: from defective virus to effective vector. *Virol J*, **2**:43, (2005).

Gourine A.V., Kasymov V., Marina N., Tang F., Figueiredo M.F., Lane S., Teschemacher A.G., Spyer K.M., Deisseroth K., and Kasparov S. Astrocytes control breathing through pH-dependent release of ATP. *Science*, **329**(5991): 571–575, (2010).

Gouwens N.W., Zeberg H., Tsumoto K., Tateno T., Aihara K., and Robinson H.P.C. Synchronization of firing in cortical fast-spiking interneurons at gamma frequencies: a phase-resetting analysis. *PLoS Comput Biol*, **6**(9), (2010).

Graber K.D. and Prince D.A. Tetrodotoxin prevents posttraumatic epileptogenesis in rats. *Ann Neurol*, **46**(2):234–242, (1999).

Gradinaru V., Thompson K.R., Zhang F., Mogri M., Kay K., Schneider M.B., and Deisseroth K. Targeting and readout strategies for fast optical neural control in vitro and in vivo. *J Neurosci*, **27**(52):14231–14238, (2007).

Gradinaru V., Thompson K.R., and Deisseroth K. eNpHR: a Natronomonas halorhodopsin enhanced for optogenetic applications. *Brain Cell Biol*, **36**(1-4): 129–139, (2008).

Gradinaru V., Zhang F., Ramakrishnan C., Mattis J., Prakash R., Diester I., Goshen I., Thompson K.R., and Deisseroth K. Molecular and cellular approaches for diversifying and extending optogenetics. *Cell*, **141**(1):154–165, (2010).

Graebenitz S., Kedo O., Speckmann E.J., Gorji A., Panneck H., Hans V., Palomero-Gallagher N., Schleicher A., Zilles K., and Pape H.C. Interictal-like

network activity and receptor expression in the epileptic human lateral amygdala. *Brain*, **134**(Pt 10):2929–2947, (2011).

Graham F.L. and van der Eb A.J. Transformation of rat cells by DNA of human adenovirus 5. *Virology*, **54**(2):536–539, (1973).

Gray C.M. and Singer W. Stimulus-specific neuronal oscillations in orientation columns of cat visual cortex. *Proc Natl Acad Sci U S A*, **86**(5):1698–1702, (1989).

Grenier F., Timofeev I., and Steriade M. Focal synchronization of ripples (80-200 Hz) in neocortex and their neuronal correlates. *J Neurophysiol*, **86**(4): 1884–1898, (2001).

Grigorieff N., Ceska T.A., Downing K.H., Baldwin J.M., and Henderson R. Electron-crystallographic refinement of the structure of bacteriorhodopsin. *J Mol Biol*, **259**(3):393–421, (1996).

Gulledge A.T. and Stuart G.J. Excitatory actions of GABA in the cortex. *Neuron*, **37**(2):299–309, (2003).

Gulyás A.I., Miles R., Sík A., Tóth K., Tamamaki N., and Freund T.F. Hippocampal pyramidal cells excite inhibitory neurons through a single release site. *Nature*, **366**(6456):683–687, (1993).

Gunaydin L.A., Yizhar O., Berndt A., Sohal V.S., Deisseroth K., and Hegemann P. Ultrafast optogenetic control. *Nat Neurosci*, **13**(3):387–392, (2010).

Gutkin B.S., Ermentrout G.B., and Reyes A.D. Phase-response curves give the responses of neurons to transient inputs. *J Neurophysiol*, **94**(2):1623–1635, (2005).

Haas K., Sin W.C., Javaherian A., Li Z., and Cline H.T. Single-cell electroporation for gene transfer in vivo. *Neuron*, **29**(3):583–591, (2001).

Haberman R.P. and McCown T.J. Regulation of gene expression in adeno-associated virus vectors in the brain. *Methods*, **28**(2):219–226, (2002).

Haberman R.P., Samulski R.J., and McCown T.J. Attenuation of seizures and neuronal death by adeno-associated virus vector galanin expression and secretion. *Nat Med*, **9**(8):1076–1080, (2003).

Hájos N. and Paulsen O. Network mechanisms of gamma oscillations in the CA3 region of the hippocampus. *Neural Netw*, **22**(8):1113–1119, (2009).

Halgren E., Babb T.L., and Crandall P.H. Responses of human limbic neurons to induced changes in blood gases. *Brain Res*, **132**(1):43–63, (1977).

Hamil N.E., Cock H.R., and Walker M.C. Acute down-regulation of adenosine A(1) receptor activity in status epilepticus. *Epilepsia*, **53**(1):177–188, (2012).

Han X. and Boyden E.S. Multiple-color optical activation, silencing, and desynchronization of neural activity, with single-spike temporal resolution. *PLoS One*, **2**(3):e299, (2007).

Han X., Qian X., Bernstein J.G., Zhou H.H., Franzesi G.T., Stern P., Bronson R.T., Graybiel A.M., Desimone R., and Boyden E.S. Millisecond-timescale optical control of neural dynamics in the nonhuman primate brain. *Neuron*, **62**(2): 191–198, (2009).a.

Han X., Qian X., Stern P., Chuong A.S., and Boyden E.S. Informational lesions: optical perturbation of spike timing and neural synchrony via microbial opsin gene fusions. *Front Mol Neurosci*, **2**:12, (2009).b.

Hasenstaub A., Shu Y., Haider B., Kraushaar U., Duque A., and McCormick D.A. Inhibitory postsynaptic potentials carry synchronized frequency information in active cortical networks. *Neuron*, **47**(3):423–435, (2005).

Hashimoto I. High-frequency oscillations of somatosensory evoked potentials and fields. *J Clin Neurophysiol*, **17**(3):309–320, (2000).

Hashimoto I., Kimura T., Fukushima T., Iguchi Y., Saito Y., Terasaki O., and Sakuma K. Reciprocal modulation of somatosensory evoked N20m primary

response and high-frequency oscillations by interference stimulation. *Clin Neurophysiol*, **110**(8):1445–1451, (1999).

Hecht S., Shlaer S., and Pirenne M.H. Energy, Quanta and Vision. *J Gen Physiol*, **25**(6):819–840, (1942).

Hegemann P., Oesterhelt D., and Bamberg E. The transport activity of the light-driven chloride pump halorhodopsin is regulated by green and blue light. *Biochimica et Biophysica Acta*, **819**:195-205, (1985).

Hegemann P., Gärtner W., and Uhl R. All-trans retinal constitutes the functional chromophore in Chlamydomonas rhodopsin. *Biophys J*, **60**(6):1477–1489, (1991).

Heinrich C., Blum R., Gascón S., Masserdotti G., Tripathi P., Sánchez R., Tiedt S., Schroeder T., Götz M., and Berninger B. Directing astroglia from the cerebral cortex into subtype specific functional neurons. *PLoS Biol*, **8**(5):e1000373, (2010).

Heiss J.D., Walbridge S., Asthagiri A.R., and Lonser R.R. Image-guided convection-enhanced delivery of muscimol to the primate brain. *J Neurosurg*, **112**(4):790–795, (2010).

Hipp J.F., Engel A.K., and Siegel M. Oscillatory synchronization in large-scale cortical networks predicts perception. *Neuron*, **69**(2):387–396, (2011).

Hodgkin A.L. and Huxley A.F. A quantitative description of membrane current and its application to conduction and excitation in nerve. *J Physiol*, **117**(4): 500–544, (1952).

Hodgkin A.L. and Huxley A.F. A quantitative description of membrane current and its application to conduction and excitation in nerve. 1952. *Bull Math Biol*, **52**(1-2):25–71; discussion 5-23, (1990).

Holland E.M., Braun F.J., Nonnengässer C., Harz H., and Hegemann P. The

nature of rhodopsin-triggered photocurrents in Chlamydomonas. I. Kinetics and influence of divalent ions. *Biophys J*, **70**(2):924–931, (1996).

Hormuzdi S.G., Pais I., LeBeau F.E., Towers S.K., Rozov A., Buhl E.H., Whittington M.A., and Monyer H. Impaired electrical signaling disrupts gamma frequency oscillations in connexin 36-deficient mice. *Neuron*, **31**(3): 487–495, (2001).

Hu B., Yang H., Dai B., Tai A., and Wang P. Nonintegrating lentiviral vectors can effectively deliver ovalbumin antigen for induction of antitumor immunity. *Hum Gene Ther*, **20**(12):1652–1664, (2009).

Hu B., Dai B., and Wang P. Vaccines delivered by integration-deficient lentiviral vectors targeting dendritic cells induces strong antigen-specific immunity. *Vaccine*, **28**(41):6675–6683, (2010).

Huber D., Petreanu L., Ghitani N., Ranade S., Hromádka T., Mainen Z., and Svoboda K. Sparse optical microstimulation in barrel cortex drives learned behaviour in freely moving mice. *Nature*, **451**(7174):61–64, (2008).

Hutcheon B. and Yarom Y. Resonance, oscillation and the intrinsic frequency preferences of neurons. *Trends Neurosci*, **23**(5):216–222, (2000).

Hwang R.Y., Zhong L., Xu Y., Johnson T., Zhang F., Deisseroth K., and Tracey W.D. Nociceptive neurons protect Drosophila larvae from parasitoid wasps. *Curr Biol*, **17**(24):2105–2116, (2007).

Ishizuka T., Kakuda M., Araki R., and Yawo H. Kinetic evaluation of photosensitivity in genetically engineered neurons expressing green algae light-gated channels. *Neurosci Res*, **54**(2):85–94, (2006).

Jacobs J., LeVan P., Chander R., Hall J., Dubeau F., and Gotman J. Interictal high-frequency oscillations (80-500 Hz) are an indicator of seizure onset areas independent of spikes in the human epileptic brain. *Epilepsia*, **49**(11): 1893–1907, (2008).

Jacobs J., Levan P., Châtillon C.E., Olivier A., Dubeau F., and Gotman J. High frequency oscillations in intracranial EEGs mark epileptogenicity rather than lesion type. *Brain*, **132**(Pt 4):1022–1037, (2009).a.

Jacobs J., Zijlmans M., Zelmann R., Chatillon C.E., Hall J., Olivier A., Dubeau F., and Gotman J. High-frequency electroencephalographic oscillations correlate with outcome of epilepsy surgery. *Ann Neurol*, **67**(2):209–220, (2010).

Jacobs M.P., Leblanc G.G., Brooks-Kayal A., Jensen F.E., Lowenstein D.H., Noebels J.L., Spencer D.D., and Swann J.W. Curing epilepsy: progress and future directions. *Epilepsy Behav*, **14**(3):438–445, (2009).b.

Janson C., McPhee S., Bilaniuk L., Haselgrove J., Testaiuti M., Freese A., Wang D.J., Shera D., Hurh P., Rupin J., Saslow E., Goldfarb O., Goldberg M., Larijani G., Sharrar W., Liouterman L., Camp A., Kolodny E., Samulski J., and Leone P. Clinical protocol. Gene therapy of Canavan disease: AAV-2 vector for neurosurgical delivery of aspartoacylase gene (ASPA) to the human brain. *Hum Gene Ther*, **13**(11):1391–1412, (2002).

Jasnow A.M., Ressler K.J., Hammack S.E., Chhatwal J.P., and Rainnie D.G. Distinct subtypes of cholecystokinin (CCK)-containing interneurons of the basolateral amygdala identified using a CCK promoter-specific lentivirus. *J Neurophysiol*, **101**(3):1494–1506, (2009).

Jasper H.H. and Andrews H.L. Brain potentials and voluntary muscle activity in man. *J. Neurophysiol.*, **1**:87-100, (1938).

Jin X., Mathers P.H., Szabó G., Katarova Z., and Agmon A. Vertical bias in dendritic trees of non-pyramidal neocortical neurons expressing GAD67-GFP in vitro. *Cereb Cortex*, **11**(7):666–678, (2001).

Jones E.G. and Peters A., editors. *Cerebral Cortex: Volume 1: Cellular Components of the Cerebral Cortex*. Plenum Press, (1984).

Jones M.S., MacDonald K.D., Choi B., Dudek F.E., and Barth D.S. Intracellular correlates of fast (>200 Hz) electrical oscillations in rat somatosensory cortex. *J Neurophysiol*, **84**(3):1505–1518, (2000).

Jung K.H., Trivedi V.D., and Spudich J.L. Demonstration of a sensory rhodopsin in eubacteria. *Mol Microbiol*, **47**(6):1513–1522, (2003).

Kahane P. and Depaulis A. Deep brain stimulation in epilepsy: what is next? *Curr Opin Neurol*, **23**(2):177–182, (2010).

Kang Y., Stein C.S., Heth J.A., Sinn P.L., Penisten A.K., Staber P.D., Ratliff K.L., Shen H., Barker C.K., Martins I., Sharkey C.M., Sanders D.A., McCray P.B., and Davidson B.L. In vivo gene transfer using a nonprimate lentiviral vector pseudotyped with Ross River Virus glycoproteins. *J Virol*, **76**(18):9378–9388, (2002).

Kaplitt M.G., Feigin A., Tang C., Fitzsimons H.L., Mattis P., Lawlor P.A., Bland R.J., Young D., Strybing K., Eidelberg D., and During M.J. Safety and tolerability of gene therapy with an adeno-associated virus (AAV) borne GAD gene for Parkinson's disease: an open label, phase I trial. *Lancet*, **369** (9579):2097–2105, (2007).

Karkar K.M., Garcia P.A., Bateman L.M., Smyth M.D., Barbaro N.M., and Berger M. Focal cooling suppresses spontaneous epileptiform activity without changing the cortical motor threshold. *Epilepsia*, **43**(8):932–935, (2002).

Karson M.A., Whittington K.C., and Alger B.E. Cholecystokinin inhibits endocannabinoid-sensitive hippocampal IPSPs and stimulates others. *Neuropharmacology*, **54**(1):117–128, (2008).

Katarova Z., Mugnaini E., Sekerková G., Mann J.R., Aszódi A., Bösze Z., Greenspan R., and Szabó G. Regulation of cell-type specific expression of lacZ by the 5'-flanking region of mouse GAD67 gene in the central nervous system of transgenic mice. *Eur J Neurosci*, **10**(3):989–999, (1998).

Katarova Z., Sekerková G., Prodan S., Mugnaini E., and Szabó G. Domain-restricted expression of two glutamic acid decarboxylase genes in midgestation mouse embryos. *J Comp Neurol*, **424**(4):607–627, (2000).

Kato H.E., Zhang F., Yizhar O., Ramakrishnan C., Nishizawa T., Hirata K., Ito J., Aita Y., Tsukazaki T., Hayashi S., Hegemann P., Maturana A.D., Ishitani R., Deisseroth K., and Nureki O. Crystal structure of the channelrhodopsin light-gated cation channel. *Nature*, **482**(7385):369–374, (2012).

Katona I., Sperlágh B., Sík A., Käfalvi A., Vizi E.S., Mackie K., and Freund T.F. Presynaptically located CB1 cannabinoid receptors regulate GABA release from axon terminals of specific hippocampal interneurons. *J Neurosci*, **19**(11): 4544–4558, (1999).

Kellinghaus C. and Lüders H.O. Frontal lobe epilepsy. *Epileptic Disord*, **6**(4): 223–239, (2004).

Kennedy J.L., Bradwejn J., Koszycki D., King N., Crowe R., Vincent J., and Fourie O. Investigation of cholecystokinin system genes in panic disorder. *Mol Psychiatry*, **4**(3):284–285, (1999).

Kerwin R., Robinson P., and Stephenson J. Distribution of CCK binding sites in the human hippocampal formation and their alteration in schizophrenia: a post-mortem autoradiographic study. *Psychol Med*, **22**(1):37–43, (1992).

Khorana H.G. Two light-transducing membrane proteins: bacteriorhodopsin and the mammalian rhodopsin. *Proc Natl Acad Sci U S A*, **90**(4):1166–1171, (1993).

Klausberger T., Marton L.F., O'Neill J., Huck J.H.J., Dalezios Y., Fuentealba P., Suen W.Y., Papp E., Kaneko T., Watanabe M., Csicsvari J., and Somogyi P. Complementary roles of cholecystokinin- and parvalbumin-expressing GABAergic neurons in hippocampal network oscillations. *J Neurosci*, **25**(42): 9782–9793, (2005).

Klein R.L., Meyer E.M., Peel A.L., Zolotukhin S., Meyers C., Muzyczka N., and King M.A. Neuron-specific transduction in the rat septohippocampal or nigrostriatal pathway by recombinant adeno-associated virus vectors. *Exp Neurol*, **150**(2):183–194, (1998).

Klein R., Ruttkowski B., Knapp E., Salmons B., Günzburg W.H., and Hohenadl C. WPRE-mediated enhancement of gene expression is promoter and cell line specific. *Gene*, **372**:153–161, (2006).

Klein R.L., Hamby M.E., Gong Y., Hirko A.C., Wang S., Hughes J.A., King M.A., and Meyer E.M. Dose and promoter effects of adeno-associated viral vector for green fluorescent protein expression in the rat brain. *Exp Neurol*, **176**(1): 66–74, (2002).

Kleinlogel S., Feldbauer K., Dempski R.E., Fotis H., Wood P.G., Bamann C., and Bamberg E. Ultra light-sensitive and fast neuronal activation with the $Ca^{2+}$-permeable channelrhodopsin CatCh. *Nat Neurosci*, **14**(4):513–518, (2011).

Kocharyan A., Fernandes P., Tong X.K., Vaucher E., and Hamel E. Specific subtypes of cortical GABA interneurons contribute to the neurovascular coupling response to basal forebrain stimulation. *J Cereb Blood Flow Metab*, **28** (2):221–231, (2008).

Kolbe M., Besir H., Essen L.O., and Oesterhelt D. Structure of the light-driven chloride pump halorhodopsin at 1.8 A resolution. *Science*, **288**(5470): 1390–1396, (2000).

Kongkaneramit L., Sarisuta N., Azad N., Lu Y., Iyer A.K.V., Wang L., and Rojanasakul Y. Dependence of reactive oxygen species and FLICE inhibitory protein on lipofectamine-induced apoptosis in human lung epithelial cells. *J Pharmacol Exp Ther*, **325**(3):969–977, (2008).

Korn H., Oda Y., and Faber D.S. Long-term potentiation of inhibitory circuits

and synapses in the central nervous system. *Proc Natl Acad Sci U S A*, **89**(1): 440–443, (1992).

Korn S.J., Giacchino J.L., Chamberlin N.L., and Dingledine R. Epileptiform burst activity induced by potassium in the hippocampus and its regulation by GABA-mediated inhibition. *J Neurophysiol*, **57**(1):325–340, (1987).

Kotin R.M., Menninger J.C., Ward D.C., and Berns K.I. Mapping and direct visualization of a region-specific viral DNA integration site on chromosome 19q13-qter. *Genomics*, **10**(3):831–834, (1991).

Kravitz A.V., Freeze B.S., Parker P.R.L., Kay K., Thwin M.T., Deisseroth K., and Kreitzer A.C. Regulation of parkinsonian motor behaviours by optogenetic control of basal ganglia circuitry. *Nature*, **466**(7306):622–626, (2010).

Kuehne W. Ueber den Sehpurpur. *Untersuch. physiol. Inst., Heidelberg*, **1(2)**:pp. 119-138, (1878).

Lagali P.S., Balya D., Awatramani G.B., Münch T.A., Kim D.S., Busskamp V., Cepko C.L., and Roska B. Light-activated channels targeted to ON bipolar cells restore visual function in retinal degeneration. *Nat Neurosci*, **11**(6): 667–675, (2008).

Laurent G., Wehr M., and Davidowitz H. Temporal representations of odors in an olfactory network. *J Neurosci*, **16**(12):3837–3847, (1996).

Lawson M.A., Zacks D.N., Derguini F., Nakanishi K., and Spudich J.L. Retinal analog restoration of photophobic responses in a blind Chlamydomonas reinhardtii mutant. Evidence for an archaebacterial like chromophore in a eukaryotic rhodopsin. *Biophys J*, **60**(6):1490–1498, (1991).

Lee J.H., Durand R., Gradinaru V., Zhang F., Goshen I., Kim D.S., Fenno L.E., Ramakrishnan C., and Deisseroth K. Global and local fMRI signals driven by neurons defined optogenetically by type and wiring. *Nature*, **465**(7299): 788–792, (2010).

Lee S.Y. and Soltesz I. Cholecystokinin: a multi-functional molecular switch of neuronal circuits. *Dev Neurobiol*, **71**(1):83–91, (2011).

Leone P., Shera D., McPhee S.W.J., Francis J.S., Kolodny E.H., Bilaniuk L.T., Wang D.J., Assadi M., Goldfarb O., Goldman H.W., Freese A., Young D., During M.J., Samulski R.J., and Janson C.G. Long-term follow-up after gene therapy for canavan disease. *Sci Transl Med*, **4**(165):165ra163, (2012).

Levine M. and Tjian R. Transcription regulation and animal diversity. *Nature*, **424**(6945):147–151, (2003).

LeWitt P.A., Rezai A.R., Leehey M.A., Ojemann S.G., Flaherty A.W., Eskandar E.N., Kostyk S.K., Thomas K., Sarkar A., Siddiqui M.S., Tatter S.B., Schwalb J.M., Poston K.L., Henderson J.M., Kurlan R.M., Richard I.H., Meter L.V., Sapan C.V., During M.J., Kaplitt M.G., and Feigin A. AAV2-GAD gene therapy for advanced Parkinson's disease: a double-blind, sham-surgery controlled, randomised trial. *Lancet Neurol*, **10**(4):309–319, (2011).

Li J. and Yuan J. Caspases in apoptosis and beyond. *Oncogene*, **27**(48): 6194–6206, (2008).

Li J., Edwards P.C., Burghammer M., Villa C., and Schertler G.F.X. Structure of bovine rhodopsin in a trigonal crystal form. *J Mol Biol*, **343**(5):1409–1438, (2004).

Li X., Quan Y., and Wainberg M.A. Controlling elements in replication of the human immunodeficiency virus type 1. *Cell Mol Biol (Noisy-le-grand)*, **43**(3): 443–454, (1997).

Li X., Gutierrez D.V., Hanson M.G., Han J., Mark M.D., Chiel H., Hegemann P., Landmesser L.T., and Herlitze S. Fast noninvasive activation and inhibition of neural and network activity by vertebrate rhodopsin and green algae channelrhodopsin. *Proc Natl Acad Sci U S A*, **102**(49):17816–17821, (2005).

Li Y.X., Schaffner A.E., and Barker J.L. Astrocytes regulate the developmental appearance of GABAergic and glutamatergic postsynaptic currents in cultured embryonic rat spinal neurons. *Eur J Neurosci*, **11**(7):2537–2551, (1999).

Liang F. and Jones E.G. Differential and time-dependent changes in gene expression for type II calcium/calmodulin-dependent protein kinase, 67 kDa glutamic acid decarboxylase, and glutamate receptor subunits in tetanus toxin-induced focal epilepsy. *J Neurosci*, **17**(6):2168–2180, (1997).

Lien C.C. and Jonas P. Kv3 potassium conductance is necessary and kinetically optimized for high-frequency action potential generation in hippocampal interneurons. *J Neurosci*, **23**(6):2058–2068, (2003).

Lima S.Q. and Miesenböck G. Remote control of behavior through genetically targeted photostimulation of neurons. *Cell*, **121**(1):141–152, (2005).

Lin E.J.D., Richichi C., Young D., Baer K., Vezzani A., and During M.J. Recombinant AAV-mediated expression of galanin in rat hippocampus suppresses seizure development. *Eur J Neurosci*, **18**(7):2087–2092, (2003).

Lin J.Y. A user's guide to channelrhodopsin variants: features, limitations and future developments. *Exp Physiol*, **96**(1):19–25, (2011).

Lin J.Y., Lin M.Z., Steinbach P., and Tsien R.Y. Characterization of engineered channelrhodopsin variants with improved properties and kinetics. *Biophys J*, **96**(5):1803–1814, (2009).

Llinás R.R. The intrinsic electrophysiological properties of mammalian neurons: insights into central nervous system function. *Science*, **242**(4886):1654–1664, (1988).

Lo D.C. Neuronal transfection using particle-mediated gene transfer. *Curr Protoc Neurosci*, **Chapter 3**:Unit 3.15, (2001).

Löscher W., Cole A.J., and McLean M.J. Commentary: physical approaches for

the treatment of epilepsy: electrical and magnetic stimulation and cooling. *Neurotherapeutics*, **6**(2):258–262, (2009).

Louis E.D., Williamson P.D., and Darcey T.M. Chronic focal epilepsy induced by microinjection of tetanus toxin into the cat motor cortex. *Electroencephalogr Clin Neurophysiol*, **75**(6):548–557, (1990).

Ludvig N., Kuzniecky R.I., Baptiste S.L., John J.E., von Gizycki H., Doyle W.K., and Devinsky O. Epidural pentobarbital delivery can prevent locally induced neocortical seizures in rats: the prospect of transmeningeal pharmacotherapy for intractable focal epilepsy. *Epilepsia*, **47**(11):1792–1802, (2006).

Luecke H., Schobert B., Richter H.T., Cartailler J.P., and Lanyi J.K. Structure of bacteriorhodopsin at 1.55 A resolution. *J Mol Biol*, **291**(4):899–911, (1999).

Luecke H., Schobert B., Lanyi J.K., Spudich E.N., and Spudich J.L. Crystal structure of sensory rhodopsin II at 2.4 angstroms: insights into color tuning and transducer interaction. *Science*, **293**(5534):1499–1503, (2001).

Mainardi M., Pietrasanta M., Vannini E., Rossetto O., and Caleo M. Tetanus neurotoxin-induced epilepsy in mouse visual cortex. *Epilepsia*, **53**(7): e132–e136, (2012).

Man D., Wang W., Sabehi G., Aravind L., Post A.F., Massana R., Spudich E.N., Spudich J.L., and Béjà O. Diversification and spectral tuning in marine proteorhodopsins. *EMBO J*, **22**(8):1725–1731, (2003).

Man-Aharonovich D., Sabehi G., Sineshchekov O.A., Spudich E.N., Spudich J.L., and Béjà O. Characterization of RS29, a blue-green proteorhodopsin variant from the Red Sea. *Photochem Photobiol Sci*, **3**(5):459–462, (2004).

Mandel R.J. CERE-110, an adeno-associated virus-based gene delivery vector expressing human nerve growth factor for the treatment of Alzheimer's disease. *Curr Opin Mol Ther*, **12**(2):240–247, (2010).

Manno C.S., Pierce G.F., Arruda V.R., Glader B., Ragni M., Rasko J.J., Rasko J., Ozelo M.C., Hoots K., Blatt P., Konkle B., Dake M., Kaye R., Razavi M., Zajko A., Zehnder J., Rustagi P.K., Nakai H., Chew A., Leonard D., Wright J.F., Lessard R.R., Sommer J.M., Tigges M., Sabatino D., Luk A., Jiang H., Mingozzi F., Couto L., Ertl H.C., High K.A., and Kay M.A. Successful transduction of liver in hemophilia by AAV-Factor IX and limitations imposed by the host immune response. *Nat Med*, **12**(3):342–347, (2006).

Marks W.J., Ostrem J.L., Verhagen L., Starr P.A., Larson P.S., Bakay R.A., Taylor R., Cahn-Weiner D.A., Stoessl A.J., Olanow C.W., and Bartus R.T. Safety and tolerability of intraputaminal delivery of CERE-120 (adeno-associated virus serotype 2-neurturin) to patients with idiopathic Parkinson's disease: an open-label, phase I trial. *Lancet Neurol*, **7**(5):400–408, (2008).

Marks W.J., Bartus R.T., Siffert J., Davis C.S., Lozano A., Boulis N., Vitek J., Stacy M., Turner D., Verhagen L., Bakay R., Watts R., Guthrie B., Jankovic J., Simpson R., Tagliati M., Alterman R., Stern M., Baltuch G., Starr P.A., Larson P.S., Ostrem J.L., Nutt J., Kieburtz K., Kordower J.H., and Olanow C.W. Gene delivery of AAV2-neurturin for Parkinson's disease: a double-blind, randomised, controlled trial. *Lancet Neurol*, **9**(12):1164–1172, (2010).

Marson A.G., Al-Kharusi A.M., Alwaidh M., Appleton R., Baker G.A., Chadwick D.W., Cramp C., Cockerell O.C., Cooper P.N., Doughty J., Eaton B., Gamble C., Goulding P.J., Howell S.J.L., Hughes A., Jackson M., Jacoby A., Kellett M., Lawson G.R., Leach J.P., Nicolaides P., Roberts R., Shackley P., Shen J., Smith D.F., Smith P.E.M., Smith C.T., Vanoli A., Williamson P.R., and group S.A.N.A.D.S. The SANAD study of effectiveness of carbamazepine, gabapentin, lamotrigine, oxcarbazepine, or topiramate for treatment of partial epilepsy: an unblinded randomised controlled trial. *Lancet*, **369**(9566): 1000–1015, (2007).

Marty S., MdaP B., and Berninger B. Neurotrophins and activity-dependent

plasticity of cortical interneurons. *Trends Neurosci*, **20**(5):198–202, (1997).

Masotti A., Mossa G., Cametti C., Ortaggi G., Bianco A., Grosso N.D., Malizia D., and Esposito C. Comparison of different commercially available cationic liposome-DNA lipoplexes: Parameters influencing toxicity and transfection efficiency. *Colloids Surf B Biointerfaces*, **68**(2):136–144, (2009).

Matsuno-Yagi A. and Mukohata Y. Two possible roles of bacteriorhodopsin; a comparative study of strains of Halobacterium halobium differing in pigmentation. *Biochem Biophys Res Commun*, **78**(1):237–243, (1977).

Mattis J., Tye K.M., Ferenczi E.A., Ramakrishnan C., O'Shea D.J., Prakash R., Gunaydin L.A., Hyun M., Fenno L.E., Gradinaru V., Yizhar O., and Deisseroth K. Principles for applying optogenetic tools derived from direct comparative analysis of microbial opsins. *Nat Methods*, **9**(2):159–172, (2012).

Mazarakis N.D., Azzouz M., Rohll J.B., Ellard F.M., Wilkes F.J., Olsen A.L., Carter E.E., Barber R.D., Baban D.F., Kingsman S.M., Kingsman A.J., O'Malley K., and Mitrophanous K.A. Rabies virus glycoprotein pseudotyping of lentiviral vectors enables retrograde axonal transport and access to the nervous system after peripheral delivery. *Hum Mol Genet*, **10**(19):2109–2121, (2001).

McCown T.J. Adeno-associated virus vector-mediated expression and constitutive secretion of galanin suppresses limbic seizure activity. *Neurotherapeutics*, **6**(2):307–311, (2009).

McNaught A.D. and Wilkinson A. *IUPAC. Compendium of Chemical Terminology, 2nd ed.* Blackwell Scientific Publications, Oxford., (1997 (online version 2012)). XML on-line corrected version: http://goldbook.iupac.org (2006-) created by M. Nic, J. Jirat, B. Kosata; updates compiled by A. Jenkins.

McPhee S.W.J., Janson C.G., Li  C., Samulski R.J., Camp A.S., Francis J., Shera

D., Lioutermann L., Feely M., Freese A., and Leone P. Immune responses to AAV in a phase I study for Canavan disease. *J Gene Med*, **8**(5):577–588, (2006).

Meisler M.H., O'Brien J.E., and Sharkey L.M. Sodium channel gene family: epilepsy mutations, gene interactions and modifier effects. *J Physiol*, **588**(Pt 11):1841–1848, (2010).

Mellanby J. and Thompson P.A. Tetanus toxin in the rat hippocampus [proceedings]. *J Physiol*, **269**(1):44P–45P, (1977).

Mellanby J., George G., Robinson A., and Thompson P. Epileptiform syndrome in rats produced by injecting tetanus toxin into the hippocampus. *J Neurol Neurosurg Psychiatry*, **40**(4):404–414, (1977).

Mellanby J., Oliva M., Peniket A., and Nicholls B. The effect of experimental epilepsy induced by injection of tetanus toxin into the amygdala of the rat on eating behaviour and response to novelty. *Behav Brain Res*, **100**(1-2):113–122, (1999).

Mellanby J. Elimination of 125 - I from rat brain after injection of small doses of 125 - I labelled tetanus toxin into the hippocampus Mellanby 1989. *Neurosci. Lett.*, , (1989).

Miesenböck G. Optogenetic control of cells and circuits. *Annu Rev Cell Dev Biol*, **27**:731–758, (2011).

Miller K.K., Hoffer A., Svoboda K.R., and Lupica C.R. Cholecystokinin increases GABA release by inhibiting a resting K+ conductance in hippocampal interneurons. *J Neurosci*, **17**(13):4994–5003, (1997).

Min N., Joh T.H., Kim K.S., Peng C., and Son J.H. 5' upstream DNA sequence of the rat tyrosine hydroxylase gene directs high-level and tissue-specific expression to catecholaminergic neurons in the central nervous system of transgenic mice. *Brain Res Mol Brain Res*, **27**(2):281–289, (1994).

Mingozzi F. and High K.A. Therapeutic in vivo gene transfer for genetic disease using AAV: progress and challenges. *Nat Rev Genet*, **12**(5):341–355, (2011).

Mitchell R.S., Beitzel B.F., Schroder A.R.W., Shinn P., Chen H., Berry C.C., Ecker J.R., and Bushman F.D. Retroviral DNA integration: ASLV, HIV, and MLV show distinct target site preferences. *PLoS Biol*, **2**(8):E234, (2004).

Mizuseki K., Diba K., Pastalkova E., and Buzsáki G. Hippocampal CA1 pyramidal cells form functionally distinct sublayers. *Nat Neurosci*, **14**(9): 1174–1181, (2011).

Modur P.N., Zhang S., and Vitaz T.W. Ictal High-Frequency Oscillations in Neocortical Epilepsy: Implications for Seizure Localization and Surgical Resection. *Epilepsia*, , (2011).

Mohajeri M.H., Figlewicz D.A., and Bohn M.C. Intramuscular grafts of myoblasts genetically modified to secrete glial cell line-derived neurotrophic factor prevent motoneuron loss and disease progression in a mouse model of familial amyotrophic lateral sclerosis. *Hum Gene Ther*, **10**(11):1853–1866, (1999).

Montgomery S.M. and Buzsáki G. Gamma oscillations dynamically couple hippocampal CA3 and CA1 regions during memory task performance. *Proc Natl Acad Sci U S A*, **104**(36):14495–14500, (2007).

Montgomery S.M., Sirota A., and Buzsáki G. Theta and gamma coordination of hippocampal networks during waking and rapid eye movement sleep. *J Neurosci*, **28**(26):6731–6741, (2008).

Morozov Y.M., Ayoub A.E., and Rakic P. Translocation of synaptically connected interneurons across the dentate gyrus of the early postnatal rat hippocampus. *J Neurosci*, **26**(19):5017–5027, (2006).

Moscioni D., Morizono H., McCarter R., Stern A., Cabrera-Luque J., Hoang A., Sanmiguel J., Wu D., Bell P., Gao G., Raper S.E.and Wilson J., and Batshaw M.

Long-term correction of ammonia metabolism and prolonged survival in ornithine transcarbamylase-deficient mice following liver-directed treatment with adeno-associated viral vectors. *Mol. Ther.*, **14**:25-33, (2006).

Müller M., Bamann C., Bamberg E., and Kühlbrandt W. Projection structure of channelrhodopsin-2 at 6 Åresolution by electron crystallography. *J Mol Biol*, **414**(1):86–95, (2011).

Nagel G., Ollig D., Fuhrmann M., Kateriya S., Musti A.M., Bamberg E., and Hegemann P. Channelrhodopsin-1: a light-gated proton channel in green algae. *Science*, **296**(5577):2395–2398, (2002).

Nagel G., Szellas T., Huhn W., Kateriya S., Adeishvili N., Berthold P., Ollig D., Hegemann P., and Bamberg E. Channelrhodopsin-2, a directly light-gated cation-selective membrane channel. *Proc Natl Acad Sci U S A*, **100**(24): 13940–13945, (2003).

Nagel G., Brauner M., Liewald J.F., Adeishvili N., Bamberg E., and Gottschalk A. Light activation of channelrhodopsin-2 in excitable cells of Caenorhabditis elegans triggers rapid behavioral responses. *Curr Biol*, **15**(24):2279–2284, (2005).

Naldini L., Blömer U., Gallay P., Ory D., Mulligan R., Gage F.H., Verma I.M., and Trono D. In vivo gene delivery and stable transduction of nondividing cells by a lentiviral vector. *Science*, **272**(5259):263–267, (1996).

Nathanson J.L. Short promoters in viral vectors drive selective expression in mammalian inhibitory neurons, but do not restrict activity to specific inhibitory cell-types. *frontiers in neural circuits*, **3**, (2009).

Nathanson J.L., Yanagawa Y., Obata K., and Callaway E.M. Preferential labeling of inhibitory and excitatory cortical neurons by endogenous tropism of adeno-associated virus and lentivirus vectors. *Neuroscience*, **161**(2):441–450, (2009).

Neve R. Viral Core Newsletter (Feb 11). http://mcgovern.mit.edu/technology/viral-vector/viral-core-newsletter, (2011).

Neville K.R. and Haberly L.B. Beta and gamma oscillations in the olfactory system of the urethane-anesthetized rat. *J Neurophysiol*, **90**(6):3921–3930, (2003).

Nilsen K.E., Walker M.C., and Cock H.R. Characterization of the tetanus toxin model of refractory focal neocortical epilepsy in the rat. *Epilepsia*, **46**(2): 179–187, (2005).

Noble F. and Roques B. *Cholecystokinin Peptides in Brain Function. Handbook of Neurochemistry and Molecular Neurobiology.* (2006).

Noe F., Vaghi V., Balducci C., Fitzsimons H., Bland R., Zardoni D., Sperk G., Carli M., During M.J., and Vezzani A. Anticonvulsant effects and behavioural outcomes of rAAV serotype 1 vector-mediated neuropeptide Y overexpression in rat hippocampus. *Gene Ther*, **17**(5):643–652, (2010).

Obeso J.A., Rothwell J.C., and Marsden C.D. The spectrum of cortical myoclonus. From focal reflex jerks to spontaneous motor epilepsy. *Brain*, **108 ( Pt 1)**:193–124, (1985).

Oesterhelt D. and Stoeckenius W. Functions of a new photoreceptor membrane. *Proc Natl Acad Sci U S A*, **70**(10):2853–2857, (1973).

Oh E., Maejima T., Liu C., Deneris E., and Herlitze S. Substitution of 5-HT1A receptor signaling by a light-activated G protein-coupled receptor. *J Biol Chem*, **285**(40):30825–30836, (2010).

O'Keefe J. and Recce M.L. Phase relationship between hippocampal place units and the EEG theta rhythm. *Hippocampus*, **3**(3):317–330, (1993).

Pagano J.S. and Vaheri A. Enhancement of infectivity of poliovirus RNA with

diethylaminoethyl-dextran (DEAE-D). *Arch Gesamte Virusforsch*, **17**(3): 456–464, (1965).

Palczewski K., Kumasaka T., Hori T., Behnke C.A., Motoshima H., Fox B.A., Trong I.L., Teller D.C., Okada T., Stenkamp R.E., Yamamoto M., and Miyano M. Crystal structure of rhodopsin: A G protein-coupled receptor. *Science*, **289** (5480):739–745, (2000).

Palfi S. ProSavin a gene therapy approach for Parkinson disease: Phase I clinical trial update. *Hum. Gene Ther.*, **21**:1364, (2010).

Pálhalmi J., Paulsen O., Freund T.F., and Hájos N. Distinct properties of carbachol- and DHPG-induced network oscillations in hippocampal slices. *Neuropharmacology*, **47**(3):381–389, (2004).

Palva S., Palva J.M., Shtyrov Y., Kujala T., Ilmoniemi R.J., Kaila K., and Näätänen R. Distinct gamma-band evoked responses to speech and non-speech sounds in humans. *J Neurosci*, **22**(4):RC211, (2002).

Panayiotopoulos C. *The Epilepsies: Seizures, Syndromes and Management.* Bladon Medical Publishing, (2005).

Paradiso B., Marconi P., Zucchini S., Berto E., Binaschi A., Bozac A., Buzzi A., Mazzuferi M., Magri E., Mora G.N., Rodi D., Su T., Volpi I., Zanetti L., Marzola A., Manservigi R., Fabene P.F., and Simonato M. Localized delivery of fibroblast growth factor-2 and brain-derived neurotrophic factor reduces spontaneous seizures in an epilepsy model. *Proc Natl Acad Sci U S A*, **106**(17): 7191–7196, (2009).

Pascual-Leone A., Tarazona F., Keenan J., Tormos J.M., Hamilton R., and Catala M.D. Transcranial magnetic stimulation and neuroplasticity. *Neuropsychologia*, **37**(2):207–217, (1999).

Paxinos G. and Watson C. *The rat atlas in stereotaxic co-ordinates*. Academic Press, (1986).

Paz J.T., Davidson T.J., Frechette E.S., Delord B., Parada I., Peng K., Deisseroth K., and Huguenard J.R. Closed-loop optogenetic control of thalamus as a tool for interrupting seizures after cortical injury. *Nat Neurosci*, , (2012).

Pebay-Peyroula E., Rummel G., Rosenbusch J.P., and Landau E.M. X-ray structure of bacteriorhodopsin at 2.5 angstroms from microcrystals grown in lipidic cubic phases. *Science*, **277**(5332):1676–1681, (1997).

Pedroarena C. and Llinás R. Dendritic calcium conductances generate high-frequency oscillation in thalamocortical neurons. *Proc Natl Acad Sci U S A*, **94**(2):724–728, (1997).

Pellizzari R., Rossetto O., Schiavo G., and Montecucco C. Tetanus and botulinum neurotoxins: mechanism of action and therapeutic uses. *Philos Trans R Soc Lond B Biol Sci*, **354**(1381):259–268, (1999).

Philippe S., Sarkis C., Barkats M., Mammeri H., Ladroue C., Petit C., Mallet J., and Serguera C. Lentiviral vectors with a defective integrase allow efficient and sustained transgene expression in vitro and in vivo. *Proc Natl Acad Sci U S A*, **103**(47):17684–17689, (2006).

Pike F.G., Goddard R.S., Suckling J.M., Ganter P., Kasthuri N., and Paulsen O. Distinct frequency preferences of different types of rat hippocampal neurones in response to oscillatory input currents. *J Physiol*, **529 Pt 1**:205–213, (2000).

Pinault D. and Deschênes M. Voltage-dependent 40-Hz oscillations in rat reticular thalamic neurons in vivo. *Neuroscience*, **51**(2):245–258, (1992).

Pitkaenen A., Schwartzkroin P., and S.L. M. *Models of Seizures and Epilepsy*. Elsevier Academic Press, (2006).

Pitler T.A. and Alger B.E. Cholinergic excitation of GABAergic interneurons in the rat hippocampal slice. *J Physiol*, **450**:127–142, (1992).

Polderman K.H. Induced hypothermia and fever control for prevention and treatment of neurological injuries. *Lancet*, **371**(9628):1955–1969, (2008).

Pool J.L. Psychosurgery in older people. *J Am Geriatr Soc*, **2**(7):456–466, (1954).

Prechtl J.C. Visual motion induces synchronous oscillations in turtle visual cortex. *Proc Natl Acad Sci U S A*, **91**(26):12467–12471, (1994).

Purcell D.F. and Martin M.A. Alternative splicing of human immunodeficiency virus type 1 mRNA modulates viral protein expression, replication, and infectivity. *J Virol*, **67**(11):6365–6378, (1993).

Radhakrishnan K. Challenges in the management of epilepsy in resource-poor countries. *Nat Rev Neurol*, **5**(6):323–330, (2009).

Rahim A.A., Wong A.M.S., Howe S.J., Buckley S.M.K., Acosta-Saltos A.D., Elston K.E., Ward N.J., Philpott N.J., Cooper J.D., Anderson P.N., Waddington S.N., Thrasher A.J., and Raivich G. Efficient gene delivery to the adult and fetal CNS using pseudotyped non-integrating lentiviral vectors. *Gene Ther*, **16** (4):509–520, (2009).

Raimondo J.V., Kay L., Ellender T.J., and Akerman C.J. Optogenetic silencing strategies differ in their effects on inhibitory synaptic transmission. *Nat Neurosci*, **15**(8):1102–1104, (2012).

Ramcharitar J.U., Tan E.W., and Fortune E.S. Global electrosensory oscillations enhance directional responses of midbrain neurons in eigenmannia. *J Neurophysiol*, **96**(5):2319–2326, (2006).

Ribak C.E., Seress L., Weber P., Epstein C.M., Henry T.R., and Bakay R.A. Alumina gel injections into the temporal lobe of rhesus monkeys cause complex partial seizures and morphological changes found in human temporal lobe epilepsy. *J Comp Neurol*, **401**(2):266–290, (1998).

Riban V., Fitzsimons H.L., and During M.J. Gene therapy in epilepsy. *Epilepsia*, **50**(1):24–32, (2009).

Richichi C., Lin E.J.D., Stefanin D., Colella D., Ravizza T., Grignaschi G., Veglianese P., Sperk G., During M.J., and Vezzani A. Anticonvulsant and

antiepileptogenic effects mediated by adeno-associated virus vector neuropeptide Y expression in the rat hippocampus. *J Neurosci*, **24**(12): 3051–3059, (2004).

Riedner B.A., Hulse B.K., Murphy M.J., Ferrarelli F., and Tononi G. Temporal dynamics of cortical sources underlying spontaneous and peripherally evoked slow waves. *Prog Brain Res*, **193**:201–218, (2011).

Roelfsema P.R., König P., Engel A.K., Sireteanu R., and Singer W. Reduced synchronization in the visual cortex of cats with strabismic amblyopia. *Eur J Neurosci*, **6**(11):1645–1655, (1994).

Roopun A.K., Simonotto J.D., Pierce M.L., Jenkins A., Nicholson C., Schofield I.S., Whittaker R.G., Kaiser M., Whittington M.A., Traub R.D., and Cunningham M.O. A nonsynaptic mechanism underlying interictal discharges in human epileptic neocortex. *Proc Natl Acad Sci U S A*, **107**(1): 338–343, (2010).

Rothman S.M. The therapeutic potential of focal cooling for neocortical epilepsy. *Neurotherapeutics*, **6**(2):251–257, (2009).

Roux E. and Borrell A. Tetanos cerebral et immunite contre le tetanos. *Ann Inst Pasteur*, **4**:225-239, (1898).

Ryu M.H., Moskvin O.V., Siltberg-Liberles J., and Gomelsky M. Natural and engineered photoactivated nucleotidyl cyclases for optogenetic applications. *J Biol Chem*, **285**(53):41501–41508, (2010).

Sabehi G., Massana R., Bielawski J.P., Rosenberg M., Delong E.F., and Béjà O. Novel Proteorhodopsin variants from the Mediterranean and Red Seas. *Environ Microbiol*, **5**(10):842–849, (2003).

Sakmar T.P. Rhodopsin: a prototypical G protein-coupled receptor. *Prog Nucleic Acid Res Mol Biol*, **59**:1–34, (1998).

Salinas E. and Sejnowski T.J. Correlated neuronal activity and the flow of neural information. *Nat Rev Neurosci*, **2**(8):539–550, (2001).

Sanjuan J., Toirac I., González J.C., Leal C., Moltó M.D., Nájera C., and Frutos R.D. A possible association between the CCK-AR gene and persistent auditory hallucinations in schizophrenia. *Eur Psychiatry*, **19**(6):349–353, (2004).

Sastry L., Johnson T., Hobson M.J., Smucker B., and Cornetta K. Titering lentiviral vectors: comparison of DNA, RNA and marker expression methods. *Gene Ther*, **9**(17):1155–1162, (2002).

Sauer J.F., Strüber M., and Bartos M. Interneurons provide circuit-specific depolarization and hyperpolarization. *J Neurosci*, **32**(12):4224–4229, (2012).

Sayin U., Osting S., Hagen J., Rutecki P., and Sutula T. Spontaneous seizures and loss of axo-axonic and axo-somatic inhibition induced by repeated brief seizures in kindled rats. *J Neurosci*, **23**(7):2759–2768, (2003).

Scanziani M. and Häusser M. Electrophysiology in the age of light. *Nature*, **461** (7266):930–939, (2009).

Schiavo G., Papini E., Genna G., and Montecucco C. An intact interchain disulfide bond is required for the neurotoxicity of tetanus toxin. *Infect Immun*, **58**(12):4136–4141, (1990).

Schiavo G., Demel R., and Montecucco C. On the role of polysialoglycosphingolipids as tetanus toxin receptors. A study with lipid monolayers. *Eur J Biochem*, **199**(3):705–711, (1991).

Schiavo G., Benfenati F., Poulain B., Rossetto O., de Laureto P.P., DasGupta B.R., and Montecucco C. Tetanus and botulinum-B neurotoxins block neurotransmitter release by proteolytic cleavage of synaptobrevin. *Nature*, **359**(6398):832–835, (1992).

Schiffmann S.N. and Vanderhaeghen J.J. Distribution of cells containing mRNA encoding cholecystokinin in the rat central nervous system. *J Comp Neurol*, **304**(2):219–233, (1991).

Schiller Y. and Najjar Y. Quantifying the response to antiepileptic drugs: effect of past treatment history. *Neurology*, **70**(1):54–65, (2008).

Schlegel R., Tralka T.S., Willingham M.C., and Pastan I. Inhibition of VSV binding and infectivity by phosphatidylserine: is phosphatidylserine a VSV-binding site? *Cell*, **32**(2):639–646, (1983).

Schobert B. and Lanyi J.K. Halorhodopsin is a light-driven chloride pump. *J Biol Chem*, **257**(17):10306–10313, (1982).

Schoenenberger P., Gerosa D., and Oertner T.G. Temporal control of immediate early gene induction by light. *PLoS One*, **4**(12):e8185, (2009).

Schrödinger, LLC The PyMOL Molecular Graphics System, Version 1.3r1. (2010).

Schuele S.U. and Lueders H.O. Intractable epilepsy: management and therapeutic alternatives. *Lancet Neurol*, **7**(6):514–524, (2008).

Shaner N.C., Campbell R.E., Steinbach P.A., Giepmans B.N.G., Palmer A.E., and Tsien R.Y. Improved monomeric red, orange and yellow fluorescent proteins derived from Discosoma sp. red fluorescent protein. *Nat Biotechnol*, **22**(12): 1567–1572, (2004).

Shigekawa K. and Dower W.J. Electroporation of eukaryotes and prokaryotes: a general approach to the introduction of macromolecules into cells. *Biotechniques*, **6**(8):742–751, (1988).

Shiramizu B., Herndier B.G., and McGrath M.S. Identification of a common clonal human immunodeficiency virus integration site in human immunodeficiency virus-associated lymphomas. *Cancer Res*, **54**(8):2069–2072, (1994).

Silfverhuth M.J., Kortelainen J., Ruohonen J., Suominen K., Niinimäki J., Sonkajärvi E., Kiviniemi V., Alahuhta S., Jäntti V., Tervonen O., and Seppänen T. A characteristic time sequence of epileptic activity in EEG during dynamic penicillin-induced focal epilepsy-A preliminary study. *Seizure*, **20**(7):513–519, (2011).

Sillanpää M. Remission of seizures and predictors of intractability in long-term follow-up. *Epilepsia*, **34**(5):930–936, (1993).

Sineshchekov O.A., Govorunova E.G., Dér A., Keszthelyi L., and Nultsch W. Photoinduced electric currents in carotenoid-deficient Chlamydomonas mutants reconstituted with retinal and its analogs. *Biophys J*, **66**(6):2073–2084, (1994).

Sineshchekov O.A., Jung K.H., and Spudich J.L. Two rhodopsins mediate phototaxis to low- and high-intensity light in Chlamydomonas reinhardtii. *Proc Natl Acad Sci U S A*, **99**(13):8689–8694, (2002).

Sisodiya S. and Manford M. *Epilepsy 2009 From Benchside to Bedside Chapter 14, Frontal Lobe Epilepsy*. (2009).

Smale S.T. and Kadonaga J.T. The RNA polymerase II core promoter. *Annu Rev Biochem*, **72**:449–479, (2003).

Somogyi P. and Klausberger T. Defined types of cortical interneurone structure space and spike timing in the hippocampus. *J Physiol*, **562**(Pt 1):9–26, (2005).

Spudich J.L. Variations on a molecular switch: transport and sensory signalling by archaeal rhodopsins. *Mol Microbiol*, **28**(6):1051–1058, (1998).

Spudich J.L., Yang C.S., Jung K.H., and Spudich E.N. Retinylidene proteins: structures and functions from archaea to humans. *Annu Rev Cell Dev Biol*, **16**: 365–392, (2000).

Steriade M. *Electroencephalography: Basic Principles, Clinical Applications, and*

*Related Fields Chapter 3 - Cellular Substrates of Brain Rhythms*. Lippincott Williams & Wilkins, (2005).

Stewart H.J., Fong-Wong L., Strickland I., Chipchase D., Kelleher M., Stevenson L., Thoree V., McCarthy J., Ralph G.S., Mitrophanous K.A., and Radcliffe P.A. A stable producer cell line for the manufacture of a lentiviral vector for gene therapy of Parkinson's disease. *Hum Gene Ther*, **22**(3):357–369, (2011).

Stierl M., Stumpf P., Udwari D., Gueta R., Hagedorn R., Losi A., Gärtner W., Petereit L., Efetova M., Schwarzel M., Oertner T.G., Nagel G., and Hegemann P. Light modulation of cellular cAMP by a small bacterial photoactivated adenylyl cyclase, bPAC, of the soil bacterium Beggiatoa. *J Biol Chem*, **286**(2): 1181–1188, (2011).

Stuber G.D., Sparta D.R., Stamatakis A.M., van Leeuwen W.A., Hardjoprajitno J.E., Cho S., Tye K.M., Kempadoo K.A., Zhang F., Deisseroth K., and Bonci A. Excitatory transmission from the amygdala to nucleus accumbens facilitates reward seeking. *Nature*, **475**(7356):377–380, (2011).

Sun W., Fu W., Mao W., Wang D., and Wang Y. Low-frequency repetitive transcranial magnetic stimulation for the treatment of refractory partial epilepsy. *Clin EEG Neurosci*, **42**(1):40–44, (2011).

Suzuki T., Yamasaki K., Fujita S., Oda K., Iseki M., Yoshida K., Watanabe M., Daiyasu H., Toh H., Asamizu E., Tabata S., Miura K., Fukuzawa H., Nakamura S., and Takahashi T. Archaeal-type rhodopsins in Chlamydomonas: model structure and intracellular localization. *Biochem Biophys Res Commun*, **301**(3):711–717, (2003).

Szabadics J., Varga C., Molnár G., Oláh S., Barzó P., and Tamás G. Excitatory effect of GABAergic axo-axonic cells in cortical microcircuits. *Science*, **311** (5758):233–235, (2006).

Szabó G., Katarova Z., and Greenspan R. Distinct protein forms are produced

from alternatively spliced bicistronic glutamic acid decarboxylase mRNAs during development. *Mol Cell Biol*, **14**(11):7535–7545, (1994).

Szabó G., Katarova Z., Körtvély E., Greenspan R.J., and Urban Z. Structure and the promoter region of the mouse gene encoding the 67-kD form of glutamic acid decarboxylase. *DNA Cell Biol*, **15**(12):1081–1091, (1996).

Tabata H. and Nakajima K. Efficient in utero gene transfer system to the developing mouse brain using electroporation: visualization of neuronal migration in the developing cortex. *Neuroscience*, **103**(4):865–872, (2001).

Takahashi T., Tomioka H.and Kamo N., and Kobatake Y. A photosystem other than PS370 also mediates the negative phototaxis of Halobacterium halobium. *FEMS Microbiol. Lett.*, **28**:161-164, (1985).

Takahashi T., Yoshihara K., Watanabe M., Kubota M., Johnson R., Derguini F., and Nakanishi K. Photoisomerization of retinal at 13-ene is important for phototaxis of Chlamydomonas reinhardtii: simultaneous measurements of phototactic and photophobic responses. *Biochem Biophys Res Commun*, **178**(3): 1273–1279, (1991).

Tamamaki N., Yanagawa Y., Tomioka R., Miyazaki J.I., Obata K., and Kaneko T. Green fluorescent protein expression and colocalization with calretinin, parvalbumin, and somatostatin in the GAD67-GFP knock-in mouse. *J Comp Neurol*, **467**(1):60–79, (2003).

Teschemacher A.G., Wang S., Lonergan T., Duale H., Waki H., Paton J.F.R., and Kasparov S. Targeting specific neuronal populations using adeno- and lentiviral vectors: applications for imaging and studies of cell function. *Exp Physiol*, **90**(1):61–69, (2005).

Theofilas P., Brar S., Stewart K.A., Shen H.Y., Sandau U.S., Poulsen D., and Boison D. Adenosine kinase as a target for therapeutic antisense strategies in epilepsy. *Epilepsia*, **52**(3):589–601, (2011).

Thomas C.E., Schiedner G., Kochanek S., Castro M.G., and Löwenstein P.R. Peripheral infection with adenovirus causes unexpected long-term brain inflammation in animals injected intracranially with first-generation, but not with high-capacity, adenovirus vectors: toward realistic long-term neurological gene therapy for chronic diseases. *Proc Natl Acad Sci U S A*, **97**(13):7482–7487, (2000).

Tiesinga P. and Sejnowski T.J. Cortical enlightenment: are attentional gamma oscillations driven by ING or PING? *Neuron*, **63**(6):727–732, (2009).

Tiesinga P., Fellous J.M., and Sejnowski T.J. Regulation of spike timing in visual cortical circuits. *Nat Rev Neurosci*, **9**(2):97–107, (2008).

Tonnesen J., Sorensen A.T., Deisseroth K., Lundberg C., and Kokaia M. Optogenetic control of epileptiform activity. *Proc Natl Acad Sci U S A*, **106**(29): 12162–12167, (2009).

Towne C., Schneider B.L., Kieran D., Redmond D.E., and Aebischer P. Efficient transduction of non-human primate motor neurons after intramuscular delivery of recombinant AAV serotype 6. *Gene Ther*, **17**(1):141–146, (2010).

Traub R.D. and Whittington M.A. *Cortical Oscillations in health and Disease*. Oxford University Press, (2010).

Traub R.D., Whittington M.A., Buhl E.H., LeBeau F.E., Bibbig A., Boyd S., Cross H., and Baldeweg T. A possible role for gap junctions in generation of very fast EEG oscillations preceding the onset of, and perhaps initiating, seizures. *Epilepsia*, **42**(2):153–170, (2001).

Trono D. *Lentiviral Vectors*. Springer Verlag, (2002).

Tsujino N., Yamanaka A., Ichiki K., Muraki Y., Kilduff T.S., ichi Yagami K., Takahashi S., Goto K., and Sakurai T. Cholecystokinin activates orexin/hypocretin neurons through the cholecystokinin A receptor. *J Neurosci*, **25**(32):7459–7469, (2005).

Tye K.M., Prakash R., Kim S.Y., Fenno L.E., Grosenick L., Zarabi H., Thompson K.R., Gradinaru V., Ramakrishnan C., and Deisseroth K. Amygdala circuitry mediating reversible and bidirectional control of anxiety. *Nature*, **471**(7338): 358–362, (2011).

Uhlhaas P.J. and Singer W. Abnormal neural oscillations and synchrony in schizophrenia. *Nat Rev Neurosci*, **11**(2):100–113, (2010).

Uhlhaas P.J., Haenschel C., Nikolić D., and Singer W. The role of oscillations and synchrony in cortical networks and their putative relevance for the pathophysiology of schizophrenia. *Schizophr Bull*, **34**(5):927–943, (2008).

Van der Velden H.A. The number of quanta necessary for the perception of light of the human eye. *Ophthalmologica*, **111**(6):321–331, (1946).

Venter J.C., Remington K., Heidelberg J.F., Halpern A.L., Rusch D., Eisen J.A., Wu D., Paulsen I., Nelson K.E., Nelson W., Fouts D.E., Levy S., Knap A.H., Lomas M.W., Nealson K., White O., Peterson J., Hoffman J., Parsons R., Baden-Tillson H., Pfannkoch C., Rogers Y.H., and Smith H.O. Environmental genome shotgun sequencing of the Sargasso Sea. *Science*, **304**(5667):66–74, (2004).

Vicente R., Gollo L.L., Mirasso C.R., Fischer I., and Pipa G. Dynamical relaying can yield zero time lag neuronal synchrony despite long conduction delays. *Proc Natl Acad Sci U S A*, **105**(44):17157–17162, (2008).

Vreugdenhil M., Hack S.P., Draguhn A., and Jefferys J.G.R. Tetanus toxin induces long-term changes in excitation and inhibition in the rat hippocampal CA1 area. *Neuroscience*, **114**(4):983–994, (2002).

Wald G. Carotenoids and the Visual Cycle. *J Gen Physiol*, **19**(2):351–371, (1935).

Wang H., Peca J., Matsuzaki M., Matsuzaki K., Noguchi J., Qiu L., Wang D., Zhang F., Boyden E., Deisseroth K., Kasai H., Hall W.C., Feng G., and Augustine G.J. High-speed mapping of synaptic connectivity using

photostimulation in Channelrhodopsin-2 transgenic mice. *Proc Natl Acad Sci U S A*, **104**(19):8143–8148, (2007).

Wang H., Sugiyama Y., Hikima T., Sugano E., Tomita H., Takahashi T., Ishizuka T., and Yawo H. Molecular determinants differentiating photocurrent properties of two channelrhodopsins from chlamydomonas. *J Biol Chem*, **284** (9):5685–5696, (2009).

Wang X. and Buzsáki G. Gamma Oscillation by Synaptic Inhibition in a Hippocampal Interneuronal Network Model. *J Neurosci*, **16(20)**:6402-641, (1996).

Wang X. and Rinzel J. Alternating and Synchronous Rhythms in Reciprocally. Inhibitory Model Neurons. *Neural Computation*, **4**:84-97, (1992).

Watson D.J., Kobinger G.P., Passini M.A., Wilson J.M., and Wolfe J.H. Targeted transduction patterns in the mouse brain by lentivirus vectors pseudotyped with VSV, Ebola, Mokola, LCMV, or MuLV envelope proteins. *Mol Ther*, **5**(5 Pt 1):528–537, (2002).

Watts D.J. and Strogatz S.H. Collective dynamics of 'small-world' networks. *Nature*, **393**(6684):440–442, (1998).

Weinberg M.S., Blake B.L., Samulski R.J., and McCown T.J. The influence of epileptic neuropathology and prior peripheral immunity on CNS transduction by rAAV2 and rAAV5. *Gene Ther*, , (2011).

Wen L., Wang H., Tanimoto S., Egawa R., Matsuzaka Y., Mushiake H., Ishizuka T., and Yawo H. Opto-current-clamp actuation of cortical neurons using a strategically designed channelrhodopsin. *PLoS One*, **5**(9):e12893, (2010).

White A., Williams P.A., Hellier J.L., Clark S., Dudek F.E., and Staley K.J. EEG spike activity precedes epilepsy after kainate-induced status epilepticus. *Epilepsia*, **51**(3):371–383, (2010).

Whittington M.A., Traub R.D., and Jefferys J.G. Synchronized oscillations in interneuron networks driven by metabotropic glutamate receptor activation. *Nature*, **373**(6515):612–615, (1995).

Whittington M.A., Traub R.D., Kopell N., Ermentrout B., and Buhl E.H. Inhibition-based rhythms: experimental and mathematical observations on network dynamics. *Int J Psychophysiol*, **38**(3):315–336, (2000).

Wiesenhofer B. and Humpel C. Lipid-mediated gene transfer into primary neurons using FuGene: comparison to C6 glioma cells and primary glia. *Exp Neurol*, **164**(1):38–44, (2000).

Wilke C., Worrell G., and He B. Graph analysis of epileptogenic networks in human partial epilepsy. *Epilepsia*, **52**(1):84–93, (2011).

Williamson L.C., Fitzgerald S.C., and Neale E.A. Differential effects of tetanus toxin on inhibitory and excitatory neurotransmitter release from mammalian spinal cord cells in culture. *J Neurochem*, **59**(6):2148–2157, (1992).

Willmore L.J., Sypert G.W., Munson J.V., and Hurd R.W. Chronic focal epileptiform discharges induced by injection of iron into rat and cat cortex. *Science*, **200**(4349):1501–1503, (1978).

Wilson E. Neurosurgical treatment for tetanus. *J Hist Neurosci*, **6**(1):82–85, (1997).

Wilson H.R. and Cowan J.D. Excitatory and inhibitory interactions in localized populations of model neurons. *Biophys J*, **12**(1):1–24, (1972).

Wilson S.P., Yeomans D.C., Bender M.A., Lu Y., Goins W.F., and Glorioso J.C. Antihyperalgesic effects of infection with a preproenkephalin-encoding herpes virus. *Proc Natl Acad Sci U S A*, **96**(6):3211–3216, (1999).

Winfree A.T. Biological rhythms and the behavior of populations of coupled oscillators. *J Theor Biol*, **16**(1):15–42, (1967).

Woldbye D.P.D., Angehagen M., Gøtzsche C.R., Elbrønd-Bek H., Sørensen A.T., Christiansen S.H., Olesen M.V., Nikitidou L., Hansen T.V.O., Kanter-Schlifke I., and Kokaia M. Adeno-associated viral vector-induced overexpression of neuropeptide Y Y2 receptors in the hippocampus suppresses seizures. *Brain*, **133**(9):2778–2788, (2010).

Wong L.F., Azzouz M., Walmsley L.E., Askham Z., Wilkes F.J., Mitrophanous K.A., Kingsman S.M., and Mazarakis N.D. Transduction patterns of pseudotyped lentiviral vectors in the nervous system. *Mol Ther*, **9**(1):101–111, (2004).

Woo M., Hakem R., Soengas M.S., Duncan G.S., Shahinian A., Kägi D., Hakem A., McCurrach M., Khoo W., Kaufman S.A., Senaldi G., Howard T., Lowe S.W., and Mak T.W. Essential contribution of caspase 3/CPP32 to apoptosis and its associated nuclear changes. *Genes Dev*, **12**(6):806–819, (1998).

Worgall S., Sondhi D., Hackett N.R., Kosofsky B., Kekatpure M.V., Neyzi N., Dyke J.P., Ballon D., Heier L., Greenwald B.M., Christos P., Mazumdar M., Souweidane M.M., Kaplitt M.G., and Crystal R.G. Treatment of late infantile neuronal ceroid lipofuscinosis by CNS administration of a serotype 2 adeno-associated virus expressing CLN2 cDNA. *Hum Gene Ther*, **19**(5): 463–474, (2008).

Worrell G.A., Parish L., Cranstoun S.D., Jonas R., Baltuch G., and Litt B. High-frequency oscillations and seizure generation in neocortical epilepsy. *Brain*, **127**(Pt 7):1496–1506, (2004).

Worrell G.A., Gardner A.B., Stead S.M., Hu S., Goerss S., Cascino G.J., Meyer F.B., Marsh R., and Litt B. High-frequency oscillations in human temporal lobe: simultaneous microwire and clinical macroelectrode recordings. *Brain*, **131**(Pt 4):928–937, (2008).

Wyatt R. and Sodroski J. The HIV-1 envelope glycoproteins: fusogens, antigens, and immunogens. *Science*, **280**(5371):1884–1888, (1998).

Wykes R.C., Heeroma J.H., Mantoan L., Zheng K., MacDonald D.C., Deisseroth K., Hashemi K.S., Walker M.C., Schorge S., and Kullmann D.M. Optogenetic and potassium channel gene therapy in a rodent model of focal neocortical epilepsy. *Sci Transl Med*, **4**(161):161ra152, (2012).

Yalkinoglu A.O., Heilbronn R., Bürkle A., Schlehofer J.R., and zur Hausen H. DNA amplification of adeno-associated virus as a response to cellular genotoxic stress. *Cancer Res*, **48**(11):3123–3129, (1988).

Yizhar O., Fenno L.E., Davidson T.J., Mogri M., and Deisseroth K. Optogenetics in neural systems. *Neuron*, **71**(1):9–34, (2011).a.

Yizhar O., Fenno L.E., Prigge M., Schneider F., Davidson T.J., O'Shea D.J., Sohal V.S., Goshen I., Finkelstein J., Paz J.T., Stehfest K., Fudim R., Ramakrishnan C., Huguenard J.R., Hegemann P., and Deisseroth K. Neocortical excitation/inhibition balance in information processing and social dysfunction. *Nature*, **477**(7363):171–178, (2011).b.

Zacks D.N., Derguini F., Nakanishi K., and Spudich J.L. Comparative study of phototactic and photophobic receptor chromophore properties in Chlamydomonas reinhardtii. *Biophys J*, **65**(1):508–518, (1993).

Zemelman B.V., Lee G.A., Ng M., and Miesenböck G. Selective photostimulation of genetically chARGed neurons. *Neuron*, **33**(1):15–22, (2002).

Zennou V., Serguera C., Sarkis C., Colin P., Perret E., Mallet J., and Charneau P. The HIV-1 DNA flap stimulates HIV vector-mediated cell transduction in the brain. *Nat Biotechnol*, **19**(5):446–450, (2001).

Zhang F., Aravanis A.M., Adamantidis A., de Lecea L., and Deisseroth K. Circuit-breakers: optical technologies for probing neural signals and systems. *Nat Rev Neurosci*, **8**(8):577–581, (2007).a.

Zhang F., Wang L.P., Brauner M., Liewald J.F., Kay K., Watzke N., Wood P.G., Bamberg E., Nagel G., Gottschalk A., and Deisseroth K. Multimodal fast optical interrogation of neural circuitry. *Nature*, **446**(7136):633–639, (2007).b.

Zhang F., Prigge M., Beyrière F., Tsunoda S.P., Mattis J., Yizhar O., Hegemann P., and Deisseroth K. Red-shifted optogenetic excitation: a tool for fast neural control derived from Volvox carteri. *Nat Neurosci*, **11**(6):631–633, (2008).

Zhang F., Gradinaru V., Adamantidis A.R., Durand R., Airan R.D., de Lecea L., and Deisseroth K. Optogenetic interrogation of neural circuits: technology for probing mammalian brain structures. *Nat Protoc*, **5**(3):439–456, (2010).

Zhang G.R., Wang X., Yang T., Sun M., Zhang W., Wang Y., and Geller A.I. A tyrosine hydroxylase-neurofilament chimeric promoter enhances long-term expression in rat forebrain neurons from helper virus-free HSV-1 vectors. *Brain Res Mol Brain Res*, **84**(1-2):17–31, (2000).

Zhao S., Cunha C., Zhang F., Liu Q., Gloss B., Deisseroth K., Augustine G.J., and Feng G. Improved expression of halorhodopsin for light-induced silencing of neuronal activity. *Brain Cell Biol*, **36**(1-4):141–154, (2008).

Zin-Ka-Ieu S., Roger M., and Arnault P. Direct contacts between fibers from the ventrolateral thalamic nucleus and frontal cortical neurons projecting to the striatum: a light-microscopy study in the rat. *Anat Embryol (Berl)*, **197**(1): 77–87, (1998).

Zufferey R., Dull T., Mandel R.J., Bukovsky A., Quiroz D., Naldini L., and Trono D. Self-inactivating lentivirus vector for safe and efficient in vivo gene delivery. *J Virol*, **72**(12):9873–9880, (1998).

# Appendix A

# Appendix: Additional Figures and Tables

Figure A.1: **Original Plasmids and Fluorophores. (a)** Schematic of original plasmids used for cloning. **(b)** Activation spectra of ChR2 and NpHR (adapted from (Zhang et al., 2007a)) **(c)** Table summarizing wavelengths required for excitation of opsins and fluorophores, and emission wavelengths for EYFP, GFP and mCherry.
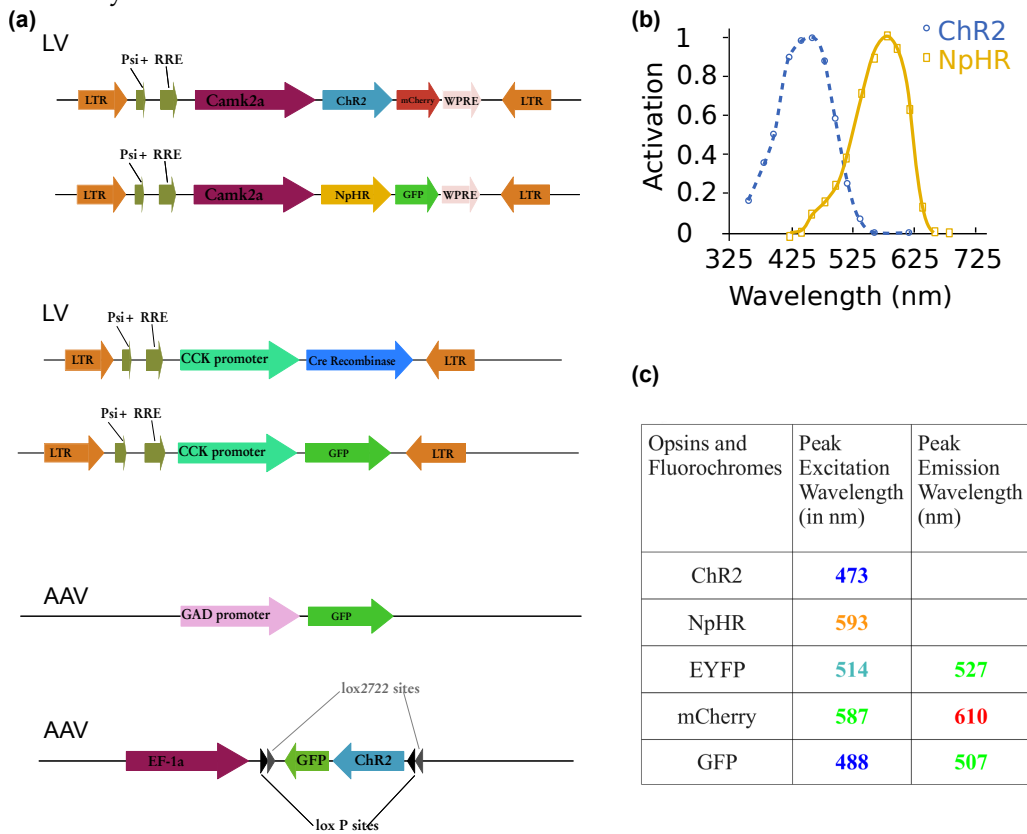


**(a)**

**(b)**

**(c)**

| Opsins and Fluorochromes | Peak Excitation Wavelength (in nm) | Peak Emission Wavelength (nm) |
|---|---|---|
| ChR2 | 473 | |
| NpHR | 593 | |
| EYFP | 514 | 527 |
| mCherry | 587 | 610 |
| GFP | 488 | 507 |

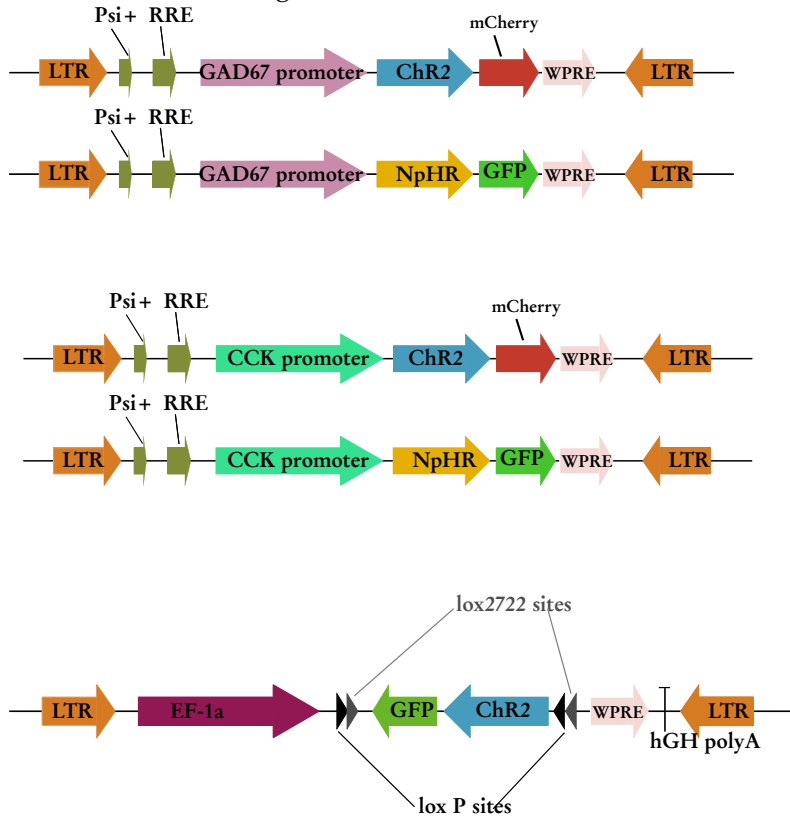Figure A.2: **Cloned Lentiviral Constructs.**

Table A.1: **Fluorophores and Filter Settings Used for Confocal Microscopy Experiments**

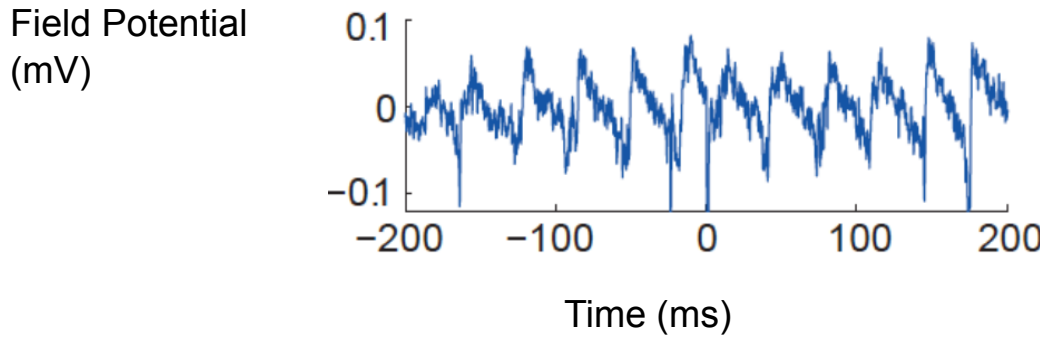| Fluorophore | Wavelength maximum [nm] | | Laser excitation wavelength [nm] | Filter set for emitted light [nm] |
|---|---|---|---|---|
| | Excitation | Emission | | |
| AF 488 | 495 | 519 | 488 | 500-570 |
| AF 568 | 578 | 603 | 532 | 570-690 |
| Tetramethyl-rhodamine | 550 | 570 | 532 | 570-690 |
| DAPI (4′,6-diamidino-2-phenylindole) | 358 | 561 | 405 | 420-490 |

Figure A.3: Induction of gamma oscillations by carbachol.Example of local field potential trace during carbachol perfusion inducing gamma oscillations of slower frequency (~22 Hz) than those elicited by ChR2 activation (~52 Hz). Pyramidal neuron held at -55 mV (from (Akam et al., 2012)).
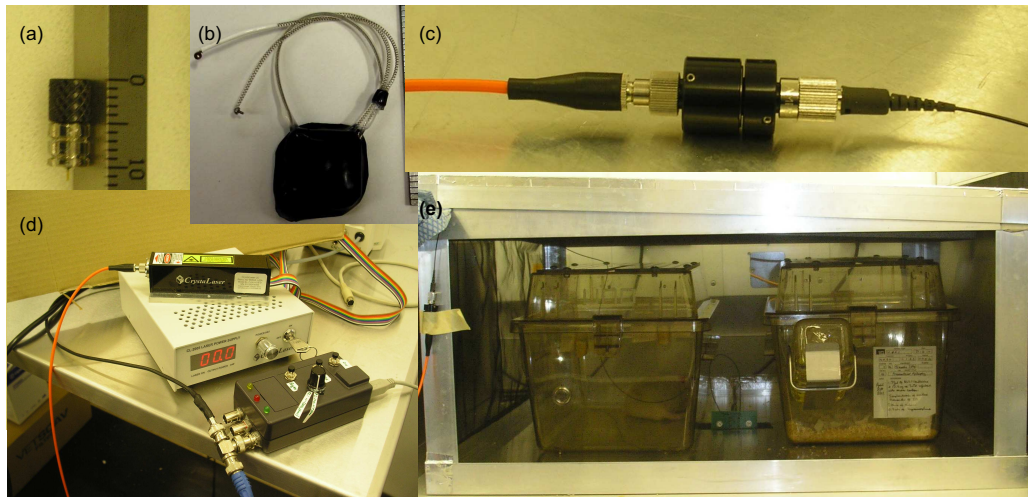


(a) Optic fibre (core diameter 200 μm, numerical aperture 0.22, cannula length 1.5 – 1.8 mm, Doric Lenses, Canada) (b)Wireless transmitter (A3019D, Open Source Instruments Inc; sampling frequency 512 Hz, bandwidth 0.7 – 160 Hz). (c) Fiberoptic patch cord (in black, right: NA 0.22, Doric Lenses) connected via a rotary commutator (center: Doric Lenses) to laser fiberoptic cable (in orange, left: Crystalaser). (d) 561nm laser (Crystalaser) connected to microcontroller (Arduino) for pulsing the laser. (e) Faraday enclosure for continuous EEG telemetry.

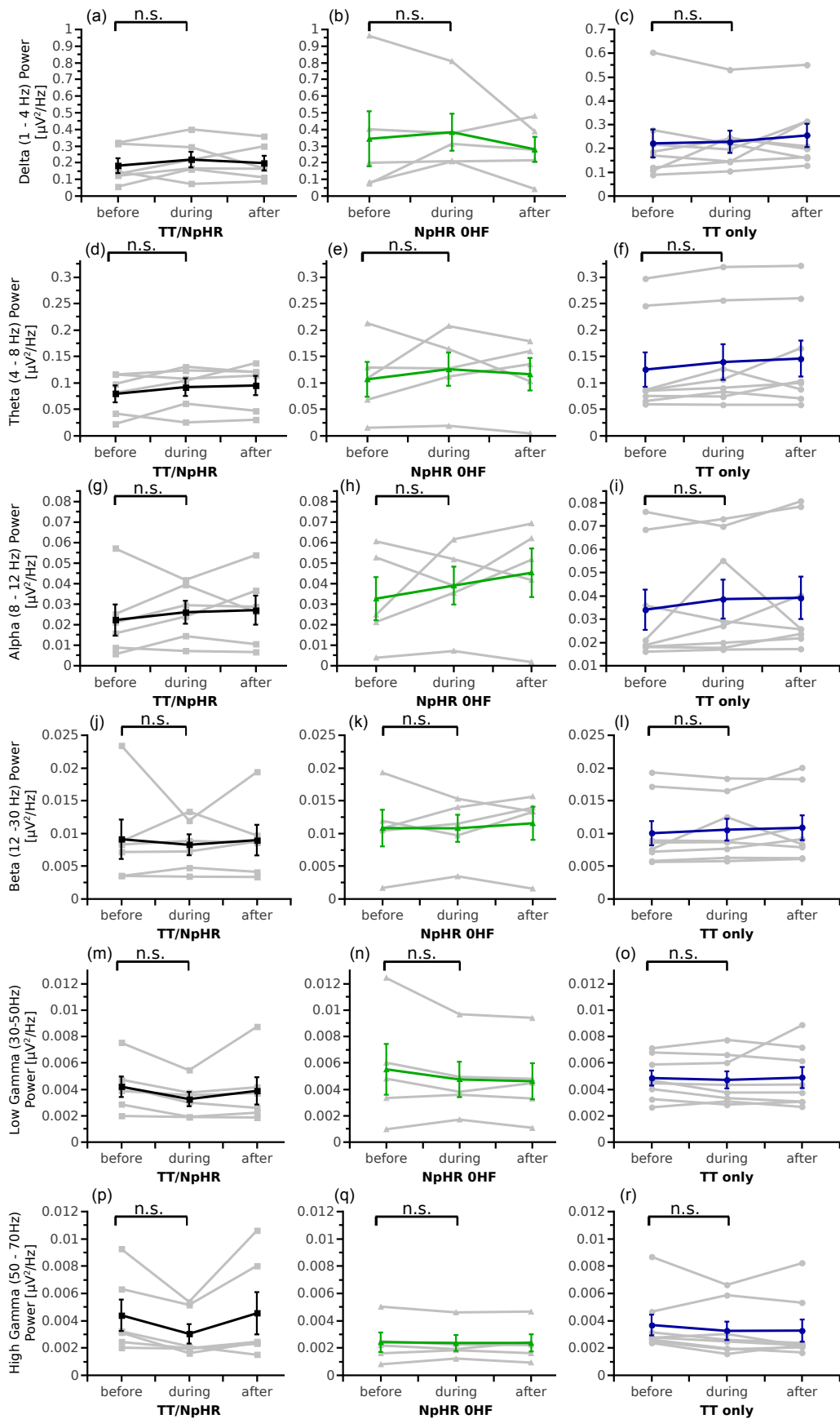Figure A.4: **Optogenetic Equipment for *In Vivo* Experiments.**

Figure A.5: **EEG Frequency Bands < 70 Hz are not affected by laser stimulation.**

| | |
|---|---|
| 5′ UTR | 5′ untranslated region |
| AAV | adeno associated virus |
| Acop-1 and Acop-2 | Archaeal type Chlamydomonas opsin 1 and 2 |
| ACSF | artificial cerebrospinal fluid |
| Ad | Adenovirus |
| AF | Alexa Fluor |
| AP | anterior-posterior |
| Arch | archaerhodopsin-3 |
| AVV | adenoviral vector |
| AVVL | anteroventral nucleus of the thalamus |
| BDNF | brain-derived neurotrophic factor |
| BR | bacteriorhodopsin |
| BSA | bovine serum albumin |
| BSS | balanced salt solution |
| CA1 | cornu ammonis 1 |
| CA3 | cornu ammonis |
| Camk2a | calcium calmodulin binding kinase 2a (promoter) |
| CaMKIIα | calcium calmodulin binding kinase II alpha (protein) |
| CB-1 | cannabinoid type 1 |
| CCK | cholecystokinin |
| cDNA | complementary deoxyribonucleic acid |
| Chop-1 and 2 | channelopsin 1 and 2 |
| ChR1 and ChR2 | channelrhodopsin-1 and -2 |
| CLN2 | ceroid lipofuscinosis |
| CMV | cytomegalovirus |
| CNS | central nervous system |
| cPPT | central polypurine tract |
| CSRA and CSRB | Chlamydomonas sensory rhodopsin A and B |
| D-PBS | Dulbecco's Phosphate-Buffered Saline |
| DAPI | 4′6-diamidino-2-phenylindole |
| DBS | deep brain stimulation |
| DEAE-Dextran | diethylaminoethyl-dextran |
| DG | dentate gyrus |
| DIV | day in vitro |
| DMEM | Dulbecco's Modified Eagle Medium |
| DOTMA | 1 |
| E14 | Embryonal day 14 |
| EEG | electroencephalographic |
| EF1a | elongation factor 1 a |
| eNPAC | AAV5-eNpHR3.0-2A-ChR2-EYFP |
| ER | endoplasmatic reticulum |
| EYFP | enhanced yellow fluorescent protein |
| FACS | Fluorescent-activated cell sorting |
| FCS | fetal calf serum |

Table A.2: **List of Abbreviations**

| | |
|---|---|
| GABA | gamma-aminobutyric acid |
| GAD | glutamic acid decarboxylase |
| GE | ganglionic eminence |
| GFAP | glial fibrillary acidic protein |
| GFP | green fluorescent protein |
| GPCR | G protein coupled receptor protein |
| HBSS | Hanks' balanced salt solution |
| Hcrt | prepro-hypocretin |
| HEK | human embryonic kidney cells |
| HFA | high frequency activity |
| HFO | high frequency oscillations |
| HIV | human immunodeficiency virus |
| HR | halorhodopsin |
| HsHR | Halobacterium salinarum |
| HSV | herpes simplex virus |
| hSyn | Synapsin |
| ILAE | International League against Epilepsy |
| IPSPs | inhibitory postsynaptic potentials |
| ITRs | inverted terminal repeats |
| IU | infectious units |
| L | lateral |
| LED | light emitting diode |
| LFP | local field potential |
| LTRs | long-terminal repeats |
| LV | lentivirus |
| Mac | a proton pump from the fungus Leptosphaeria maculans |
| MIT | Massachusetts Institute of Technology |
| MoMLV | Moloney murine leukaemia virus |
| NMDA | N-Methyl-D-aspartate |
| NPY | neuropeptide Y |
| p0 | postnatal day 0 |
| p20 | postnatal day 20 |
| PBS | phosphate buffered saline |
| PCR | polymerase chain reaction |
| PD | Parkinson's Disease |
| PDL | Poly-D-Lysine |
| PFA | paraformaldehyde |
| PRC | phase response curve |
| qPCR | quantitative PCR |
| rAAVs | recombinant AAVs |
| s.c. | subcutaneous |
| SEM | standard error of mean |
| SFO | step-function opsins |
| SIN | self-inactivating vectors |
| SOZ | seizure onset zone |
| SRI | sensory rhodopsin I and II |

Table A.3: **List of Abbreviations - continued**

| | |
|---|---|
| Thy1 | Thymocyte differentiation antigen 1 |
| TT | tetanus toxin |
| V | vertical |
| VFO | very fast oscillation |
| VFs | visual fields |
| VSV | vesicular stomatitis virus |
| VSVg | G-Protein of vesicular stomatitis virus |
| WPRE | Woodchuck Hepatitis Virus Post-transcriptional Regulatory Element |
| YFP | yellow fluorescent protein |

Table A.4: **List of Abbreviations - continued**